EXPANDING THE SULFUR CHEMICAL TOOLBOX: SYNTHESIS AND STUDY OF SMALL MOLECULE CARBONYL SULFIDE DONORS AND HYDROGEN SULFIDE PROBES

by

CAROLYN M. LEVINN

A DISSERTATION

Presented to the Department of Chemistry and Biochemistry
and the Graduate School of the University of Oregon
in partial fulfillment of the requirements
for the degree of
Doctor of Philosophy

September 2020

DISSERTATION APPROVAL PAGE

Student: Carolyn M. Levinn

Title: Expanding the Sulfur Chemical Toolbox: Synthesis and Study of Small Molecule Carbonyl Sulfide Donors and Hydrogen Sulfide Probes

This dissertation has been accepted and approved in partial fulfillment of the requirements for the Doctor of Philosophy degree in the Department of Chemistry and Biochemistry by:

Dr. Darren W. Johnson	Chairperson
Dr. Michael D. Pluth	Advisor
Dr. Victoria J. DeRose	Core Member
Dr. Matthew F. Barber	Institutional Representative

and

Kate Mondloch	Interim Vice Provost and Dean of the Graduate School

Original approval signatures are on file with the University of Oregon Graduate School.

Degree awarded September 2020

DISSERTATION ABSTRACT

Carolyn M. Levinn

Doctor of Philosophy

Department of Chemistry and Biochemistry

September 2020

Title: Expanding the Sulfur Chemical Toolbox: Synthesis and Study of Small Molecule Carbonyl Sulfide Donors and Hydrogen Sulfide Probes

Hydrogen sulfide (H_2S) has recently been recognized as an important biological signaling molecule, with roles in regulating many biological processes, including neuromodulation and inflammation, as well as many disease states, such as diabetes and Alzheimer's disease. Due to these diverse biological functions, there is great interest in better understanding the complex roles of H_2S in biology and studying how we can utilize this molecule as a potential therapeutic. To accomplish these goals, researchers need chemical tools, such as H_2S donors and probes, that act with precision in biological settings.

The research presented in this dissertation falls into primarily two aims: 1) obtaining a better mechanistic understanding of the thiocarbamate COS/H_2S donor scaffold and developing novel COS/H_2S donors, and 2) studying and applying H_2S detection motifs to novel H_2S probes. Chapter I is an introduction into the biological roles of H_2S. Chapter II is a review of current H_2S donor molecules with an emphasis on COS delivering systems. Chapter III expands upon previously reported cytotoxic esterase-triggered thiocarbamate donors, demonstrating that the observed toxicity and rate of COS release can be attenuated predictably by changing the rate of ester hydrolysis, but not through electronic modulation of the payload. Chapter IV uses *N*-methylation to

investigate the mechanism of COS release from thiocarbamates and shows that electron-poor payloads have a more complex reaction landscape than previously recognized. Additionally, Chapter IV describes the application of the *N*-alkylation strategy to the development of dithiocarbamate CS_2 donors and oligomeric COS donors. Chapter V reports the development of a COS-releasing Alzheimer's prodrug.

To address aim 2, Chapter VI provides an overview of detection methods and probes for H_2S. Chapter VII details using a chemiluminescent core to survey different H_2S-senstitive triggering motifs and reports a bright platform for aqueous detection of H_2S. Chapter VIII demonstrates using a nanohoop rotaxane as a fluorescent probe for H_2S. Chapter IX summarizes where the field of H_2S research currently stands, and includes a broader scientific policy argument that highlights the need for increased transparency and destigmatization around publishing failed results across all of science.

This dissertation includes previously published and unpublished co-authored materials.

CURRICULUM VITAE

NAME OF AUTHOR: Carolyn M. Levinn

GRADUATE AND UNDERGRADUATE SCHOOLS ATTENDED:

University of Oregon, Eugene
University of Illinois at Urbana Champaign, Urbana
State University of New York College at Geneseo, Geneseo

DEGREES AWARDED:

Doctor of Philosophy, Chemistry, 2020, University of Oregon
Master of Science, Chemistry, 2017, University of Illinois at Urbana Champaign
Bachelor of Science, Chemistry, 2014, State University of New York College at Geneseo

AREAS OF SPECIAL INTEREST:

Reactive Sulfur Species in Biology
Small Molecule Organic Synthesis
Organic Chemistry

PROFESSIONAL EXPERIENCE:

Graduate Teaching Fellow, University of Oregon, 2020
Graduate Teaching Fellow, University of Illinois at Urbana-Champaign, 2014-2015

GRANTS, AWARDS, AND HONORS:

NSF Graduate Research Fellowship, University of Illinois at Urbana-Champaign, 2016

Roger Adams Fellowship, University of Illinois at Urbana-Champaign, 2015

ACS Division of Organic Chemistry Undergraduate Award, SUNY Geneseo, 2014

Phi Beta Kappa, SUNY Geneseo, 2014

Goldwater Scholar, SUNY Geneseo, 2013

Presidential Scholar, SUNY Geneseo, 2013

PUBLICATIONS:

Otteson, C. E.; Levinn, C. M.; Van Raden, J. M. Pluth, M. D.; Jasti, R. Nanohoop [2]rotaxane as size-selective reactive turn-on fluorescent probe for H_2S. *Manuscript in preparation.*

Levinn, C. M.; Mancuso, J. L.; Lutz, R. E.; Hendon, C. H.; Pluth, M. D. N-Methylation Provides Insights into Mechanism of Carbonyl Sulfide Release from Self-Immolative Thiocarbamates. *Manuscript in preparation.*

Levinn, C. M.; Pluth, M. D. A Direct Comparison of Triggering Motifs on Chemiluminescent Probes for Hydrogen Sulfide Detection in Water. *Manuscript in preparation.*

Levinn, C. M.; Cerda, M. M.; Pluth, M. D. Activatable Small Molecule H_2S Donors. *Antioxid. Redox Signal.* **2020**, *32*, 96-109.

Levinn, C. M.; Cerda, M. M.; Pluth, M. D. Development and Application of Carbonyl-Sulfide-Based Donors for H_2S Delivery. *Acc. Chem. Res.* **2019**, *52*, 2723-2731.

Levinn, C. M.; Steiger, A. K.; Pluth, M. D. Esterase-Triggered Self-Immolative Thiocarbamates Provide Insights into COS Cytotoxicity. *ACS Chem. Biol.* **2019**, *14*, 170-175.

ACKNOWLEDGMENTS

First and foremost, I would like to thank my family. They have always been there for me and leave me with no doubt that they always will be. To my parents, Doris and Mitch for always loving and supporting me, while still pushing me to ask the hard questions and think outside the box. To my brother Ben for being a grounding voice on what grad school is, and what it should not be, and for always welcoming me into your home. To Sandy, the smartest and most selfless person I know, you are my forever best friend, and I would not be where I am today if I didn't have you to look up to. To Oma and Opa, to Nanny and Poppa. Thank you for a lifetime of support.

Next, I would like to thank Professor Mike Pluth, for taking a chance and accepting me as a transfer into his lab. He has been a great boss and mentor and has always made sure to support me both academically and professionally. I went to Mike and said I wanted to work in science policy, and his response was great let's make that happen, and has supported me every step of the way. I would like to also thank my committee, Professors Darren Johnson, Matt Barber, and Vickie DeRose, for seeing my potential and encouraging me. The University of Oregon Chemistry Department is one of the most supportive departments that I have ever heard of, and I am lucky to have had the privilege of working with you all.

To my undergraduate professors at SUNY Geneseo who made me fall in love with chemistry, Cristina and Dave Geiger, Eric Helms, and Dave Johnson – thank you for introducing me to the strange puzzle that is organic chemistry. To Professor Steve Zimmerman at the University of Illinois, for always having my back and giving me a safe place in a dangerous environment. I learned a lot about how to be a leader from you, and

I appreciate all that you've done for me.

To my labmates past and present – Dr. Toby Sherbow, Dr. Dan Seidencranz, Dr. Matt Cerda, Annie Gilbert, Turner Newton, Sarah Bolton, Dr. Yu Zhao – you have made me a better scientist and a better person, and I would not have made it through graduate school without you. To Rachel Lutz, one of the most generous and hard-working people I've ever met, I have loved getting to work with you. Driven and resilient, you are the Elle Woods we all need in our lives. To all of the researchers I have collaborated with, Claire Otteson, Dr. Jeff Van Raden, Professor Ramesh Jasti, Jenna Mancuso, Hannah Hashimoto, Professor Chris Hendon, Professor Mi Hee Lim, thank you for all of your time, effort and patience with me. To my UIUC crew, Dr. Kali Miller, Dr. Kim Basset, Dr. Elena Montoto, and (soon to be) Dr. Sarah Perlemutter, you carried me through some of the worst times, and have celebrated with me some of the best times, and I appreciate everything you've done for me. To Dr. Emma Southgate, Dr. Chris Bemis, Dr. Mikiko Okumura, Bry-guy Reynolds, Chris Huck, and Stef Nakamata Huynh – the best of the brightest Super Starlahs. To all of my UO friends and family, especially Annie, Dani, Kira, Gabby, Josh, Claire, Dan, Kiana, and Thais, thank you for everything. To my Sophie, the sassiest sidekick. And finally, to Andrew, who has been my rock for the past year, thank you for being on my team.

Lastly, I would like to thank the University of Oregon, the National Science Foundation (NSF/GRFP DGE-1309047, CHE-1427987, CHE-1625529, ACI-1548562), the National Institutes of Health (R01GM113030), and the Camille and Henry Dreyfus Foundation for funding the research in this dissertation.

To my parents – thank you for everything, I love you.

TABLE OF CONTENTS

Chapter Page

Chapter Page

LIST OF FIGURES

Figure Page

Figure Page

Figure Page

Figure Page

Figure Page

Figure Page

CHAPTER I

HYDROGEN SULFIDE AS AN IMPORTANT BIOMOLECULE

This chapter includes previously published and co-authored material from Levinn, C.M.; Cerda, M.M.; Pluth, M.D. Activatable Small-Molecule Hydrogen Sulfide Donors. *Antioxid. Redox Signal.* **2020**, *32* (2), 96-109. This review was co-written by Dr. Matthew M. Cerda and Carolyn M. Levinn, with editorial assistance from Professor Michael D. Pluth.

Hydrogen sulfide (H_2S), historically dismissed as a toxic and malodorous gas, has emerged in the scientific community as an important biological signaling molecule.[1-3] The physicochemical properties of H_2S have been studied extensively, and we refer the interested reader to recent reviews that cover this area in depth.[4-9] Since its initial recognition as a relevant biomolecule, diverse scientific communities ranging from chemists to physiologists have focused on in investigating the role of H_2S in various biosystems.

H_2S is produced endogenously in mammals primarily from cysteine through the action of three main enzymes. Cystathionine-β-synthase (CBS) is primarily localized in the nervous system, brain, and liver; cystathionine-γ-lyase (CSE) produces H_2S primarily in the cardiovascular system; and 3-mercaptopyruvate sulfurtransferase (3-MST) is localized in the mitochondria.[1, 10] Investigations into the biological roles of H_2S have established its critical roles in different disease states and pathologies in almost every human organ system (Figure 1).[11-14] As brief examples, H_2S plays important roles in the central nervous system, participates in neurotransmission, and has been shown to have

neuroprotective effects, specifically in mouse models of Parkinson's disease.[15-17] Additionally, H_2S upregulates GSH production in the brain during periods of high oxidative stress and contributes to regulating key sodium channels in neuronal cells.[17] In the respiratory system, H_2S plays roles in different conditions, including chronic obstructive pulmonary disease (COPD), pulmonary fibrosis, and hypoxia-induced pulmonary hypertension.[18] In the cardiovascular system, H_2S mitigates oxidative stress and is well established to reduce myocardial injury related to ischemia-reperfusion injury.[19-21] Moreover, lower circulating H_2S levels are found in experimental models of heart failure, and CSE-deficient mice exhibit greater cardiac disfunction after transverse aortic constriction, both of which suggest additional roles of H_2S in heart failure.[22]

More broadly, H_2S interacts through several signaling pathways, such as the KATP channels, and promotes angiogenesis by the Akt and phosphatidylinositol 3-kinase (PI3K) pathways.[23] Low levels of H_2S has been demonstrated to promote cell proliferation and migration.[24-25] More recently, a study of psoriasis patients demonstrated lower serum H_2S levels than healthy patients, underscoring the potential role H_2S plays in skin protection and repair.[26] As a whole, the established pathophysiological targets of H_2S are incredibly diverse, and include activities as an established antiapoptotic,[27] anti-inflammatory,[28-30] and antioxidative agent,[31] as well as contributing to many other processes.

With such a broad range of biological targets and activities, significant effort has focused on investigating and understanding the direct effects of H_2S on specific systems with a long-term goal of leveraging these insights to deliver H_2S-related therapeutic

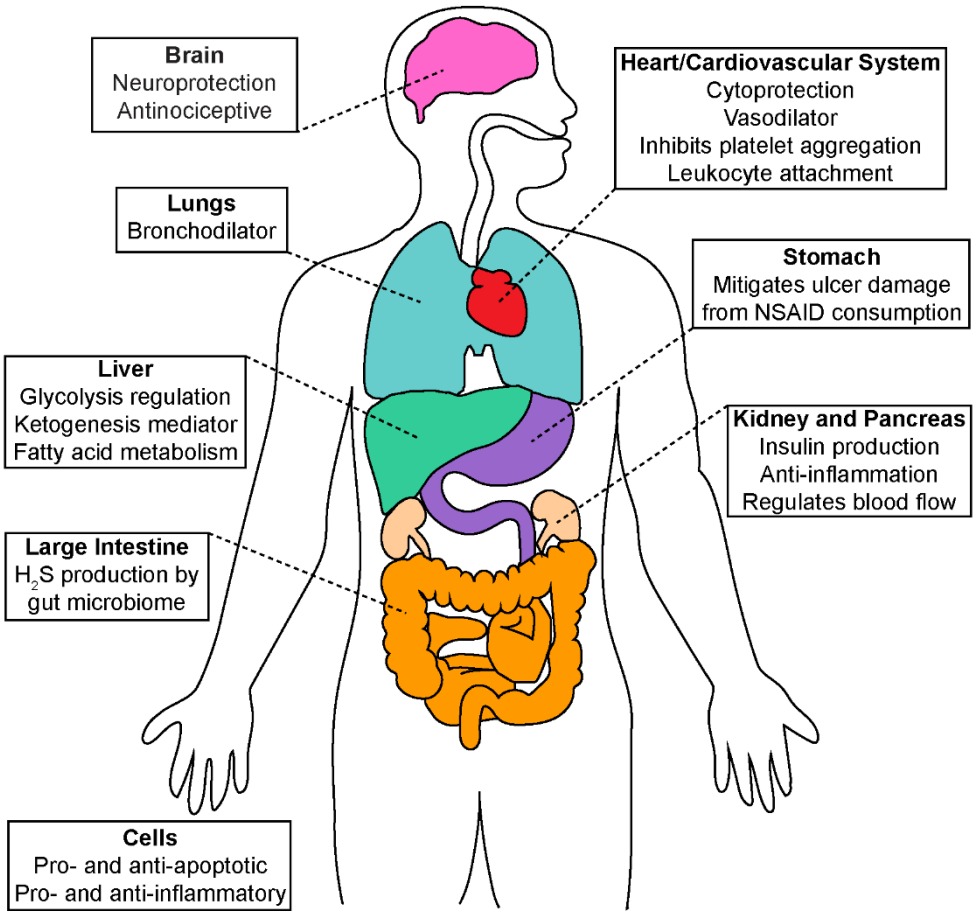

Figure 1.1 Selected roles of H_2S in major organ systems

interventions. This has led to the development of many small molecule chemical 'tools,' designed to aid biologists in their quest to determine the exact role of H_2S in different systems. Among these tools are H_2S donors, which can deliver one or more equivalents of H_2S to the desired system, as well as H_2S probes, which provide an optical response upon reaction with one or more equivalents of H_2S.

The research discussed in this dissertation describes contributions to this toolbox for studying H_2S in biology. Chapter II provides a comprehensive review of the know triggerable H_2S donors, and then Chapters III and IV detail the development of different esterase-triggered self-immolative thiocarbamate COS/H_2S donor scaffolds and the

thorough mechanistic investigation that they enable. Chapter V highlights preliminary work on the development of a COS-releasing prodrug for Alzheimer's disease. Chapter VI provides an introduction to different methods of H_2S detection and different small molecule probes, and Chapters VII and VIII describe the preparation and reactivity of a novel chemiluminescent and fluorescent probe for H_2S, respectively. Chapter IX summarizes the work presented and discusses what challenges still face the field of H_2S research. This Chapter also argues for the increased publication of failed or incomplete results across all disciplines as a means to reduce costs and redundancy in science. Chapters I through III include previously published, co-authored material. Chapters IV through IX include unpublished, co-authored material.

CHAPTER II

ACTIVATABLE SMALL-MOLECULE HYDROGEN SULFIDE DONORS

This chapter includes previously published and co-authored material from Levinn, C.M.; Cerda, M.M.; Pluth, M.D. Activatable Small-Molecule Hydrogen Sulfide Donors. *Antioxid. Redox Signal.* **2020**, *32* (2), 96-109. This review was co-written by Dr. Matthew M. Cerda and Carolyn Levinn, with editorial assistance from Professor Michael D. Pluth. This chapter also includes previously published and co-authored material from Levinn, C.M.; Cerda, M.M.; Pluth, M.D. Development and Application of Carbonyl Sulfide-Based Donors for H_2S Delivery. *Acc. Chem. Res.* **2019**, *52* (9), 2723-2731. This review was likewise co-written by Dr. Matthew M. Cerda and Carolyn Levinn, with editorial assistance from Professor Michael D. Pluth.

2.1 Introduction to H_2S Donors

The controlled delivery of H_2S has been a long-standing challenge due to the inherent chemical properties of H_2S. At physiological pH, the weak acidity of H_2S (pK_a ~ 7.0) results in a speciation of ~70% hydrosulfide anion (SH^-) and ~30% H_2S gas. In the presence of oxygen, and especially in the presence of redox-active metals, H_2S is readily oxidized and leads to the formation of polysulfides,[32] thus complicating the quantification of active H_2S concentrations. To avoid the direct use of H_2S gas, most biological studies have used sodium hydrosulfide (NaSH) and sodium sulfide (Na_2S) as convenient sources of H_2S. The addition of these inorganic sulfide salts to a buffered aqueous solution, however, results in a rapid, almost instantaneous increase in H_2S concentration followed

by a gradual decrease due to volatilization of H_2S gas.[33] This fast release of H_2S is in stark contrast to the rate of H_2S production by CBS and CSE measured under similar conditions.[34] These factors drive the need to develop alternative sources of H_2S which better mimic the rate of endogenous H_2S production.

Many reported H_2S donor systems respond to specific exogenous or biocompatible stimuli to release H_2S.[5, 9, 35-41] Such activation profiles allow for donor activities to be tuned to respond to specific activators and stimuli present in a given system. Although there is no single universal "ideal donor," certain donor classes provide distinct advantages and useful properties. For example, donors should have readily accessible control compounds that can be used to clearly delineate observed biological activities and outcomes associated with H_2S from those of donor byproducts. Similarly, donors that respond to specific stimuli enable experiments in which H_2S delivery can be controlled or triggered by specific activators. Coincident with these primary needs, significant advances in the development of triggerable H_2S donors have occurred in the past five years, with key examples including donors activated by light, various pH regimes, enzymes, biological thiols, and H_2O_2.

In developing activatable H_2S-releasing donors, a number of primary strategies have emerged, which are summarized briefly below but are expanded on in various sections of this chapter. The first commonly used strategy is to replace an oxygen atom in a molecule with a sulfur, such that hydrolysis releases H_2S. A second common strategy is to develop systems that generate an intermediate persulfide, which can be subsequently cleaved by thiols, such as GSH or cysteine, to generate H_2S and a disulfide. A third strategy is to develop systems that release carbonyl sulfide (COS) as an intermediate,

which can be quickly converted to H_2S the ubiquitous mammalian enzyme carbonic anhydrase (CA).[42] These three general approaches are summarized in Figure 2.1 and will be discussed briefly throughout the chapter. The mechanisms of H_2S release from the donor scaffolds shown are listed in Appendix A.

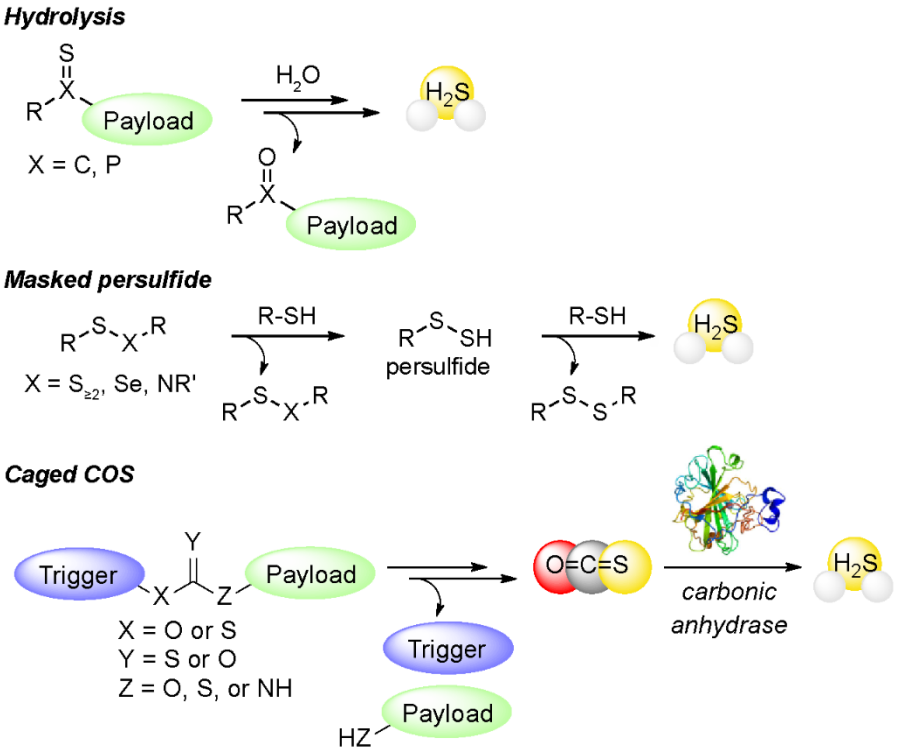

Figure 2.1 General strategies for H_2S release from different classes of small molecule donors.

2.2 Hydrolysis-Based and pH-Sensitive Donors

Numerous H_2S donors are activated by hydrolysis mechanisms, and most of these respond through acid-mediated pathways. Figure 2.2 shows the structures of these donors and the pH value or ranges at which the compounds have been reported to release H_2S. This class of H_2S donors provide the unique opportunity to target specific diseases, cells, and/or organelles in which acidic microenvironments are present. As a simple example, thioacetamide can function as a pH-activated H_2S donor in extremely acidic

environments (pH 1.0) and was initially used for the precipitation of dissolved metals as metal sulfides from acidic solutions for qualitative analysis.[43] We note the inherent toxicity of thioacetamide has severely limited the use of this H_2S donor in biological studies. As interest in the chemical biology of H_2S has grown, the use of related thioamides as H_2S donors has expanded to include various aryl thioamides, which are highlighted in a review.[44] Other simple small molecules have also been reported as pH-activated H_2S donors. For example, both thioglycine and thiovaline release H_2S in the presence of bicarbonate (HCO_3^-) at physiological pH.[45] Both of these thioamino acids were demonstrated to increase intracellular cGMP levels and promote vasorelaxation in mouse aortic rings, with both being more efficacious and potent than **GYY4137**.

One of the most commonly-used, **GYY4137**, is a water-soluble H_2S donor that draws inspiration from Lawesson's Reagent,[46] which is traditionally used in organic synthesis to prepare various organosulfur compounds.[47] The release of H_2S from **GYY4137** occurs slowly at physiological pH, but can be accelerated under acidic conditions (pH < 3.0).[48] Relative to other pH-sensitive H_2S donors, the biological activities of **GYY4137** have been studied extensively and are highlighted in a separate review in this Forum. To tune the rate of pH-dependent H_2S release from P=S motifs related to **GYY4137**, Xian and co-workers investigated the use of analogous phosphorodithioates as H_2S donors.[49] The inclusion of phenolic groups was found to enhance the rates of H_2S release at physiological pH, whereas alkyl alcohols decreased the efficiency of H_2S production consistent with the enhanced leaving group ability of phenols relative to alkyl alcohols. Moreover, pretreatment of H9c2 mouse

cardiomyocytes with these H_2S donors provided significant cytoprotection against H_2O_2-induced oxidative damage. Interestingly, analogous experiments with **GYY4137** failed to

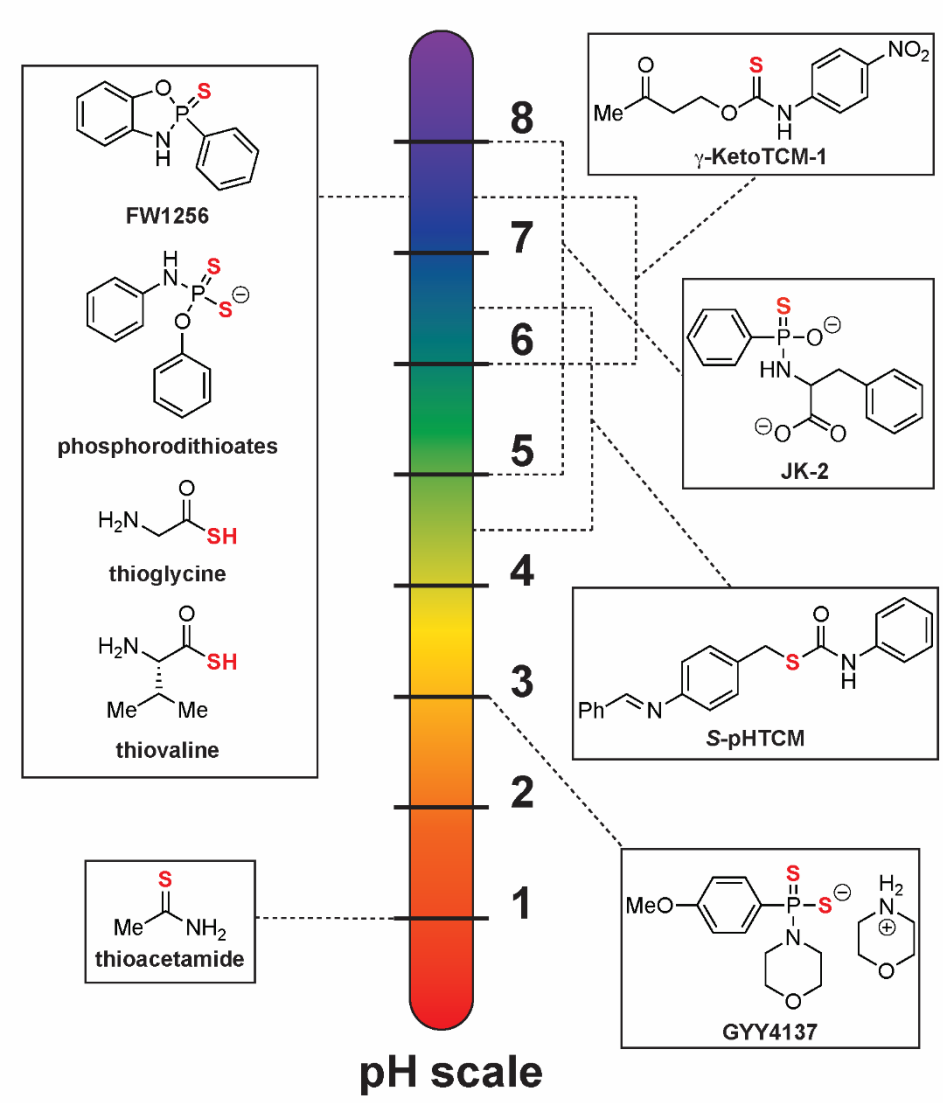

Figure 2.2 Hydrolysis-activated H_2S donors. The pH windows shown represent specific pH values or pH windows in which H_2S release was reported or in which H_2S release was reported to be optimal.

provide similar results due to the inherent cytotoxicity of this donor at higher concentrations. In a follow-up study of phosphorodithioate-based H_2S donors by Dymock and co-workers, they prepared a library of derivative compounds and examined the H_2S-

releasing properties of these compounds.[50] The cyclized derivative **FW1256** displayed relatively high levels of H_2S release and potent cytotoxicity against MCF7 breast cancer cells. In 2016, this concept was revisited by Xian and co-workers leading to the design of **GYY4137** derivatives, including **JK-2**, that bear a pendant nucleophile that can participate in an intramolecular cyclization to generate H_2S.[51] H_2S release was demonstrated within a range of pH 5.0 to 8.0, with significant enhancements in releasing efficiency over **GYY4137**. Moreover, treatment with **JK-2** resulted in significant reductions in infarction size in a myocardial ischemia-reperfusion injury mouse model.

In an alternative approach, our group recently reported pH-sensitive donors including **γ-KetoTCM-1**, that function through intermediate COS release, which will be discussed further in Chapter 2.6. This system was inspired by the use of 4-hydroxy-2-butanone esters to prepare self-immolative carbamate polymers that undergo β-elimination to generate CO_2 as a function of pH.[52] The release of H_2S from **γ-KetoTCM-1** was measured over a range of pH values (6.0 to 8.0), with increasing rates in more basic solution. The H_2S release half-life could be modified by structural tuning, and the donors provided anti-inflammatory activity in RAW 264.7 cells.[53] More recently, we reported a self-immolative thiocarbamate (***S*-pHTCM**) with a pendant aryl imine trigger as a pH-sensitive donor that releases COS/H_2S.[54] Notably, this triggering motif was designed to be activated within a specific acidic pH window and showed optimal cleavage rates between pH 4.3 and 7.3.

2.3 Thiol-Activated Donors

Compounds activated by biological thiols, including cysteine and reduced glutathione (GSH), represent the largest class of small-molecule H_2S donors (Figure 2.3a and 2.3b). The activation of many of these compounds proceed through persulfide intermediates, although others function through poorly understood mechanisms. The fundamental role and abundance of biological thiols, especially GSH, allows researchers to use these nucleophiles to probe the effects of H_2S donor administration. Expanding from thioacetamide, many aryl thioamides have been reported as H_2S donors. These compounds are stable at physiological pH and exhibit a cysteine-dependent H_2S release, yet the mechanism of H_2S release is unclear.[44] Despite the low H_2S-releasing efficiencies, such compounds possess unique pharmacological activities. The use of structurally-related iminothioethers as cysteine-activated H_2S donors was reported by Martelli and co-workers in 2017.[55] H_2S release from these donors was evaluated in buffer containing 4 mM cysteine and releasing efficiencies were dependent on donor derivatization. In isolated rat hearts, two donors were demonstrated to reverse the effects of angiotensin II induced reduction in basal coronary flow, and studies on human aortic smooth muscle cells showed that these donors exhibited membrane hyperpolarizing effects. The mechanism of cysteine-mediated H_2S release from iminothioethers remains unclear.

Aryl isothiocyanates were first reported as cysteine-activated H_2S donors in 2014 by Calderone and co-workers.[56] Although release efficiency from these compounds was relatively low and required millimolar levels of cysteine for release, the isothiocyanates were found to cause membrane hyperpolarization of vascular smooth muscle cells and vasorelaxation in coronary arteries, both of which are consistent with H_2S release. In

2019, Huang and co-workers investigated the mechanism of H_2S release from aryl isothiocyanates, and their data suggest that H_2S release proceeds through a native chemical ligation-type mechanism after initial attack on the isothiocyanate by the sulfhydryl group of cysteine.[57] Also building from a native chemical ligation mechanistic approach,[58] our group reported in 2018 that thionoesters, which are structural isomers of thioesters commonly used in native chemical ligation, respond selectively to cysteine over other thiols to release H_2S with >80% efficiency.[59] Mechanistic investigations demonstrated that the N to S acyl transfer step was the rate-limiting step of this reaction. We later expanded this approach to demonstrate that dithioesters, which are more synthetically diversifiable than thionoesters, release H_2S selectively in the presence of cysteine.[60] This approach has also been extended to provide fluorescent H_2S donors activated in the presence of cysteine (**CysP-1**).[61] Proceeding through a key N to S acyl transfer step, Xian and co-workers showed that acyl-protected geminal dithiols react selectively to release H_2S in the presence of cysteine, through generation of an unstable geminal dithiol intermediate.[62] Expanding to bioactive thioketone derivatives, Zhu and co-workers demonstrated during an investigation into the metabolism of clopidogrel (Plavix) that an intermediate metabolite containing a thioenol motif releases H_2S efficiently at physiological pH, suggesting possible future application of these and related compounds as H_2S donor motifs.[63]

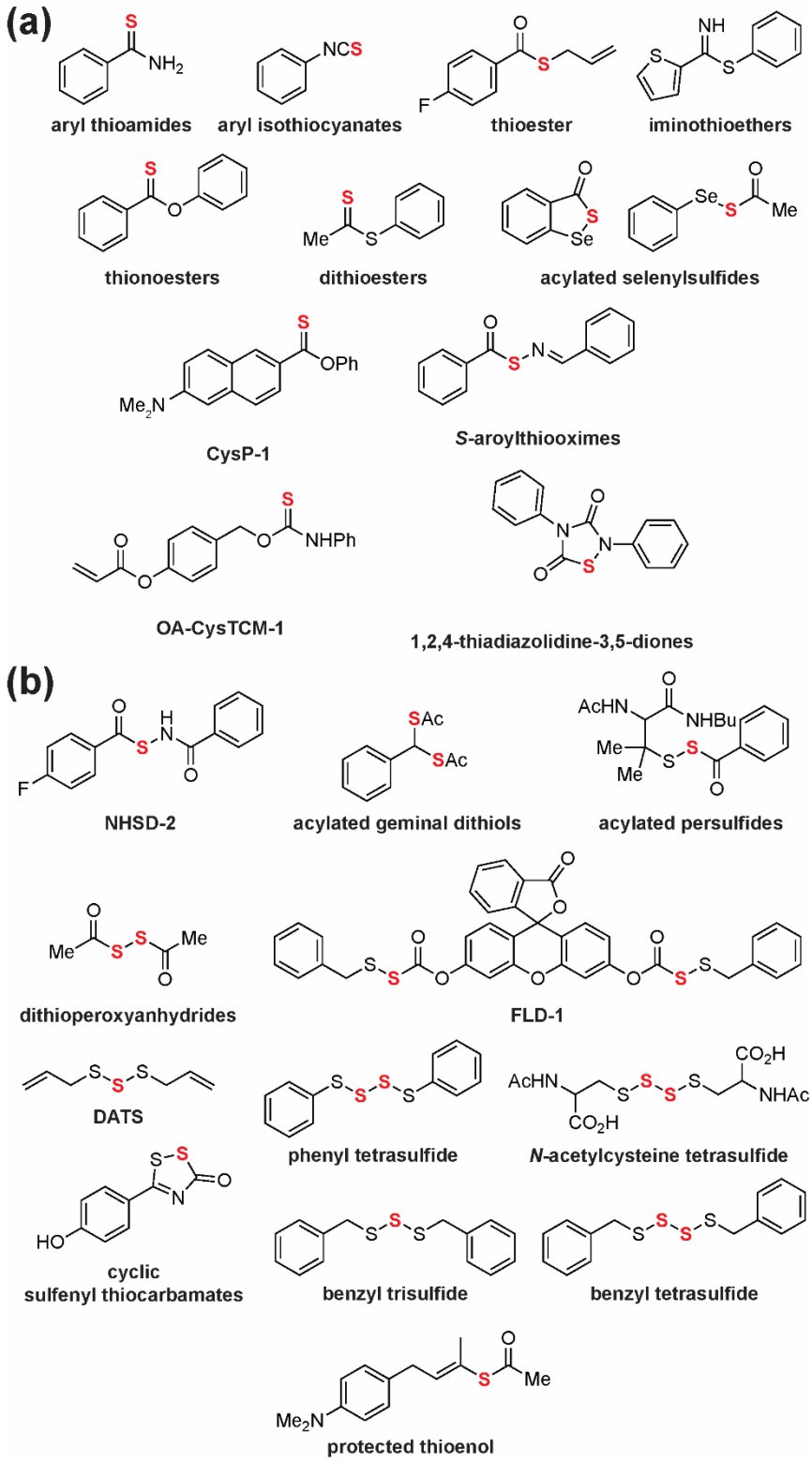

Figure 2.3 Structures of donor compounds activated in the presence of biological thiols. (a) H_2S donors activated in the presence of cysteine. (b) H_2S donors activated in the presence of cysteine and GSH

Inspired by the unique reactivity of S-N motifs present in *S*-nitrosothiols, Xian and co-workers developed a series of compounds termed "*N*-mercapto donors" and demonstrated H_2S release in the presence of cysteine.[64] The mechanism of H_2S release from these donors proceeds through the *N*-acylation of cysteine and generation of cysteine persulfide as the key H_2S-releasing intermediate. This class of donors was later expanded on in the development of **NHSD-2**, which exhibited significant cardioprotective effects in a murine model of myocardial-ischemia reperfusion injury.[65] Also leveraging the generation of intermediate persulfide motifs, Xian and co-workers investigated the use of protected cysteine and penicillamine persulfide derivatives as H_2S donors in the presence of cysteine and GSH.[66] These compounds function by initial attack on the donor by cysteine to generate a cysteine persulfide, which undergoes subsequent reaction with thiols to generate H_2S. These donors also provided H_2S-related protection against in vivo murine models of myocardial ischemia reperfusion injury. Matson and co-workers reported the related *S*-aroylthiooxime class of compounds, which release H_2S in the presence of cysteine and can be tuned predictably by simple electronic modulation.[67] H_2S release from these compounds likely proceeds by initial attack by cysteine on the donor to release an iminothiol intermediate, which further reacts with cysteine to generate a cysteine persulfide intermediate en route to H_2S release. More recently, the intermediate persulfide generation from S-X hybrid systems was further leveraged by Xian and co-workers to develop a series of cyclic[68] and acyclic sulfur-selenium compounds,[69] which generate H_2S-releasing persulfides and analogous selenylsulfides (RSeSH) in the presence of cysteine. In an alternative approach, Galardon and co-workers reported that dithioperoxyanhydrides also function as H_2S donors through the intermediate generation

of persulfides in the presence of GSH and cysteine.[70] These compounds were demonstrated to induce vasorelaxation in isolated rat aortic rings. In general, the use of persulfides as H_2S-releasing species has been of particular interest because a number of H_2S signaling mechanisms involve persulfidation of cysteine residues. In parallel to these developments, different methods of direct persulfide generation in water are of significant interest and advances have been recently reviewed.[71]

An often overlooked yet uncontrolled method of generating H_2S from persulfide intermediates is by treatment of organic polysulfides with thiols.[72] The most widely used organic polysulfide, diallyl trisulfide (**DATS**), is a simple organosulfur compound readily isolated from alliums including garlic.[73] In the presence of thiols, **DATS** is reduced to generate allyl persulfide, which is further reduced by thiols to generate H_2S. We note that although diallyl disulfide (**DADS**) is often used in the literature as an H_2S donor, its apparent H_2S-releasing activity has been demonstrated to be a result of a **DATS** impurities.[74] Both experimental and computational results support the lack of direct H_2S release from **DADS** in the presence of thiols, except for a minor, slow pathway involving attack at the □-carbon by a thiol to generate an allyl persulfide intermediate.[75] Consistent with this slow release, the generation of H_2S from thioester donors reported by Xu and co-workers is likely due to the intermediate release of allyl thiol and subsequent oxidation to form **DADS**, which results in slow H_2S donation.[76] Expanding investigations into H_2S from organic polysulfides, our group recently reported *bis*(aryl)- and *bis*(alkyl)-tetrasulfides as H_2S donors and demonstrated that tetrasulfides release more H_2S than trisulfides, as expected.[77] In comparing a series of benzyl di-, tri-, and tetra-sulfides,[78] we confirmed cysteine and GSH mediated H_2S release occurs exclusively from dibenzyl

trisulfide and dibenzyl tetrasulfide, which is consistent with the presence of sulfane sulfur.[79] A related study by Quinn and co-workers highlighted the efficient release of H_2S from polysulfide-based donors built around polyethylene glycol / trisulfide / cholesterol conjugates that assemble into supramolecular macrostructures.[80]

COS-based H_2S donors that are activated by thiols have also been reported. In 2018, we reported a small library of sulfenyl thiocarbonate motifs including **FLD-1** that undergoes thiol-mediated decomposition to generate COS.[81] By using a fluorophore as a payload released upon COS/H_2S donation, these donors provide a fluorescent response that correlates linearly with COS/H_2S release and allows for spatiotemporal resolution of cellular COS/H_2S release in live cell imaging. We also reported cysteine-selective COS-based H_2S donors, such as **OA-CysTCM-1**, which utilized a cysteine-mediated cyclization to activate a self-immolative donor motif.[82] A large library of 1,2,4-thiadiazolidine-3,5-diones was reported by Caliendo and co-workers that was demonstrated to release H_2S in the presence of cysteine. We note the proposed mechanism of donor activation in this system proceeds through an anionic thiocarbamate intermediate, which likely results in the direct release of COS with concomitant hydrolysis to H_2S.[83] COS-based H_2S donors are discussed more in depth in Chapter 2.6.

2.4 Photoactivated Donors

The ability to control H_2S donation using external bio-orthogonal stimuli that selectively activate the desired compound in the presence of diverse biological functional groups, is a powerful method that has garnered significant interest. Of such strategies, photoactivatable donors offer the potential for high spatiotemporal control of H_2S release

(Figure 2.4). Photocaged species react upon exposure to specific wavelengths of light to cleave a protecting group and reveal, in these cases, an H_2S-releasing moiety. This approach allows for non-invasive triggering of H_2S release in cells *in vitro* and the potential for photo-triggering on skin or at shallow sub-cutaneous levels.[84-85] The first photoactivated H_2S donor **Photo-gem-dithiol** was reported by Xian and co-workers in 2013, in which a *bis*-orthonitrobenzyl protected geminal-dithiol undergoes a Norrish type II rearrangement upon irradiation (λ_{irr} = 365 nm) to unmask an unstable gem-dithiol intermediate that is subsequently hydrolyzed to release H_2S.[86] Sulfide release was confirmed using the methylene blue assay, as well as through fluorescence imaging with HeLa cells. Moreover, these donors displayed pH-dependent H_2S release, consistent with other donors involving hydrolysis of gem-dithiols, an acid-mediated process. Similar photocleavable gem-dithiol scaffolds (λ_{irr} = 365 nm) have since been incorporated into water-soluble polymers and block copolymer nanoparticles,[87-88] as well as upconverting nanoparticles, which absorb low energy near-IR (NIR) light (λ_{irr} = 980 nm) and emit UV to visible light, that can trigger H_2S release.[89]

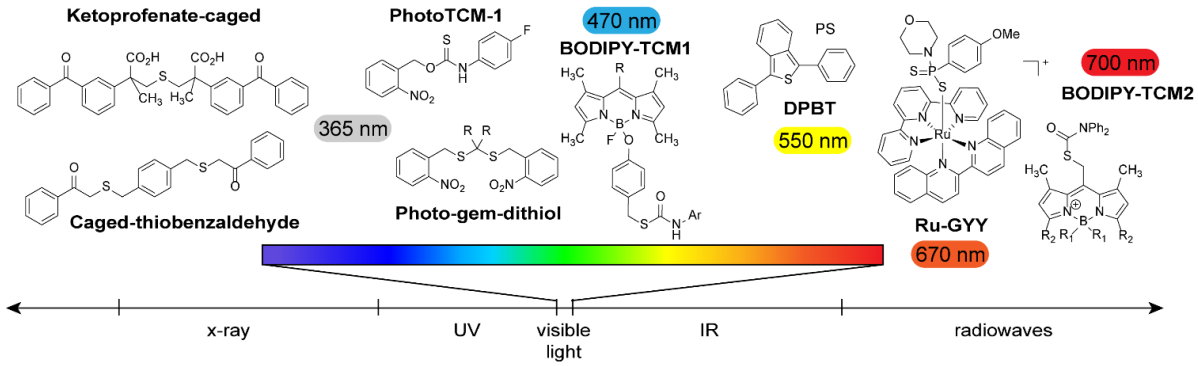

Figure 2.4 Structures and excitation wavelengths of selected photoactivable H_2S donors. PS indicates photosensitizer. IR, infrared; UV, ultraviolet.

An alternative photocontrollable H_2S donor was reported by Nakagawa and co-workers, which centers around a functionalized thioether that releases H_2S directly after photocleavage of the protecting groups, rather than relying on a subsequent hydrolysis step. Initially employing 2-nitrobenzyl photoactivatable groups, this approach was expanded to incorporate **ketoprofenate photocages** to avoid the production of the potentially-deleterious 2-nitrosobenzaldehyde byproduct.[90] These donors were further adapted to function by photoexcitation (λ_{irr} = 325-385 nm) of xanthone chromophores.[91] **Photocaged thiobenzaldehydes** have also been used as light-activated H_2S donors. In these systems, irradiation (λ_{irr} = 355 nm) reveals a thiobenzaldehyde intermediate that requires a subsequent nucleophilic attack by an amine to liberate the H_2S.[92] Such donors have been incorporated into both water-soluble H_2S releasing polymers and hydrogels. One benefit of this approach is that the byproduct of photolysis is simply acetophenone, which is a benign and FDA-approved excipient.

Expanding to visible light photoexcitation, You and co-workers harnessed the photogeneration of singlet oxygen to trigger H_2S release. Photoirradiation (λ_{irr} = 500-550 nm) of a photosensitizer in the presence of ambient oxygen and 1,3-diphenylisobenzothiophene (**DPBT**) generated an unstable endoperoxide intermediate, which undergoes rapid fragmentation to generate 2-benzoylbenzophenone and H_2S.[93] This system was incorporated into artificial vesicles or polymersomes, which enabled H_2S generation in water. An interesting advantage of this system is that the photoirradiation wavelengths are dictated by the choice of photosensitizer rather than the donor itself, which allows for a broad range of wavelengths to be used (λ_{ex} = 380 – 550 nm demonstrated).

In a hybrid system, Wilson and co-workers reported a red-light activated complex of GYY-4137 and a common ruthenium photocage (**Ru-GYY**), that releases H_2S upon irradiation (λ_{irr} = 626 nm).[94] Interestingly, although GYY-4137 is known to spontaneously hydrolyze in aqueous systems, complexation to the ruthenium metal center suppresses this H_2S release. The authors were thus able to demonstrate controlled H_2S release from this donor, as well as its activity against a model of ischemia-reperfusion injury in H9c2 heart myoblast cells. The Singh lab recently reported a novel optical-readout based phototriggered H_2S donor. Harnessing Excited-State Intramolecular Proton Transfer (ESIPT), which had been previously applied to monitoring nitric oxide donation[95] among other analytes, they developed a *p*-hydroxyphenacyl triggered donor that releases H_2S under irradiation (λ_{irr} = 410 nm), while simultaneously shifting the fluorescence of the donor.[96] This change in fluorescence allowed for H_2S release to be monitored, and was demonstrated to function in HeLa cells.

A number of photoactivatable COS-based H_2S donors have also been reported. In 2017, our group reported the first light-activated COS-based H_2S donor, **PhotoTCM-1**, in which an *o*-nitrobenzyl protecting group masked a caged thiocarbamate, which was cleaved upon irradiation (λ_{irr} = 365 nm) to release COS.[97] COS-based photolabile H_2S donors are discussed in Chapter 2.6.

2.5 Enzyme-Activated Donors

Because H_2S has a myriad of biological targets, disentangling the effects of sulfide delivery in specific environments can be challenging. One approach to overcome this difficulty is to incorporate an enzymatically cleaved trigger on a sulfide donor. This

approach allows for donors to be developed that are stable until the activating group is cleaved or modified by the target enzyme to release H_2S or an H_2S equivalent, such as COS. This strategy has the benefit of being readily tuned to specific triggering groups and enzyme pairs. In addition, utilizing an enzyme to carry out the donor activation event does not consume cellular nucleophiles or thiols, which could otherwise perturb the redox balance of related reactive sulfur species – an inherent challenge with many thiol-triggered H_2S donors.

The first enzyme-triggered H_2S donor, **HP-101**, was reported by Binghe Wang and co-workers in 2016 (Figure 2.5). In this system, esterase-mediated cleavage of an acyl protecting group on the donor motif was used to generate an unstable phenolic intermediate that subsequently underwent an intramolecular lactonization with a pendant thioacid to release H_2S.[98] Esterases are expressed in most tissue types and are involved in the activation or metabolism of approximately 10% of drugs (Figure 2.5b).[99] One benefit of this design is that the rate of H_2S release could be tuned by varying the identity of the ester triggering group or by modifying the geminal-dimethyl substitution in the "trimethyl lock" backbone to facilitate lactonization. Notably, Wang and co-workers were able to conjugate this sulfide-donating scaffold to the non-steroidal anti-inflammatory drug (NSAID) naproxen, forming an activatable H_2S-drug hybrid.

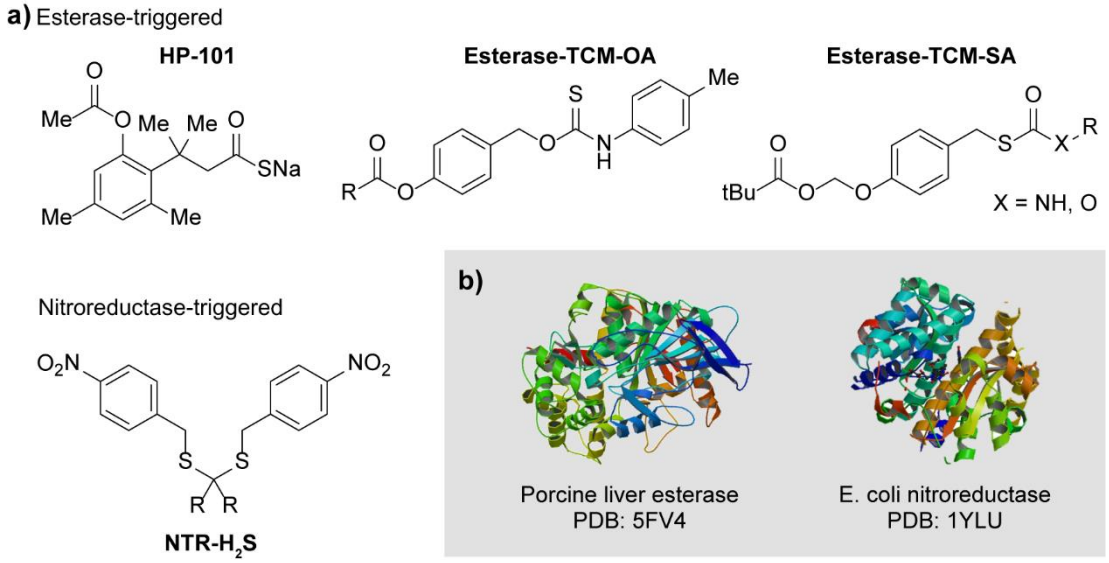

Figure 2.5 Enzyme-activated donors and associated enzymes. (a) Structures of enzymatically triggered COS and H_2S donors. (b) Structures of PLE and *Escherichia coli* NTR.

Chakrapani and co-workers further expanded work on enzyme-triggered donor platforms to develop donors activated by bacterial nitroreductase (NTR) (Figure 2.5b). NTRs are frequently found in bacteria and are also upregulated under hypoxic conditions in different cell types.[100-101] The NTR-mediated reduction of the electron-withdrawing nitro groups on **NTR-H_2S** to the corresponding aniline, with the nitrogen lone pair now free to resonate through to release the iminoquinone methide was used to reveal a geminal-dithiol intermediate that hydrolyzes in buffer to generate H_2S (Figure 2.5a). H_2S release was confirmed and measured in these systems using monobromobimane and fluorescence assays. These donors have been used to study the role of H_2S in the intracellular redox balance and development of antibiotic resistance in bacteria, specifically E. coli.[102]

In 2017, both Chakrapani and co-workers and our group independently reported esterase-activated donors that functioned through the intermediacy of COS release. In these approaches, self-immolative thiocarbamates or thiocarbamates functionalized with ester motifs were enzymatically activated to release COS, which is rapidly metabolized to H_2S by CA, rather than H_2S directly. These and other COS-releasing donors will be discussed further in Chapter 2.6.[103-104]

2.6 COS-Releasing H_2S Donors

As an alternative approach to previously reported donors that release H_2S directly, we were inspired by the conversion of carbonyl sulfide (COS) by carbonic anhydrase (CA) to H_2S.[105] COS is the most abundant sulfur-containing gas in Earth's atmosphere, and we as well as others have recently leveraged COS as vehicle for H_2S delivery.[106] Currently, enzymatic pathways for the mammalian biosynthesis of COS have not been identified, but a number of different metalloenzymes that can convert COS to H_2S, most notably, the ubiquitous mammalian enzyme CA. A primary physiological role of CA is regulation of blood pH by conversion of CO_2 to bicarbonate (K_{cat}/K_M = 8 x 10^7 M^{-1} s^{-1} for bovine CA-II), but as a relatively promiscuous enzyme, CA can also metabolize COS to H_2S and CO_2, with high catalytic efficiency (K_{cat}/K_M = 2.2 x 10^4 M^{-1} s^{-1} for bovine CA-II).[107-110]

In 2016, we reported a new approach to access H_2S donors by leveraging the efficient hydrolysis of COS to H_2S by CA.[111] We drew inspiration from the widely-employed strategy of using triggerable self-immolative carbamates to deliver a payload in response different stimuli (Figure 2.6a). Because such scaffolds extrude CO_2 as a

byproduct of the self-immolative decomposition, we reasoned that replacing the carbamate core with a thiocarbamate would result in COS release. In this design, the caged-thiocarbamates can be engineered to respond to specific biologically-relevant stimuli to deliver COS, which in turn is rapidly converted to H_2S by CA (Figure 2.6b,c).

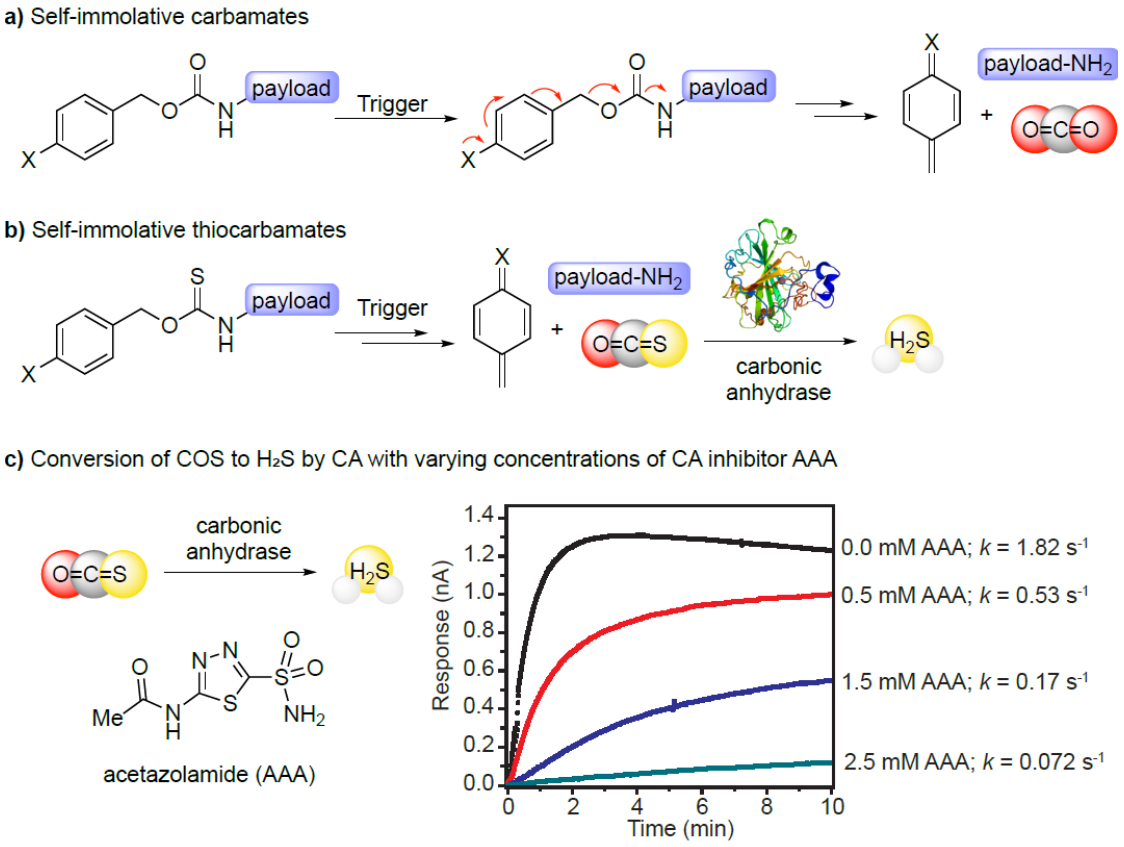

Figure 2.6 (a) Design and mechanism of self-immolative carbamates and (b) self-immolative thiocarbamates. (c) Conversion of COS to H_2S by CA in the presence of acetazolamide at varying concentrations measured by a sulfide-selective electrode.

The high modularity of this scaffold allows for a "plug and play" approach to H_2S donor design, in which both the trigger and the payload can be readily modified to accomplish different goals (Figure 2.7a). Importantly, the analogous carbamates, which release CO_2 rather than COS, serve as key H_2S-depleted control compounds that can help to separate the effects of the organic byproducts from that of COS/H_2S release.

Additionally, the triggerless control, which maintains the thiocarbamate core but lacks the self-immolative triggering group, provides an additional control compound that helps to account for any effects observed as a result of the thiocarbamate moiety. In our first application of this general design, we reported self-immolative thiocarbamates in the development of the first analyte-replacement COS/H_2S fluorescent probe (Figure 2.7b). With an azide as the triggering group and methyl rhodol as the payload, treatment with NaSH yielded both COS/H_2S release and a fluorescent turn-on response.[111] Importantly, this design provided a first step toward addressing the common challenge of analyte consumption in activity-based systems. We have since expanded the strategy of triggered COS/H_2S release to encompass a wide range of triggering events and stimuli (Figure 2.7c).

Stimuli Responsive COS-based H_2S Donors

In an early application of stimulus-responsive COS/H_2S donors, we developed systems in which a boronate ester, which is converted to a phenol by ROS, was used as the trigger (Figure 2.8a).[112] This system combined the known role of boronate esters as ROS scavengers with the cytoprotective effects of H_2S to access enhanced cytoprotection against ROS. Using an H_2S-selective electrode, we demonstrated the hydrogen peroxide (H_2O_2)-dependent release of COS/H_2S from the thiocarbamate, but not from carbamate or triggerless control compounds, in the presence of CA. We also established the ability of these ROS-activated donors to release COS/H_2S in live cell environments. For example, treatment of HeLa cells incubated with an H_2S-selective fluorescent probe and the ROS-

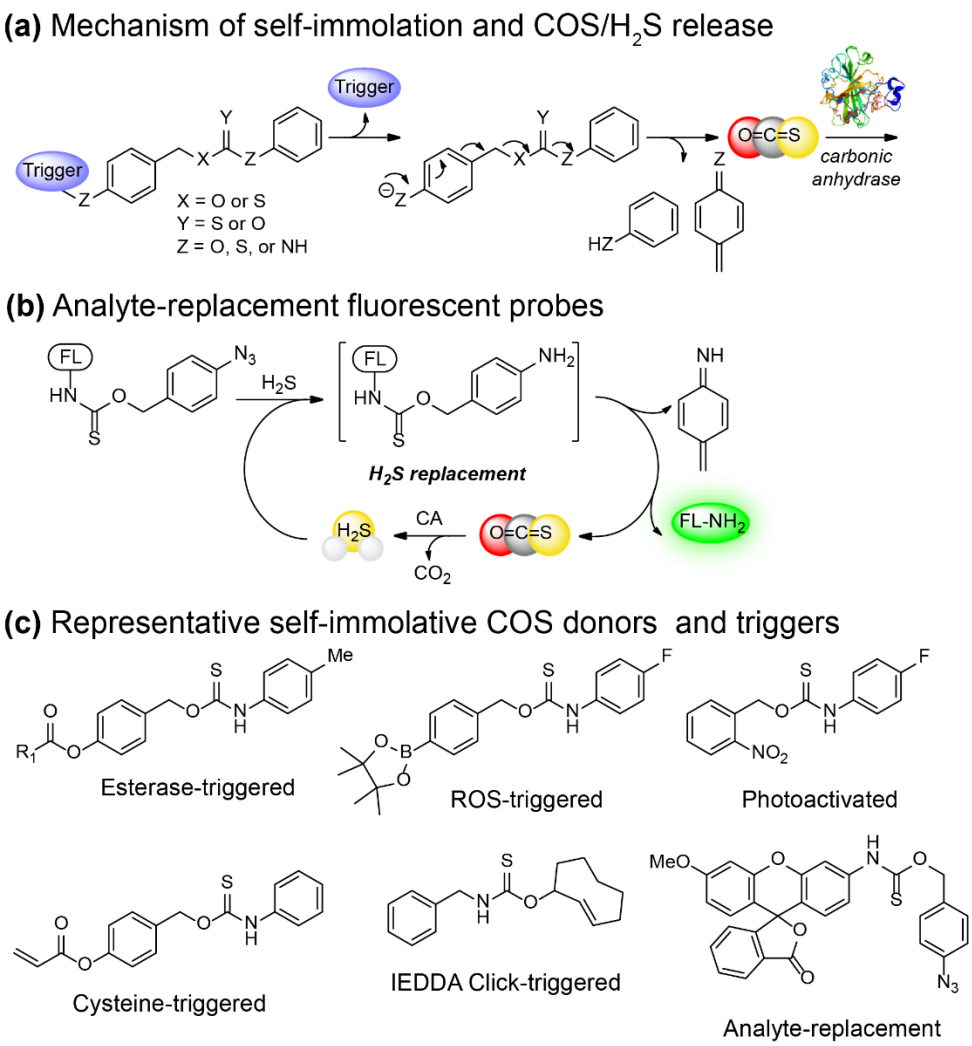

Figure 2.7 (a) Mechanism of self-immolation and subsequent conversion of COS to H_2S by CA. (b) Development of analyte-replacement fluorescent probes. (c) Current examples self-immolation-based COS/H_2S donors reported to date by our lab.

activated donor exhibited an H_2S-derived fluorescence response when treated with exogenous H_2O_2. Similarly, endogenous levels ROS produced by stimulation with phorbol myristate acetate (PMA) could also trigger COS/H_2S release from the donors, as demonstrated in RAW 264.7 cells. Moreover, the thiocarbamate donors showed significant cytoprotective effects against exogenous H_2O_2 in HeLa cells. The carbamate control compound also proved slightly cytoprotective, although to a much lesser extent

than the sulfide-releasing donors (Figure 2.8b), which was likely due to partial H_2O_2 consumption by the boronate trigger. These results highlight the benefit of having key control compounds to fully disentangle the observed biological effects of the release H_2S from that of other donor components or byproducts. A further systematic study of analogous boronate-containing molecules with variable COS-releasing motifs, including *O*- and *S*-alkyl thiocarbamates, *O*- and *S*-alkyl thiocarbonates, and dithiocarbonates, demonstrated the broad applicability and tunability of this platform in triggerable COS/H_2S delivery.[113]

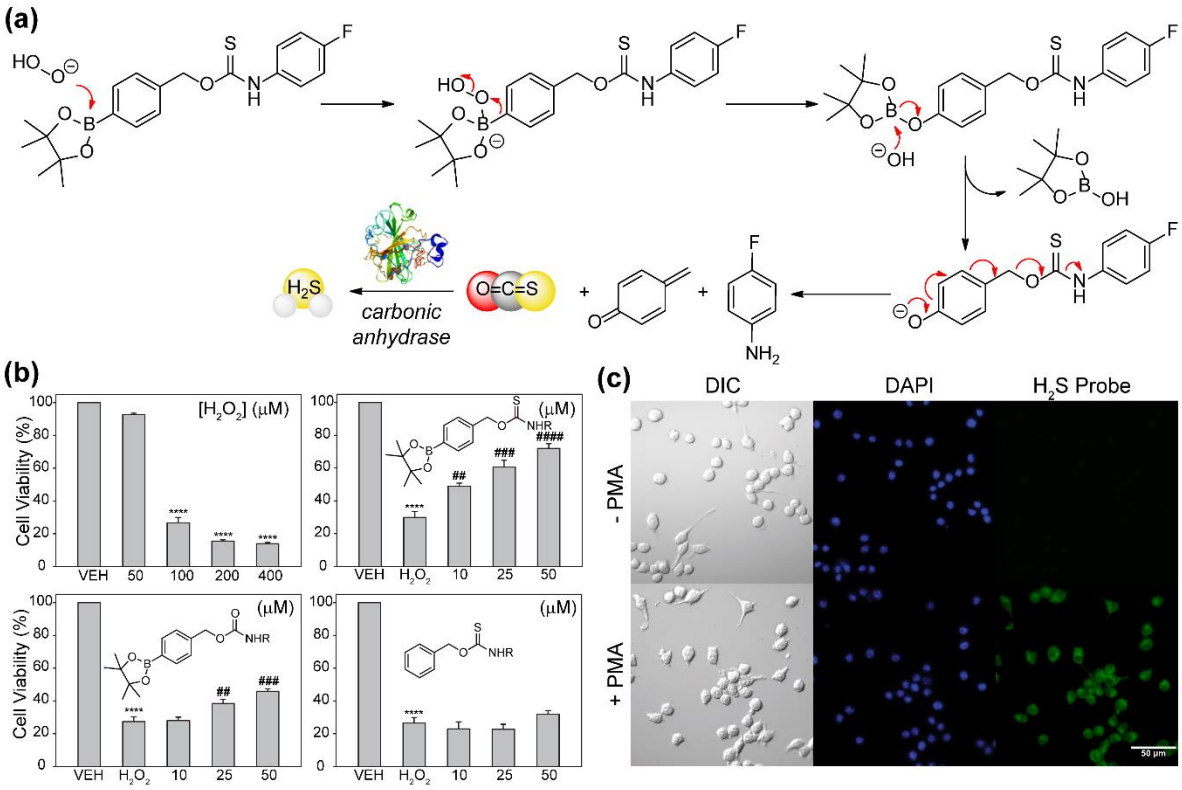

Figure 2.8 (a) Representative reaction scheme and mechanism for H_2O_2-triggered COS/H_2S release. (b) Cytotoxicity of Bpin-triggered thiocarbamate donor, Bpin-triggered carbamate control, and triggerless thiocarbamate control. (c) Imaging ROS-scavenging upon stimulation with PMA in RAW 264.7 cells.

The self-immolative thiocarbamate COS donor scaffold has also been used in common bio-orthogonal activation mechanisms, such as photoactivation. In proof-of-concept studies, we reported the first light-activated COS/H_2S donor equipped with a photocleavable *o*-nitrobenzyl group. Upon irradiation (λ = 365 nm), the benzyl alcohol is cleaved *via* a Norrish type II mechanism, revealing one equivalent of COS and an aniline payload (Figure 2.9). The rate of H_2S release from this system was found to increase with the addition of electron-donating methoxy substituents on the *o*-nitrobenzyl group consistent with previous findings.[97] Building from this work, light-triggered COS release has also been recently reported using BODIPY-derived photolabile groups.[114-115]

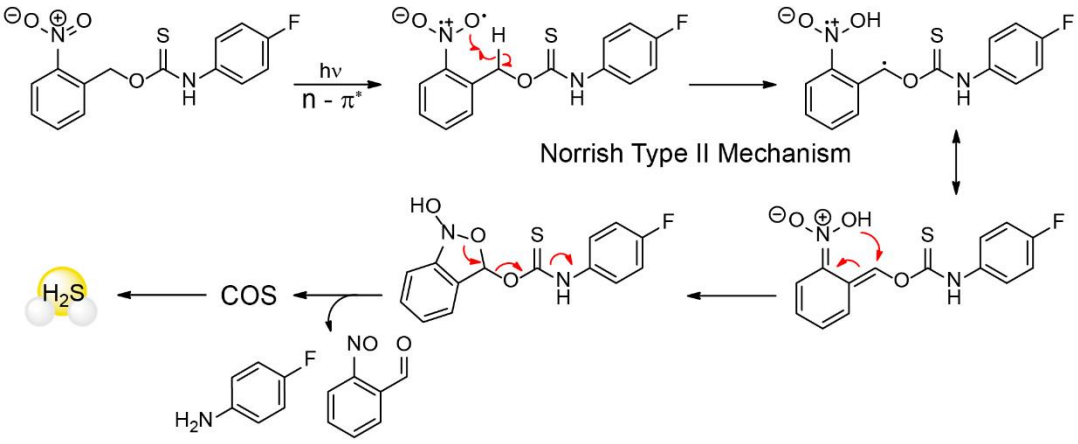

Figure 2.9 Mechanism of self-immolation from photocleavable thiocarbamate COS/H_2S donors.

In vivo, H_2S is produced primarily through cysteine catabolism. In an effort to better mimic the conditions of endogenous H_2S production, we applied the established chemistry of the Strongin ligation to prepare a cysteine-selective COS/H_2S donor. (Figure 2.10) The mechanism of COS release proceeds through nucleophilic attack by cysteine into an acrylate, followed by subsequent cyclization by the pendant amine, and finally in

elimination to uncage the thiocarbamate moiety. Due to the requirement of a nearby amine in the mechanism, this donor has an inherent selectivity towards cysteine over other biological thiols including reduced glutathione (GSH). The sulfide release of this donor was shown in bEnd.3 cells using an H_2S-selective fluorescent probe.[82]

One limitation of many triggerable donor scaffolds is the consumption of biological nucleophiles to initiate release of the desired product, thus perturbing the cellular homeostasis. We envisioned using an enzymatically-triggered reaction as a potential solution, thus enabling activation without depleting the levels of cellular nucleophiles.[103-104] By appending a small ester to the 4-hydroxybenzyl alcohol core,

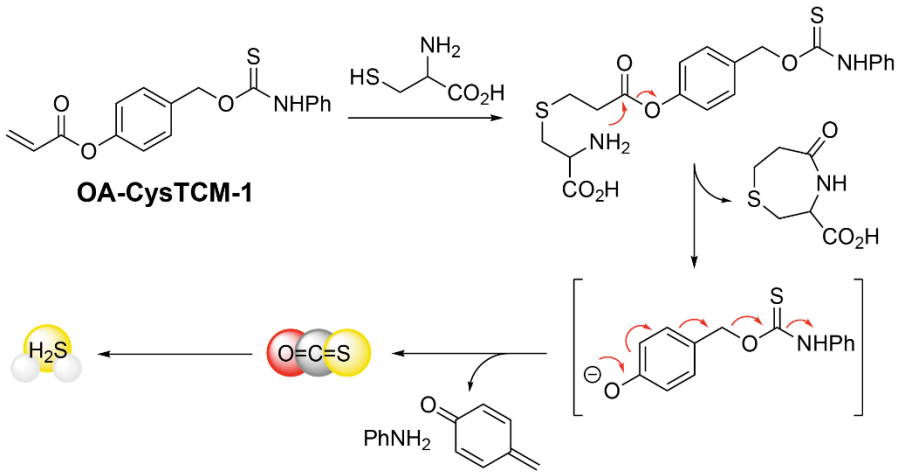

Figure 2.10 Mechanism of COS-release from OA-CysTCM-1 in the presence of cysteine with subsequent hydrolysis of COS to H_2S by carbonic anhydrase.

exposure to intracellular esterases should reveal the corresponding phenolate, which undergoes the same 1,6-self-immolative cascade to generate COS (Figure 2.11a). Employing a thiocarbamate with a *t*-butyl ester trigger and a *p*-tolyl payload yielded fast COS/H_2S donors as determined by a H_2S-selective electrode in the presence of porcine liver esterase (PLE). Further studies revealed that this donor led to almost complete cell

death even at the low concentration of 10 µM in BEAS2B, whereas neither the triggerless or H_2S-depleted control compounds showed any toxicity at those concentrations. Additionally, neither GYY4137 or AP39, two commonly used H_2S donors were toxic at these levels. Most surprisingly, the thiocarbamate was much more cytotoxic than Na_2S, which is often described to be toxic due to the immediate bolus of H_2S released under physiological conditions (Figure 2.11b). These results highlight the crucial need for adequate control compounds to delineate observed activities of COS/H_2S from those attributable to organic byproducts of donor activation.[104]

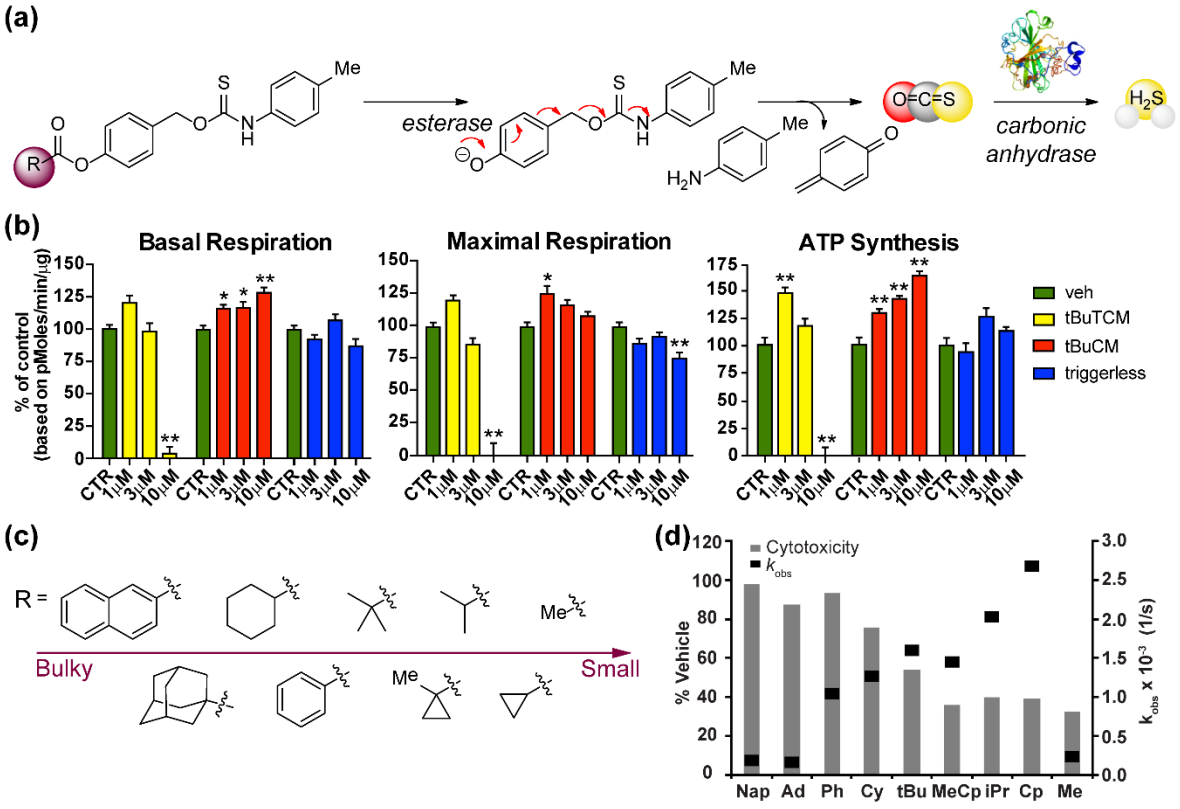

Figure 2.11 Altered cytotoxicity via steric modulation for esterase-triggered COS/H_2S donors. (a) Mechanism of self-immolation of esterase-triggered COS donors. (b) Inhibition of mitochondrial bioenergetics with the tert-Butyl triggered COS donor in BEAS2B cells. (c) Library of different ester size thiocarbamates prepared. (d) The relationship between COS release rate and observed cytotoxicity at 100 µM in HeLa cells for a library of different esterase-triggered COS donors of varying ester size.

The unique toxicity profile of the *t*-butyl ester thiocarbamate led us to hypothesize that either the specific subcellular localization of the compound caused cell death, or that a build-up of COS itself directly inhibited mitochondrial bioenergetics. To investigate the latter hypothesis, we prepared a series of esterase-triggered COS donors equipped with esters of varying sizes (Figure 2.11c).[116] The rate of small ester cleavage by esterases is likely faster than the rate of COS hydrolysis by CA (up to 5.8×10^5 M^{-1} s^{-1} compared to 2.2×10^4 M^{-1} s^{-1} for bovine CA II), which could lead to a potentially toxic buildup of COS in the cell.[108] Changing the size of an ester significantly changes the rate of cleavage by esterases, and we proposed that donors with small esters would exhibit high levels of cytotoxicity, whereas those with bulkier groups would have little effect on cell viability.[117] Consistent with this hypothesis, we demonstrated that the rate of ester hydrolysis directly correlates with the observed cytotoxicity in HeLa cells, supporting the idea that COS may function as more than a simple H_2S shuttle (Figure 2.11d). Despite the toxicity of the small ester donors, this report outlined a suite of COS donors with tunable rates of release, the utility of which was highlighted with fluorescent cell-imaging of the cyclohexyl ester thiocarbamate.[116] This research is discussed in depth in Chapter III. A similar series of *S*-alkyl thiocarbamate esterase-triggered COS donors were reported by the Chakrapani group, which display comparable toxicity at 50 μM in human breast cancer MCF-7 cells, however rates of H_2S release were found to be slightly slower.[103]

One challenge associated with the 1,6-self-immolative thiocarbamate scaffold is the release of an electrophilic para-quinone methide. As one approach to address this limitation, and also to demonstrate the compatibility of our approach with common biorthogonal chemistry, we developed a “click-and-release” donor, in which COS release

is triggered through an inverse-electron demand Diels Alder reaction (IEDDA) with a *trans*-cyclooctene moiety fused to a thiocarbamate (Figure 2.12). Experiments with both bovine and sheep plasma and blood proved that endogenous levels of CA are sufficient for the hydrolysis of the released COS to H_2S.[118]

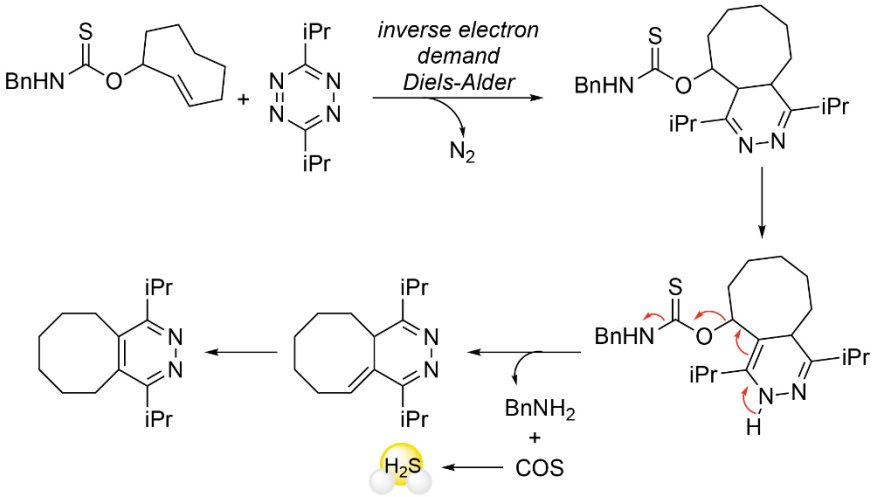

Figure 2.12 Mechanism of 'click-and-release' biorthogonal COS donor.

COS-based H_2S Donors with Optical Readouts

To assess the validity of our donors *in vitro*, we utilize spectrophotometric methods of H_2S detection such as the methylene blue assay.[119] In cells, the use of H_2S-selective fluorescent probes[120-122] consumes the generated H_2S and interferes with our ability to fully observe the effect of H_2S production on cells. To prevent this undesired analyte consumption, we envisioned coupling a spectroscopic response to COS/H_2S release by appending a COS-releasing moiety to a chromophore which would generate a spectroscopic signal concomitantly with the release of COS. This class of donors provides novel chemical tools to visualize COS/H_2S release by UV/Vis or fluorescence

spectroscopy and allows us to minimize the number of external components needed to visualize H_2S release in complex biological systems.

In our initial approach, we designed an analogous self-immolation scaffold which undergoes *β*-elimination at physiological pH to generate methyl vinyl ketone, COS, and release an amine-based payload (Figure 2.13a).[123] The use of *p*-nitroaniline (PNA) as the payload allows for optical monitoring of H_2S release from **γ-KetoTCM1** by measuring the UV/Vis absorbance of PNA (λ_{max} = 381 nm) (Figure 2.13b). Importantly, UV-Vis spectroscopy showed that PNA formation correlated directly with H_2S generation measured using the methylene blue assay, which confirmed that the optical response can be used as a direct proxy for H_2S release (Figure 2.13c).

The incorporation of a spectroscopic handle also allowed us to conduct a series of kinetic experiments to probe the effect of pH on COS/H_2S release from this donor by UV/Vis spectroscopy. At physiological pH, this donor releases H_2S slowly over 30 h with a measured pseudo-first order rate constant (k_{obs}) of 4.52(2) x10^{-5} s^{-1}. The rate of H_2S release from this donor can be tuned as a function of pH, and the observed rates of H_2S release in basic solutions (pH 8.0, k_{obs} = 12.6(2) x10^{-5} s^{-1}) consistent with a mechanism of *β*-elimination. Additionally, we were able to decrease the rate of H_2S release by installing a methyl group at the *α*-position resulting in modulation of the *α*-proton acidity. The addition of bovine serum albumin (5 mg/mL) led to a significant increase in the rate of H_2S release at pH 7.4 (k_{obs} = 81(3) x10^{-5} s^{-1}) suggesting that this donor could function in complex biological environments and benefit from protein microenvironments. In further support of biological combability, the addition of biological nucleophiles including cysteine, GSH, and lysine did not impact H_2S release. Moreover, H_2S release from **γ-**

KetoTCM1 was observed in HeLa cells, as evidenced by the fluorescence response from an H_2S-responsive probe.

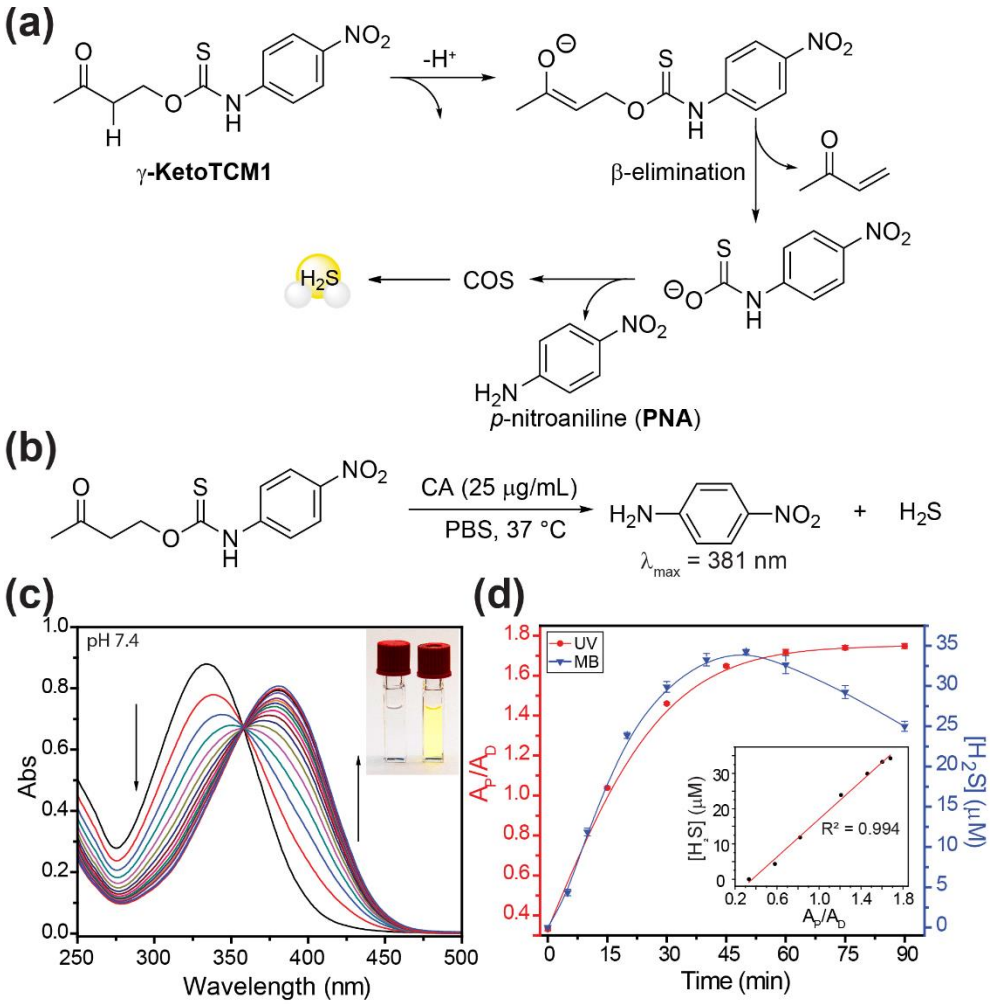

Figure 2.13 (a) Mechanism of COS/H_2S release from γ-KetoTCM1. (b) Conditions for measuring H_2S release from γ-KetoTCM1. (c) Measurement of PNA formation over time by UV/vis spectroscopy. (d) Correlation between measured [H_2S] and PNA formation by the methylene blue assay and UV/vis spectroscopy.

To improve optical signal to be more compatible with biological samples, we also developed fluorescent turn-on donors that become fluorescent after release of COS/H_2S. To accomplish this goal, we relied on the reactivity of sulfenyl thiocarbonates towards thiols to generate a disulfide, COS, and alcohol-based payload (Figure 2.14a). By a simple, one-step procedure, we prepared a small library of fluorescein-caged sulfenyl thiocarbonates to serve as fluorescent, COS-based H_2S donors with **FLD-1** serving as the model fluorescent donor (Figure 2.14b).[81] The addition of excess cysteine (100 μM) to 10 μM **FLD-1** in the presence of carbonic anhydrase at pH 7.4 resulted in a fluorescent enhancement of over 500-fold consistent with the formation of fluorescein upon consumption of the donor motif (Figure 2.14c). Using a monofunctionalized sulfenyl thiocarbonate derivative to simplify the reaction kinetics, we demonstrate the formation of fluorescein monitored by fluorescence spectroscopy can be directly correlated to H_2S release measured by the methylene blue assay and confirms the validity of this approach to prepare fluorescent H_2S/COS donors. The release of H_2S from **FLD-1** was found to occur exclusively in the presence of thiols including cysteine and GSH over other biological nucleophiles including lysine, serine, and H_2O_2. To assess the biological compatibility of **FLD-1**, we examined the activation of this donor by endogenous thiols and concomitant H_2S release by use of 7-azido-4-methylcoumarin (**C7-Az**), an H_2S-selective fluorescent probe in HeLa cells. The treatment of HeLa cells with **FLD-1** (50 μM) resulted in a fluorescent turn-on of **C7-Az** and fluorescent signal corresponding to the formation of fluorescein (Figure 2.14c). An overlay of both channels reveals an even cellular distribution suggesting good uptake of **FLD-1** and confirms the compatibility of this donor in live cells. Taken together, **γ-KetoTCM-1** and **FLD-1** are the first examples

of COS-based H_2S donors with an incorporated optical readout and provide visual chemical tools for probing the biological effects of H_2S.

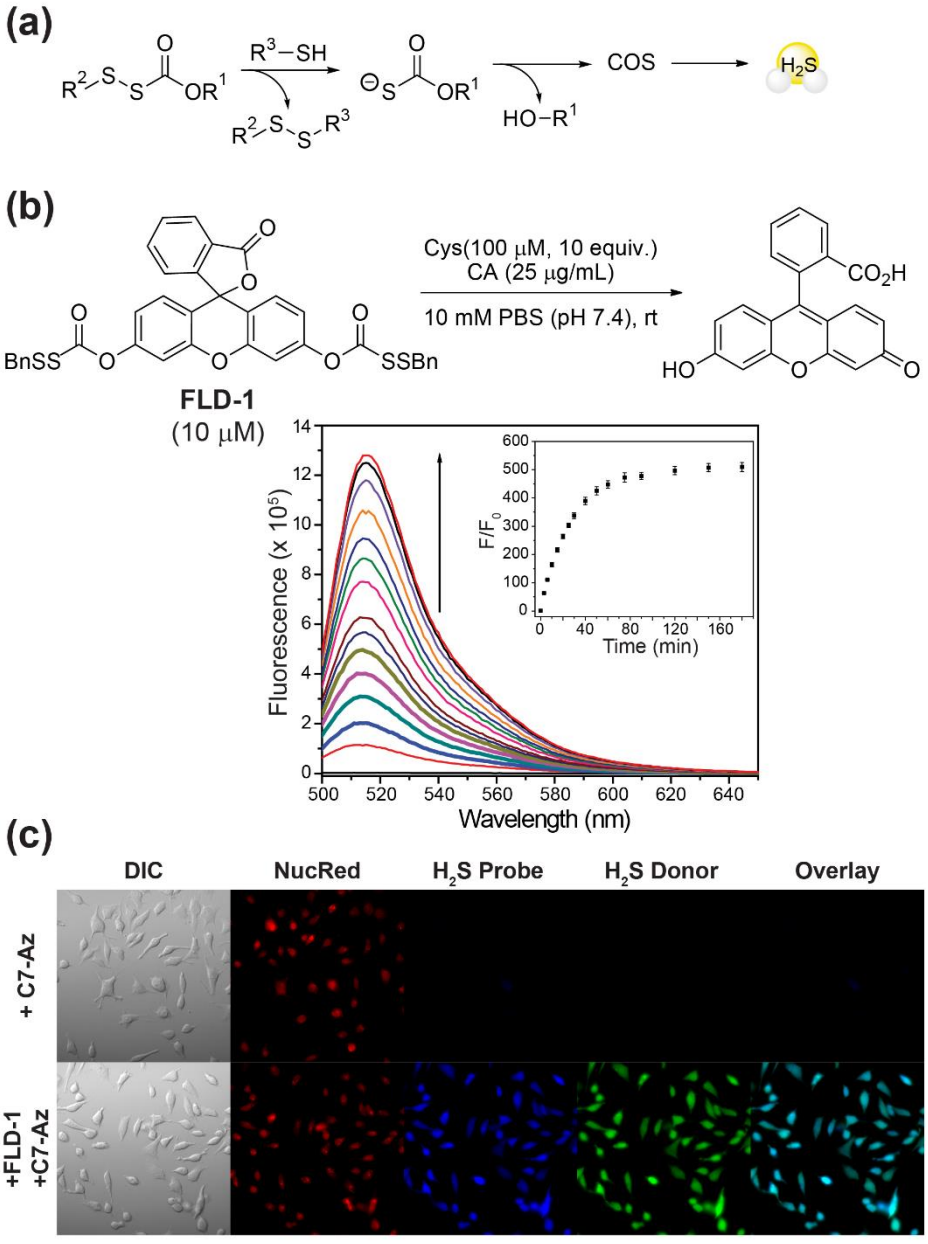

Figure 2.14 (a) Mechanism of thiol-mediated, COS/H_2S release from sulfenyl thiocarbonates. (b) Structure of FLD-1 and release of H_2S from FLD-1 (10 μM) in the presence of cysteine (100 μM, 10 equiv.) in the presence of carbonic anhydrase in 10 mM PBS (pH 7.4) monitored by fluorescence spectroscopy (λ_{ex} = 490 nm, λ_{em} = 500-650 nm). (c) Imaging of cellular H_2S release from FLD-1 (50 μM) in HeLa cells.

2.7 Donor Conclusion and Outlook

The development of activatable small-molecule H_2S donors has been one of the most significant advances in the field of H_2S chemical biology over the past 5 to 10 years. The donors covered in this chapter can collectively be viewed as a toolbox that chemists, biologists, and physiologists can use to probe the chemical biology of H_2S under various conditions and begin to assess the biological impacts of COS. To both further our studies and to advance the field, we envision further investigating the potential roles of COS in sulfur biology, and developing more donors to accomplish this. My efforts towards this are described in Chapters 3-5 of this dissertation.

CHAPTER III

ESTERASE-TRIGGERED SELF-IMMOLATIVE THIOCARBAMATES PROVIDE INSIGHTS INTO COS CYTOTOXICITY

This chapter includes previously published and co-authored material from Levinn, C.M.; Steiger, A.K.; Pluth, M.D. Esterase-Triggered Self-Immolative Thiocarbamates Provide Insights into COS Cytotoxicity. *ACS Chem. Biol.* **2019**, *14* (2), 170-175. This manuscript was written by Carolyn M. Levinn and Dr. Andrea K. Steiger, with editorial assistance by Professor Michael D. Pluth. The project in this chapter was conceived by Carolyn M. Levinn and Andrea K. Steiger, and the experimental work was performed by Carolyn M. Levinn and Andrea K. Steiger.

3.1 Introduction

Hydrogen sulfide (H_2S), the most recent addition to the gasotransmitter family,[1] plays important physiological roles in the cardiovascular,[124] respiratory, as well as other organ systems.[125] Significant interest in both research and therapeutic approaches for H_2S delivery has led to the development of a library of synthetic small molecules that release H_2S (H_2S donors) by using different strategies.[5, 9, 39, 87, 126] In one recently-developed approach, our group, as well as others, has reported H_2S donors based on the triggerable, self-immolative decomposition of thiocarbamates to release carbonyl sulfide (COS), which is rapidly hydrolyzed to H_2S by the ubiquitous mammalian enzyme carbonic anhydrase (CA).[42] This COS-dependent H_2S-releasing strategy is highly tunable and

allows for triggering of H_2S release by a variety of stimuli, including ROS,[127-128] nucleophiles,[129] cysteine,[130] and light.[114-115, 131]

In addition to functioning as a precursor for CA-mediated H_2S release, COS is the most prevalent sulfur-containing gas in Earth's atmosphere and plays important roles in the global sulfur cycle. Despite this significance, few studies have investigated the physiological properties of COS directly.[106] Currently, there are no established mechanisms of eukaryotic COS biosynthesis, although it has been shown that acetylcholine stimulation of porcine coronary artery (PCA) leads to an observed increase in COS, indicating that muscarinic acetylcholine receptors could play a role in regulating COS synthesis.[132] Additionally, it has been detected in the headspace of PCA and cardiac muscle,[132] suggesting potential endogenous production. Although simple methods for the direct detection of COS in aqueous solutions are not currently available, COS can be detected through GC-MS analysis or by other spectroscopic methods. Moreover, COS has also been recognized as a potential exhaled breath biomarker for a variety of diseases, including cystic fibrosis[133] as well as liver disease and rejection,[134-135] which suggests a possible role in disease physiology. The consumption of COS by CA is well established and COS toxicity closely resembles that of H_2S, which is likely due to CA-mediated hydrolysis within mucous membranes upon exposure. The rapid conversion of COS to H_2S, with an associated rate constant of 2.2×10^4 $M^{-1}s^{-1}$ (for bovine CA II), makes COS a convenient source of sulfide, but also makes disentangling the chemical biology of COS from H_2S inherently challenging.[136]

We recently reported an esterase-triggered COS-mediated H_2S donor,[104] wherein ester cleavage reveals an intermediate phenol that undergoes a 1,4-self-immolation

cascade to release COS, followed by rapid hydrolysis to H_2S. Contrary to previous reports of similar donors, however, these compounds exhibit significant cytotoxicity and fully inhibited major mitochondrial bioenergetic pathways in bronchial epithelium BEAS2B cells. Similar cytotoxicity profiles were not observed for other H_2S donors, including NaSH, GYY4137, or AP39, at similar concentrations. Furthermore, the analogous CO_2-releasing carbamate control compound was non-cytotoxic, confirming that the observed cytotoxicity or bioenergetics impacts were not due to organic byproducts of donor activation. Taken together, these results led to the hypothesis that the observed effects could be due to a buildup of COS. Supporting this hypothesis, the rate of small ester cleavage by mammalian esterases is likely faster (~$5.1x10^4$ – $5.8x10^5$ $M^{-1}s^{-1}$) than the rate of CA-mediated COS hydrolysis to H_2S,[117, 136] which would result in a buildup of intracellular COS. Here we extend this hypothesis by preparing a library of esterase-cleaved COS-releasing donors in which the steric bulk of the ester and the electronic properties of the aniline payload are modified. We demonstrate that the differential cytotoxicity of these donors maps to the COS release rates, thus furthering the hypothesis that COS may exert different biological effects than H_2S alone (Figure 3.1).

3.2 Results and Discussion

To further investigate whether the cytotoxicity of these esterase-activated COS/H_2S donors could be related to COS directly, we chose to probe the relationship between COS release rates and the corresponding cytotoxicity. We hypothesized that if COS buildup was responsible for the observed cytotoxicity, then esters cleaved more quickly should result in increased cell death, whereas esters cleaved more slowly should

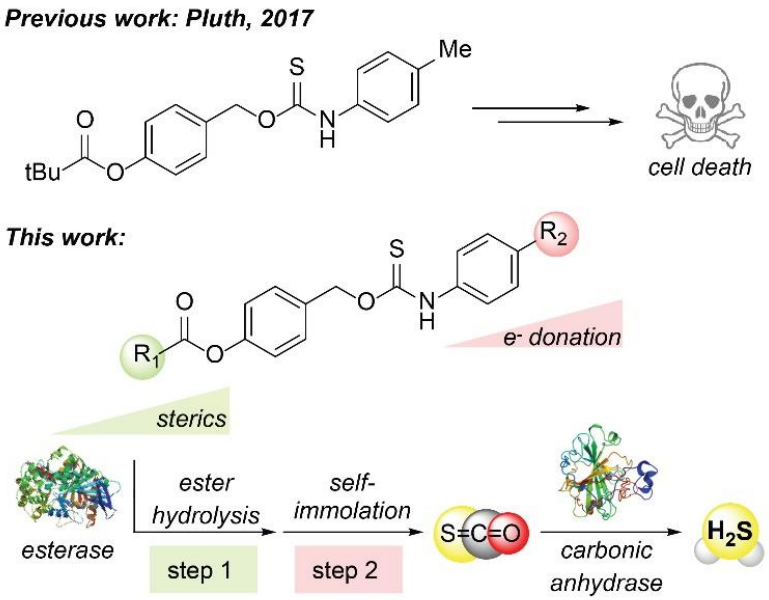

Figure 3.1 Esterase-triggered thiocarbamate-based H_2S donors exhibit increased cytotoxicity, potentially due to the buildup of intracellular COS.

have a diminished effect. In the esterase-activated donors, the rate of COS release depends not only on the rate of ester cleavage ("triggering"), but also on the rate of self-immolative decomposition. There have been a number of reports demonstrating that rate of esterase activity varies directly with the steric bulk of the ester being cleaved,[137-138] providing a rational strategy for manipulating the rate of triggering by intracellular esterases. Similarly, recent work has demonstrated that the electronics of the amine payload can affect the rate of thiocarbamate self-immolation.[127, 139]

To probe the effects of steric bulk on the rate of COS release and cytotoxicity of esterase-triggered COS donors, we prepared a library of thiocarbamates functionalized with different esters. To prepare the donors, we first treated 4-hydroxy benzyl alcohol with different alkyl and aryl carbonyl chlorides to afford the corresponding esters. Reaction with *p*-tolyl isothiocyanate furnished the desired thiocarbamates (**TCM1** to **TCM9**) in 14-90% yield (Figure 3.2a). In parallel, we also prepared the carbamate

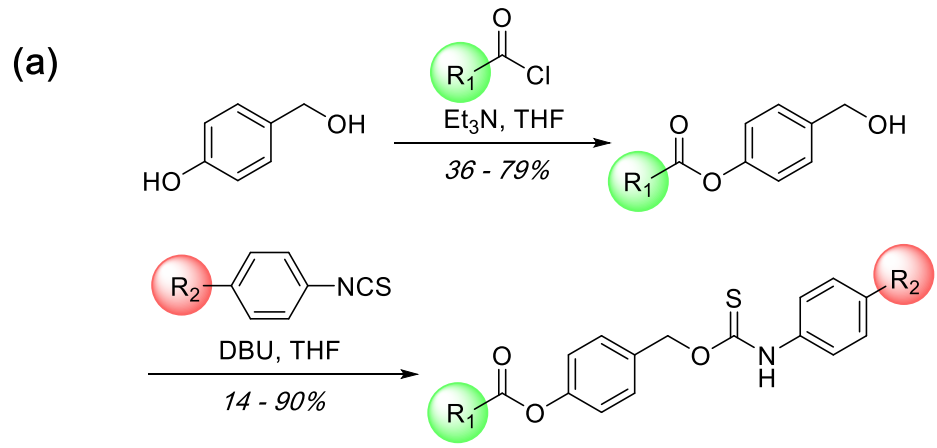

	R_1	X	yield
TCM1	Me	S	14%
TCM2	Cp	S	39%
TCM3	iPr	S	31%
TCM4	MeCp	S	61%
TCM5	tBu	S	64%
TCM6	Ph	S	22%
TCM7	Cy	S	29%
TCM8	1-Ad	S	26%
TCM9	2-Nap	S	76%
CM1	Me	O	36%
CM2	Cp	O	57%
CM3	iPr	O	52%
CM4	MeCp	O	90%
CM5	tBu	O	83%
CM6	Ph	O	79%
CM7	Cy	O	79%
CM8	1-Ad	O	53%
CM9	2-Nap	O	71%

	R_2	X	yield
TCM10	Ph	S	45%
TCM5	Me	S	64%
TCM11	H	S	55%
TCM12	F	S	58%
TCM13	CF_3	S	51%
TCM14	NO_2	S	47%
CM10	Ph	O	56%
CM5	Me	O	83%
CM11	H	O	78%
CM12	F	O	75%
CM13	CF_3	O	90%
CM14	NO_2	O	80%

Figure 3.2 (a) Synthetic scheme for the development of a library of esterase-activated thiocarbamate COS/H_2S donors (**TCM1** – **14**). (b) Table showing all compounds used in this study (**TCM1** – **14** and **CM1** – **14**) with yields.

control compounds, which release CO_2 rather than COS, by treatment of the carbonyl chloride intermediates with p-tolyl isocyanate (Figure 3.2b). To investigate the role of electronic modulation of the aniline payload on the rate of self-immolation and cytotoxicity of these compounds, a similar synthetic sequence was followed to access

esterase-triggered COS donors with electron-rich and electron-deficient amine payloads, (**TCM10** to **TCM14**).

With the library of esterase-activated COS/H_2S donors in hand, we next measured the H_2S release from these compounds in the presence of CA (Isozyme II from bovine erythrocytes) and porcine liver esterase (PLE). Direct detection of H_2S using a sulfide-selective electrode is simple and fast, but analogous methods do not exist for rapid COS detection directly in solution. For this reason, we added excess CA to these experiments to ensure no buildup of COS and used the detection of H_2S as an indirect measurement of COS release. We treated compounds **TCM1** – **TCM9** (Figure 3.2b, left) and **TCM10** – **TCM14** (Figure 3.2b, right) with 5 U/mL PLE in the presence of CA (25 μg/mL) in PBS buffer (pH 7.4) and observed H_2S release from each of compounds using a H_2S-sensitive electrode. These data confirm that physiologically relevant amounts of CA and PLE are sufficient to result in H_2S release from each of these donors. Consistent with our expectation that steric changes to the esters would results in different cleavage rates, we observed significantly different H_2S release rates and efficiencies from the donor compounds containing a variety of different ester groups (Figure 3.3a). For example, donors with bulkier esters (cyclohexyl (**TCM7**), adamantyl (**TCM8**), or naphthyl (**TCM9**), yellow, orange, and light blue traces, respectively) generated H_2S more slowly than those with smaller esters (methyl (**TCM1**), t-butyl (**TCM5**), or methyl cyclopropyl (**TCM4**), dark green, grey, and magenta traces, respectively). This qualitatively confirms that donors containing larger ester groups produce COS/H_2S more slowly, consistent with slower hydrolysis by PLE.

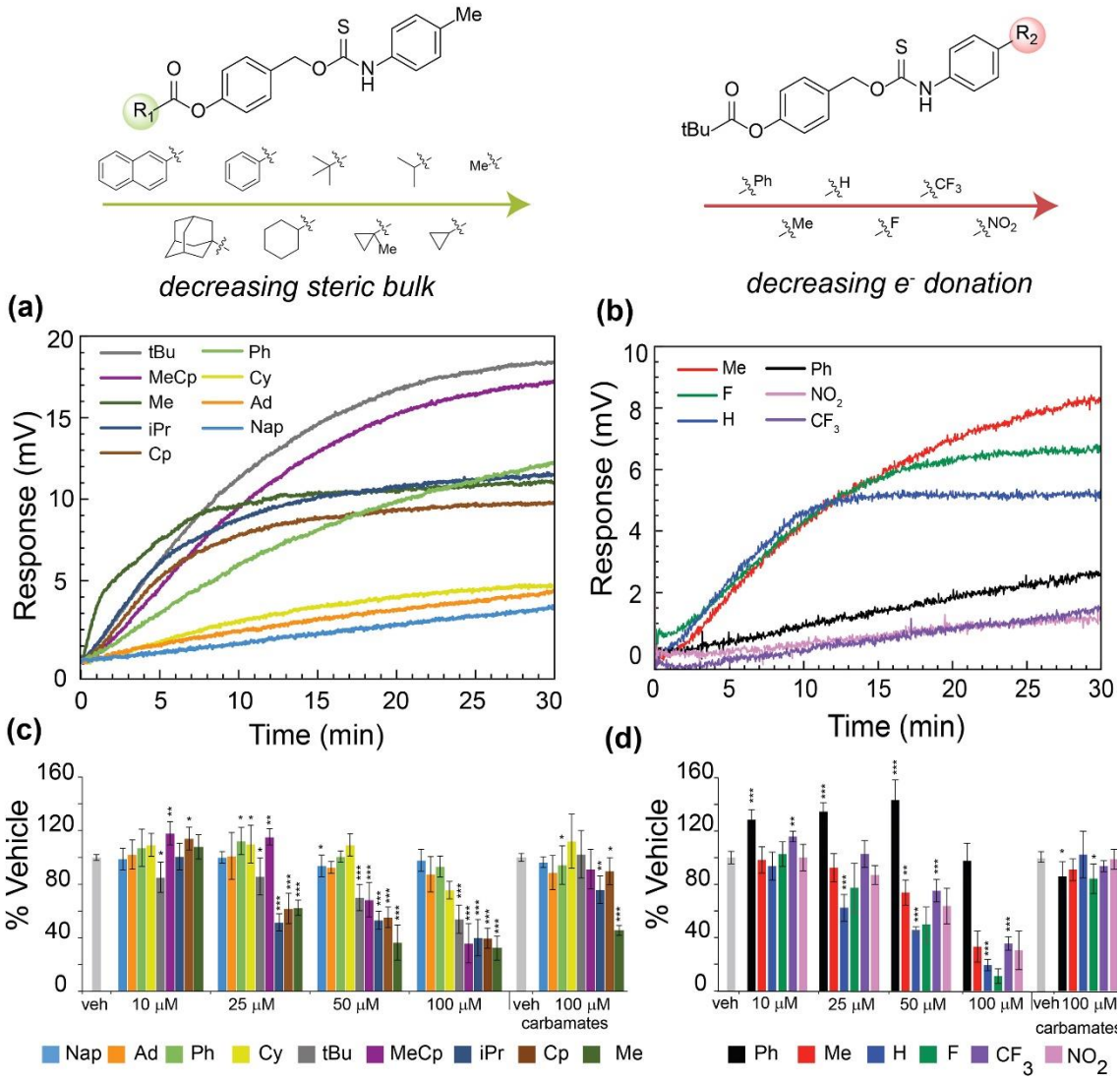

Figure 3.3 H_2S release curves for compounds (a) **TCM1** – **TCM9** and (b) **TCM5**, **TCM10** – **TCM14**) in the presence of PLE (5 U/mL) and CA (25 μg/mL) at pH 7.4. (c and (d) Cytotoxicity of compounds in HeLa cells. Data for donors (**TCM1** – **TCM14**) is shown for 10 – 100 μM and compared to the cytotoxicity of the carbamate control compounds (**CM1** – **CM14**) at 100 μM. (c) Cytotoxicity data for donors containing varying ester groups (**TCM1** – **TCM9**), with steric bulk of the ester group decreasing from left to right. (d) Cytotoxicity data for donors containing varying amine payloads (**TCM5**, **TCM10** – **TCM14**), with electron donating-ability of the payload decreasing from left to right. Results are expressed as mean (±) SD (n=6). The values that are significantly different by Student's t test are indicated by asterisks as follows: ***, $p < 0.001$ **, $p < 0.01$; *, $p < 0.05$. (e) Dual-axis comparison of cytotoxicity of various ester-containing donors at 100 μM and the rate of H_2S release from these compounds in the presence of PLE and CA. (f) Table of the rates of H_2S release and percent cell viability of various ester-containing donors at 100 μM.

H_2S release kinetics were also compared for a library of t-butyl ester functionalized donors containing a variety of electronically modulated amine payloads. We hoped to systematically decrease the rate of COS release through the introduction of electron-donating groups, although acidification of the N-H proton of the thiocarbamate has been reported to decrease the rate of COS release from similar donors functionalized with electron-withdrawing groups as well.[127] Consistent with this hypothesis, the introduction of either strongly electron-withdrawing (NO_2 (**TCM14**), CF_3 (**TCM13**), pink and purple traces, respectively) or electron-donating (Ph (**TCM10**), black trace) groups decreased the rate and efficiency of the donors, indicating that both electron-withdrawing and electron-donating groups slow down the rate of self-immolation following esterase hydrolysis. The donors containing weakly electronically modified amine payloads **TCM5**, **TCM11**, and **TCM12**) appear to have very similar initial rates (Figure 3.3b).

We next sought to determine whether the observed differences in COS/H_2S release rates translated to differences in cytotoxicities of compounds **TCM1** – **TCM14**. To probe these effects, we incubated HeLa cells with the COS donor compounds at 10, 25, 50, and 100 μM for 90 minutes and measured the resultant cell viability against the vehicle using the formazan dye-based CCK-8 cytotoxicity assay. We found that the cytotoxicity of the donors increased as the size of the ester decreased (Figure 3.3c), with the smallest ester (Me, **TCM1**) resulting in about 70% cell death at 100 μM. No significant cell death was observed, however, when cells were incubated with 100 μM of **TCM9**, which requires hydrolysis of a much larger naphthyl ester and has a much slower rate of COS/H_2S release. To confirm that the observed cytotoxicity was not due to the

organic byproducts of the donor constructs after activation, we also investigated the cytotoxicity of the corresponding carbamate control compounds (**CM1** – **CM14**) using the same conditions. Overall, we found significantly less cytotoxicity of all of the carbamates up to 100 μM. No significant trend was observed in the cytotoxicity of the donors as the electronics of the payload were changed. While many of these donors (**TCM5**, **TCM11** – **TCM14**) were cytotoxic, even as low as 25 μM, we did not find any correlation between cytotoxicity and the electronics of the amine payload (Figure 3.3d). Since the mechanism of decomposition of these donors may change due to acidification of the N-H proton, the cytotoxicity likely does not correspond to the rate of COS production.

This work provides evidence that cellular accumulation of COS is cytotoxic. Importantly, the cytotoxicity observed from many of these COS donors was completely eliminated when HeLa cells were incubated with the analogous, CO_2-releasing carbamates, which control for all other byproducts, suggesting that COS may be directly responsible for the observed effects. Cell death is dose-dependent for all of the cytotoxic COS-releasing compounds, and in general, the most cytotoxic donors were also found the have the most rapid kinetics of H_2S release in the presence of CA (Figure 3.3e and 33.3f). Overall, the hypothesis that the inclusion of a larger ester on these donors would decrease the rate of hydrolysis and prevent the build-up of COS was found to hold true. We were not able to systematically decrease the rate of COS release through electronic modulation of the amine payloads, but did find that both strongly electron-withdrawing and electron-donating groups diminished COS/H_2S release, consistent with two previously suggested effects: that electron-donating groups decrease the rate of self-immolation, and electron-

withdrawing groups can result in a change in the mechanism of H_2S release due to acidification of the N-H proton on the thiocarbamate.[127] Due to a potential change in mechanism supported by a decrease in H_2S production from donors containing electron-withdrawing payloads, it is impossible to correlate the cytotoxicity of these particular donors with their rate of COS/H_2S release.

In addition to providing new insights into the differential impacts of COS and H_2S, this work also increases the tools available for increasing basal H_2S concentrations without the need for external triggering mechanisms or consumption of cellular nucleophiles. To confirm that these donors release COS/H_2S in a cellular environment, we incubated 100 μM Cy-TCM (**TCM7**) with SF7-AM in HeLa cells and observed an increase in fluorescence corresponding to H_2S donation from the scaffold (**Figure 3.4**).[140] This confirms the basic cellular viability of this compound as an H_2S donor. Although the faster-releasing donors are too cytotoxic for use as efficacious H_2S donors, the slower-releasing donors provide a library of enzyme-activated COS/H_2S donors viable for use in cell-based experiments.

3.3 Conclusions

In conclusion, this work supports the hypothesis that rapid accumulation of COS likely results in cytotoxicity.[104] Conclusively disentangling the effects of COS delivery from the physiological effects of H_2S will require a systematic study of COS, the various CA isoforms, and the potential for subcellular localization of COS delivery from various donors. The work reported here suggests the likely role of COS in the cytotoxicity of many of these compounds and provides an important piece of early evidence that COS

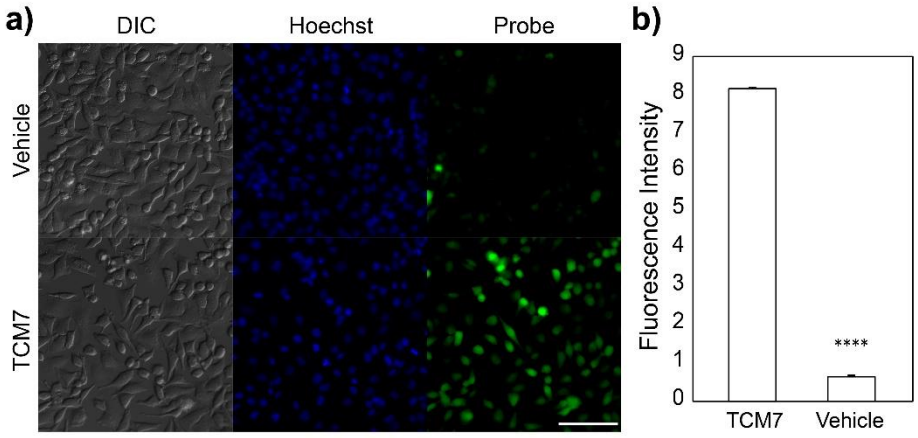

Figure 3.4 (a) Live-cell imaging of H_2S release from **TCM7** in HeLa cells. HeLa cells were treated with SF7-AM (5 µM) and Hoechst (5 µg/mL) for 30 min, washed, and incubated with FBS-free DMEM containing **TCM7** (100 µM, bottom) or DMSO (0.5%, top) for one hour. Cells were then washed and imaged in PBS. Scale bar = 100 µm. (b) Relative integrated fluorescence intensity of cells treated with **TCM7** versus vehicle treated cells.

delivery may produce a cellular response that is different than that observed from H_2S alone.

Despite the tunability shown by altering the ester subsituent across a suite of esterase-triggered slef-immolative thiocarbamates, we were surprised to not the lack of a correlation between electron-withdrawing nature of the payload and rate of H_2S release. Chapter IV discusses the use of N-Methyl thiocarbamates to probe the true mechanism of self-immolation and COS-release from thiocarbamates, and reports a new platform for thiocarbamate and dithiocarbamate synthesis.

3.4 Experimental Details

General Materials and Methods.

Reagents were purchased from Sigma-Aldrich or Tokyo Chemical Industry (TCI) and used as received. SF7-AM was synthesized as previously reported.[141] Spectroscopic grade, inhibitor-free THF was deoxygenated by sparging with argon followed by passage through a Pure Process Technologies solvent purification system to remove water. Deuterated solvents were purchased from Cambridge Isotope Laboratories and used as received. Silica gel (SiliaFlash F60, Silicycle, 230-400 mesh) was used for column chromatography. ^{1}H, $^{13}C\{^{1}H\}$, and ^{19}F NMR spectra were recorded on a Bruker 500 or 600 MHz instrument (as indicated). Chemical shifts are reported in ppm relative to residual protic solvent resonances. Mass spectrometric measurements were performed on a Xevo Waters ESI LC/MS instrument or by the University of Illinois, Urbana Champaign MS facility. H_2S electrode data were acquired with a Unisense H_2S Microsensor Sulf-100 connected to a Unisense Microsensor Multimeter. All air-free manipulations were performed under an inert atmosphere using standard Schlenk techniques or an Innovative Atmospheres N_2-filled glove box. HeLa cells were purchased from ATCC (Manassas, Virginia, USA). Cell imaging experiments were performed on a Leica DMi8 fluorescence microscope, equipped with an Andor Zyla 4.2+ sCMOS detector. Fluorescence intensity measurements were calculated using Fiji (ImageJ).[142] Fluorescence intensities were measured in Fiji, with images scaled to 32-bit, and the error is reported as the standard mean error.

H_2S Electrode Experiments

Scintillation vials containing 20.00 mL of phosphate buffer (140 mM NaCl, 3 mM KCl, 10 mM phosphate, pH 7.4) were prepared in an N_2-filled glovebox. The Unisense electrode was inserted into the vial and the vial was capped with a split-top septum to minimize oxidation. The current was allowed to equilibrate prior to starting the experiment. With moderate stirring, the CA stock solution (50 µL, CAII from Bovine Erythrocytes) was injected, followed by subsequent injections of TCM stock solution (50 µL) and PLE stock solution (100 µL). H_2S release was monitored until leveling off.

CCK-8 Cell Viability Experiments

HeLa cells were cultured in Dulbecco's modified Eagle's medium (DMEM) supplemented with 10% fetal bovine serum (FBS) and 1% penicillin/streptomycin at 37 °C under 5% CO_2. 96-well plates were seeded with 15,000 cells/well overnight then washed, incubated in FBS-free DMEM containing vehicle (0.5% DMSO), TCA (10-100 µM), or carbamate (10 – 100 µM) for 90 minutes. Cells were then washed with PBS and CCK-8 solution (1:10 in FBS-free DMEM) was added to each well, and cells were incubated for 1-2 hours at 37 °C under 5% CO_2. The absorbance at 450 nm was measured using a microplate reader and the cell viability was measured and normalized to the vehicle group. Results are expressed as mean (±) SD (n=6). P values were calculated using a Student's T-test in Excel compared to DMSO alone.

Cell Imaging

HeLa cells were cultured in Dulbecco's modified Eagle's medium (DMEM) supplemented with 10% fetal bovine serum (FBS) and 1% penicillin/streptomycin at 37 °C under 5% CO2. Imaging dishes were seeded with HeLa cells overnight and then washed and incubated with SF7-AM (5 µM) and Hoechst 33342 (5 µg/mL) in FBS-free DMEM for 30 min. Cells were then washed with PBS and incubated with either Cy-TCM (100 µM) or vehicle (DMSO, 0.5%) in FBS-free DMEM for 60 minutes prior to being washed with PBS and imaged. Imaging was performed once, and the fluorescence intensities were calculated from the images shown, with 77 cells in the TCM images and 116 cells in the control.

Synthesis

General procedure for the synthesis of phenol esters. 4-Hydroxy benzyl alcohol (1.0 equiv.) was dissolved in anhydrous THF (0.1 M solution), under and atmosphere of N_2. The solution was cooled to 0 °C, followed by addition of Et_3N. The reaction mixture was let stir for 5 minutes, after which the carbonyl chloride was added dropwise over 20 minutes. The resultant mixture was stirred at 0 °C until the completion of the reaction indicated by TLC. The reaction was quenched by adding brine (30 mL), and the aqueous solution was extracted with ethyl acetate (3 x 20 mL). The organic layers were combined, dried over anhydrous $MgSO_4$, and concentrated under reduced pressure. The crude product was purified by silica column chromatography. Full spectroscopic data for each compound is reported in Appendix B. The preparation of MeCp-OH is also reported in Appendix B.

General procedure for preparation of thiocarbamates

The functionalized benzyl alcohol (1.0 equiv.) was dissolved in anhydrous THF (0.2 M solution) under an atmosphere of N_2. Aryl isothiocyanate (1.1 equiv.) was added, followed by DBU (1.25 equiv.) at 0 °C. The resultant mixture was warmed to rt and stirred monitored by TLC. The reaction was quenched upon observation of by-product formation by TLC by addition of brine (20 mL), and extracted with EtOAc (3 x 20 mL). The combined organic layers were dried over anhydrous $MgSO_4$ or Na_2SO_4, concentrated under reduced pressure, and purified by silica column chromatography. Full spectroscopic data for each compound is reported in Appendix B.

General procedure for preparation of carbamate controls

Functionalized benzyl alcohol (1.0 equiv.) was dissolved in anhydrous THF (0.1 M solution) under an atmosphere of N_2. Aryl isocyanate (0.90 equiv.) was added, followed by DBU (1.25 equiv.) at 0 °C. The resultant mixture was warmed to rt and stirred monitored by TLC. The reaction was quenched upon observation of by-product formation by TLC by addition of brine (20 mL), and extracted with EtOAc (3 x 20 mL). The combined organic layers were dried over anhydrous $MgSO_4$, concentrated under reduced pressure, and purified by silica column chromatography. Full spectroscopic data for each compound is reported in Appendix B.

CHAPTER IV

PREPARATION AND COMPUTATIONAL INVESTIGATION OF N-METHYL SELF-IMMOLATIVE THIOCARBAMATES AND DITHIOCARBAMATES

This chapter includes unpublished and co-authored material. The manuscript in Chapter 4.1 was written by Carolyn M. Levinn with editorial assistance by Professor Michael D. Pluth. The project in this chapter was conceived by Carolyn M. Levinn. The experimental work was performed by Carolyn M. Levinn and Rachel E Lutz. The computational experiments were performed by Jenna L. Mancuso with assistance from Professor Christopher H. Hendon. The project in Chapter 4.2 was conceived by Carolyn M. Levinn with insight from Professor Michael D. Pluth. The experimental work was performed by Carolyn M. Levinn and Rachel E Lutz. The computational experiments were performed by Hannah E. Hashimoto, with assistance from Jenna L. Mancuso.

Chapter 4.1 N-Methylation Provides Insights into the Mechanism of Carbonyl Sulfide Release from Self-Immolative Thiocarbamates

4.1.1 Introduction

Since its recent classification as a third gasotransmitter, alongside carbon monoxide and nitric oxide, there has been significant interest in studying the role of hydrogen sulfide (H_2S) in various biological systems.[3] H_2S has been shown to exhibit cardioprotective properties, mitigating the oxidative stress from myocardial infarction and ischemia-reperfusion events.[19, 143] Additionally, there have been promising reports

regarding the role of H_2S in treatments for various neurodegenerative diseases,[16, 144] including Parkinson's[145] and Alzheimer's diseases.[146] However, many of these reports show conflated and confusing effects: H_2S has been shown to have both pro-[147] and anti-inflammatory,[148-149] as well as both pro-[150] and anti-apoptotic[151-152] effects, depending on the specific study or assay. These findings, both promising and confusing, have led many research groups to develop a broad array of chemical tools for studying H_2S in biology to better understand the physiochemical properties of this molecule. These tools include donor platforms capable of delivering known quantities of H_2S (or H_2S equivalents) at controllable rates, the state of the art of which can be delivered in response to a specific stimuli.[153]

One class of H_2S donor that has recently become popular is self-immolative thiocarbamates which, in response to a specific triggering stimulus, collapse to reveal some payload and an equivalent of carbonyl sulfide (COS), which is rapidly converted to H_2S by the enzyme carbonic anhydrase (CA) (Figure 4.1a).[106, 154] There are many advantages of these systems over other triggered scaffolds. Thiocarbamates are relatively easily prepared, and are modular in that the triggering moiety and the payload can be interchanged to create diverse libraries of donors that release in response to many types of both external and internal stimuli, including endogenous levels of peroxide,[113, 128] bio-orthogonal chemistry,[118] enzymes,[103-104] thiols,[82] acid,[155] and light.[97, 114-115] Perhaps most importantly, the self-immolative thiocarbamate scaffold is adaptable for the preparation of two critical control compounds: the triggerless, which controls for any biological response due to the core thiocarbamate scaffold, and the sulfur-deplete, CO_2-releasing

control, which controls for any response resulting from the byproducts of self-immolation.

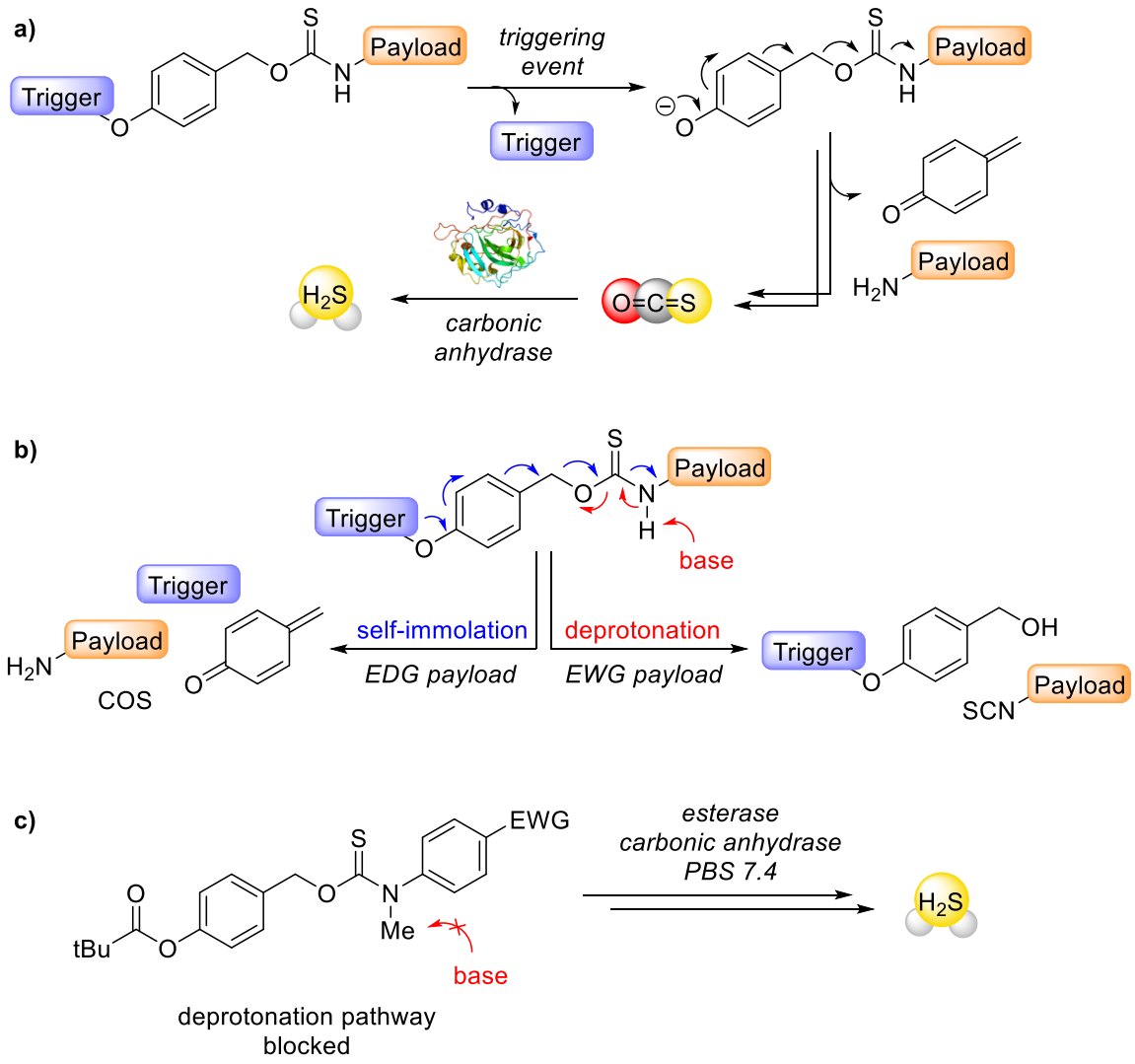

Figure 4.1. (a) Mechanism of COS/H_2S release from self-immolative thiocarbamates. (b) Proposed competing breakdown pathways of thiocarbamates with different payloads; left (blue) indicating the productive COS-releasing pathway with electron-rich payloads, right (red) indicating unproductive deprotonation-based pathway, which does not release COS. (c) This work: N-Methylation of thiocarbamates should block deprotonation, allowing for more electron-poor payloads to be appended to thiocarbamate COS donors.

Recently, we reported a series of esterase-triggered thiocarbamates with aniline payloads encompassing a broad range of electronic properties, with the hypothesis that

more electron-deficient anilines would favor an increased rate of self-immolation by stabilizing the charge build-up on the nitrogen atom in the COS-releasing transition state.[156] However, experimentally the rate of COS release (monitored through H_2S formation with an H_2S-sensitive electrode) did not follow any obvious trend correlating with σ_p values. Understanding that Hammett parameters are based on a system designed with benzoic acid (not directly translatable) we felt that this warranted deeper investigation.

One explanation for the divergence in COS-release rates from standard Hammet parameters, is competition with a second, unfavorable pathway. In the case of strongly electron-withdrawing amine payloads, wherein the electron poor payload acidifies the thiocarbamate N-H, resultant deprotonation could reveal an isothiocyanate and benzylic alcohol. Since this pathway is non-productive, one would expect low rates and levels of detectable H_2S to be observed (Figure 1b). Indeed, this competing mechanism has been proposed in similar systems, but to the best of our knowledge has not yet been investigated in detail.[113, 157]

Here, to test this hypothesis, we block deprotonation by methylating the carbamate nitrogen and assess the relative rates of release (Figure 4.1c). We report the synthesis of a suite of N-Me esterase-triggered thiocarbamates, roughly analogous to the parent N-H derivatives reported in 2019, as well as their H_2S/COS release curves. We further present a mechanistic analysis of both productive, and unproductive reaction trajectories to reveal large thermal barriers towards isothiocyanate formation, and propose a more likely alternative route for electron-withdrawing substituents.

4.1.2 Results and Discussion

Previous syntheses of thiocarbamates involve the addition of a benzyl alcohol or a benzyl mercaptan into the corresponding isothiocyanate or isocyanate.[156] Initial attempts to methylate after thiocarbamate formation, while facile for the carbamate, yielded only the undesired *S*-Me isomer when applied to thiocarbamate systems. However, addition of one equivalent of an *N*-Me aniline into thiocarbonyldiimidazole (TCDI) produced the asymmetric mixed thiourea, which could be further reacted with a benzyl alcohol to access the desired *N*-Me *O*-alkyl thiocarbamates. Following this protocol, we prepared a suite of *N*-Me TCMs covering a range of electronic payload properties (Figure 4.2). It is noteworthy that following a similar sequence of steps we prepared the analogous *S*-alkyl isomers, however were unable to observe COS/H_2S release from these donors via the methylene blue assay (Appendix C, Figure C.34).

In the preparation of the coupling partners for the synthesis of the *S*-alkyl N-Me thiocarbamates, the reactivity was greatly enhanced by methylating the remaining imidazole to the imidazolium.[158] (Figure 4.3a) Thiocarbamate syntheses with these activated coupling partners proceeded in high yields under mild conditions. However, attempts to activate the *O*-alkyl thiourea coupling partners in this way yielded instead the *S*-Me isothiouronium species, which proved inactive in the desired coupling reaction (Figure 4.3b).

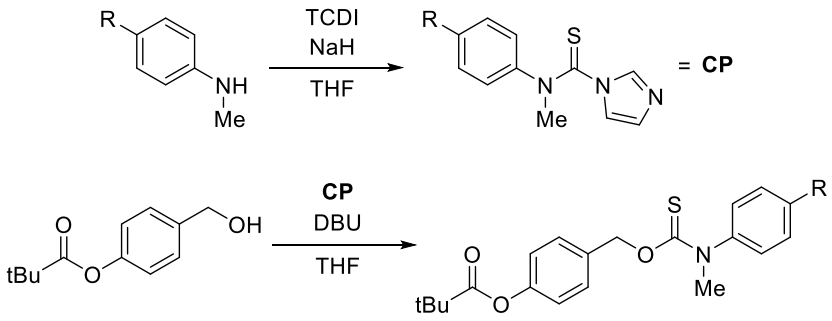

		coupling partner		thiocarbamate	
EWG	R = NO_2	CP-NO_2	26%	MeTCM-NO_2	33%
	R = CF_3	CP-CF_3	81%	MeTCM-CF_3	10%
	R = OCF_3	CP-OCF_3	60%	MeTCM-OCF_3	14%
	R = F	CP-F	55%	MeTCM-F	21%
	R = H	CP-H	75%	MeTCM-H	19%
	R = Me	CP-Me	99%	MeTCM-Me	22%
EDG	R = OMe	CP-OMe	95%	MeTCM-OMe	9%

Figure 4.2. Synthesis and yields of coupling partners and final *O*-alkyl N-Me thiocarbamate COS/H_2S donors.

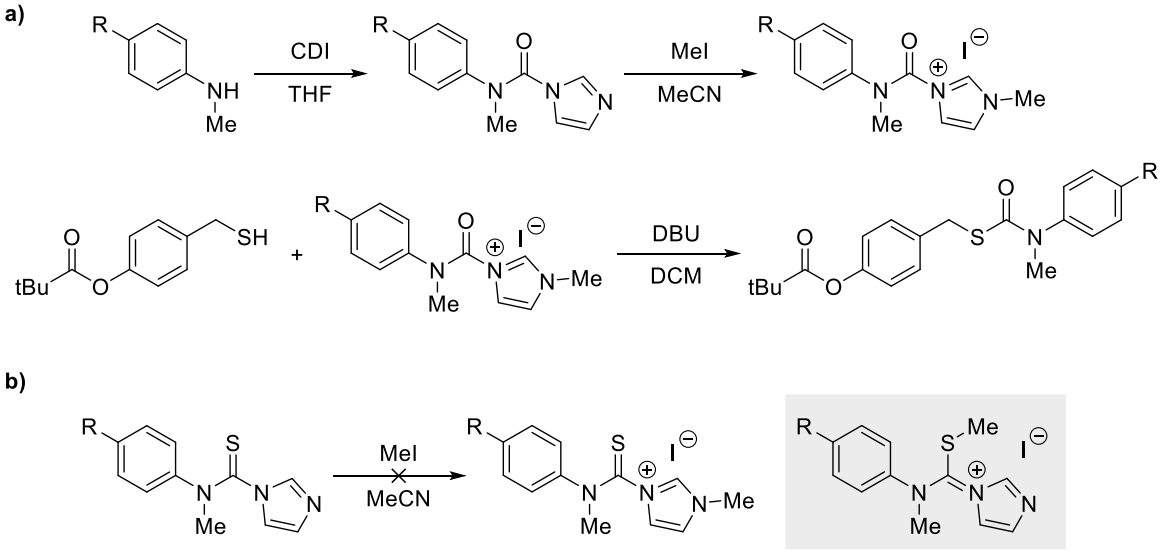

Figure 4.3. a) Preparation of activated coupling partner for synthesis of *S*-alkyl N-Methyl thiocarbamate COS/H_2S donors. b) Application of the same strategy for activated *O*-alkyl coupling partners instead yielded undesired *S*-Methylation.

With the methylated O-alkyl thiocarbamate donors in hand, the rates of COS/H_2S release were surveyed using the colorimetric methylene blue assay (Figure 4.4).[159] We measured H_2S release from the thiocarbamates (50 μM) in phosphate-buffered saline solutions (10 mM PBS 7.4) with 2% DMSO in the presence of carbonic anhydrase (50 μg/mL) and porcine liver esterase (5 U/mL) at 25 °C. The methylene blue aliquots were filtered through a 0.5 micron syringe filter before absorbances were measured, due to the highly acidic methylene blue cocktail solution causing the protonated PLE to crash out of solution, causing high variance in absorbance; all experiments were performed in quadruplicate. We hypothesized that installing electron-withdrawing substituents on the payload would increase the observed rate of H_2S/COS release, with the *p*-NO_2 donors being the most efficient. What we observed, however, was less straightforward. The donors with the most electron-rich payloads release H_2S at the slowest rates and efficiencies, with a rough correlation of rates increasing as electron density decreased. This peaked at the *p*-F payload, and then the observed rates decreased as the aniline substituents were more electron withdrawing.

To directly compare the effects of the *N*-Methylation on the rate of COS/H_2S release from thiocarbamates, we again measured the H_2S release from *p*-NO_2 and *p*-Me *N*-H thiocarbamate donors. Indeed, *N*-Methylation dramatically increased the observed H_2S release from the *p*-NO_2 donor relative to the N-H. However, the N-Me *p*-Me thiocarbamate was significantly slower and less efficient than the N-H donor. While the increase in observed H_2S release in the *p*-NO_2 series from N-H to the N-Me supports the hypothesis that the undesired, unproductive isothiocyanate pathway was being blocked,

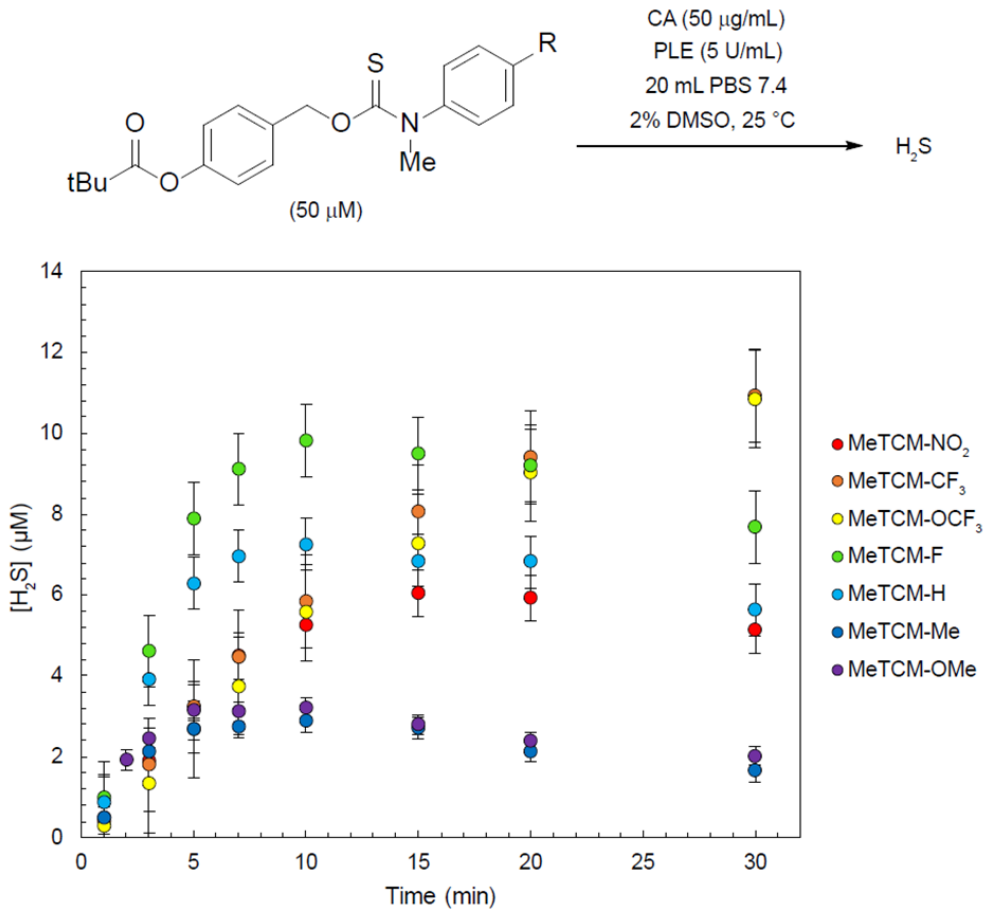

Figure 4.4 H_2S release profiles of *O*-alkyl N-Me thiocarbamate donors, as measured by the methylene blue assay.

we were surprised to find the N-H *p*-Me TCM still showed the fastest initial rate of H_2S release, prompting computational exploration of reaction pathways (Figure 4.5).

To probe possible side reaction pathways, all ground state and transition state geometries were fully equilibrated using density functional theory (DFT) as implemented in Gaussian09. The hybrid functional B3LYP was employed in conjunction with the triple-ζ Pople basis set and additional diffuse and polarization functions on all atoms (6-311++G(d,p)) using a superfine grid and tight convergence criteria for all calculations. A self-consistent reaction field was included with the dielectric constant of water using the

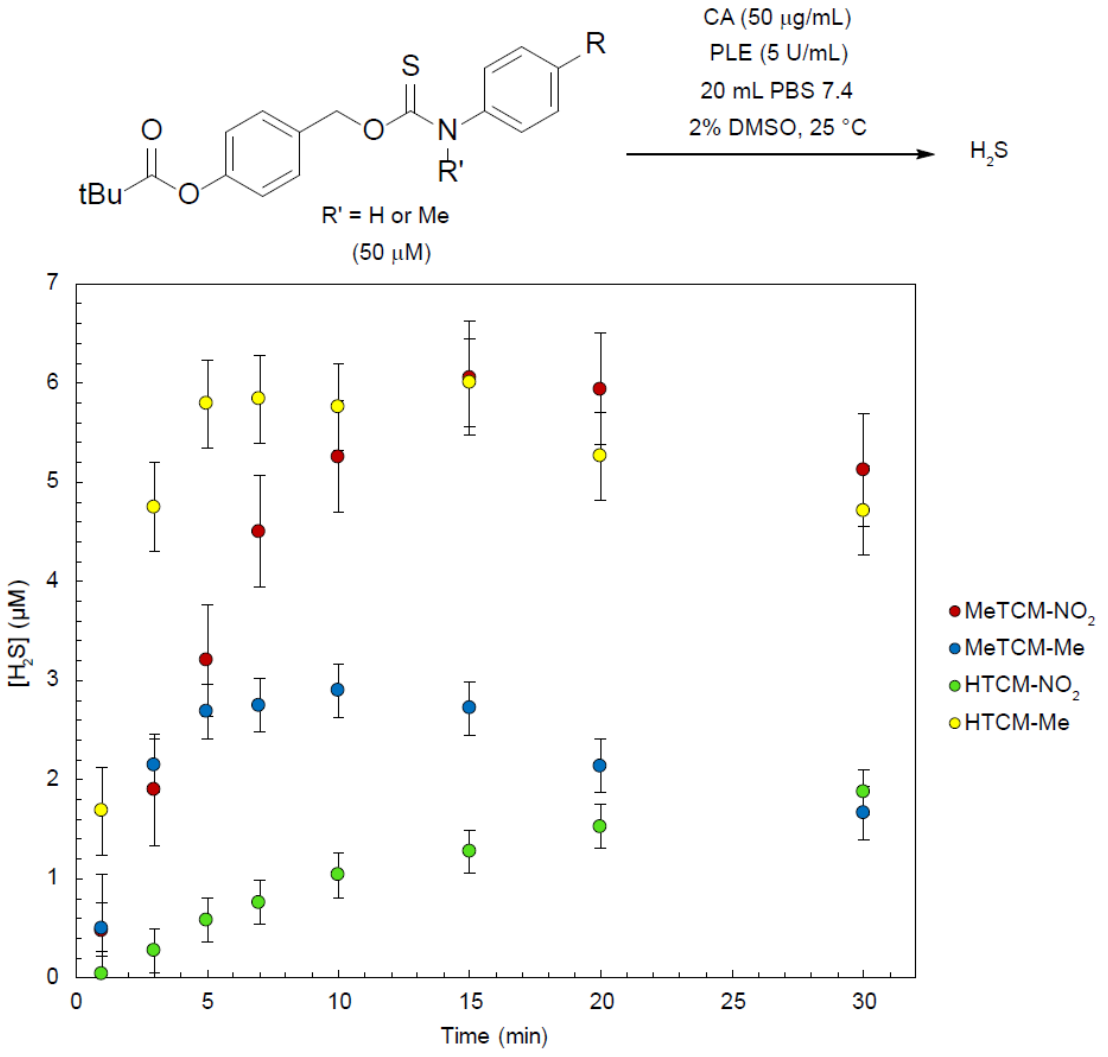

Figure 4.5. H_2S release profiles of select *O*-alkyl N-Me and N-H thiocarbamate donors, as measured by the methylene blue assay.

polarizable continuum model in order to simulate the biological environment. In addition to the expected 1,6-self-immolation and COS extrusion route (Figure 4.6a, black), we identified continuous routes for I) deprotonation of the thiocarbamate N-H to release an isothiocyanate, as is often cited (Figure 4.6a red, alternate path I), and protonation of the thiocarbamate anion following payload release with subsequent hydrolysis to yield an aniline and an equivalent of thiocarbonic acid (Figure 4.6a blue, alternate path II).

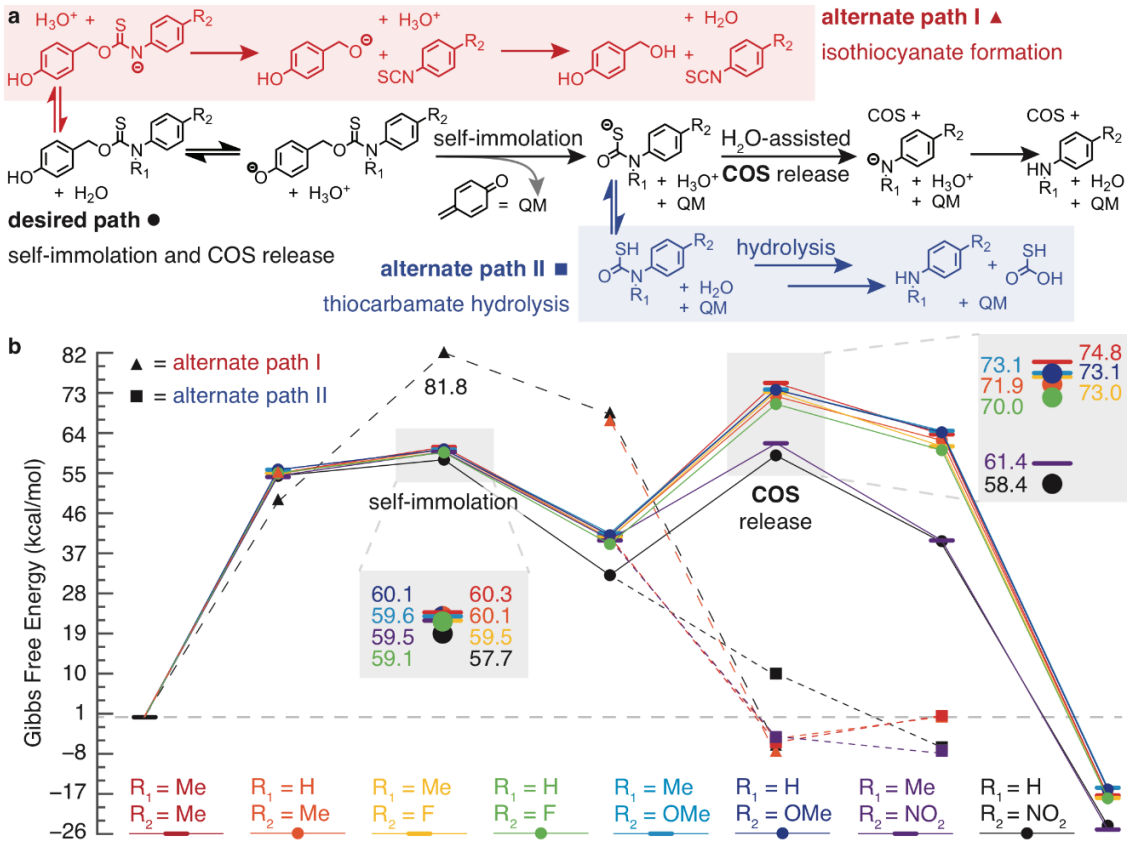

Figure 4.6 (a) The intended reaction pathway for thiocarbamate scaffolds where R_1 = H, Me and R_2 = Me, F, OMe, NO_2 is shown in black with alternate paths I and II depicted in red/triangles and blue/squares, respectively, that were investigated computationally in this study. (b) Gibbs Free Energy coordinate diagram comparing the relative energies of each proposed reaction pathway recovered from B3LYP/6-311++G** including the PCM for water as implemented in Gaussian09

Along the desired pathway, thiocarbamate methylation is expected to reduce reaction rates due to mild electron-donation into the formally anionic pathway, which is reflected in both the experimental (Figure 4.5) and computation data (Figure 4.6b). Additionally, *N*-Methylation provides a steric 'lock' on the conformation of the thiocarbamate. *O*-alkyl thiocarbamates are known to have restricted rotation about the thioamide bond, requiring elevated temperatures to resolve the rotameric peaks by NMR spectroscopy. Methylating the thiocarbamate nitrogen exaggerates that phenomenon,

effectively locking the aryl ring of the payload out of plane with the thiocarbamate moiety and minimizing orbital overlap, which can also slow the rate of COS-extrusion.

As expected, comparing the zero-point energy corrected energy barriers for the rate-determining step of COS-release from the thiocarbamate anions we see that scaffolds with electron-donating groups in the R_2-position have higher activation barriers for COS release, while donors with electron-withdrawing groups in the R_2 position have lower barriers. However, the relative barriers to the rate-determining step for donors where $R_2 = NO_2$ (MeTCM-NO_2 and HTCM-NO_2) indicate they should release H_2S much more efficiently than experimentally observed. To examine whether this reduced production is the result of N-H acidification, we explored deprotonation of the N-H scaffold following the expected competing pathway to isothiocyanate formation (alternative path I, Figure 4.6b black triangles). Deprotonation of the N-H in HTCM-NO_2 is indeed expected to occur – as evidenced by the relative stability of the resulting anion compared with deprotonation of the phenol trigger – yet, the activation barrier for benzyl alcohol release is > 20 kcal/mol greater than the rate-determining step for COS release, indicating that this pathway is largely inactive. However, the reversible deprotonation of the acidified thiocarbamate N-H when R_2=NO_2 still likely plays a role in reduced rates of H_2S production. For HTCM-Me, deprotonation at the nitrogen and oxygen are effectively the same (cf. 54.8(6) and 54.9(2) kcal/mol, respectively) and the transition state for isothiocyanate formation could not be isolated – saddlepoint searches returned small molecule byproducts rather than an activated complex – but it we would expect it to be considerably less stable compared to when $R_2 = NO_2$.

After investigating plausible reaction intermediates and activated complexes we uncovered a more likely competing pathway: alternate path II (black squares, Figure 4.6b). In this scheme, protonation of the thiocarbamate anion yields a thiocarboxylic acid motif that can hydrolyze to release thiocarbonic acid. Indeed, there are prior reports of thiocarbonic acid dimer complexes decomposing to produce two equivalents of COS and H_2O, which in this system can be converted to H_2S by CA.[160] Potential energy surface scans performed to identify the activation barrier for water attack at the thiocarboxylic acid carbonyl reveal a barrierless transition (Appendix C, Figure C.36) to higher energy zwitterionic intermediates, for which equilibrium structures could not be found. Still, the path is generally "downhill" thermodynamically. Notably, hydrolysis to complete alternate path II is exergonic for R_2=NO_2 scaffolds but (slightly) endergonic when R_2=Me (squares and small dashed lines, Figure 4.6b). We also considered the direct release of H_2S by hydrolysis of the thiocarbamate SH as an alternative path, however zero H_2S is detected by the methylene blue assay for HTCM-NO_2 without addition of CA, indicating that any H_2S released comes from a COS-based pathway. (Appendix C, Figure C.35).

Chapter 4.1.3 Conclusions

In conclusion, we have designed a platform for the synthesis of *N*-alkyl self-immolative thiocarbamate COS donors, which we have shown to have vastly different rates of H_2S release than the free N-H analogs. *N*-Methylation makes accessible thiocarbamates with highly electron poor payloads, which previously were shown to either release H_2S very slowly or not at all. With quantum mechanical analysis of COS

release from *O*-alkyl thiocarbamates, we show that the often cited isothiocyanate formation route is likely not operative, at least in aqueous systems. While, the unexpectedly low levels of H_2S release from thiocarbamates with electron-withdrawing payloads are indeed the result of increased competition from side reactions due to the acidity of the N-H, they are also likely a function of the electrophilicity of the carbonyl in the thiocarbamate anion, which are not as competitive in systems with more electron-rich payloads Methylating the nitrogen of the thiocarbamate blocks some of these side pathways, which increases the rate of H_2S release and subsequent utility of thiocarbamate donors with electron poor payloads, such as nitroanilines or most fluorophores. Across many diverse thiocarbamate COS donor scaffolds, we have observed aniline payloads with a 4-Fluoro substituent to be some of the most efficient[128, 156], potentially as an optimal combination of electronegative and deactivating, but still electron-donating enough to prevent side-reactivity. We anticipate these findings will inform researchers in future H_2S donor design, and will expand the chemical space available with thiocarbamate COS donors to now more reasonably include electron poor payloads. In Chapter 4.2 we expand this N-Me coupling partner platform to the synthesis of dithiocarbamates as potential CS_2 donors.

Chapter 4.1.4 Materials and Methods

Synthesis Materials and Methods: Reagents were purchased from Sigma-Aldrich, VWR, or Tokyo Chemical Industry (TCI) and used as received. Spectroscopic grade, inhibitor-free THF was deoxygenated by sparging with argon followed by passage through a Pure Process Technologies solvent purification system to remove water.

Deuterated solvents were purchased from Cambridge Isotope Laboratories and used as received. Silica gel (SiliaFlash F60, Silicycle, 230–400 mesh) was used for column chromatography. ^{1}H, $^{13}C\{^{1}H\}$, and ^{19}F NMR spectra were recorded on a Bruker 500 or 600 MHz instrument (as indicated). Chemical shifts are reported in parts per million relative to residual protic solvent resonances. Mass spectrometric measurements were performed by the University of Illinois, Urbana–Champaign MS facility. All air-free manipulations were performed under an inert atmosphere using standard Schlenk techniques or an Innovative Atmospheres N_2-filled glovebox.

General Procedure for the Synthesis of N-Me Coupling Partners:

General procedure A: para-substituted N-Me aniline (1.0 equiv.) and TCDI (2.0 equiv.) were dissolved in anhydrous THF (0.15 M solution based on aniline) in a flame-dried round-bottomed flask equipped with a magnetic stirbar under an inert N_2 atmosphere. The reaction was refluxed at 70 °C overnight, then the solvent removed under reduced pressure. The crude residue was re-dissolved in EtOAc, quenched with brine, and extracted with EtOAc (3 x 20 mL). The combined organic layers were dried over anhydrous $MgSO_4$, and purified via silica column chromatography (1:1 Hex:EtOAc).

General procedure B: para-substituted N-Me aniline (1.0 equiv.) and TCDI (1.2 equiv.) was dissolved in anhydrous THF (0.1 M solution based on aniline) and cooled to 0 °C in an ice bath under an inert N_2 atmosphere. NaH (1.1 equiv.) was added, and the reaction mixture was allowed to slowly warm to room temperature and stir overnight. The reaction mixture was quenched with brine, extracted with EtOAc (3 x 20 mL), and the

combined organic layers were dried over anhydrous $MgSO_4$, and purified via silica column chromatography (1:1 Hex:EtOAc).

General Procedure for the Synthesis of N-Me Thiocarbamates: 4-(hydroxymethyl)phenyl pivalate (1.0 equiv.) and an N-Me Coupling Partner (1.1 equiv.) was dissolved in anhydrous THF (0.1 M solution), and put under an atmosphere of N_2. DBU (1.2 equiv.) was added, and the reaction was let stir at room temperature, monitored by TLC. Upon completion, the reaction mixture was quenched with brine, extracted with EtOAc (3 x 10 mL), the combined organic layers were dried over anhydrous $MgSO_4$, and the crude product purified by silica gel column chromatography (4:1 Hexanes:EtOAc).

Computational Methods: Density functional theory (DFT) as implemented in Gaussian09 with the hybrid functional B3LYP and the triple-ζ Pople basis set with diffuse and polarization functions on all atoms (6-311++G(d,p)) was employed to equilibrate all intermediate and transition state structures. A superfine grid and tight convergence criteria were used for all calculations. A self-consistent reaction field was included with the dielectric constant of water using the polarizable continuum model in order to simulate the biological environment. Vibrational analysis was further performed to recover thermodynamic values, including the zero-point energy correction, and to ensure ground state structures each had zero negative frequencies, while all activated complexes had exactly one corresponding to the appropriate bond breaking/forming reaction coordinate.

H_2S Detection Materials and Methods: Phosphate buffered saline (PBS) tablets (1X, CalBioChem) were used to prepare buffered solutions (140 mm NaCl, 3 mm KCl, 10 mm phosphate, pH 7.4) in deionized water. Buffer solutions were sparged with nitrogen to remove dissolved oxygen and stored in an Innovative Atmosphere nitrogen-filled glovebox. Donor stock solutions (in DMSO) were prepared inside a nitrogen-filled glovebox immediately before use. PLE stock solutions (in PBS) were freshly prepared in an N_2-filled glovebox immediately before use. CA stock solutions (in PBS) were freshly prepared in a nitrogen-filled glovebox immediately before use.

General Procedure for Measuring H_2S Release with the Methylene Blue Assay (MBA): Scintillation vials containing 20 mL of 10 mm PBS (pH 7.4) with 2% DMSO were prepared in a nitrogen-filled glovebox. To these solutions, 100 μL of 10 mg mL^{-1} CA and 50 μL of a 20 mM DMSO donor stock were added for final concentrations 50 μg mL^{-1} and 50 μM, respectively. Immediately prior to PLE addition, 0.5 mL solutions of methylene blue cocktail were prepared. The methylene blue cocktail solution contains: 200 μL of 30 mm FeCl3 in 1.2 m HCl, 200 μL of 20 mm N,N-dimethyl-*p*-phenylene diamine in 7.2 m HCl, and 100 μL of 1 % (w/v) $Zn(OAc)_2$. To begin an experiment, 100 μL of 1000 U/mL PLE stock solution was added for a final concentration of 5 UmL^{-1}. At set time points after the addition of PLE, 500 μL reaction aliquots were added to the methylene blue cocktail solutions and incubated for 1 h at room temperature shielded from light, then filtered through a 0.5 micron syringe filter into disposable 1.5 mL cuvettes. Absorbance values at 670 nm were measured 1 h after addition of reaction aliquot. Each experiment was performed in quadruplicate unless stated otherwise.

UV/Vis spectra were acquired on an Agilent Cary 60 UV/Vis spectrophotometer equipped with a Quantum Northwest TC-1 temperature controller set at 25±0.05 °C.

4.2 N-Me Dithiocarbamates as Potential Carbon Disulfide Donors

4.2.1 Introduction

Alongside COS and H_2S, carbon disulfide (CS_2) is another interesting sulfur-containing biomolecule, and in fact shares many characteristics with other recognized small molecule bioregulators (SMB).[161] CS_2 is small, nonpolar, and membrane permeable. Much like H_2S, CS_2 was originally dismissed as an environmental toxin, but has been since found to have potential therapeutic effects. And although there is no direct evidence yet for endogenous enzymatic production of CS_2 in mammals, there are ancillary indicators of endogenous production, including high levels of CS_2 on in exhaled breath of patients with a variety of disease states.[162-164] CS_2 is unreactive towards spontaneous hydrolysis in biological systems, yet its electrophilic carbon center is a target for thiols, and it readily inserts into metal ligand bonds to form strongly chelating ligands on enzyme metal centers.[161] The extent to which the potential signaling chemistry of CS_2 mirrors that of other known small biomolecules suggests a need for the development of reliable CS_2 donors to parse out its exact roles in the body, and whether it should be more seriously considered as an SMB.

To this end, there are few known small molecule CS_2 donors in the literature.[165] Previous work in our lab attempted to adapt the self-immolative thiocarbamate scaffold to release CS_2, by exchanging the thiocarbamate oxygen for a sulfur atom to produce dithiocarbamates (DTCM).[127] However, spontaneous direct extrusion of H_2S from the

intermediate dithiocarbamate anion was observed from these donors, a phenomenon enhanced with increasing the electron-withdrawing character of the payload (Figure 4.7a). We envisioned applying the same N-Me mixed thiourea coupling partners used to prepare N-Me thiocarbamates in Chapter 4.1 for the synthesis of N-Me dithiocarbamate CS_2 donors that are not susceptible to competitive H_2S release (Figure 4.7b). Herein we report the synthesis of different N-Me DTCMs and initial attempts to observe CS_2 release from these molecules.

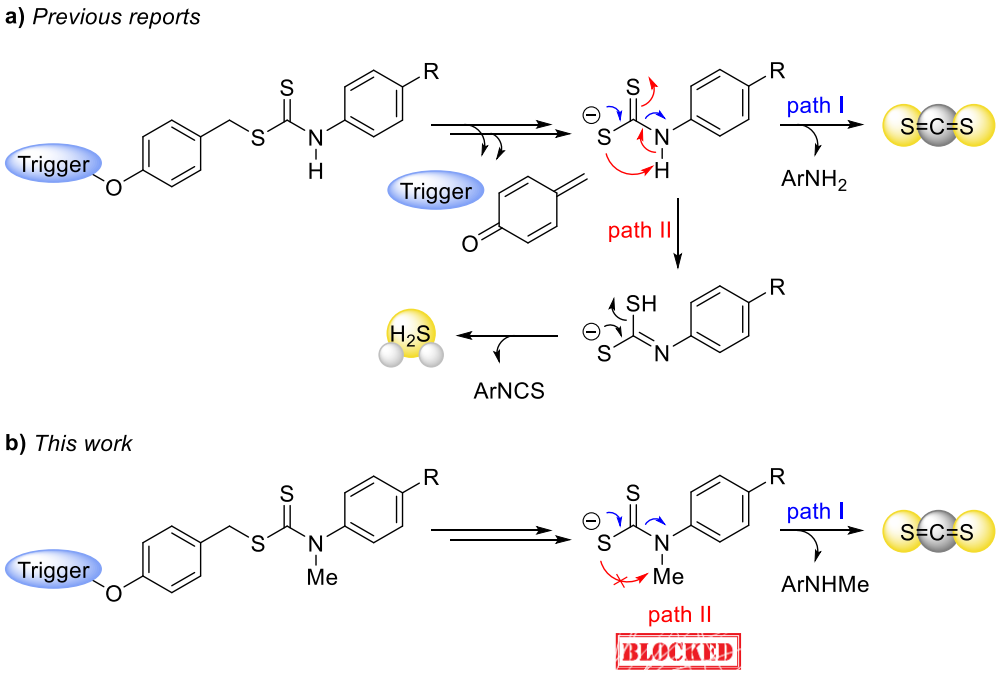

Figure 4.7 (a) Competing pathways for sulfur extrusion from N-H dithiocarbamates. Path I (blue) follows dithiocarbamate collapse to reveal CS_2. Path II (red) involves isomerization of the dithiocarbamate anion followed by direct release of H_2S alongside an aryl isothiocyanate. (b) This work: N-methyl dithiocarbamates as CS_2 donors that cannot directly release H_2S through path II.

4.2.2 Results and Discussion

Although there are a number of reported methods for the detection and quantification of CS_2, these methods present with very high detection limits, often significantly higher than 20 µM, which presents a challenge for measuring CS_2 release form donors at biologically relevant concentrations.[166] Therefore, we designed our initial CS_2 donors to have a payload with an optical response, in order to monitor donor breakdown by the growth of the payload signal. To this end, we selected an N-methyl-4-nitroaniline payload (PNA), which has a UV-vis absorbance maximum at ~ 415 nm.

Our initial CS_2 donor design contained an esterase-triggering motif, analogous to the N-Me TCMs in Chapter 4.1. Starting from 4-hydroxybenzyl alcohol, selective esterification of the phenol followed by bromination of the benzylic alcohol and nucleophilic attack with potassium thioacetate installed the required sulfur atom.[127] Deprotection of the acetate to the free thiol and addition into CP-NO_2 afforded the target donor molecule tBu-DTCM in 64% yield (Figure 4.8). With tBu-DTCM in hand, we attempted to measure PNA formation by UV-vis spectroscopy. A solution of 50 µM tBu-DTCM in PBS 7.4 with 2% DMSO at room temperature was treated with 5 U/mL PLE, and the absorbance spectrum was collected from 250 to 600 nm every two minutes. Unfortunately, over the course of an hour no significant peaks appeared at 415 nm. (Figure 4.9)

To further investigate the ability of N-Me dithiocarbamates to deliver CS_2, we turned to NMR spectroscopy. CS_2 has a distinctive signal in the ^{13}C NMR spectrum at 193 ppm in DMSO-d_6 (Appendix, Figure G.5), which should allow for facile monitoring of CS_2 formation. However, due to the low signal to noise level in the NMR spectrum

after addition of esterase to the system, we sought to exchange the tBu ester trigger for an azide, which can be reduced by a phosphine to initiate a self-immolative cascade. Synthesis of the azide-triggered donor followed the same sequence as for tBu-DTCM,

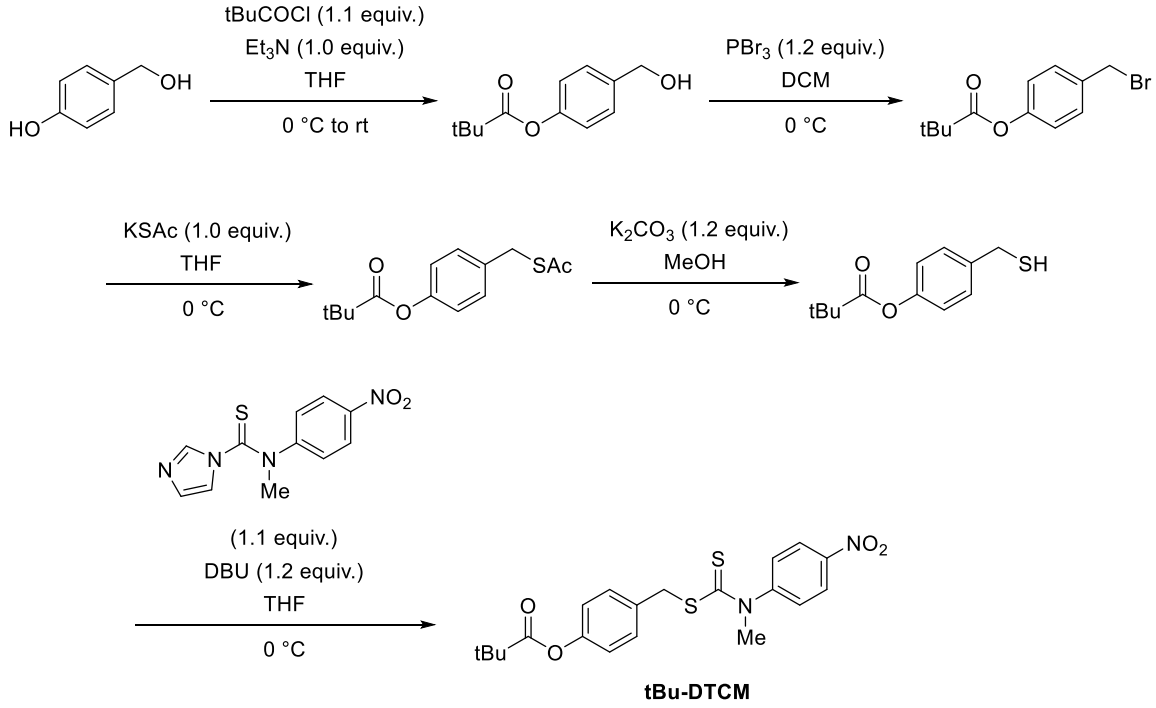

Figure 4.8 Synthesis of tBu-ester triggered p-NO_2 N-Me DTCM CS_2 donor tBu-DTCM.

using 4-azidobenxyl alcohol prepared through a Sandmeyer reaction of 4-aminobenzyl alcohol, instead of 4-(hydroxymethyl)phenyl pivalate (Figure 4.10). With this donor N3-DTCM in hand, we first attempted NMR studies in D_2O/DMSO-d_6 solvent mixtures to more closely mimic a biologically relevant system, but N3-DTCM was insoluble in water mixtures at concentrations required for reasonable NMR experiments. Therefore, NMR spectra were taken in CD_3CN. A baseline ^1H and $^{13}C\{^1H\}$ NMR spectrum was collected of N3-DTCM alone, and then again after addition of excess Et_3P. After 2 hours to allow

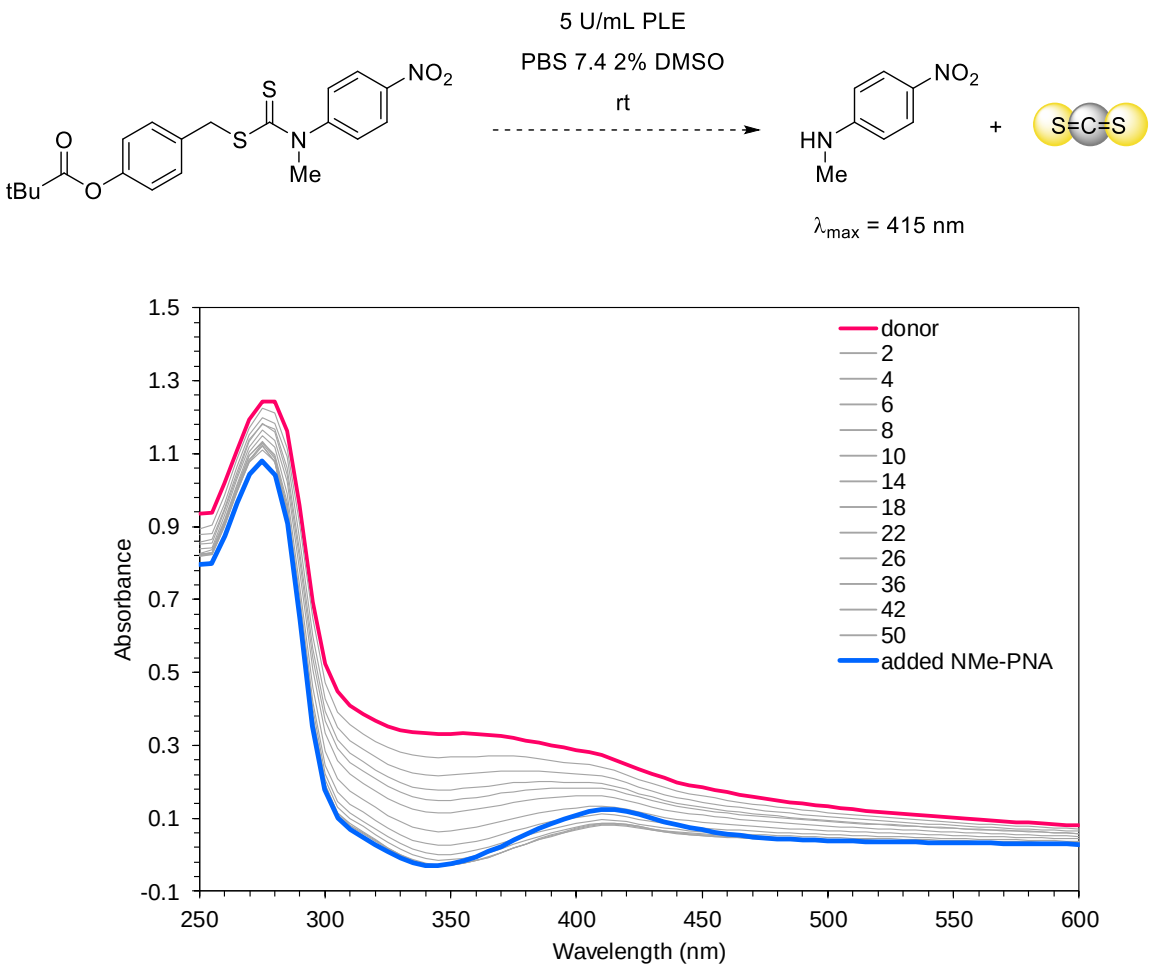

Figure 4.9 Absorbance spectra of 50 µM tBu-DTCM in PBS 7.4 with 2% DMSO at room temperature with 5 U/mL PLE. The pink trace is the initial scan with the donor added, and the blue trace is addition of exogenous PNA after 60 minutes.

for complete reaction of the phosphine with the azide, D_2O was added to cleave the formed iminophosphorane, which should have triggered self-immolation and release of CS_2. By ^1H NMR spectroscopy, it is clear that the azide was reduced to the amine from the upfield shift of the methylene peak, at around 4.5 ppm in the initial scan (Figure 4.11,

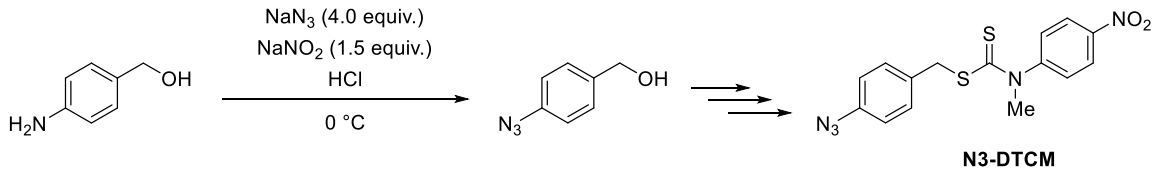

Figure 4.10 Synthesis of azide-triggered N-Me DTCM CS_2 donor N3-DTCM.

top trace) to around 4.32 ppm after addition of Et_3P and D_2O (Figure 4.11). Additionally, the signals from the protons on the azide-appended aryl ring shift significantly upfield upon azide reduction, clearly showing a shift in the electronic nature of the ring. Interestingly, the peaks corresponding to the payload PNA do not deviate an appreciable amount from their initial scan (Figure 4.11). To confirm whether or not N3-DTCM released CS_2 under the NMR reaction conditions, we turned to the $^{13}C\{^1H\}$ NMR spectra (Figure 4.12). While we can observe a change in the spectrum after addition of both Et_3P and D_2O, there are no apparent peaks from 190 – 195 ppm, which would be expected if CS_2 were formed. A small amount of a genuine sample of CS_2 was added to the reaction tube, to see precisely where the carbon signal would appear under these exact conditions, which served to underline that no detectable CS_2 was released throughout the course of the reaction (Figure 4.12).

To gain some insight as to why we could not detect any CS_2 release from the two prepared N-Me DTCM CS_2 donors when analogous COS- and CO_2-releasing (thio)carbamates function as expected, we turned to computational investigations. To probe reaction pathways, all ground state and transition state geometries for carbamate, thiocarbamate, and dithiocarbamate breakdown were fully equilibrated using density functional theory (DFT) as implemented in Gaussian09. The hybrid functional B3LYP

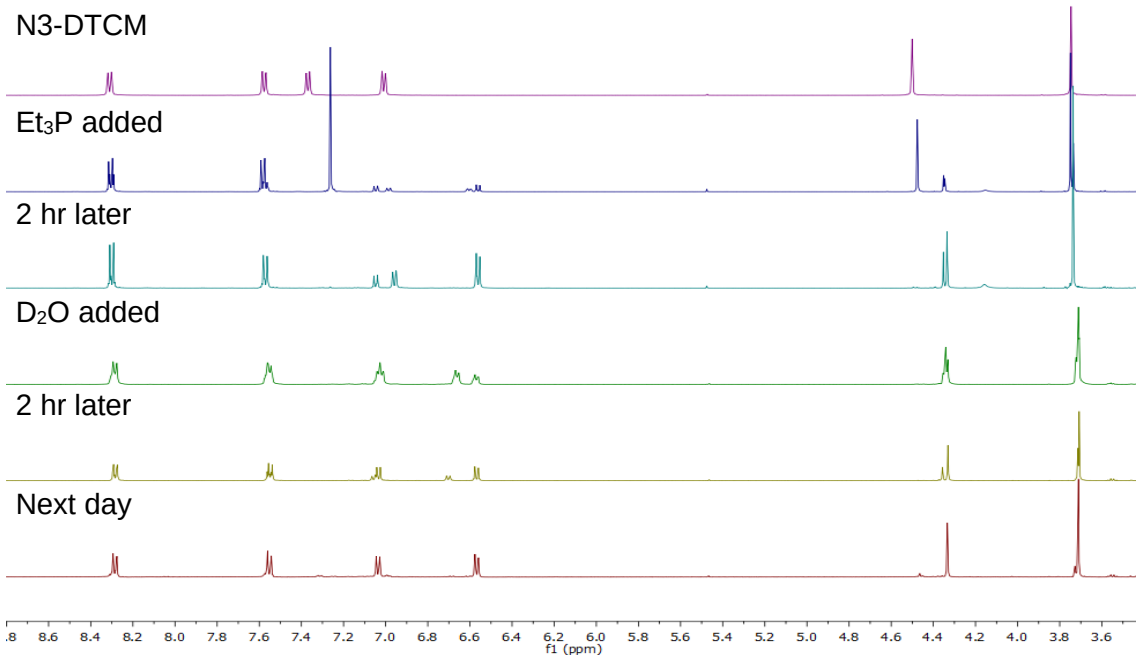

Figure 4.11 Stack of NMR ^{1}H NMR spectra of N3-DTCM in CD_3CN and its reaction with Et_3P and D_2O at various time intervals.

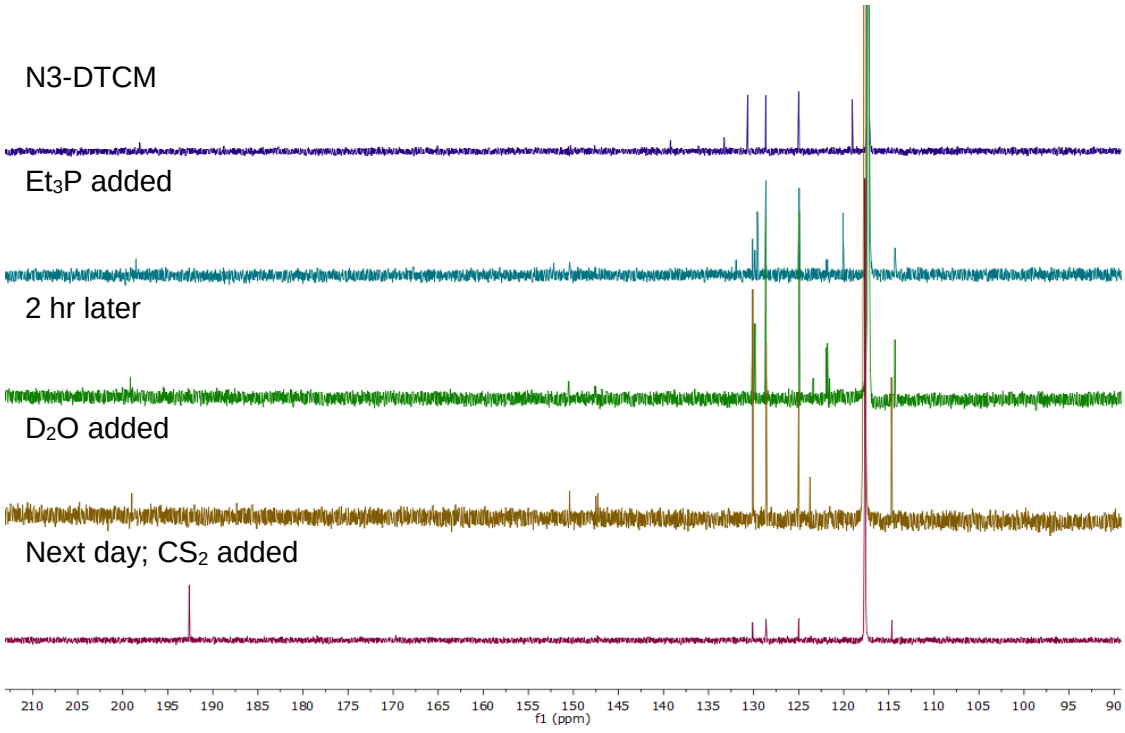

Figure 4.12 Stack of $^{13}C\{^{1}H\}$ NMR spectra of N3-DTCM in CD_3CN and its reaction with Et_3P and D_2O at various time intervals. The bottom spectrum (purple) is the reaction tube with additional exogenous CS_2 added.

was employed in conjunction with the triple-ζ Pople basis set and additional diffuse and polarization functions on all atoms (6-311++G(d,p)) using a superfine grid and tight convergence criteria for all calculations. A self-consistent reaction field was included with the dielectric constant of water using the polarizable continuum model in order to simulate the biological environment.

The calculated relative energies of the intermediates and transition states for CO_2, COS, and CS_2 release from carbamates, thiocarbamates, and dithiocarbamates, respectively, are plotted in Figure 4.13. The phenolate before self-immolation is set equal to zero for each data set. From these data it is clear that while the energies of the phenolate and the carbamate/thiocarbamate anion are relatively similar for the COS and CO_2-releasing systems, in the case of the dithiocarbamate the energy required to extrude CS_2 is almost four times more than CO_2 and five times more than COS. Based on this, we hypothesize that in the case of self-immolative dithiocarbamates, when isothiocyanate extrusion is not possible, self-immolation still occurs, but the subsequent dithiocarbamate anion gets trapped in an energy well, is protonated, or reacts as a nucleophile in an unproductive side reaction, without extruding CS_2. Previous reports of dithiocarbamate anions from the Peter Ford group have shown that even with strongly stabilized leaving groups such as imidazoles as the payload, dithiocarbamate salts are relatively inert under physiological conditions, and require strongly acidic conditions to decompose.[165] These results, taken with the lack of observable CS_2 release by UV-vis and NMR spectroscopy from the N-Me DTCMs studied, suggest that dithiocarbamates are not a suitable platform for CS_2 delivery, and should not be investigated further for that purpose.

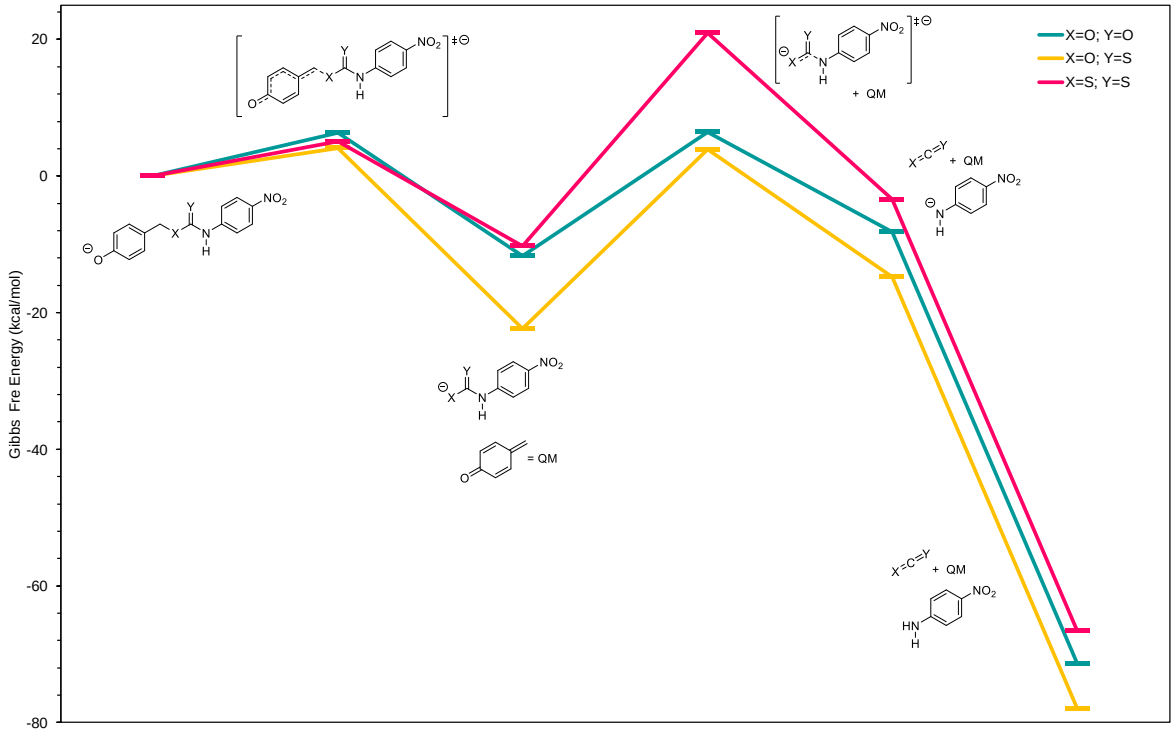

Figure 4.13 Calculated energy coordinate diagram for CO_2, COS, and CS_2 extrusion from self-immolative carbamates, thiocarbamates, and dithiocarbamates, respectively. All ground state and transition state geometries for carbamate, thiocarbamate, and dithiocarbamate breakdown were fully equilibrated using density functional theory (DFT) as implemented in Gaussian09. The hybrid functional B3LYP was employed in conjunction with the triple-ζ Pople basis set and additional diffuse and polarization functions on all atoms (6-311++G(d,p)) using a superfine grid and tight convergence criteria for all calculations. A self-consistent reaction field was included with the dielectric constant of water using the polarizable continuum model in order to simulate the biological environment.

4.2.3 Conclusions

In this chapter we report the synthesis of different types of triggerable N-Me dithiocarbamates, and preliminary investigations into their ability to donate CS_2. We were unable to detect and CS_2 release by NMR spectroscopy or UV-vis spectroscopy. Computational studies indicate that the energy barrier for CS_2 extrusion from the

dithiocarbamate anion is prohibitively high, and that the forward reaction does not proceed without forcing conditions. Thus, we believe that self-immolative dithiocarbamates are not a suitable platform for adaption to CS_2 donation. We expect these results to guide future researchers in their study of CS_2 as a potential small molecule bioregulator.

In Chapter V we expand our work on the development of small molecules for the donation of biologically active sulfur species to the synthesis and study of Memantine-DTS, a COS-releasing prodrug for the treatment of Alzheimer's Disease.

4.2.4 Materials and Methods

Synthesis Materials and Methods: Reagents were purchased from Sigma-Aldrich, VWR, or Tokyo Chemical Industry (TCI) and used as received. Spectroscopic grade, inhibitor-free THF was deoxygenated by sparging with argon followed by passage through a Pure Process Technologies solvent purification system to remove water. Deuterated solvents were purchased from Cambridge Isotope Laboratories and used as received. Silica gel (SiliaFlash F60, Silicycle, 230–400 mesh) was used for column chromatography. ^{1}H, $^{13}C\{^{1}H\}$, and ^{19}F NMR spectra were recorded on a Bruker 500 or 600 MHz instrument (as indicated). Chemical shifts are reported in parts per million relative to residual protic solvent resonances. Mass spectrometric measurements were performed by the University of Illinois, Urbana–Champaign MS facility. All air-free manipulations were performed under an inert atmosphere using standard Schlenk techniques or an Innovative Atmospheres N_2-filled glovebox.

General Procedure for the Synthesis of Benzyl Mercaptans: Trigger-functionalized benzyl alcohol (1.0 equiv.) was dissolved in DCM (0.1 M solution) and cooled to 0 °C and put under an atmosphere of N_2 and equipped with an outlet needle. PBr_3 (1.2 equiv.) was added dropwise, and the reaction was let stir until TLC analysis indicated that the reaction had gone to completion. The reaction mixture was quenched with brine and a dilute aqueous $NaHCO_3$ solution, extracted with DCM, the combined organic layers were dried over anhydrous $MgSO_4$, and purified by silica gel column chromatography. The resulting benzyl bromide was dissolved in THF (0.1 M solution), cooled to 0 °C, and KSAc (1.0 equiv.) was added. The reaction was let stir, monitored by TLC. Upon completion, the reaction mixture was quenched with brine, extracted with EtOAc, dried over anhydrous $MgSO_4$, and purified *via* silica gel column chromatography. The resulting benzyl thioacetate was dissolved in MeOH (0.1 M solution), cooled to 0 °C, and K_2CO_3 (1.2 equiv.) was added. The reaction was let stir at 0 °C until deprotection was complete, as determined by TLC, at which point it was quenched with brine, extracted with EtOAc, dried over $MgSO_4$, concentrated, and brought forward without further purification.

General Procedure for the Synthesis of N-Methyl Dithiocarbamates: Prepared trigger-functionalized benzyl mercaptan (1.0 equiv.) was combined with an N-Me coupling partner (1.1 equiv.) and dissolved in THF (0.1 M solution) at 0 °C under an atmosphere of N_2. DBU (1.2 equiv.) was added slowly, and the reaction was let stir monitored by TLC. Upon completion, the reaction mixture was quenched with brine, extracted with EtOAc, the combined organic layers were dried over anhydrous $MgSO_4$,

and the crude mixture was purified *via* silica gel column chromatography to yield the desired N-Me DTCMs.

Spectroscopy Materials and Methods: UV/Vis spectra were acquired on an Agilent Cary 60 UV/Vis spectrophotometer equipped with a Quantum Northwest TC-1 temperature controller set at 25±0.05 °C.

Computational Methods: Density functional theory (DFT) as implemented in Gaussian09 with the hybrid functional B3LYP and the triple-ζ Pople basis set with diffuse and polarization functions on all atoms (6-311++G(d,p)) was employed to equilibrate all intermediate and transition state structures. A superfine grid and tight convergence criteria were used for all calculations. A self-consistent reaction field was included with the dielectric constant of water using the polarizable continuum model in order to simulate the biological environment. Vibrational analysis was further performed to recover thermodynamic values, including the zero-point energy correction, and to ensure ground state structures each had zero negative frequencies, while all activated complexes had exactly one corresponding to the appropriate bond breaking/forming reaction coordinate.

CHAPTER V

MEMANTINE-DTS AS A COS-RELEASING PRODRUG FOR ALZHEIMER'S DISEASE

This chapter includes unpublished and co-authored material. The project in this chapter was conceived by Carolyn M. Levinn. The experimental work was performed by Carolyn M. Levinn, with feedback from Professor Michael D. Pluth. Biological studies were performed with Professor Mi Hee Lim, Jong-Min Suh, and Eunju Nam at the Korea Advanced Institute of Science and Technology (KAIST). This work is ongoing.

5.1 Introduction

Alzheimer's disease (AD) is a chronic neurodegenerative disease that often leads to dementia, with symptoms progressing from short-term memory loss to disorientation, often accompanied by mood swings, loss of control over bodily functions, and ultimately death.[167] AD is the sixth-leading cause of death in the United States, and that number is increasing dramatically. From 2000 to 2017, the number of deaths from AD have more than doubled, increasing by 145%. This increase comes at a high price – the global cost of AD is estimated to be $605 billion, roughly equivalent to 1% of the entire world's GDP.[168] Despite such remarkable statistics, and an obvious motivation for study, the cause of Alzheimer's disease is not well understood, and there is no known cure or treatment that can stop its progression.[169]

While the cause of AD is not known, recent studies have shown that hydrogen sulfide (H_2S) plays a role in its neuropathology.[167] H_2S is produced endogenously throughout the body from L-cysteine (Cys) and homocysteine (Hcy) by three enzymes: cystathionine β-synthase (CBS), cystathionine γ-lyase (CSE), and 3-mercaptopyruvate sulfurtransferase (3MST) along with cysteine aminotransferase (CAT).[5] The primary source of H_2S in the brain comes from CBS, which is expressed in the hippocampus and cerebellum, although there is 3MST also localized to neurons.[167] AD patients often present decreased levels of *S*-adenosylmethionine,[170] one of the activators of CBS, as well as increased levels of Hcy, a key substrate for CBS.[171] Additionally, measured levels of H_2S and CBS activity are significantly lower in AD patients.[172] Taken together, these findings suggest that H_2S generation is disrupted in the AD brain, and that there is potential for H_2S supplementation to be a therapeutic for AD patients. Indeed, Giuliani and coworkers reported in 2013 that treatment of AD mouse and rat models with H_2S significantly protected against degradation of cognitive function associated with the disease.[173]

With this in mind, we sought to design a prodrug for treatment of AD that would simultaneously release H_2S, or an H_2S equivalent such as COS, alongside the known FDA-approved AD drug memantine.[174] In 2019 the Rapposelli group reported Memit, a memantine prodrug equipped with an isothiocyanate, a functional group known to release H_2S in the presence of thiols (Figure 5.1 left).[175] The researchers were able to demonstrate H_2S release from Memit, but the efficiency was very low with only approximately 1.5 μM of H_2S release from a 1000 μM buffered solution of Memit, which corresponds to a 0.15% efficiency.[175] In this chapter, I report progress toward the

development of Mem-DTS, which is a highly efficient COS-releasing prodrug for the treatment of Alzheimer's Disease (Figure 5.1 right).

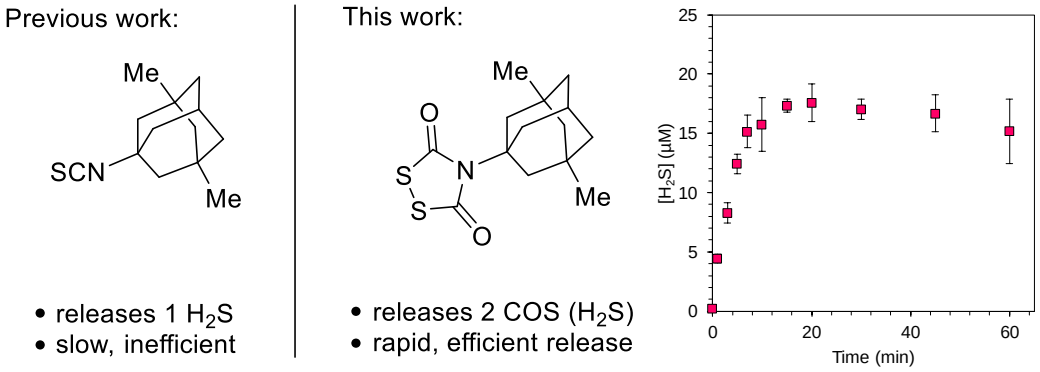

Figure 5.1. Previously reported H_2S-releasing AD prodrug Memit (left). This work with Mem-DTS, a more efficient COS/H_2S-releasing AD prodrug (right).

5.2 Results and Discussion

A new platform for COS-donation with concomitant release of an amine was recently reported by our lab, which proceeds via thiol attack into the persulfide of a dithiasuccinoyl (DTS) to release COS and a sulfenylthiocarbamate, as shown in Figure 5.2a.[176] The sulfenylthiocarbamate can then undergo a second attack by a cysteine release a second equivalent of COS, cystine, and an amine payload. Although there are not easily accessible control compounds for the DTS scaffold, it has the advantage of only releasing a benign disulfide and the amine payload without any electrophilic byproducts. This clean platform of COS/H_2S release is highly desirable for a prodrug designed for the central nervous system, and we envisioned readily adapting it to release memantine.

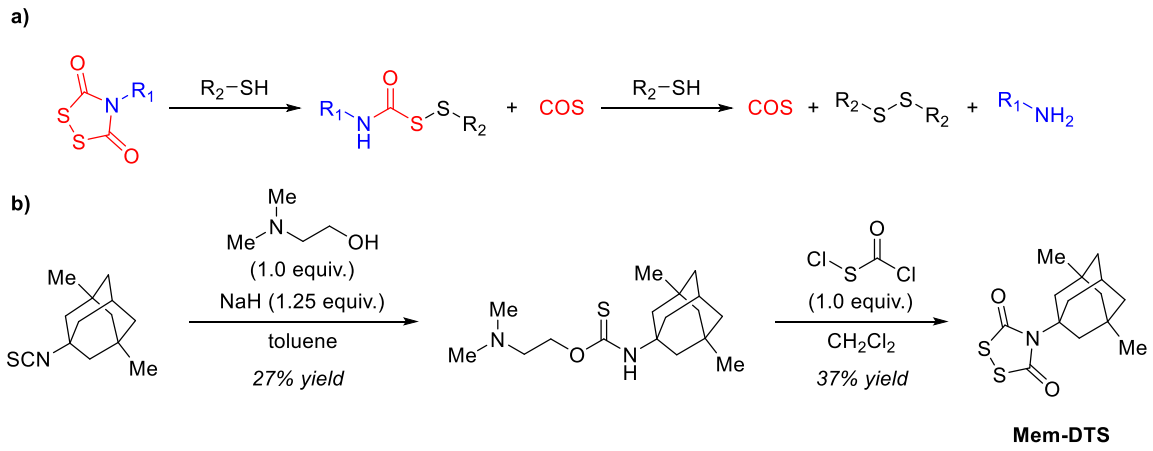

Figure 5.2 (a) Mechanism of COS release from DTS donor compounds. COS can then be rapidly converted to H_2S by the enzyme carbonic anhydrase. (b) Synthesis of **Mem-DTS.**

To prepare **Mem-DTS**, nucleophilic attack of *N*,*N*-dimethylethanolamine into memantine isothiocyanate in the presence of base formed a thiocarbamate intermediate, which was cyclized into **Mem-DTS** upon reaction with chlorocarbonylsulfenyl chloride in a 37% yield (Figure 5.2b). Previous tertiary alkyl dithiasuccinoyl COS donors were prepared in comparable yields,[176] it is likely that nucleophilic attack by the *N*,*N*-dimethylethanolamine into the memantine isothiocyanate is hindered by the steric bulk of the adamantyl scaffold. The viability of **Mem-DTS** as an H_2S donor was then assessed. Treatment of a 25 µM solution of **Mem-DTS** in pH 7.4 PBS buffer with 25 µg/mL of carbonic anhydrase and 20 equivalents of L-Cys at room temperature yielded about 17 µM of H_2S after 20 minutes, which corresponds to an approximately 35% efficiency (Figure 5.3).

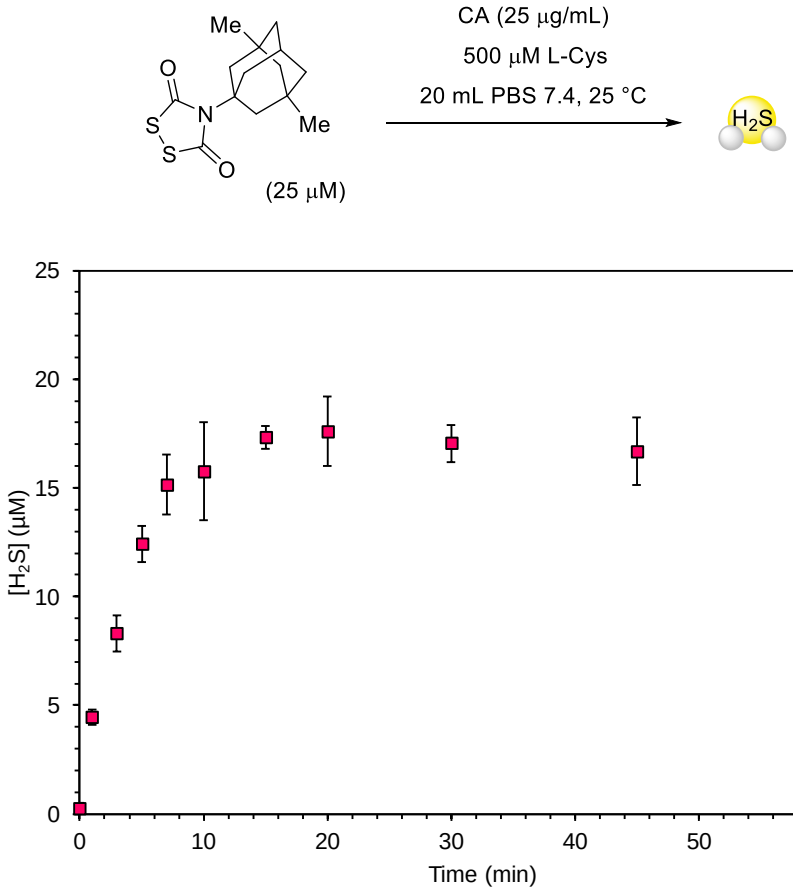

Figure 5.3 H_2S release curve from 25 μM **Mem-DTS** in PBS 7.4 buffer with 20 equiv. L-Cys. Data points are an average of four trials, error bars represent standard deviation across four trials.

Encouraged by these promising H_2S-release curves, we next turned to studying **Mem-DTS** in a biological setting. In collaboration with Professor Mi Hee Lim at the MetalloNeuroChemistry Laboratory at KAIST, we examined the effect of **Mem-DTS** on the toxicity of $A\beta_{42}$ in human SH-SY5Y Neuroblastoma Cells. $A\beta_{42}$ is a beta amyloid peptide that is thought to be a main cause of AD pathogenesis, as it tends to aggregate and form plaques more rapidly than other characteristic Aβ peptides.[177] However, in a suite of experiments with varying incubation times, **Mem-DTS** did not demonstrate any significant ability to recover the toxicity of Aβ in the cell line tested. One possible reason

for why there was no observed effect could be that the second nucleophilic attack by cysteine (or any biological thiol in the case of cell studies) into the sulfenyl thiocarbamate did not occur. Previous computational studies show that this step has a high energy barrier for bulky alkyl amine-derived DTS compounds, which might lead to the memantine not being released.[176] Interestingly however, the memantine control also had no significant ability to reduce the cytotoxicity of $A\beta_{42}$ in human SH-SY5Y cells. These studies are currently still ongoing, and we anticipate reporting the outcomes in the near future.

5.3 Conclusions

In conclusion, we have reported the synthesis and study of **Mem-DTS**, an H_2S-releasing prodrug for the treatment of AD. While there was no protective effect of **Mem-DTS** found against $A\beta_{42}$ in human SH-SY5Y cells, **Mem-DTS** did demonstrate rapid and efficient COS release, and studies into this compound as a potential therapeutic are ongoing. These results will guide our lab's future research on COS-releasing H_2S donors, as we move to adapt that platform for more in-depth and targeted biological applications.

Chapters II through V have described research into the development and mechanistic understanding of COS donors, which we hope will enable biologists to more precisely study the effects of H_2S in biological systems. Chapter VI provides an introduction to another important tool in the gasotransmitter research: fluorescent and optical response probes for visualizing H_2S *in vivo* and *in vitro*.

5.4 Experimental

Synthesis Materials and Methods: Reagents were purchased from Sigma-Aldrich, VWR, or Tokyo Chemical Industry (TCI) and used as received. Spectroscopic grade, inhibitor-free THF was deoxygenated by sparging with argon followed by passage through a Pure Process Technologies solvent purification system to remove water. Deuterated solvents were purchased from Cambridge Isotope Laboratories and used as received. Silica gel (SiliaFlash F60, Silicycle, 230–400 mesh) was used for column chromatography. ^{1}H, ^{13}C{^{1}H}, and ^{19}F NMR spectra were recorded on a Bruker 500 or 600 MHz instrument (as indicated). Chemical shifts are reported in parts per million relative to residual protic solvent resonances. Mass spectrometric measurements were performed by the University of Illinois, Urbana–Champaign MS facility. All air-free manipulations were performed under an inert atmosphere using standard Schlenk techniques or an Innovative Atmospheres N_2-filled glovebox.

Synthesis of Mem-DTS: In a flame-dried round bottom flask under nitrogen, sodium hydride (1.25 equiv) and *N* ,*N*-dimethylethanolamine were added to anhydrous toluene (20 mL). After stirring briefly until gas evolution ceased, Memantine isothiocyanate (1.0 equiv) was added dropwise. The reaction was stirred at room temperature for 3 h under nitrogen, quenched with H_2O, and extracted with EtOAc. The combined organic layers were washed with brine, dried over anhydrous $MgSO_4$, and purified by column chromatography. The resulting thiocarbamate was brought through to form Mem-DTS. To a flame-dried round bottom flask under N_2, chlorocarbonylsulfenyl chloride (1.0 equiv) was added to anhydrous DCM (20 mL). In a separate vial, the preformed

thiocarbamate (1.0 equiv) was dissolved in anhydrous DCM (1 mL) and added dropwise to the reaction. The reaction mixture was stirred at room temperature for 1 h, after which it was quenched with 1 M HCl (15 mL). The organic layer was separated and washed with deionized water and brine. The resultant organic layer was dried over anhydrous $MgSO_4$ and purified *via* preparative thin layer chromatography (1:1 DCM:Hex) to yield 302 mg of a colorless oil (37% yield). ^{1}H NMR (500 MHz, $CDCl_3$) δ (ppm): 2.33 (d, *J* = 3.33 Hz, 2H), 2.27 (p, *J* = 3.33 Hz, 1H), 1.46 (dt, *J* = 2.90, 12.55, 2H), 1.33 (dd, *J* = 2.90, 12.55, 2H), 1.25 (dt, *J* = 2.90, 12.55, 1H), 1.19 (d, *J* = 12.55, 1H), 0.91 (s, 6H). ^{13}C{^{1}H} NMR (151 MHz, $CDCl_3$) δ (ppm): 168.84, 72.22, 50.03, 44.68, 42.17, 37.48, 33.46, 30.88, 30.23.

H_2S Detection Materials and Methods: Phosphate buffered saline (PBS) tablets (1X, CalBioChem) were used to prepare buffered solutions (140 mm NaCl, 3 mm KCl, 10 mm phosphate, pH 7.4) in deionized water. Buffer solutions were sparged with nitrogen to remove dissolved oxygen and stored in an Innovative Atmosphere nitrogen-filled glovebox. Donor stock solutions (in THF) were prepared inside a nitrogen-filled glovebox immediately before use. L-Cys stock solutions (in PBS) were freshly prepared in an N_2-filled glovebox immediately before use. CA stock solutions (in PBS) were freshly prepared in a nitrogen-filled glovebox immediately before use.

General Procedure for Measuring H_2S Release with the Methylene Blue Assay (MBA): Scintillation vials containing 20 mL of 10 mm PBS (pH 7.4) were prepared in a nitrogen-filled glovebox. To these solutions, 50 µL of 10 mg mL^{-1} CA and 50 µL of a 20 mM

THF donor stock were added for final concentrations 25 μg mL^{-1} and 50 μM, respectively. Immediately prior to L-Cys addition, 0.5 mL solutions of methylene blue cocktail were prepared. The methylene blue cocktail solution contains: 200 μL of 30 mm $FeCl_3$ in 1.2 m HCl, 200 μL of 20 mm N,N -dimethyl-*p*-phenylene diamine in 7.2 m HCl, and 100 μL of 1 % (w/v) $Zn(OAc)_2$. To begin an experiment, 20 equivalents of an L-Cys stock solution in PBS 7.4 was added for a final concentration of 500 μm. At set time points after the addition of L-Cys, 500 μL reaction aliquots were added to the methylene blue cocktail solutions and incubated for 1 h at room temperature shielded from light. Absorbance values at 670 nm were measured 1 h after addition of reaction aliquot. Each experiment was performed in quadruplicate unless stated otherwise. UV/Vis spectra were acquired on an Agilent Cary 60 UV/Vis spectrophotometer equipped with a Quantum Northwest TC-1 temperature controller set at 25±0.05 °C. It is noteworthy that dithiasuccinoyls are not stable in DMSO.

CHAPTER VI

INTRODUCTION TO REACTION-BASED H_2S DETECTION METHODS AND H_2S PROBES

Alongside the expansion of the H_2S donor toolbox as discussed in Chapter 2, there has been extensive research into the development of novel reaction-based optical readout H_2S probes over the past decade. This topic has been the subject of numerous extensive and comprehensive reviews, and so will only be briefly surveyed in this introduction.[178-181] The general design principle for reaction-based probes involves a functional group on the probe that reacts selectively with the analyte of interest over other small molecules that might be present in the system, which triggers the release or turn on of some optical readout moiety, such as a fluorophore or luminophore (Figure 6.1).[178] The most widely studied and utilized optical response has been fluorescence, although much progress has been made in bio- and chemiluminescence, as well as photoacoustic detection. The key advantage of these systems over other common approaches for detection and/or quantification, such as the methylene blue assay or H_2S-selective electrodes, is the compatibility of reaction-based probes with live cell applications. Fluorescent and luminescent probes can be used directly in live animals and cells without destroying the specimen in study, which allows researchers to monitor and detect transient reactive species *in vivo*.

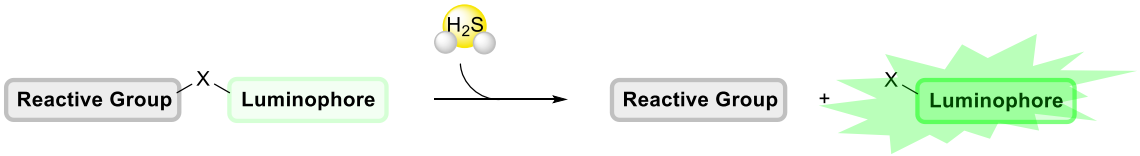

Figure 6.1 General principle for turn-on reaction based H_2S probe design: a luminophore is quenched, and upon selective reaction with H_2S or HS^-, the luminophore is released and an optical response is observed.

The inherent chemistry of H_2S makes this small molecule amenable to a diverse array of detection motifs. H_2S is a weak acid with a pK_a of 7.0 and under physiological conditions 80% of this molecule exists as HS^-, which is a potent nucleophile. Additionally, H_2S/HS^- is redox active, interacting with the sulfane-sulfur pool in biology, and can strongly chelate or ligate different metal centers.[5] Exploiting these properties, researchers have designed a wide variety of reaction-based triggers for this analyte, ranging from electrophilic triggers and copper metal-based triggers to reduction-based triggers.

The most common motif employed in fluorescent or luminescent reaction-based H_2S probes is azide reduction.[178] In these systems, a fluorogenic amine is masked as an azide, which decreases electron delocalization, rendering the molecule non-emissive. Exposure to H_2S reduces the azide to an amine, which in many cases can be coupled to a fluorescent turn on by judicious choice of fluorophore. Due to the ease of installation and the prevalence of fluorophores with key pendant amines, aryl azide-based H_2S probes have found widespread use in biological studies. However, in 2015 our group reported a detailed mechanistic study of the azide reduction by H_2S, which revealed that this process consumes two equivalents of HS^-, and releases hydrogen disulfide (H_2S_2), which can go on to further react with biological thiols and perturb thiol equilibria.[182] Additionally, although azides are often considered as 'biorthogonal' functional groups, and have gained

notoriety in the copper catalyzed azide-alkyne 'click' reaction in chemical biology,[183] there have also been reports of azide reduction by cytochrome P450, which can lead to false responses.[184] Despite these drawbacks, azide-based H_2S probes have seen some of the most widespread use, and many specialized systems have been developed, such as the cell-trappable SF7-AM, which have enabled high quality localized cell imaging of H_2S donors, greatly advancing the field.[185]

Electrophilic probes for H_2S have also gained momentum over the past five years, largely due to the diversity in accessible and suitable electrophilic motifs. Such electrophilic groups include dinitrophenyl (DNP) ether and nitrobenzoxadiazole (NBD) triggers, which react *via* a nucleophilic aromatic substitution (S_NAr) mechanism, as well as disulfide, diselenide, selenylsulfide, sulfonate, sulfonamide, sulfoxide, vinyl chloride, and aldehyde triggers, among others (Figure 6.2).[178] From this laundry list of groups that react with H_2S/HS^-, it is obvious why there are so many probes that rely on the nucleophilicity of this analyte. One challenge however with electrophilic recognition systems is that there are many highly nucleophilic biomolecules, and selectivity for just H_2S/HS^- can be difficult to achieve, and these probes can be susceptible to false positives from hydrolysis and other biological nucleophiles.

Lastly, the third most common method for reaction-based H_2S sensing is through copper chelation and precipitation. Paramagnetic Cu(II) can accept the excited state electrons of many fluorophores, and so when complexed to Cu^{2+}, organic chelators quench nearby covalently attached fluorophores. Exposure to H_2S results in CuS formation and precipitation, liberating the fluorophores to create a turn-on response.[181] Similarly, there have also been fluorescent probes reported in which Cu or other metal

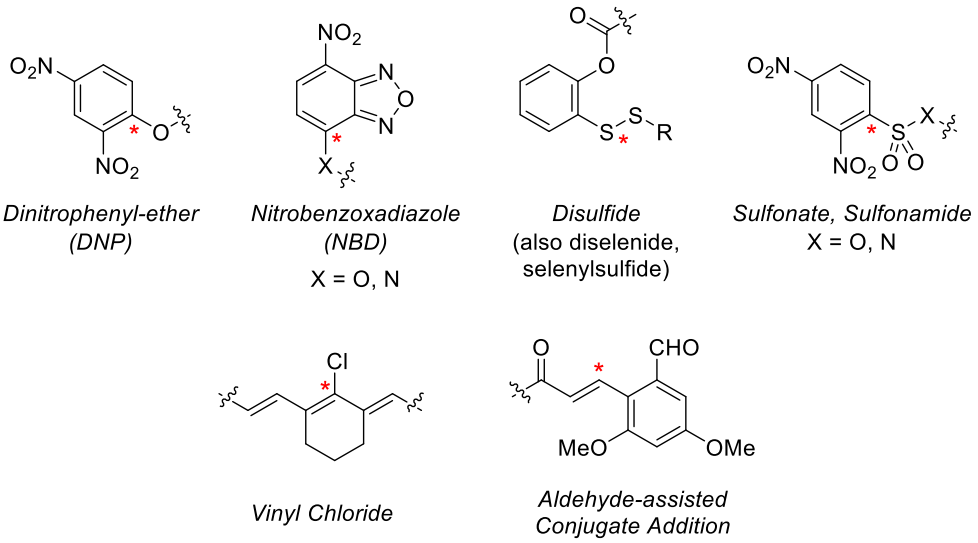

Figure 6.2 Common electrophilic functional groups and motifs used in luminescent probes for H_2S. The sites of nucleophilic attack by HS^- are marked in red.

chelation keeps the probe in a turned-on state, which is then turned off when exposed to H_2S to generate the metal sulfide product. Although Cu-based H_2S probes show a lot of promise, they have not seen widespread adoption in mainstream biological studies of H_2S, and have the potential to react with other cellular reductants.

Contrasting the significant diversity in the triggering motifs for H_2S probes, there is notably less variation in the actual optical response scaffolds. When focusing on fluorescent probes, the vast majority of H_2S detection molecules rely on the same few scaffolds: coumarin,[186] BODIPY,[187] fluorescein and rhodamine,[188] cyanine,[189] dansyl,[190] and naphthalimide[191] dyes for fluorescence; and luminol,[192] luciferin,[193] and Schaap's dioxetane[194] for chemi- and bioluminescence. The most recently discovered fluorophore that has seen widespread adoption in sensing technologies is the BODIPY system, which was discovered in 1968, but has really earned increasing interest over the last three

decades.[187] Prior to BODIPY, most fluorophores and luminophores had been known since the early 1900's.

The research presented in Chapter 8 aims to challenge that fluorophore status quo, introducing nanohoop rotaxanes as turn-on fluorescent probes for H_2S. These probes rely on the photophysical properties of carbon nanohoops, a novel class of fluorophore. Chapter 7 on the other hand discusses the comparison of two distinct H_2S detection motifs – aryl azides (reduction-based) and 2,4-dinitrophenol (nucleophilic attack-based) – on a bright chemiluminescent core scaffold in the development of an improved chemiluminescent probe that can selectively detect H_2S in aqueous systems.

CHAPTER VII

A DIRECT COMPARISON OF TRIGGERING MOTIFS ON CHEMILUMINESCENT PROBES FOR HYDROGEN SULFIDE DETECTION IN WATER

This chapter contains previously unpublished coauthored work. This manuscript was written by Carolyn M. Levinn and edited by Professor Michael D. Pluth. The project in this chapter was conceived of by Carolyn M. Levinn and Professor Michael D. Pluth. The experimental work in this chapter was performed by Carolyn M. Levinn.

7.1 Introduction

Hydrogen sulfide (H_2S) is the third recognized gasotransmitter and an important biomolecule,[3, 195] with roles in cardio-[196] and neuroprotection,[197] wound healing,[198-199] and mitigating oxidative stress and associated damage.[200-201] As brief examples of these biological roles, H_2S-producing enzymes are found to be overexpressed in diabetic rat models, with subsequent inhibition of enzymatic H_2S production resulting in reduced hyperglycemia.[202] Conversely, in rat models of Parkinson's disease (PD), brain H_2S levels are significantly lower than healthy control animals, and treatment with exogenous NaSH reverses the progression of PD symptoms.[144, 203-204] These and other diverse roles of H_2S in biological systems have motivated the development of chemical tools for detection and delivery of H_2S and related reactive sulfur species. New approaches for detection and quantification have expanded in the last decade, with novel fluorescent

probes providing front-line methods for imaging and measuring changes in biological H_2S levels in cell culture, as well as more complex, experiments.[181, 205] Complementing fluorescent probe design and deployment however, other approaches for H_2S detection and imaging are needed to investigate and disentangle the roles of H_2S in more complex systems.[154, 206]

Parallel to fluorescent probe development, chemiluminescent probes provide an alternative approach for biological imaging that often results in lower background signals and greater tissue penetration due to the lack of excitation requirements.[207-208] In addition, the lack of an external excitation source leads to reduced autofluorescence, photobleaching and phototoxicity, and background interference. Chemiluminescent platforms utilize a chemical reaction that generates an excited state intermediate, which emits photons upon relaxation back to ground state. Similarly, bioluminescent probes require enzymatic activation to generate a luminescent response, with the most common example being the luciferin / luciferase platform.[209] These favorable properties have led to the wide adoption of chemiluminescent and bioluminescent probes as important tools for bioimaging and biochemical studies.[210-213] Demonstrating the diversity of this approach, prior probes have been developed for a wide array of small biomolecules, including hydrogen peroxide,[214] singlet oxygen,[215] formaldehyde,[216] nitroxyl,[217] as well as other analytes.

When compared to the number of fluorescent probes developed for H_2S detection, there are relatively few chemiluminescent or bioluminescent methods. The first report of chemiluminescent H_2S detection was described by our group in 2013, in which H_2S-mediated azide reduction was used to generate luminol.[218-219] Early bioluminescent H_2S

probes based on caged-luciferin were reported by Lu and Li in 2015 and also leveraged H_2S-mediated azide reduction to trigger the response.[220-221] In 2014, the first chemiluminescent probe for H_2S based on Shaap's dioxetane[222] was reported by Sozmen and coworkers, and utilized the H_2S-responsive 2,4-dinitrophenol-based S_NAr trigger. This probe, however, required harsh basic conditions (pH 12) to generate a chemiluminescence response, which significantly limited potential applications in biological applications.[223] More recently, in 2015 the Lippert group reported a similar dioxetane-based chemiluminescent H_2S probe, with electronegative substituents ortho to the phenoxide, that utilized H_2S-mediated azide reduction to initiate a 1,6-self-immolative decay to reveal the luminogenic phenoxide. These probes alone only displayed a moderate chemiluminescent signal under biologically relevant conditions, but the signal could be enhanced by the addition of 20% Emerald II Enhancer, a surfactant-dye adduct that red-shifted and amplified the luminescence, to result in up to a 400-fold turn-on response (Figure 7.1a).[224] Motivated by the scarcity of chemiluminescent probes for H_2S detection, we report here the preparation and direct comparison of two H_2S probes with distinct triggering mechanisms on a bright platform for chemiluminescent imaging in aqueous systems (Figure 7.1b).

7.2 Results and Discussion

To compare the efficacy of different H_2S sensing strategies, we chose to use the bright chemiluminescent dioxetane platform recently reported by the Shabat lab.[194] This luminophore contains a slightly deactivating chloride ortho to both the phenol and the dioxetane, as well as an extended strongly electron-withdrawing group para to the

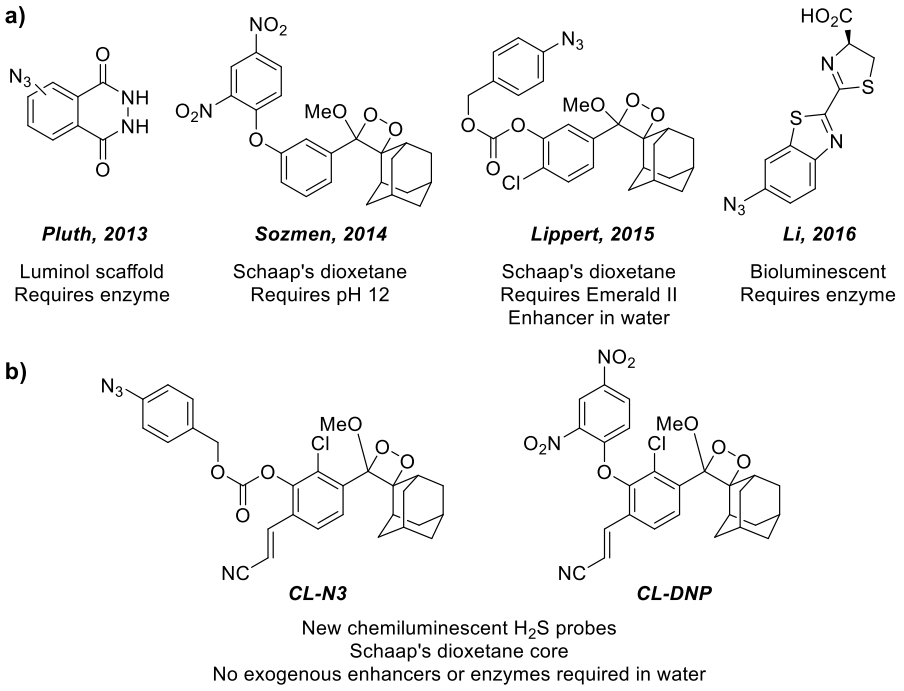

Figure 7.1. a) Selected examples of prior chemiluminescent or bioluminescent H_2S probes. b) This work: two novel dioxetane-based chemiluminescent probes for H_2S with distinct triggering mechanisms.

dioxetane and is almost 1000x brighter than previous related cores.[224-225] Although azide reduction is a more common approach to H_2S detection, the rate of this reaction is often slower than S_NAr-based detection methods.[226] Based on these considerations, we focused our approach to include the H_2S-responsive azide and 2,4-dinitrophenol (DNP) groups, which undergo H_2S-mediated reduction to the parent amine and nucleophilic aromatic substitution, respectively. Key distinctions between these are that the S_NAr based triggering system requires only one equivalent of H_2S to initiate luminescence,[227] whereas reduction of an azide requires two equivalents, and releases polysulfides, which are biologically-relevant reactive sulfur species.[182] Also, the most common linker for the azide is a 4-azido benzyl alcohol tethered with a carbonate, the self-immolation of which

releases a para amino-quinone methide, which could potentially react with nucleophiles. (Figure 7.2a).

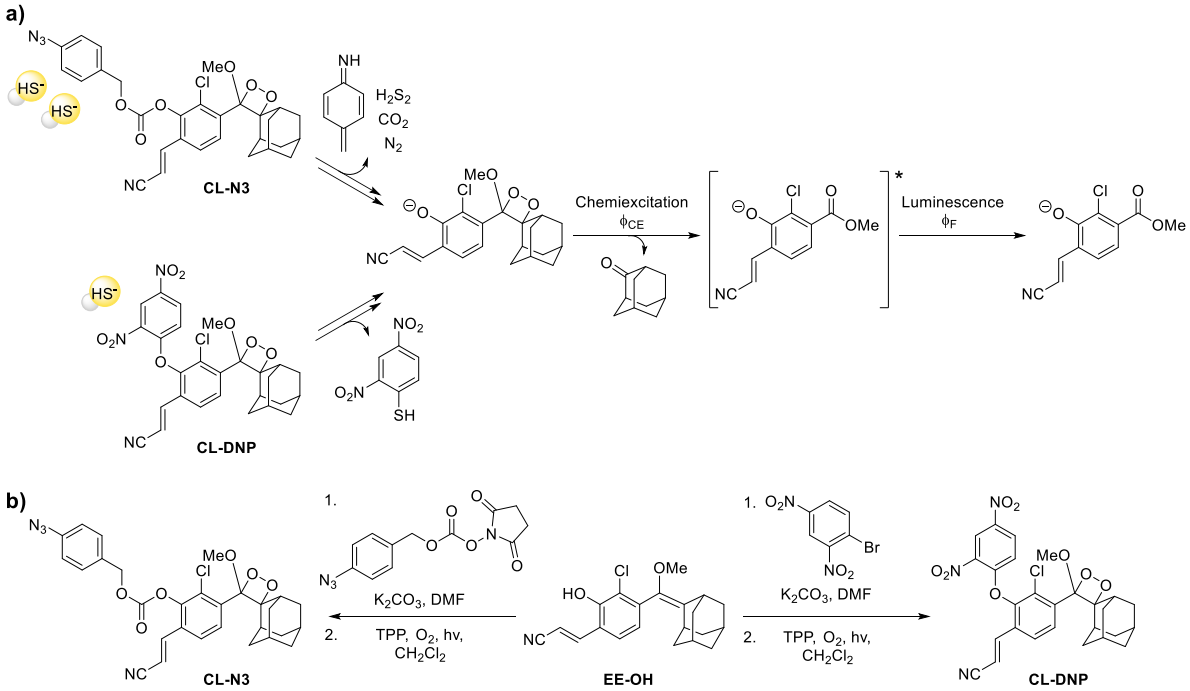

Figure 7.2. a) Mechanism and byproducts of H_2S-mediated turn-on of chemiluminescent probes **CL-N3** and **CL-DNP**. b) Synthesis of the two probes **CL-N3** and **CL-DNP** from a known phenol intermediate, **EE-OH**.

To prepare these chemiluminescent probes, we reacted H_2S-responsive motifs with the previously-reported enol-ether phenol core **EE-OH**,[194] followed by singlet oxygen oxidation (Figure 7.2b). We initially used the Acid Red/Rose Bengal photosensitizer system for singlet oxidation step, which has been used previously in the presence of azides,[228] but were unable to access clean alkene oxidation without azide photoreduction. We found, however, that using tetraphenyl porphyrin (TPP)[229] as the photosensitizer allowed for the reaction to be run in CH_2Cl_2, which slows the decay of the generated singlet oxygen, reduces the reaction time, and decreases the amount of azide

decomposition from light exposure.[230] These same photooxidation conditions were also used to prepare **CL-DNP**. We note that the final DNP product is significantly less photosensitive than **CL-N3**, which enabled greater scalability and a 76% yield over two steps compared to the 16% yield for the azide system.

Having prepared the two target probes, we next measured the chemiluminescent response from the reaction of **CL-N3** and **CL-DNP** with H_2S. We first measured the response in organic solution to eliminate potential complications with solubility, aggregation, or quenching in water. Our expectation was that the rate difference between **CL-N3** and **CL-DNP** would be smaller in water due to prior reports demonstrating the enhanced rate of H_2S-mediated azide reduction in organic solution, which compared on aqueous systems.[182] Upon treatment of a 25 μM solution each probe with 100 equivalents of NaSH in THF we observed a significant increase in luminescence. Over the course of 30 minutes, the **CL-N3** probe resulted in a luminescence turn on of more than 2600-fold, which was larger than the approximately 1450-fold luminescence turn on for **CL-DNP** (Figure 7.3a, and Appendix F). Prior reports of a suite of chemiluminescent probes for the detection of cathepsin B have similarly shown that altering the triggering motif while maintaining the same dioxetane core can significantly impact the rate of probe activation, which was attributed to differences in solubility.[231] In this case, however, the difference in observed emission from **CL-N3** and **CL-DNP** is likely due to the absorbance of the 2,4-dinitrothiophenol produced (λ_{max} = 450 nm)[232] generated from **CL-DNP**, which overlaps with the probe emission spectrum.

Having demonstrated that both the azide- and DNP-based probes function in THF, we next investigated the chemiluminescent responses in buffered aqueous conditions.

Upon addition of **CL-N3** to degassed PBS buffer, we were surprised to observe a moderate, but almost immediate, increase in luminescence, even prior to the addition of NaSH. with an over 3000 intensity unit jump. This reproducible result suggests that the triggering group on **CL-N3** may be unstable under aqueous conditions, possibly due to hydrolysis at the electrophilic carbonate, which limits the suitability of this probe for use in more complex biological imaging studies (Figure 7.3b, inset). Due to the un-triggered turn on of **CL-N3** in PBS 7.4, the normalized turn-on response of **CL-N3** with 100 equiv. of NaSH relative to with no analyte added was only 7-fold. By contrast, the **CL-DNP** probe appeared to be stable in PBS 7.4 buffer, with the 100-fold increase in luminescence only observed upon NaSH addition (Figure 7.3b).

Based on the greater stability of **CL-DNP** and significant luminescent response, we next carried out selectivity studies to confirm that the primary response is observed for H_2S. In these experiments, we treated **CL-DNP** with 100 equivalents of different analytes at 37 °C and measured the integrated luminescence response over 30 minutes. As expected, we observed a significant luminescence response for H_2S, with high selectivity over GSH, Cys, and Lys (Figure 7.4a). We chose to limit our selectivity investigations to these analytes due to the significant body of prior work in the literature that has demonstrated that primary cross-reactivity can occur with other biological nucleophiles, whereas little or no reactivity of the DNP group is observed with other potential biological reactants, including metal ions, reactive oxygen species, and reducing agents.[179, 233] For comparison, we have also included the integrated response in THF under identical conditions, which shows significant increase in overall luminescent signal.

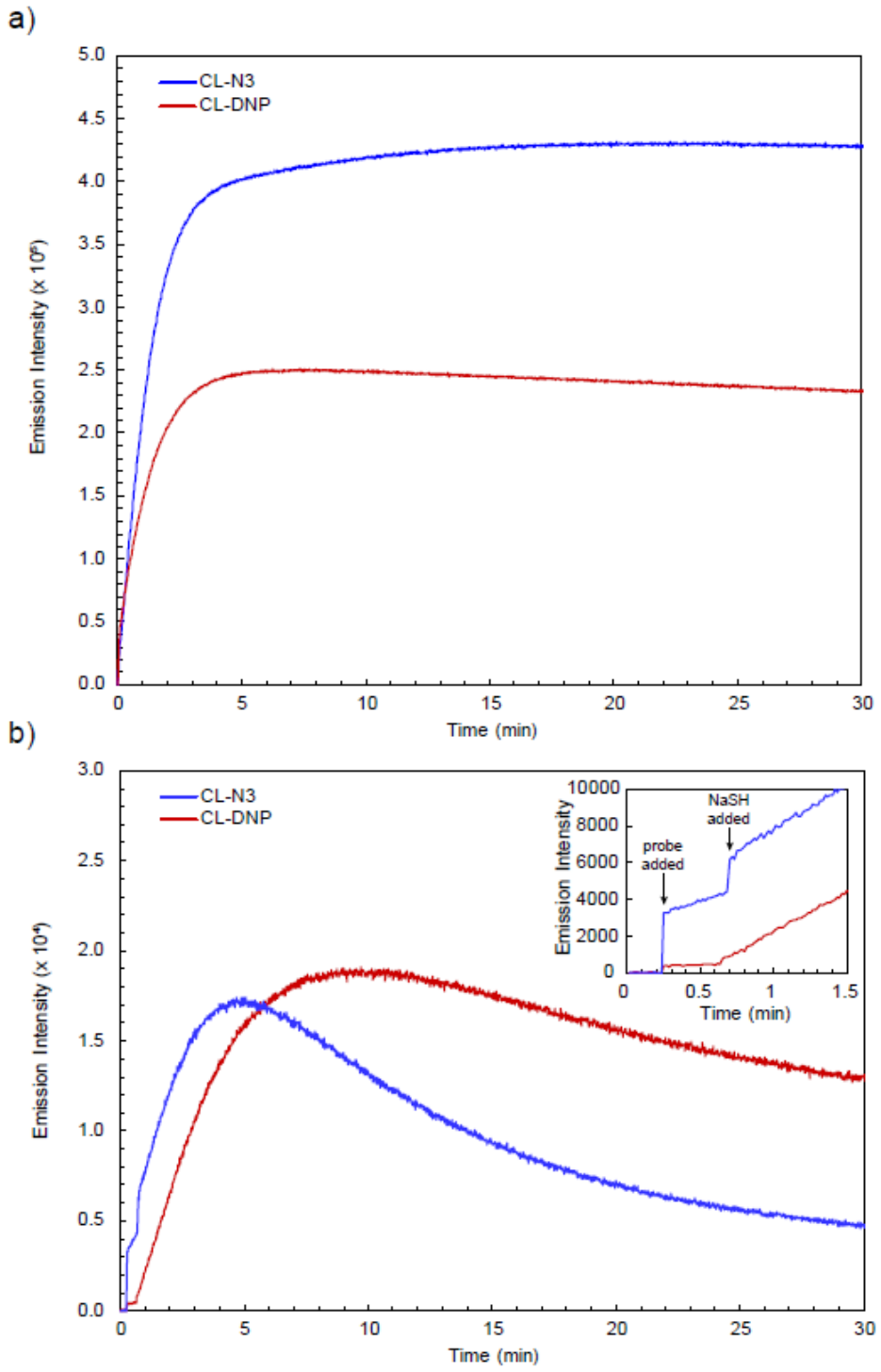

Figure 7.3. a) Luminescent response of 25 µM solutions of **CL-N3** and **CL-DNP** in THF to 100 equiv. of NaSH over 30 minutes at 37 °C. b) Luminescent response of 25 µM solutions of **CL-N3** and **CL-DNP** in degassed 10 mM PBS 7.4 buffer with 5% DMSO to 100 equiv. of NaSH over 30 minutes at 37 °C. The inset shows the first 1.5 minutes of the experiment. The probe was added after about 20 seconds, and the NaSH was added after about 40 seconds, as denoted in the plot.

Notably, this probe does not require an enzyme activator nor exogenous luminescence enhancer to function in aqueous environments.

Additionally, the average integrated chemiluminescent response to varying concentrations of H_2S in buffer was assessed, with ratios ranging from zero to 167 equivalents of NaSH. Even at less than 10 equivalents of exogenous NaSH, there is an integrated 9.0 x 10^6 turn-on response relative to the background signal over just 30 minutes. (Figure 7.4b) At lower concentrations of NaSH, it is likely that the triggering S_NAr reaction is not fully complete after 30 minutes, resulting in a lower integrated emission than expected.

7.3 Conclusions

In summary, we have reported two bright chemiluminescent probes for H_2S detection that function without the need of brightness enhancers, surfactants, or enzyme activation. We demonstrated that the more commonly used azide-trigger displayed moderate autoactivation of the probe, which suggests instability in aqueous conditions in this system. In contrast, the DNP-triggered probe is more stable and synthetically accessible, and is selective for H_2S over other biological nucleophiles. In a broader context, aryl azides can be reduced to the parent amine by the by cytochrome P450 enzymes,[184] whereas DNP groups are unlikely to be similarly triggered. These factors suggest that alternative approaches to the commonly used azide-reduction strategy may be more fruitful in biological settings. While we cannot conclude that these results are necessarily representative of a general trend for all azide and DNP-triggering events, they do indicate that certain triggering mechanisms might not be cleanly translatable across

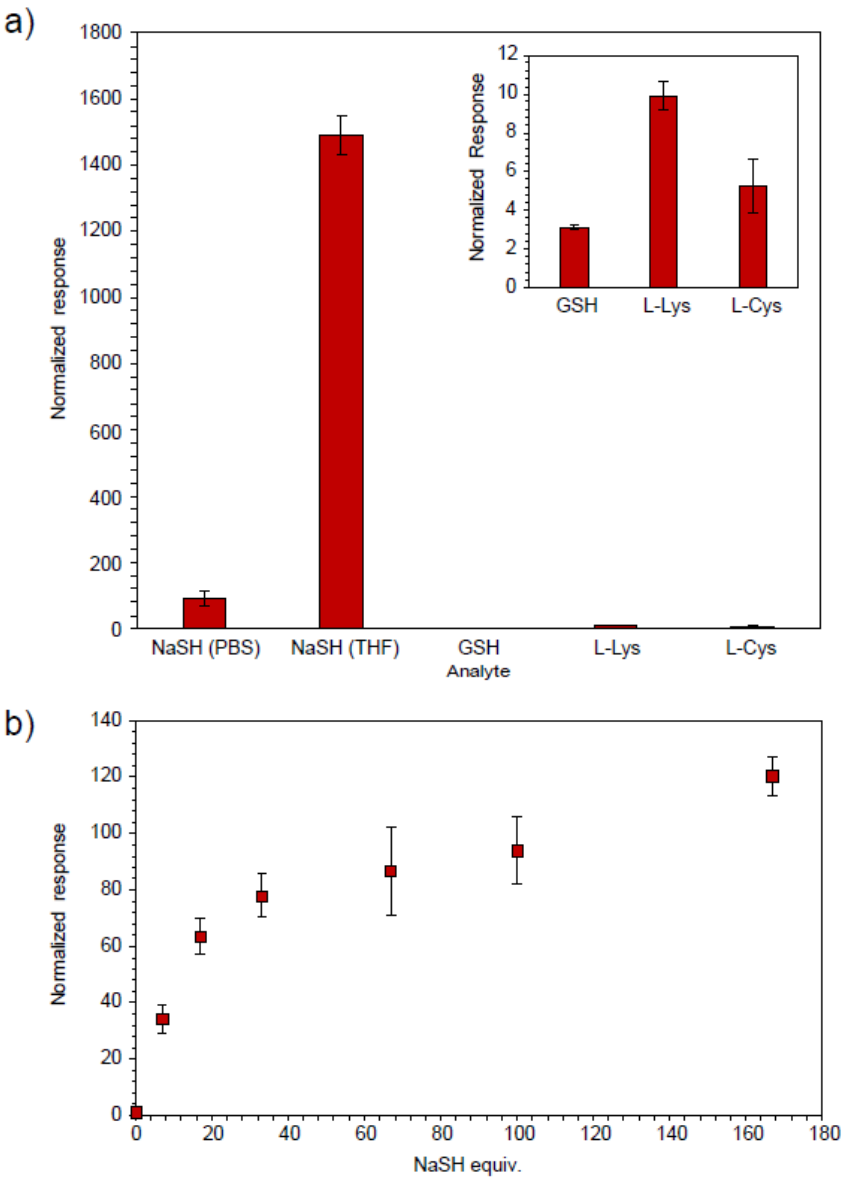

Figure 7.4. a) Selectivity studies for **CL-DNP**. The THF trial was performed in air-free unstabilized THF at 37 °C with 100 equivalents of NaSH and integrated over 30 minutes. All other trials were performed at 37 °C in 10 mM degassed PBS 7.4 buffer with 5% DMSO, and 100 equivalents of analyte integrated over 30 minutes. Inset is zoomed in view of L-Lys, L-Cys, and GSH experiments. b) Normalized chemiluminescent response of **CL-DNP** to varying equivalencies of NaSH. All trials other than the zero equivalence performed in triplicate at 37 °C in 10 mM degassed PBS 7.4 buffer with 5% DMSO and integrated over 30 minutes.

different detection platforms. We anticipate that the observed spontaneous untriggered turn-on of **CL-N3** and the apparent stability of **CL-DNP** in aqueous buffer will help inform scientists' choices when using chemiluminescence to monitor H_2S levels.

Chapter VIII of this dissertation discusses a novel rotaxane-based fluorescent H_2S probe. This system relies on the inherent fluorescence of the curved cycloparaphenylenes, and is the first fluorescent probe for H_2S detection involving this newly discovered fluorophore.

7.4 Experimental

Materials and Methods: Reagents were purchased from Sigma-Aldrich, Tokyo Chemical Industry (TCI), Fisher Scientific, or VWR and used directly as received. Silica gel (SiliaFlash F60, Silicycle, 230−400 mesh) was used for column chromatography. Deuterated solvents were purchased from Cambridge Isotope Laboratories (Tewksbury, Massachusetts, USA). ^{1}H and $^{13}C\{^{1}H\}$ NMR spectra were recorded on Bruker 500 MHz or Bruker 600 MHz NMR instruments at the indicated frequencies. Chemical shifts are reported in parts per million (δ) and are referenced to residual protic solvent resonances. The following abbreviations are used in describing NMR couplings: (s) singlet, (d) doublet, (b) broad, and (m) multiplet. IR spectra were measured on a Thermo Scientific Nicolet 6700 RT-IR using an ATR attachment. Mass spectrometric measurements were performed by the University of Illinois, Urbana Champaign MS facility, or on a Xevo Waters ESI LC/MS instrument. Phosphate buffered saline (PBS) tablets (1X, CalBioChem) were used to prepare buffered solutions (140 mM NaCl, 3.0 mM KCl, 10 mM phosphate, pH 7.4) in deionized water. Buffer solutions were sparged with nitrogen to remove dissolved oxygen

and stored in an Innovative Atmosphere nitrogen-filled glovebox. All stock solutions were freshly prepared using degassed solvents immediately before use. Anhydrous sodium hydrogen sulfide (NaSH) was purchased from Strem Chemicals and handled under nitrogen. L-Cysteine and L-Lysine were purchased from TCI. Reduced glutathione was purchased from Aldrich. Stock solutions of the analytes were prepared in 10 mM PBS 7.4 buffer or DMSO under nitrogen immediately prior to use and were introduced into buffered solutions with an air-tight Hamilton syringe. Note: **CL-N3** and **CL-DNP** are not air-sensitive, but protection of reaction solution from O_2 was to prevent H_2S oxidation. To ensure accurate measurements and to prevent decomposition of potentially reactive species, all experiments were performed under an inert atmosphere unless otherwise indicated. Chemiluminescence measurements were measured using a Quanta Master 40 spectrofluorometer (Photon Technology International) equipped with a Quantum Northwest TLC-50 temperature controller at 37.0 ± 0.05 °C. All chemiluminescent measurements were made under an inert atmosphere in septum-sealed cuvettes obtained from Starna Scientific and were repeated at in triplicate.

Synthesis of Phenol Core: Core phenol **EE-OH** was prepared according to the literature procedures. Spectral data is in agreement with those reported in the literature (Figure 7.5).[194, 234]

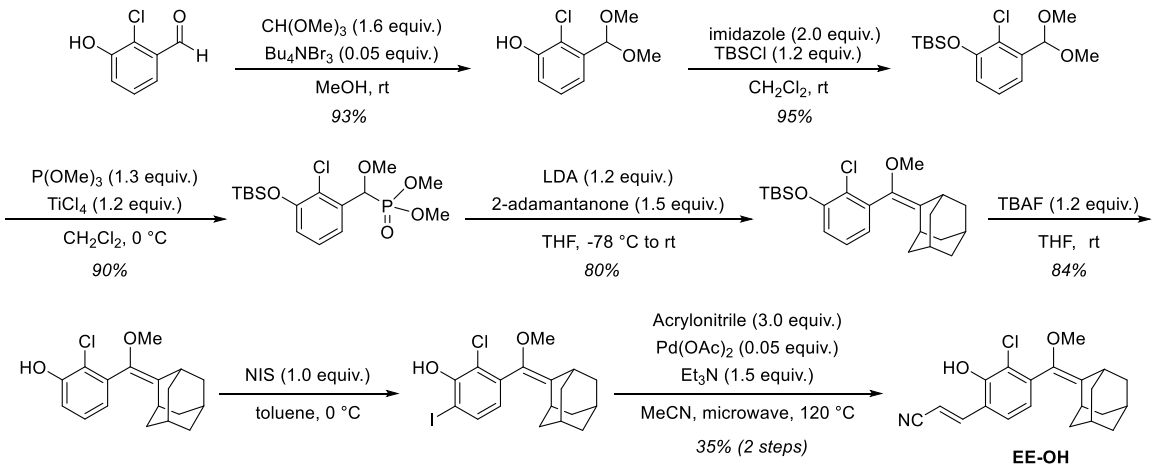

Figure 7.5 Synthesis of EE-OH.

Synthesis of CL-DNP: The synthesis of **CL-DNP** is shown in Figure 7.6. **EE-OH** (100 mg, 0.281 mmol, 1.0 equiv.), 2,4-dinitrobromobenzene (76 mg, 0.31 mmol, 1.1 equiv.), and K_2CO_3 (78 mg, 0.56 mmol, 2.0 equiv.) were dissolved in dry DMF (3 mL) and stirred overnight under N_2. The reaction mixture was quenched with brine and extracted with EtOAc (3 x 10 mL). The combined organic layers were washed with 5% aqueous LiCl (4 x 10 mL), dried over anhydrous $MgSO_4$, concentrated under vacuum, and purified by silica column chromatography to yield 113 mg of a white solid. The crude DNP-enol ether product (110 mg, 0.211 mmol, 1.0 equiv.) was dissolved in CH_2Cl_2 (40 mL) and transferred to a large test tube. TPP (10 mg, 0.016 mmol, 0.05 equiv.) was added and mixed. The reaction tube was clamped with the bottom 2 inches in an ice water bath and a steady stream of O_2 was bubbled through a 9-inch Pasteur pipette into the solution while the reaction mixture was illuminated with a flood lamp. The reaction was run for three hours and with more CH_2Cl_2 was added every 20 minutes to maintain an approximately constant volume. The reaction was monitored by removing aliquots and measuring the ^1H NMR spectrum.

After completion of the reaction, the crude reaction mixture was concentrated and purified by preparatory TLC (1:1 Hex:EtOAc, 1000 µm thick silica) to yield **CL-DNP** as a white solid (110 mg, 76% yield over two steps). ^{1}H NMR (600 MHz, $CDCl_3$) δ (ppm): 8.93 (d, *J*=2.73 Hz, 1H), 8.28 (bs, 1H), 8.23 (d, *J*=8.49 Hz, 1H), 7.73 (d, *J*=8.49 Hz, 1H), 7.47 (d, *J*=16.72 Hz, 1H), 6.48 (bs, 1H), 6.19 (d, *J*=16.72 Hz, 1H), 3.19 (s, 3H), 2.99 (s, 1H), 2.09 (d, *J*=13.31 Hz, 1H), 1.93 (bs, 1H), 1.83 (d, *J*=13.31 Hz, 2H), 1.76-1.56 (m, 7H), 1.48 (dd, *J*=13.05, 2.97 Hz, 1H), 1.40 (d, *J*=12.98 Hz, 1H), 1.17 (d, *J*=13.05 Hz, 1H). ^{13}C{^{1}H} NMR (151 MHz, $CDCl_3$) δ (ppm): 153.97, 147.20, 142.23, 141.84, 138.63, 137.68, 131.99, 130.20, 129.02, 127.08, 125.76, 122.83, 116.81, 115.43, 111.15, 102.94, 96.32, 49.86, 36.30, 33.85, 33.67, 32.65, 32.02, 31.55, 31.49, 26.00, 25.67. IR (cm^{-1}) 2916.7, 2859.4, 2222.0, 1736.4, 1610.0, 1537.6, 1392.5, 1346.2, 1266.3, 1227.4, 1217.3, 1068.9. HRMS m/z $[M + Na]^+$ calcd. for $[C_{27}H_{24}N_3O_8ClNa]^+$ 576.1150, found 576.1151.

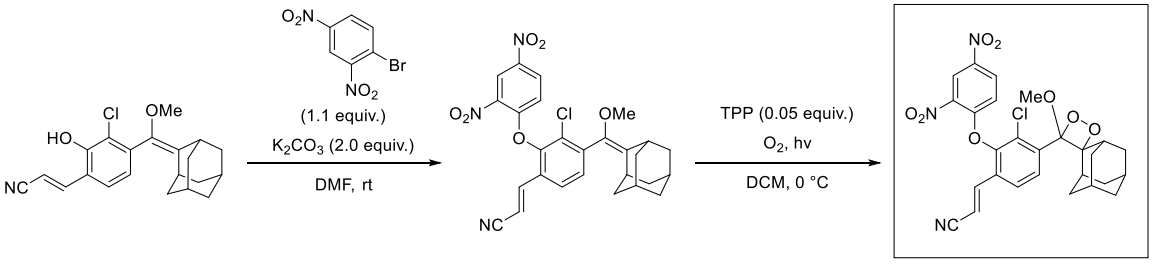

Figure 7.6 Synthesis of CL-DNP.

Synthesis of CL-N3: The synthesis of **CL-N3** is shown in Figure 7.7. **EE-OH** (515 mg, 1.45 mmol, 1.2 equiv.) and the azide carbonate coupling partner (350 mg, 1.21 mmol, 1.0 equiv.)[228] were dissolved in 20 mL of 4:1 THF:CH_2Cl_2 under N_2. DMAP (221 mg, 1.81 mmol, 1.5 equiv.) and Et_3N (0.67 mL, 4.83 mmol, 4.0 equiv.) were added, and the resultant reaction mixture was stirred overnight protected from light. The reaction mixture was quenched with brine and extracted with EtOAc (3 x 20 mL). The combined organic layers

were dried over anhydrous $MgSO_4$, concentrated under vacuum, and purified by preparatory TLC (1:1 Hex:EtOAc, 1000 µm silica thickness). The resulting N3-enol ether (120 mg, 0.226 mmol, 1.0 equiv.) was then dissolved in CH_2Cl_2 (40 mL) and transferred to a large test tube. TPP (7 mg, 0.01 mmol, 0.05 equiv.) was added and mixed. The reaction tube was clamped with the bottom 2 inches in an ice water bath, and a steady stream of O_2 was bubbled through a 9-inch Pasteur pipette into the solution while the reaction mixture was illuminated with a flood lamp. The reaction was run for three hours and with more CH_2Cl_2 was added every 20 minutes to maintain an approximately constant volume. The reaction was monitored by removing aliquots and measuring the ^{1}H NMR spectrum. The crude reaction mixture was concentrated and purified by preparatory TLC (2:1 Hex:EtOAc, 1000 µm silica thickness) to yield **CL-N3** as a white solid (87 mg 16% yield as a white solid). ^{1}H NMR (500 MHz, $CDCl_3$) δ (ppm): 8.08 (d, *J*=8.44 Hz, 1H), 7.56 (d, *J*=8.44 Hz, 1H), 7.42 (m, 3H), 7.07 (d, *J*=8.48 Hz, 2H), 6.01 (d, *J*=16.76 Hz, 1H), 5.29 (s, 2H), 3.19 (s, 3H), 3.01 (bs, 1H), 2.21 (d, *J*=13.28 Hz, 1H), 1.92 (bs, 1H), 1.83 (m, 2H), 1.73 (m, 4H), 1.65 (m, 1H), 1.59 (m, 2H), 1.46 (dd, *J*=12.92, 3.00 Hz, 1H), 1.33 (dd, *J*=13.48, 3.00 Hz, 1H). ^{13}C{^{1}H} NMR (126 MHz, $CDCl_3$) δ (ppm): 151.68, 146.16, 142.70, 141.10, 136.39, 131.06, 130.69, 130.34, 129.53, 127.42, 124.67, 119.40, 117.14, 111.35, 101.63, 96.39, 70.93, 49.81, 36.50, 33.90, 33.61, 32.41, 32.14, 31.56, 31.52, 26.11, 25.76. IR (cm^{-1}) 2910.9, 2858,4, 2221.32, 2110.0, 1767.4, 1508.4, 1453.1, 1397.9, 1376.5, 1210.7, 1180.2, 1128.8, 1104.6, 1068.6. HRMS m/z $[M + Na]^+$ calcd. for $[C_{29}H_{27}N_4O_6ClNa]^+$ 585.1517, found 585.1529.

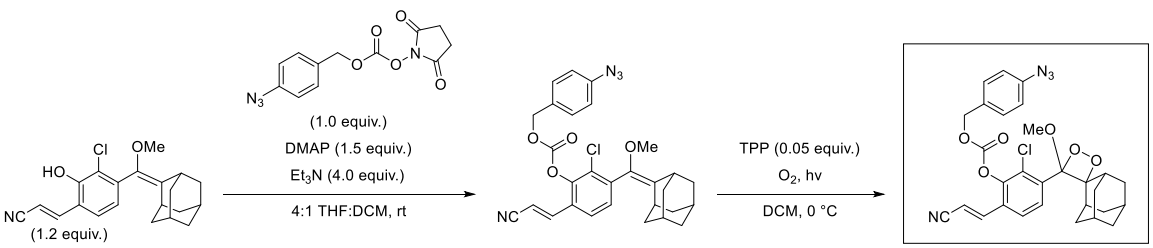

Figure 7.7 Synthesis of CL-N3.

Chemiluminescence Studies: For all chemiluminescence experiments, excitation slits were closed, and the excitation wavelength set to 800 nm. An excitation wavelength input was required for the instrument to run, however this should in no way interfere with the measurement of chemiluminescent output. Emission slits were set to 4.0 mm, and the wavelength measured at was 525 nm. Scans were taken every second for at least 30 minutes. All experiments performed in triplicate.

General Procedure in THF: In a septum sealed cuvette, 3.0 mL of degassed air-free THF was incubated for 5 minutes at 37 °C, after which data collection was started. To the cuvette 15 µL of a 5 mM THF stock of probe was added using an airtight Hamilton syringe to make a 25 µM solution, then approximately 20 seconds later analyte was added with an airtight Hamilton syringe. Data was collected for at least 30 minutes after analyte was added.

General Procedure in PBS: In a septum sealed cuvette, 3.0 mL of a solution of degassed 10 mM PBS 7.4 buffer with 5% DMSO was incubated for 5 minutes at 37 °C, after which data collection was started. To the cuvette 15 µL of a 5 mM THF stock of probe was added using an airtight Hamilton syringe to make a 25 µM solution, then approximately 20

seconds later analyte was added with an airtight Hamilton syringe. Data was collected for at least 30 minutes after analyte was added.

Preparation of Stock Solutions: In small HPLC vials, 500 mM NaSH, L-Cys, and L-Lys stocks were prepared in degassed Millipore water, and 15 µL were added for 100 equiv. experiments. Due to poor solubility, 250 mM GSH stocks were prepared in degassed Millipore water, and 30 µL GSH stock was added to the cuvette to reach 100 equiv. For the variable concentration NaSH experiments, the aliquots added were 0, 1, 2.5, 5, 10, 15, and 25 µL, to reach 0, 7, 17, 33, 67, 100, and 167 equivalents, respectively.

Calculating Normalized Turn-On Response: Data for four blank baseline response trials were collected with 25 µM of either CL-DNP or CL-N3 in either THF or PBS 7.4 with 5% DMSO at 37 °C for 30 minutes, with no analyte added. Identical fluorimeter parameters were used for each experiment: the excitation slits were closed, and the excitation wavelength set to 800 nm. Emission slits were set to 4.0 mm, and the wavelength measured at was 525 nm. Scans were taken every second for at least 30 minutes. Background luminescence measurements were recorded and subtracted from all experiments when calculating the normalized luminescence response. For the experiments monitoring turn-on response of **CL-DNP** to varying concentrations of NaSH, all trials other than the zero equivalence performed in triplicate at 37 °C in 10 mM degassed PBS 7.4 buffer with 5% DMSO and integrated over 30 minutes, and normalized relative to 25 µM **CL-DNP** in PBS 7.4 buffer with 5% DMSO with no analyte added. For the selectivity studies with **CL-DNP**, the THF trial was performed in air-free unstabilized

THF at 37 °C with 100 equivalents of NaSH added from a degassed aqueous stock solution and integrated over 30 minutes. All other trials were performed at 37 °C in 10 mM degassed PBS 7.4 buffer with 5% DMSO, and 100 equivalents of analyte added from degassed aqueous stock solutions and integrated over 30 minutes. The THF trial is the average normalized turn-on response of three independent trials relative to 25 μM **CL-DNP** in THF with no analyte added.

CHAPTER VIII

A NOVEL NANOHOOP ROTAXANE-BASED TURN-ON FLUORESCENT PROBE FOR THE DETECTION OF HYDROGEN SULFIDE

This chapter contains previously unpublished coauthored work. This manuscript was written by Carolyn M. Levinn and edited by Professor Michael D. Pluth. The project in this chapter was conceived of by Carolyn M. Levinn and Dr. Jeff Van Raden with insight from Claire E. Otteson, Professor Ramesh Jasti, and Professor Michael D. Pluth. The experimental work in this chapter was performed by Carolyn M. Levinn and Claire E. Otteson.

5.1 Introduction

The synthesis of mechanically interlocked molecules (MIMs) has taken off since the emergence of active template (AT) methods just over a decade ago.[235-236] MIMs have gained immense interest due to the range of unique properties that arise from the mechanical bonds present in structures like catenanes and rotaxanes.[237-238] For example, these structures can be engineered to have selective molecular recognition sites that would be otherwise not accessible using traditional supramolecular interactions or covalent bonding, suggesting their utility in selective biological sensing and delivery applications.[239-240] Recent work from the Jasti group highlighted the synthesis of rotaxanes – MIMs comprising a dumbbell shaped rod threaded through a macrocycle – wherein the macrocyclic component is a carbon nanohoop.[241] In this study they showed

that the inherent fluorescence of these macrocycles can be modulated via the incorporation of a quencher (3,5-dinitrobenzyl alcohol) in the thread unit of the rotaxane, rendering the molecule non-emissive in the interlocked state. This property was leveraged to create a turn-on fluorescent fluoride sensor whereby a fluoride-triggered silyl deprotection of the thread component results in dethreading of the macrocycle and a turn-on fluorescent signal (Figure 8.1, top).[241] With this proof-of-concept example for nanohoop [2]rotaxanes as fluorescent sensors and their previous success in the development of biocompatible nanohoops, they turned toward developing turn-on fluorescent sensors for a biologically relevant analyte. Due to their bright, readily tunable fluorescence and biocompatibility, nanohoops are poised to become a new class of biological fluorophores, and their macrocyclic nature makes them uniquely valuable for developing multifunctional biological probes.[242-246] Further, considering the small, rigid pore of nanohoop mN[6]CPP, suggests the exceptional flexibility in the design of nanohoop [2]rotaxanes, as very little bulk is required to retain the interlocked structure, highlighting the wealth of possibilities when considering the interlocked architectures that can be synthesized using nanohoop macrocycles.

In collaboration with the Jasti lab, we sought to adapt this novel class of sensors to detect hydrogen sulfide (H_2S), a small, nucleophilic, signaling molecule.[1] In the last decade, researchers have made a variety of tools including H_2S donors and probes to elucidate the physiological roles of this gasotransmitter.[153-154, 178, 247] One major hurdle in creating these tools is the need for selectivity when sensing this analyte in the presence of several other biologically relevant sulfides and other reactive sulfur species. We hypothesized that *via* rational design of a rotaxane-based sensor, we could enhance this

selectivity due to the highly sterically congested environment created via the mechanical bond. There are many different groups known to react with H_2S that have been previously incorporated into donor/probe scaffolds, many of which operate via nucleophilic attack by the reactive sulfide, as discussed in Chapter 6.[178] Based on this, we proposed that a dinitrophenol (DNP) group would both quench the fluorescence of the macrocycle and act as an electrophilic reaction partner with H_2S (or more specifically HS^-) in a nucleophilic aromatic substitution reaction (S_NAr) via the mechanism proposed in the bottom of Figure 8.1. We reasoned that the steric environment created by the mechanical bond should only allow attack by very small nucleophiles, i.e. H_2S, giving a selective turn-on fluorescent probe.

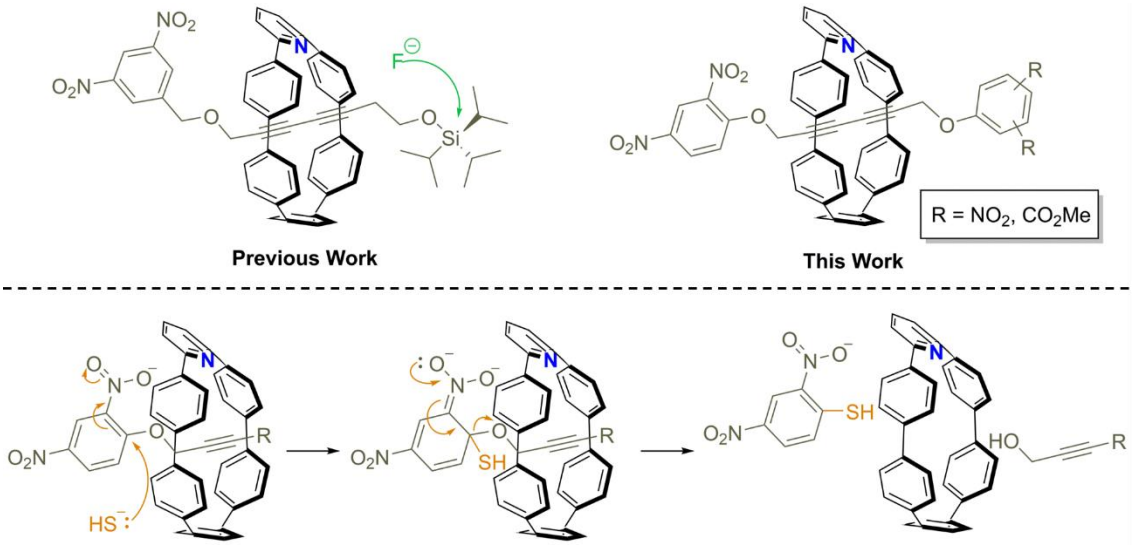

Figure 8.1. Top: structure of (left) previously published fluoride-sensing rotaxane and (right) proposed H_2S-sensing rotaxane; bottom: proposed mechanism of rotaxane dethreading in the presence of HS^-.

8.2 Results and Discussion

Utilizing the same methodologies previously established for the active-metal templating of nanohoop [2]rotaxanes we chose to continue working with previously

published mN[6]CPP as our macrocycle due to its small size and rigid nature.[241] To create the thread, we used a Cadiot-Chodkiewicz (CC) coupling to create a di-yne conjunction between our 2,4-DNP stopper units.[248-249] This was accomplished *via* deprotonation of 2,4-dinitrophenol and installation of a propargyl group to obtain our proteo-coupling partner. From this our halogenated coupling partner was easily accessible via treatment with $AgNO_2$ and NBS to obtain the alkynyl bromide in good yield (Figure 8.2a). With both thread components in hand along with our macrocycle we were able to obtain our interlocked product via AT-CC coupling in the presence of $[Cu(MeCN)_4]PF_6$, giving our desired symmetric rotaxane (**SR**) in 13% yield (Figure 8.2b). Notably, the yellow solid was non-fluorescent in the solid or solution state. For control studies, free thread **ST** was also synthesized via similar methods, utilizing pyridine in the place of the m[6]CPP. Following a similar protocol we also prepared an asymmetric rotaxane (**AR**) using dimethyl 5-hydroxyisophthalate in place of one of the 2,4-DNP groups, as well as the free thread (**AT**) for control experiments (Figure 8.2c).

With our rotaxanes in hand we next sought to test the dethreading of the nanohoop in the presence of H_2S, so we first turned to ^1H NMR spectroscopy. Figure 8.3 illustrates the immediate response of both rotaxanes **SR** and **AR** to introduction of tetrabutylammonium hydrosulfide or TBASH (an organic-soluble source of HS^-) in acetonitrile-d_3. This rapid dethreading is further seen in fluorescence studies of the sensor. **SR** shows a steady increase in fluorescence upon the introduction of 10 equivalents of TBASH (Figure 8.4),[250] and the rate of fluorescence turn-on is increased dramatically with increasing concentrations of TBASH added (Appendix G, Figure G.15). Excitingly we see very little fluorescence turn-on in the presence of PhSNa, a

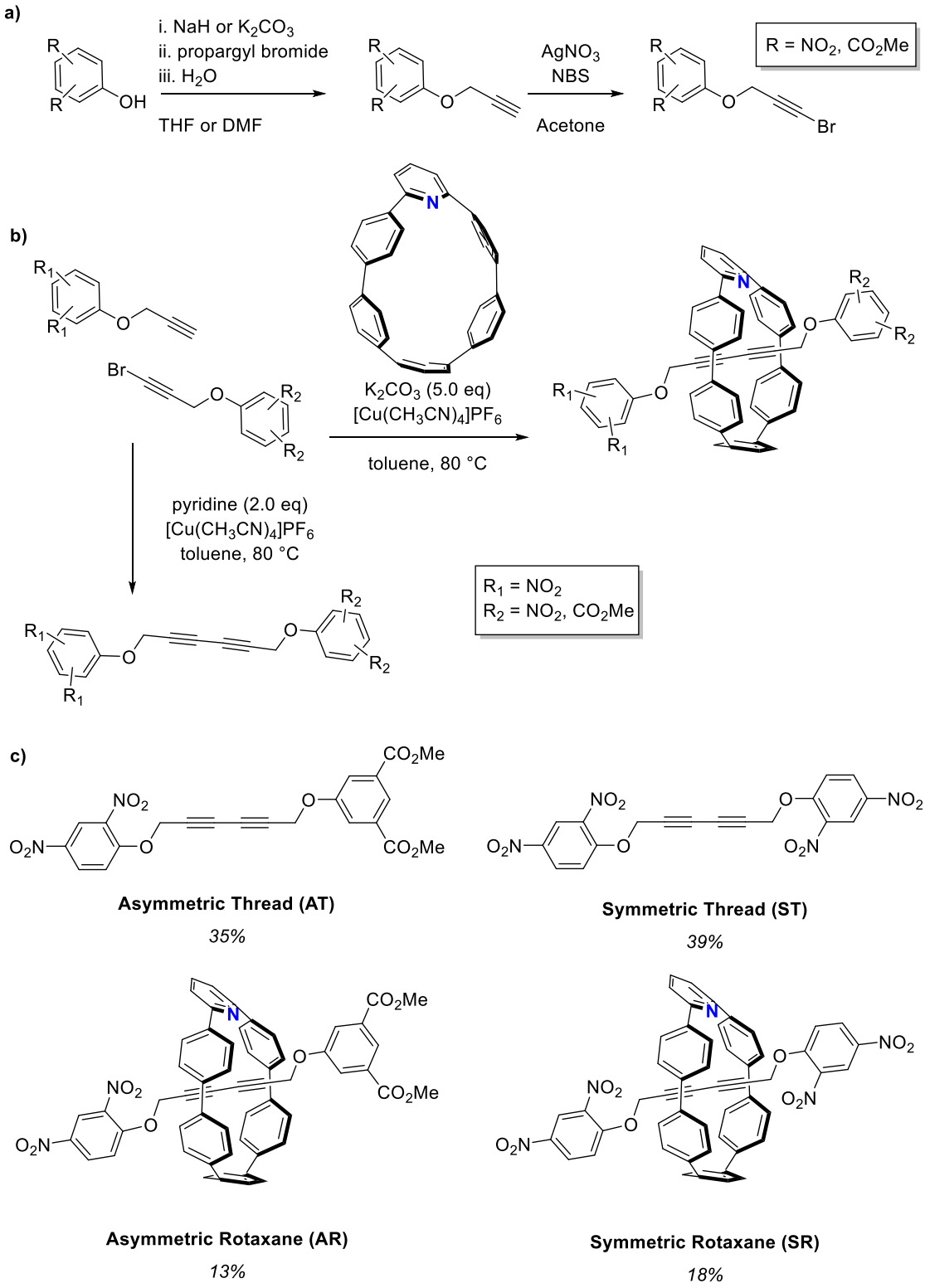

Figure 8.2 (a) General synthesis of alkyne coupling partners for the preparation of the rotaxane thread. (b) General synthesis of both the symmetric and asymmetric free threads, and the asymmetric and symmetric nanohoop rotaxanes. (c) Structures and yields of prepared rotaxanes and threads.

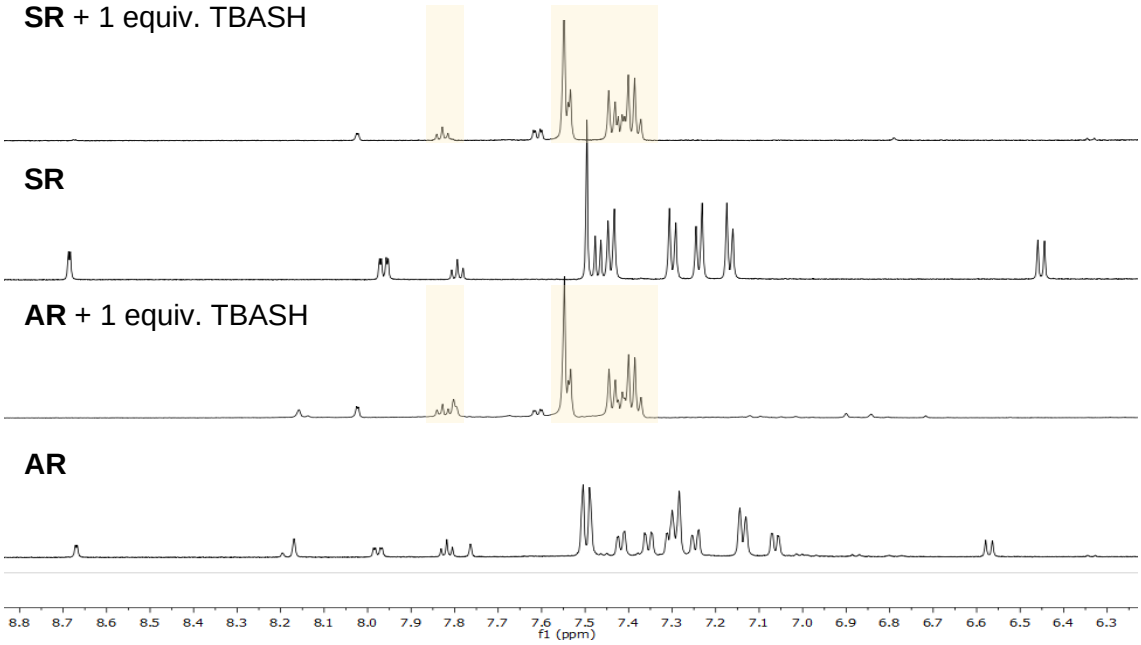

Figure 8.3 ^{1}H NMR spectra of rotaxanes SR and AR in acetonitrile-d_3 before and after addition of 1 equiv. of TBASH. Highlighted in yellow is the fluorescent macrocycle post-dethreading.

more sterically demanding sulfide, suggesting successful manipulation of the reactivity of our thread *via* mechanically interlocking (Figure 8.5).

When similar fluorescence turn-on experiments were performed on the asymmetric rotaxane **AR**, a strong fluorescence signal was observed upon excitation at 310 nm in acetonitrile, even without added nucleophile (Figure 8.6). Initially, this extra peak from around 350 – 450 nm in the emission spectrum was dismissed as an artifact of poor solubility, however the peak was still present when diluted with DMSO and other solubilizers. Additionally, this fluorescence signal did not diminish significantly upon addition of 10 equivalents of TBASH, while the expected m[6]CPP fluorescence signal did grow in, albeit at a slower rate than with the **SR** H_2S probe. We do not expect that this peak between 350 and 450 nm is due to poor solubility, because if that were the case

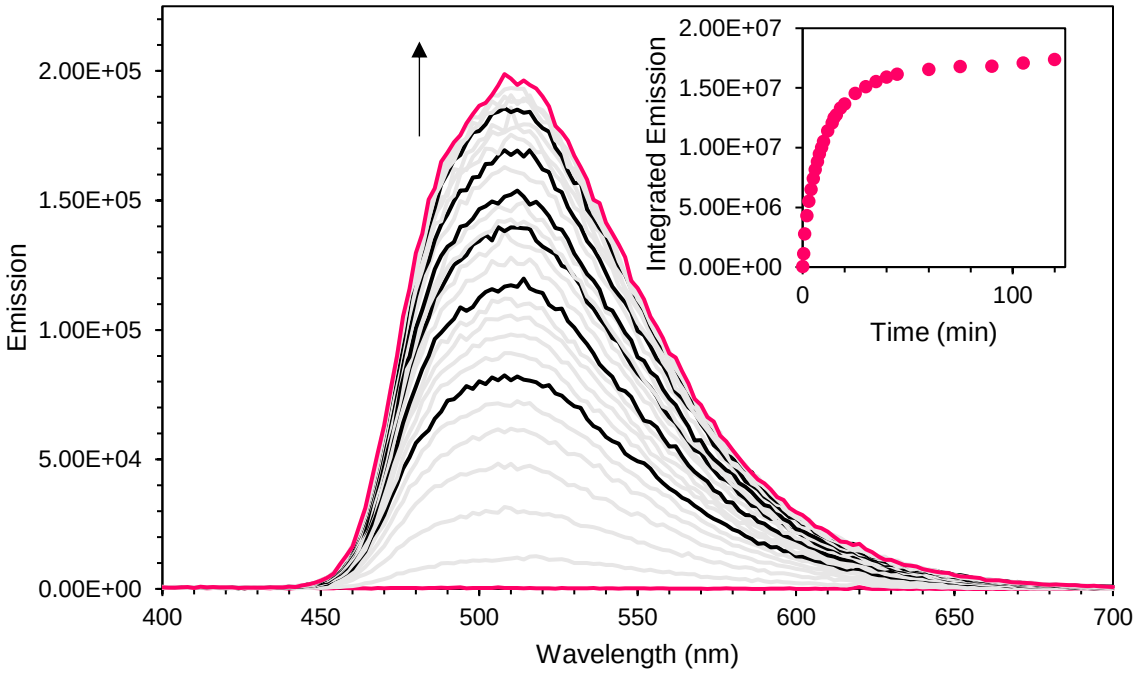

Figure 8.4 Turn-on fluorescent response of 25 µM SR in degassed acetonitrile upon addition of 10 equiv. of TBASH. Excitation wavelength set to 310 nm, all slit widths set to 0.5 mm. Inset plot is the integrated emission integrated from 400 – 700 nm.

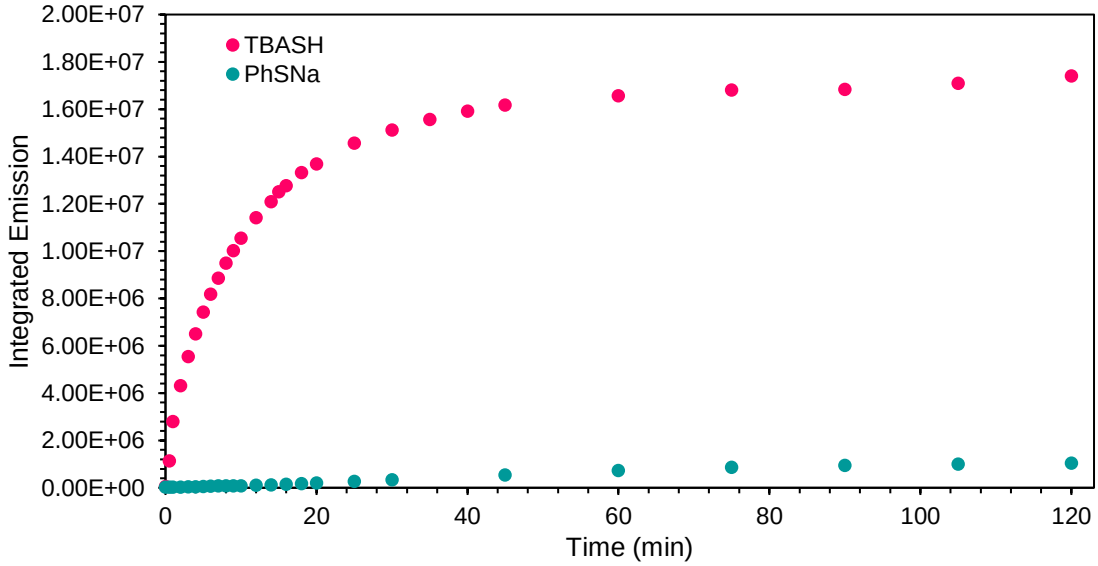

Figure 8.5 Integrated fluorescent emission response of 25 µM SR in MeCN to 10 equivalents of either TBASH (pink) or PhSNa (green). Excitation wavelength set to 310 nm, all slit widths set to 0.5 mm, emission integrated from 400 – 700 nm.

we would expect that it would decrease as the signal from the dethreaded rotaxane increased.

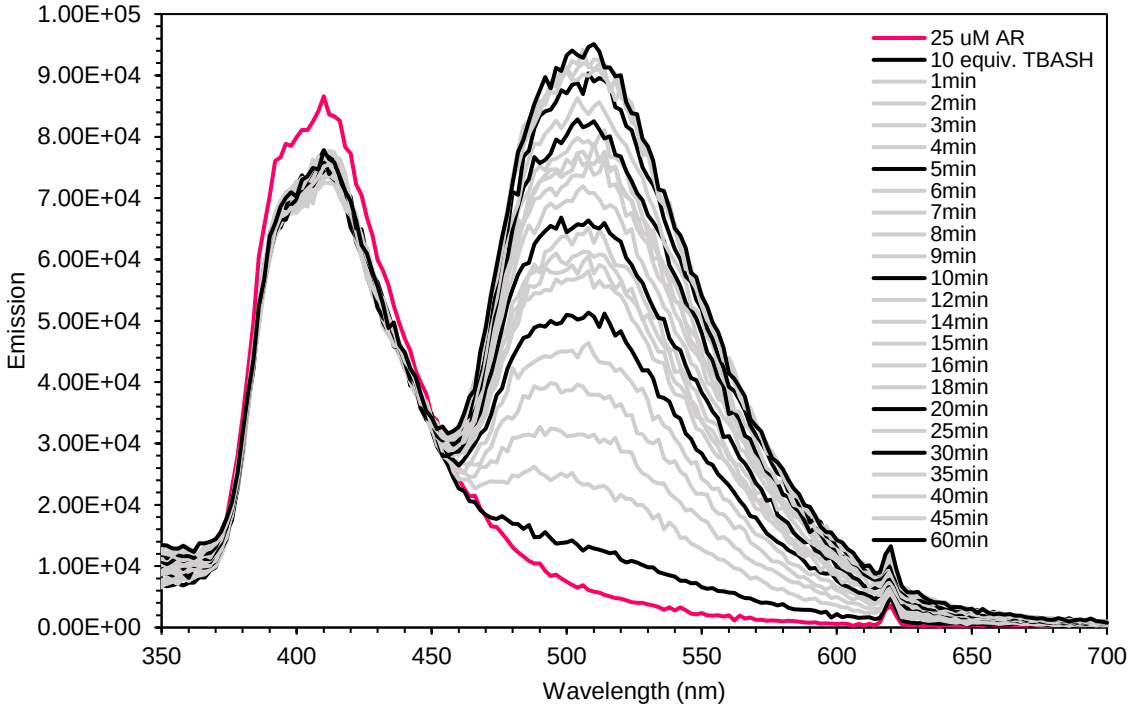

Figure 8.6 Turn-on fluorescent response of 25 µM AR in degassed acetonitrile upon addition of 10 equiv. of TBASH. Excitation wavelength set to 310 nm, all slit widths set to 0.5 mm, with a scan step size of 2 nm.

To further investigate the inherent fluorescence of **AR**, we then measured the fluorescence spectrum of the free asymmetric thread **AT**. To our surprise, when excited at 310 nm in acetonitrile, **AT** exhibited a strong peak in the emission spectrum with a maximum intensity at around 330 nm (Figure 8.7). To our knowledge, chemical structures of this type have not previously been reported to be fluorescent, however preliminary computational studies performed in the Jasti lab indicate that this phenomenon is while unexplained, somewhat general for bis-alkynyl rotaxane threads. Notably, the λ_{max} of the fluorescence spectrum for the free thread **AT** (330 nm) and the

asymmetric rotaxane **AR** before addition of sulfide (410 nm) are approximately 80 nm apart from each other, indicating that the trapping of the thread inside the m[6]CPP as a rotaxane does dramatically affect its chemical environment, and likely will impact its reactivity.

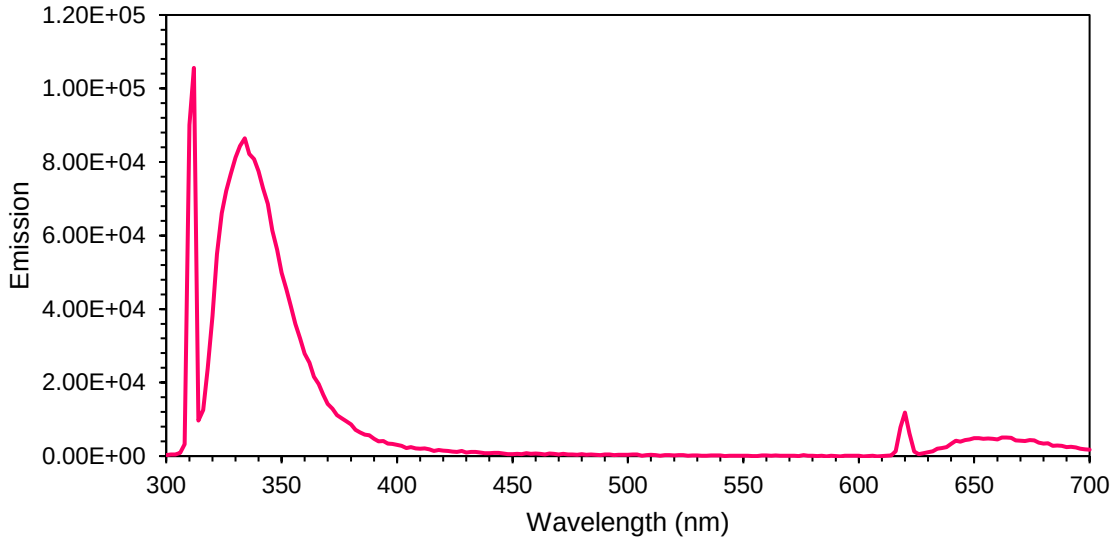

Figure 8.7 Fluorescence spectrum of 25 μM of Asymmetric Thread (**AT**) in acetonitrile. Excitation wavelength set to 310 nm, all slit widths set to 0.5 mm.

8.3 Conclusions

In conclusion, in this chapter we report the first nanohoop rotaxane-based turn-on fluorescent probe for H_2S and have demonstrated selectivity for HS^- over a second small molecule thiolate, PhSNa. We have also demonstrated that a rotaxane with a mixed thread can be employed as a sensor in this system, which lays the foundation for future probes where one head of the thread is an H_2S (or other analyte) sensing motif, while the other is a targeting group. Interestingly, we found that the free bis-alkynyl thread **AT** exhibited fluorescence independent of the nanohoop of the rotaxane, and current studies are ongoing to fully elucidate the nature and limits of its photophysical properties.

Additionally, while the experiments discussed in this chapter were all performed in organic solution a probe needs to function in aqueous systems in order to be a useful tool for bioimaging, the Jasti and Pluth labs have collaborated in the past to solubilize CPPs for fluorescent imaging in cells. We anticipate using a nanohoop with a pendant alkyne for the rotaxane will allow for solubilizing and targeting groups to be appended through a Cu-catalyzed click reaction, which will greatly broaden the applicability of this system.

Chapter 8.4 Materials and Methods

General Experimental Details: Moisture/air sensitive reactions were carried out under nitrogen atmosphere using standard Schlenk technique with flame-dried glassware cooled under an inert atmosphere of nitrogen. Solvents used for moisture/air sensitive reactions were dried by filtration through alumina and stored under an inert argon atmosphere. Silica column chromatography was conducted with Zeochem Zeoprep 60 Eco 40-63 μm silica gel and automated flash chromatography was performed using a Biotage Isolera One. Recycling gel permeation chromatography (GPC) was performed using a Japan Analytical Industry LC-9101 preparative HPLC with JAIGEL-1H/JAIGEL-2H columns with $CHCl_3$. Absorbance and fluorescence spectra were obtained in a 1 cm Quartz cuvette with dichloromethane, or deionized water using an Agilent Cary 60 or Cary 100 UV-vis spectrometer and a Quanta Master 40 spectrofluorometer (Photon Technology International) equipped with a Quantum Northwest TLC-50 temperature controller at 25.0 ± 0.05 °C. IR spectra were measured on a Thermo Scientific Nicolet 6700 RT-IR using an ATR attachment.

NMR spectra were recorded at 500 MHz or 600 MHz on a Bruker Advance-III-HD NMR spectrometer. All ^{1}H NMR spectra were referenced to either in CD_3CN (referenced to MeCN, δ 1.96 ppm), $CDCl_3$ (referenced to TMS, δ 0.00 ppm). All ^{13}C NMR spectra are referenced to residual $CDCl_3$ (77.16 ppm). All reagents were obtained commercially. Compounds S1, S2, S3, and S4 (below) were prepared according to literature procedure.

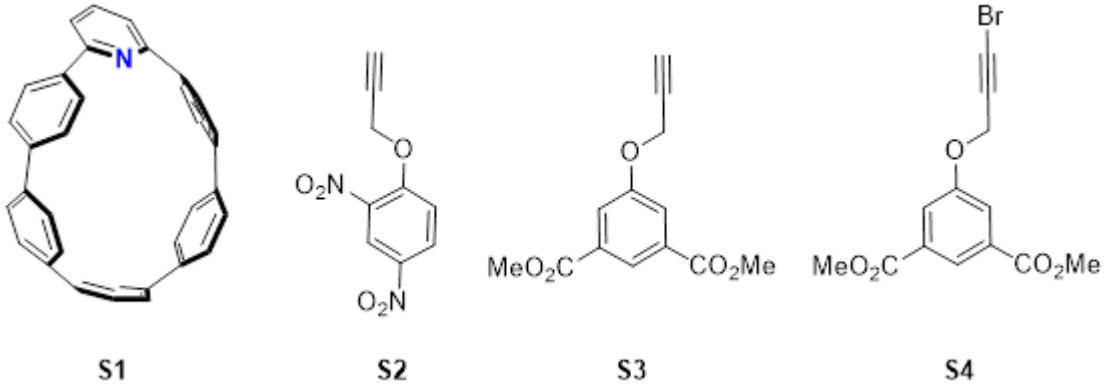

S1 S2 S3 S4

Figure 8.8 Previously reported compounds used in the research described in Chapter 8

Synthesis and Characterization: General Synthesis of Compounds

Relevant NMR spectra are shown in Appendix G, Figures G.1 – G.8.

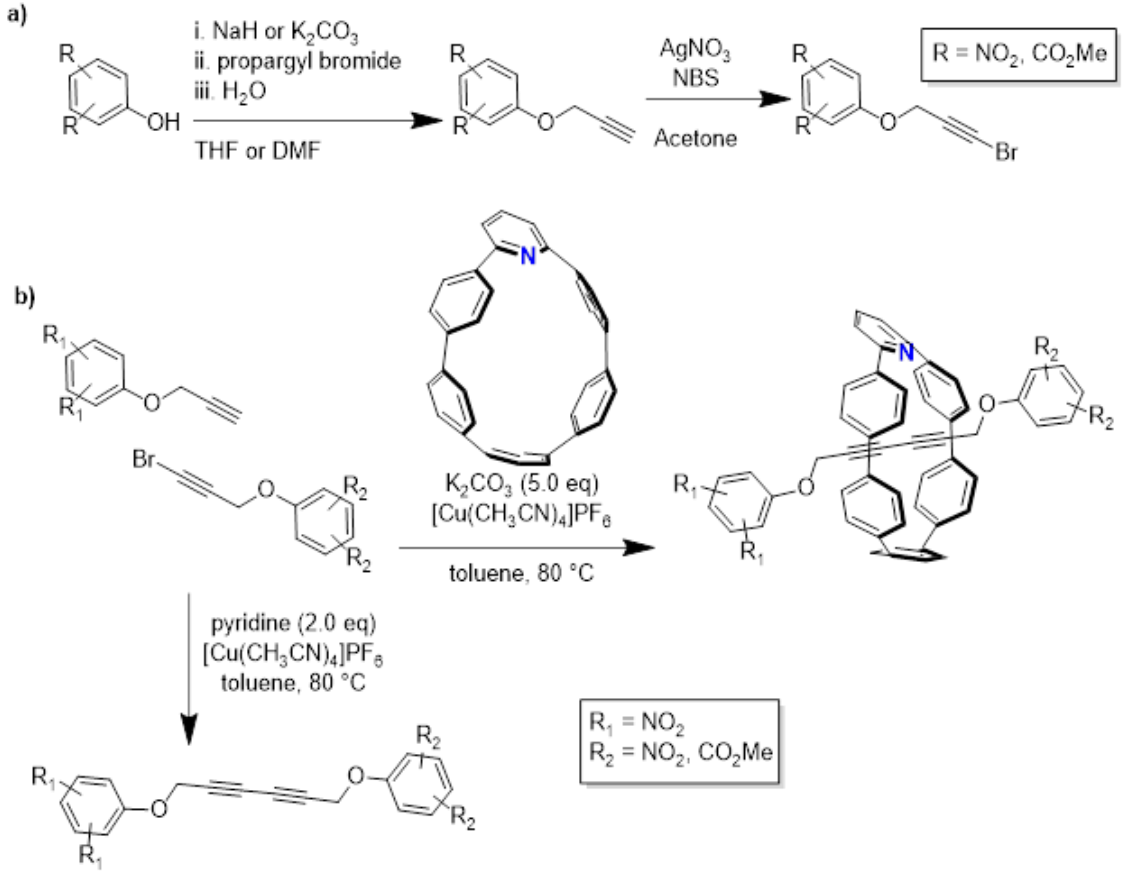

Figure 8.9 (a) Synthesis of thread components including **S2-S4.** (b) Synthesis of rotaxanes (using macrocycle **S1**) and free threads

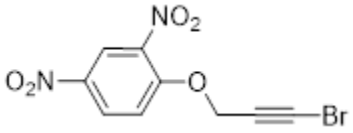

To a 50 mL flask equipped with magnetic stir bar was added **S2** (0.101 mg, 0.450 mmol, 1.00 equiv.) followed by the addition of $AgNO_3$ (0.139 mg, 0.473 mmol, 1.05 equiv.) and NBS (0.121 mg, 0.675 mmol, 1.50 equiv.) and 25 mL acetone. After stirring 1h at room temperature, the solvent was removed under reduced pressure. The resulting brown solid

was loaded onto a short SiO_2 plug which was subsequently washed with 100% hexanes before eluting the product in 100% dichloromethane to yield the product as a straw-colored solid (0.132 mg, 95%.) ^{1}H NMR (500 MHz, Chloroform-*d*) δ 8.77 (d, *J* = 2.7 Hz, 1H), 8.47 (dd, *J* = 9.3, 2.8 Hz, 1H), 7.38 (d, *J* = 9.2 Hz, 1H), 5.01 (s, 2H). ^{13}C NMR (126 MHz, Chloroform-*d*) δ 155.03, 140.90, 139.42, 128.86, 122.01, 115.09, 72.30, 58.67, 51.66. IR: 3113.63, 3088.81, 2237.22, 1599.99, 1513.09. MS (TOF MS El+) (m/z): [M]+ calculated for $C_9H_5BrN_2O_4$, 299.9382; found, 299.9382.

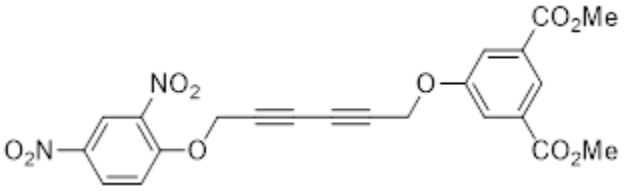

Asymmetric Thread (AT): To a flame-dried 25 mL round bottom flask equipped with a magnetic stir bar was added **S2** (0.0282 mg, 0.127 mmol, 1.00 equiv.) **S4** (0.0400 mg, 0.127 mmol, 1.00 equiv.) and $[Cu(CH_3CN)_4]PF_6$ (0.0237 mg, 0.0635 mmol, 0.500 equiv.), followed by five cycles of evacuation and refill with N_2. A septum was placed on the flask followed by the addition of 10.0 mL toluene and the addition of pyridine (0.0205 mL, 0.254 mmol, 2.00 equiv.) The reaction was heated to 80 °C with stirring for 48 hours, with reaction progress monitored by TLC. Once complete, the reaction was cooled to room temperature and the solvent was removed under reduced pressure. The crude solid was purified by automated flash chromatography, eluted with 100% dichloromethane to obtain the product as a dark yellow solid (20.7 mg, 35%.) ^{1}H NMR (500 MHz, Chloroform-*d*) δ 8.77 (d, J = 2.8 Hz, 1H), 8.47 (dd, J = 9.2, 2.8 Hz, 1H), 8.33 (t, J = 1.5 Hz, 1H), 7.78 (d, J = 1.4 Hz, 2H), 7.34 (d, J = 9.2 Hz, 1H), 5.04 (s, 2H), 4.85

(s, 2H), 3.95 (s, 6H). ^{13}C NMR (126 MHz, Chloroform-*d*) δ 165.85, 157.31, 154.82, 141.06, 139.44, 132.07, 128.93, 124.14, 122.05, 120.19, 115.12, 75.51, 73.61, 71.46, 70.81, 58.17, 56.52, 29.71.

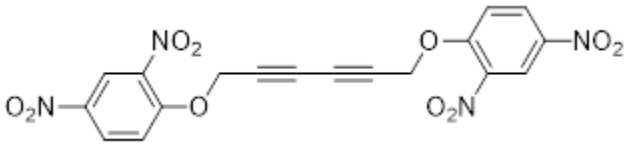

Symmetric Thread (ST): To a flame-dried 25 mL round bottom flask equipped with a magnetic stir bar was added **S2** (0.0295 mg, 0.133 mmol, 1.00 equiv.) **S5** (0.0400 mg, 0.133 mmol, 1.00 equiv.) and $[Cu(CH_3CN)_4]PF_6$ (0.0248 mg, 0.0664 mmol, 0.500 equiv.), followed by five cycles of evacuation and refill with N_2. A septum was placed on the flask followed by the addition of 10.0 mL toluene and the addition of pyridine (0.0210 mL, 0.266 mmol, 2.00 equiv.) The reaction was heated to 80 °C with stirring for 48 hours, with reaction progress monitored by TLC. Once complete, the reaction was cooled to room temperature and the solvent was removed under reduced pressure. The crude solid was purified by automated flash chromatography, eluted with 100% dichloromethane to obtain the product as a pale brown oily solid (23.1 mg, 39%.) ^{1}H NMR (500 MHz, Acetone-d_6) δ 8.76 (d, J = 2.8 Hz, 1H), 8.58 (dd, J = 9.3, 2.8 Hz, 1H), 7.72 (d, J = 9.3 Hz, 1H), 5.27 (s, 2H). ^{13}C NMR (126 MHz, Acetone-d_6) δ 155.63, 141.84, 140.49, 129.73, 122.09, 116.70, 74.34, 59.61, 51.28. IR: 3261.68, 3109.02, 3920.58, 2873.83, 1746.35, 1624.01, 1593.32, 1514.87, 1478.71.

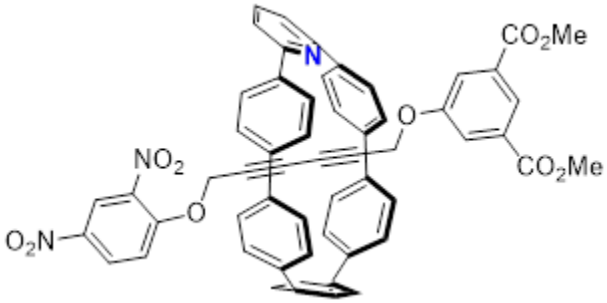

Asymmetric Rotaxane (AR): To a flame-dried 25 mL round bottom flask equipped with a magnetic stir bar was added **S2** (0.0146 mg, 0.0656 mmol, 1.50 equiv.) **S4** (0.0207 mg, 0.0656 mmol, 1.50 equiv.), **S1** (0.0200 mg, 0.0437 mmol, 1.00 equiv.), oven-dried K_2CO_3 (0.0302 g, 0.218 mmol, 5 equiv.) and $[Cu(CH_3CN)_4]PF_6$ (0.0155 mg, 0.0415 mmol, 0.950 equiv.), followed by five cycles of evacuation and refill with N_2. A septum was placed on the flask followed by the addition of 10.0 mL toluene. The reaction was heated to 80 °C with stirring for 48 hours, with reaction progress monitored by TLC. Once complete, the reaction was cooled to room temperature and quenched with an NH_3-EDTA (3 mL) solution then allowed to stir for 10 min. The layers were separated and the aqueous phase was washed with dichloromethane (3x 20 mL). The combined organic phase was then washed with H_2O (3x 20 mL) and brine (1x 20 mL) then dried over sodium sulfate, filtered and concentrated to yield an oily yellow solid. The crude material was purified by automated flash chromatography, eluted with 50-100% dichloromethane and hexanes to separate residual **S1** from the product. The resulting yellow solid was then purified via size exclusion chromatography to give the product as a bright yellow solid (5.1 mg, 13%.) ^{1}H NMR (500 MHz, Chloroform-*d*) δ 8.62 (d, *J* = 2.7 Hz, 1H), 8.35 (d, *J* = 1.5 Hz, 1H), 7.82 (t, *J* = 7.8 Hz, 1H), 7.78 (dd, *J* = 9.3, 2.8 Hz, 1H), 7.52 (d, *J* = 1.9 Hz, 2H), 7.48 (m, 4H) 7.41 (s, 2H), 7.39 (d, *J* = 2.0 Hz, 2H), 7.34 (d, *J* = 8.9 Hz, 4H), 7.27-

7.25 (m, 4H) 7.15 – 7.09 (m, 4H), 7.06 – 7.00 (m, 3H), 5.83 (d, *J* = 9.2 Hz, 1H), 3.96 (s, 6H), 3.56 (s, 2H), 3.23 (s, 2H). ^{13}C NMR (126 MHz, Chloroform-*d*) δ 166.04, 160.01, 157.40, 154.63, 141.43, 140.60, 138.24, 138.08, 136.45, 136.08, 131.98, 130.58, 129.74, 129.47, 128.85, 128.65, 128.31, 127.98, 127.83, 127.67, 127.05, 125.73, 123.81, 121.36, 119.93, 117.00, 114.17, 74.67, 72.18, 69.95, 58.32, 55.86, 29.86, 22.84, 14.27.

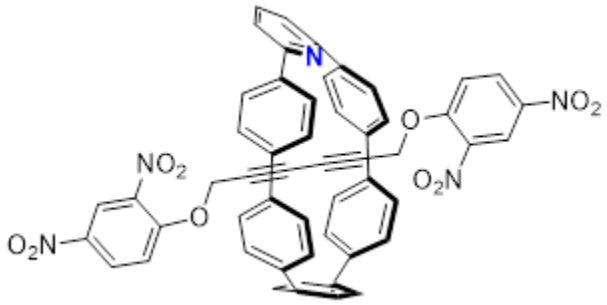

Symmetric Rotaxane (SR): To a flame-dried 25 mL round bottom flask equipped with a magnetic stir bar was added **S2** (0.0146 mg, 0.0656 mmol, 1.50 equiv.) **S5** (0.0193 mg, 0.0656 mmol, 1.50 equiv.), **S1** (0.0200 mg, 0.0437 mmol, 1.00 equiv.), oven-dried K_2CO_3 (0.0302 g, 0.218 mmol, 5 equiv.) and $[Cu(CH_3CN)_4]PF_6$ (0.0155 mg, 0.0415 mmol, 0.950 equiv.), followed by five cycles of evacuation and refill with N_2. A septum was placed on the flask followed by the addition of 10.0 mL toluene. The reaction was heated to 80 °C with stirring for 48 hours, with reaction progress monitored by TLC. Once complete, the reaction was cooled to room temperature and quenched with an NH_3-EDTA (3 mL) solution then allowed to stir for 10 min. The layers were separated and the aqueous phase was washed with dichloromethane (3x 20 mL). The combined organic phase was then washed with H_2O (3x 20 mL) and brine (1x 20 mL) then dried over sodium sulfate, filtered and concentrated to yield an oily yellow solid. The crude material was purified by automated flash chromatography, eluted with 50-100% dichloromethane

and hexanes to separate residual **S1** from the product. The resulting yellow solid was then purified via size exclusion chromatography to give the product as a bright yellow solid (7.2 mg, 18%.) ^{1}H NMR (500 MHz, Chloroform-*d*) δ 8.69 (d, *J* = 2.8 Hz, 2H), 7.99 (dd, *J* = 9.2, 2.8 Hz, 2H), 7.86 (t, *J* = 7.7 Hz, 1H), 7.50 (d, *J* = 8.3 Hz, 6H), 7.41 (d, *J* = 8.8 Hz, 4H), 7.20 (s, 8H), 7.13 (d, *J* = 8.7 Hz, 4H), 6.14 (d, *J* = 9.2 Hz, 2H), 3.60 (s, 4H). ^{13}C NMR (126 MHz, Acetone-d_6) δ 159.89, 154.60, 141.48, 140.70, 140.48, 139.50, 138.32, 137.86, 136.76, 136.42, 129.74, 128.32, 128.07, 127.90, 127.86, 127.82, 121.14, 116.54, 114.96, 71.74, 70.71, 58.29 ppm. IR: 2961.39, 2161.17, 1603.02, 1521.13, 1484.22. MS (TOF MS ES+) (m/z): [M]+ calculated for $C_{53}H_{33}N_5O_{10}$, 899.2227; found, 900.2304.

Photophysical Studies: Stock solutions of the rotaxane probes, nanohoop, threads, and TBAHS or PhSNa were prepared in degassed DCM or MeCN under nitrogen immediately prior to use and were introduced into cuvettes filled with 3 mL degassed MeCN with an air-tight Hamilton syringe. Note: Although the rotaxane probes and individual components are not air-sensitive, H_2S is known to react with oxygen. To ensure accurate measurements and to prevent decomposition of potentially reactive species, all experiments were performed under an inert atmosphere unless otherwise indicated. Fluorescence was measured using a Quanta Master 40 spectrofluorometer (Photon Technology International) equipped with a Quantum Northwest TLC-50 temperature controller at 25.0 ± 0.05 °C. All fluorescence measurements were made under an inert atmosphere in septum-sealed cuvettes obtained from Starna Scientific, with both excitation and emission slit widths set to 0.4 mm. Fluorescence spectra were collected with 0.1 s integration and 2 nm step size. UV/Vis spectra were acquired on an

Agilent Cary 60 or Agilent Cary 100 UV/Vis spectrophotometer equipped with a Quantum Northwest TC-1 temperature controller set at 25 ± 0.05 °C. TBASH[250] and PhSNa[251] were prepared according to the literature.

Reaction of Symmetric Rotaxane (SR) with Varying Concentrations of TBASH: A 10 mM stock solution of symmetric rotaxane S9 was prepared in DCM and a 100 mM stock solution of TBASH was prepared in MeCN under N_2. 3.0 mL of degassed MeCN in a septum sealed cuvette was scanned as a blank for both fluorescence and absorbance, after which 7.5 µL of the rotaxane solution was added to make a 25 µM solution. 7.5, 37.5, or 75 µL of 100 mM TBASH stock was added for the 10, 50, and 100 equivalent reactions, respectively. For Fluorescence, the excitation wavelength was set to 310 nm, and the emission was measured from 350 – 700 nm, with a 2 nm step size. Absorbance was measured from 250 – 700 nm. Fluorescence and absorbance spectra are shown in Appendix G, Figures G.9 – G.17.

CHAPTER IX

CONCLUDING REMARKS: WHERE WE ARE AND WHERE WE NEED TO GO IN HYDROGEN SULFIDE RESEARCH AND SCIENCE PUBLISHING

This chapter contains an unpublished perspective on the state of science publishing today. The perspective was conceived of and written by Carolyn M. Levinn, with editorial assistance from Michael D. Pluth. This chapter also includes previously published and co-authored material from Levinn, C.M.; Cerda, M.M.; Pluth, M.D. Development and Application of Carbonyl Sulfide-Based Donors for H_2S Delivery. *Acc. Chem. Res.* **2019**, *52* (9), 2723-2731. This review was co-written by Dr. Matthew M. Cerda and Carolyn Levinn, with editorial assistance from Professor Michael D. Pluth.

9.1 Concluding Remarks: Future Directions in the Field of H_2S Research

When the Pluth Lab started working in the area of H_2S donation and sensing, the field was relatively new. However, over the past few years, the number of general tools for the study of H_2S has grown almost exponentially. Now there are many tools available for researchers to work with, and it is time for scientists to dive deeper into the next layer of H_2S chemical biology.

This dissertation covers the work I've done over the fast three years, developing new H_2S probes and donors, and working to better understand the mechanics of the commonly employed thiocarbamate platform. One way I approached the study of thiocarbamates was by altering the payload motif – from N-H to N-methyl anilines

(Chapter 4). This work only scratched the surface – it would be interesting to study different payload scaffold in more depth. For example, if the thiocarbamate nitrogen was locked into a cyclic motif, both alkyl or aryl – how would that impact the reactivity? Could such modifications impact not just the rate of COS release, but also the rate-determining or product-determining step? Additionally, a lot of time and effort has been invested in designing donors with different triggering motifs, which has greatly advanced the field of H_2S research. outbuilding from this work, a next logical step would relate to the development of donor with more targeted systems. We have shown there to be different apparent cytotoxicity with different COS donors, and a large factor in that is likely differences in subcellular localization. Making COS donors with the same triggering motif that are targeted to different organelles could have a significant impact on our understanding of COS toxicity relative to that of H_2S.

Similarly, further investigations are needed into the potential direct toxicity of COS. We have shown that smaller esterase-triggered COS donors exhibit significant cytotoxicity at concentrations as low as 10 μM, whereas the COS-depleted controls, Na_2S, and other small-molecule direct H_2S donors have no effect. This observation raises the question of whether COS has activity independent of that of H_2S. Although we have demonstrated that the cytotoxicity of small molecule esterase-triggered donors correlates directly with the rate of COS release, fully disentangling the effects of COS delivery from the physiological effects of H_2S is a complex problem, and remains an unmet challenge in the field. Furthermore, although there are many different isoforms of CA, little is known about the different reactivity toward COS and CO_2, with available data showing that the commonly-used bovine CA-II has a significantly higher catalytic

efficiency toward its native substrate CO_2 (8×10^7 $M^{-1}s^{-1}$) than for COS (2.2×10^4 $M^{-1}s^{-1}$).[107-108] There is a relative dearth of knowledge about the activities of different CA isoforms toward COS, and how the subcellular localizations of the enzyme isoforms effects the observed toxicity of different COS donors.

Another outstanding challenge is that of COS detection. Although COS can be detected through GC-MS analysis or other spectroscopic methods, there are currently no simple methods available for the detection of COS directly in aqueous solution, which significantly limits the ability to accurately study COS in biological systems. For example, although COS has been detected in the headspace of porcine coronary artery and cardiac muscle, with the current technology it cannot be conclusively determined whether that COS was from mammalian or bacterial origin.[132] To truly advance the field of biological COS research, solution-phase COS probes and detection methods need to be developed. With the rapidly growing interest in COS as both a vehicle for H_2S delivery and as a distinct biomolecule, we anticipate that these knowledge gaps will be filled through the collective efforts of the gasotransmitter research community, and that a new category of COS-based targeted tools and therapeutics will emerge.

9.2 Learning from our Mistakes: We have a Scientific and Fiscal Obligation to Publish Failed Results

One of the great things about science is that it is supposed to be self-correcting by nature. Researchers and theorists publish their hypotheses, data, and interpretations, which form the basis for future iterations of experiments and analyses. These subsequent studies either support and further validate the earlier findings or provide new evidence

contrary to initial interpretations. In many cases, such debates can live on in the literature for many years, often fueling the development of new methods to test experimental hypotheses that were as-of-yet inaccessible in earlier investigations. The more data that is available in these scenarios, even results that are inconclusive or seemingly uninteresting at the time, the more complete the analyses can be. From this perspective, all data are useful; all data are good data. Yet there remains a remarkable hesitation by researchers to publish null results or results that do not fit perfectly into the tidy package of a final manuscript.

This growing trend of only including positive data in published work is leading to a narrower and potentially less accurate view of science – cherry-picking only the data that agrees with what has been previously reported lends a clear bias to the research, which not only propagates inaccuracies, but also provides an incomplete picture of the real boundaries of new methods or ideas.[252-254] Additionally, not making public what experiments did or did not work creates significant redundancy and waste: wasted time, wasted materials, and wasted money. Clearly some redundancy is important and serves as a key check in the literature, but this utility is lost if these experiments – both positive and negative – are not published in the first place. And while there is undoubtably a benefit in researcher training to learn how to fail, reassess, and try something new, there is certainly room enough in science to accomplish this without wasting effort and mental health on experiments that others have already proven will fail.

The growing reluctance to publish less interesting or null results comes at a cost. In 2016, the US federal government funded more than half (54%) of the academic research and development efforts in the US.[255] In total, this amounts to approximately

$38.8 billion dollars, which is about 1.1% of the estimated $3,561 billion in tax revenue collected by the government that year.[256] This is a lot of money (although arguably not enough), and the economic benefits to fundamental research are high and measurable.[257-258] Without better information stewardship, however, we as a community are often inadvertently asking taxpayers to fund researchers to perform experiments that others have likely tried and know not to be successful. Pushing more information out to the scientific community helps to inform what techniques and methodologies work on what systems, establish and expand the limits of what can be done, and define key needs for future investigation. All of these aspects maximize efficiency, both in researcher training and scientific discovery.

We believe that this is especially tangible in chemistry. Using organic synthesis as an example, one can easily run hundreds of experiments or design and prepare novel compounds that end up not performing a desired function or are incompatible with later steps in a synthetic sequence.[259] Such results are rarely published, or if they are may end up buried in the experimental section of an embargoed PhD thesis. Such compounds or reactions, however, help define the real substrate scope of new methodologies, displaying limitations or functional group tolerance on unique substrates that would otherwise not be tested. The characterization of intermediates, whether or not useful to the original story, can guide future researchers in trying to decipher what they themselves have prepared. Such unwanted or uninteresting compounds may prove to be of high value in the future in areas of chemistry that have yet to be discovered and expanded. In essence, future researchers may want to make a compound that has already been prepared but was never published because it did not fit cleanly into an overarching narrative. By not making this

information available and accessible, we are in many cases hindering the field, slowing progress, and wasting time and other resources in the scientific community, as well as the limited taxpayer money. Put simply, we have an obligation to publish scientifically sound, "failed" results, not just ones packaged in a nice, neat success story.

This principle of increasing the dissemination of all data, useful or not, gained some traction in the early 2010's with a number of publishing platforms establishing entire journals designated for publishing negative or null results.[260-261] Such efforts, however, have met limited success. Many of the journals folded within a few years, due in part to the fact that publishing null results is not incentivized by most academic structures, such as impact factors, citation rates, or journal prestige.[253, 262]

Learning from these failed publishing experiments, the question remains: how can we, the creators and consumers of scientific information and outcomes, ensure that this information is available? Is there a place in the scientific literature for unsuccessful experiments and failed results? Some might argue that no – including failed experiments would decrease general readability of the literature, exploding a four page communication into a 300 page saga. Or, one might contend that failed results often lead to spin-off projects within the same labs, and that disseminating that information puts researchers, especially those early in their careers, at risk of being scooped by more established competing labs that have more resources.

One potential solution could involve publishing on open-access multi-component platforms, such as Octopus, currently under development by a team led by Dr. Alexandra Freeman.[263-265] This approach rejects the classical idea of publishing a paper or article as a 'unit' of science – instead favoring a system where any researcher can publish a result

or an idea as a piece in the chain of research, rather than as a completed story. Such platforms offer many more opportunities for often overlooked or insignificant results, both negative and positive, to be made public.

Another solution could be requiring that any federally funded research projects publish their results, both negative and positive, within a set time frame of the end of the grant period. Such a system would provide a time buffer for labs to develop spin-off projects from unanticipated findings, but still ensures that all information is eventually made public, hopefully minimizing redundancy without reward.

More broadly, this is a conversation that needs to be had, with potential solutions and paths forward discussed and debated at length. While there is no one perfect solution right now, increasing visibility of the problem can help, and, there are some relatively straight-forward ways that people can start. As an open access platform, most supplemental information (SI) files are available even without subscriptions to the specific journal. A starting solution could be including a second SI file, or even just a subsection in the normal SI, that includes experiments that were tried and unsuccessful, or that were successful but did not go anywhere or were not pursued. In fact, some researchers are already including similar sections in their SIs.[266-267] One major limitation of this solution is that such files are not generally indexed, which makes broad capture of the information less likely, however this approach would put the results where at least researchers in that field who would likely benefit the most might be most likely to find it. This certainly would look different from field to field, and of course is more tractable in some areas than others. However, in some areas, such as synthetic organic chemistry, the obvious barriers are not so high, and this would be a good place to start.

We are confident that even small steps toward this larger goal can provide a real impact, both with regard to scientific rigor and economic sensibility. We have a duty to the taxpayers to maximize our efficiency as best as possible, while maintaining high research standards. We view that the field of chemistry is poised to play a leadership role in this endeavor, and challenge chemists to think about new ways of publishing the full results of their work.

APPENDIX A

SUPPLEMENTARY CONTENT FOR CHAPTER II

Appendix A is the supplementary appendix for Chapter II of this dissertation. It includes the general H_2S-releasing mechanisms of the various compounds reported in Chapter II.

Hydrolysis-Activated Donors

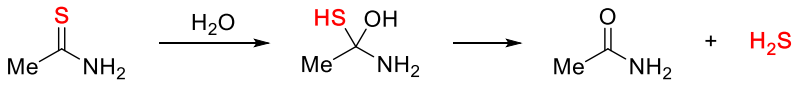

Scheme A.1 Mechanism of hydrolysis-mediated H_2S release from thioacetamide

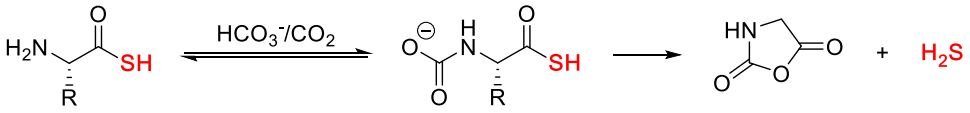

Scheme A.2 Mechanism of H_2S release from thioaminoacids (R = Me or H) in the presence of bicarbonate (HCO_3^-)

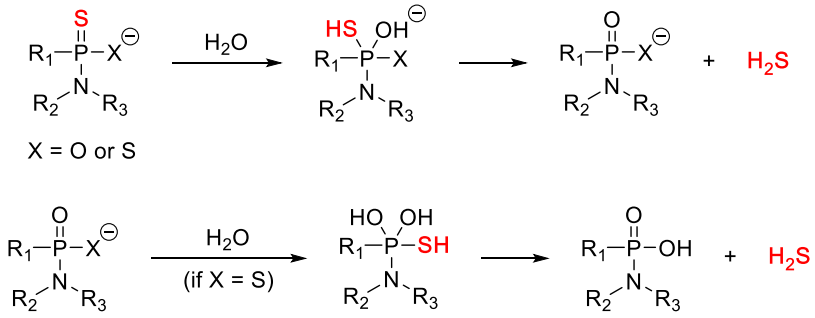

Scheme A.3. Generalized hydrolysis mechanism of H_2S release from **GYY4137,** phosphorodithioates, and **FW1256**

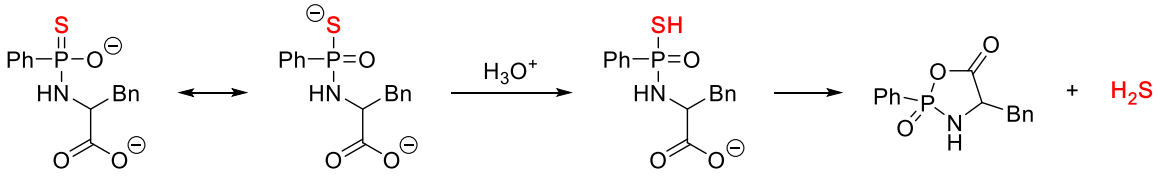

Scheme A.4 Mechanism of acid-mediated H_2S release from **JK-2**

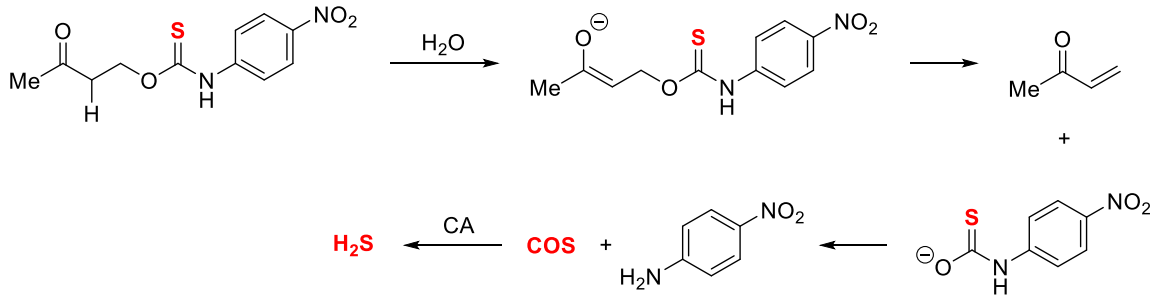

Scheme A.5 Mechanism of COS/H_2S release from **γ-KetoTCM-1** in the presence of carbonic anhydrase (CA)

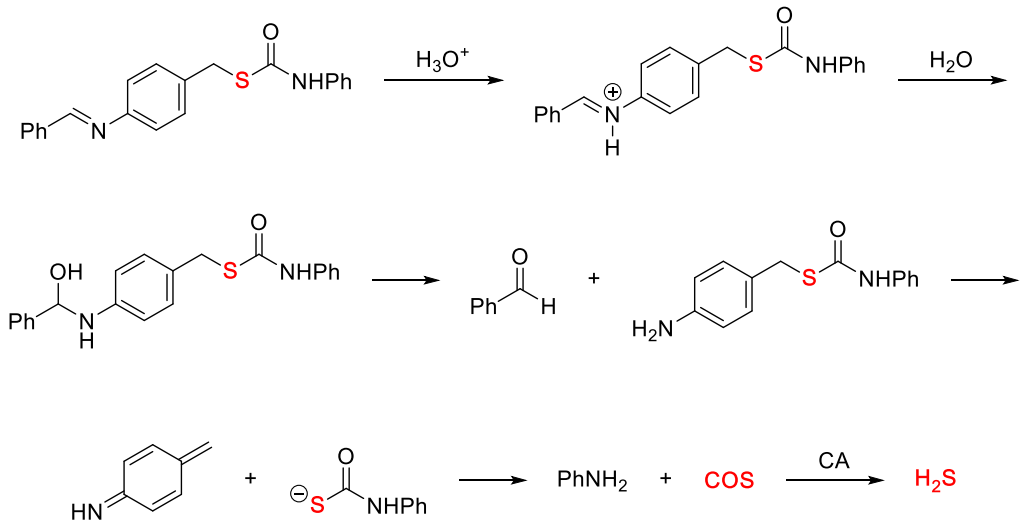

Scheme A.6 Mechanism of COS/H_2S release from ***S*-pHTCM** *via* imine hydrolysis in the presence of carbonic anhydrase (CA)

Thiol-Activated Donors

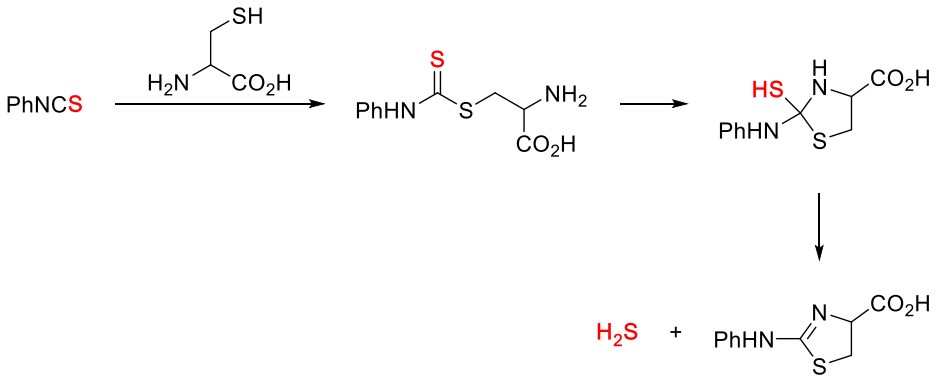

Scheme A.7 Mechanism of cysteine-activated H_2S release from arylisothiocyanates

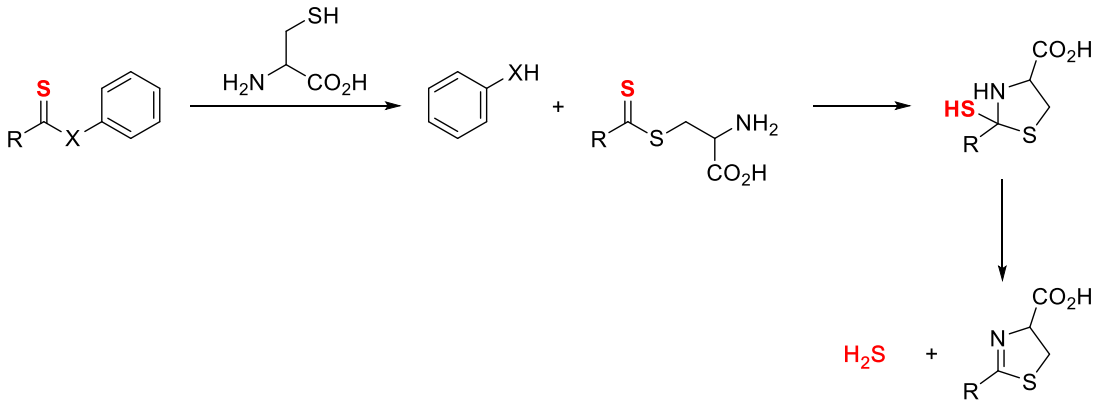

Scheme A.8 Mechanism of cysteine-mediated H_2S release from thionoesters (R = Ph, X = O) and dithioesters (R = alkyl or aryl, X = S)

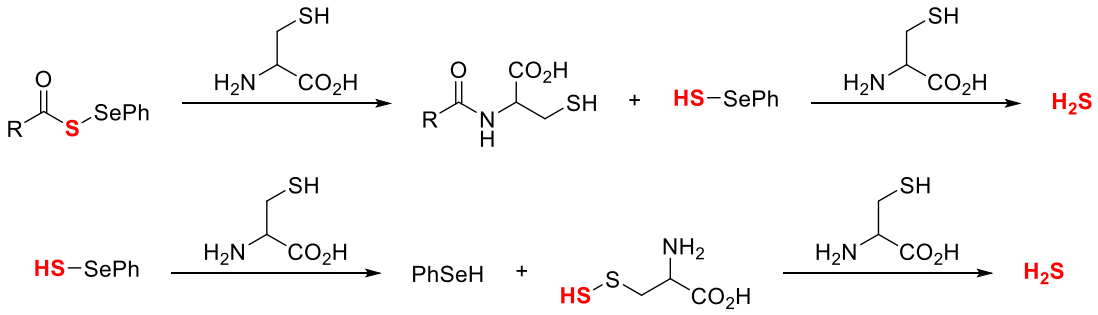

Scheme A.9 Mechanism of cysteine-mediated H_2S release from cyclic and acyclic acylated selenylsulfides

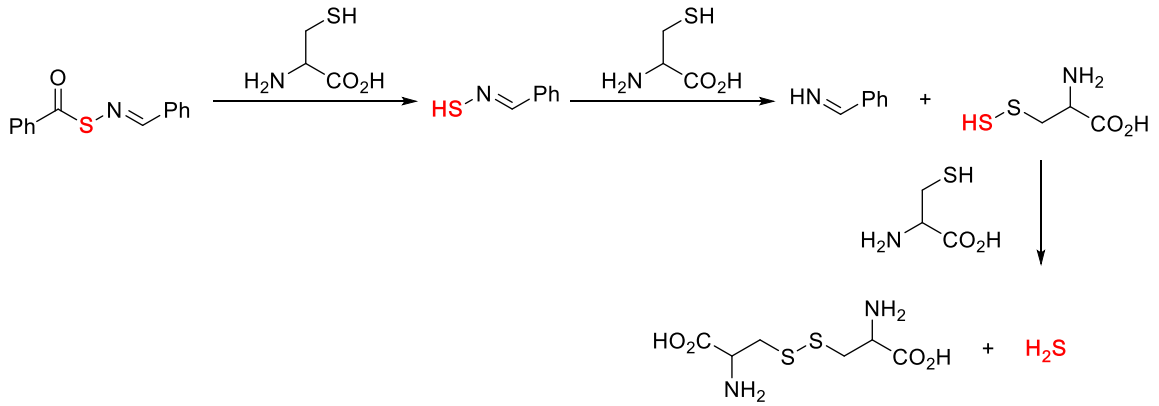

Scheme A.10 Mechanism of cysteine-mediated H_2S release from *S*-aroylthiooxime-based donors

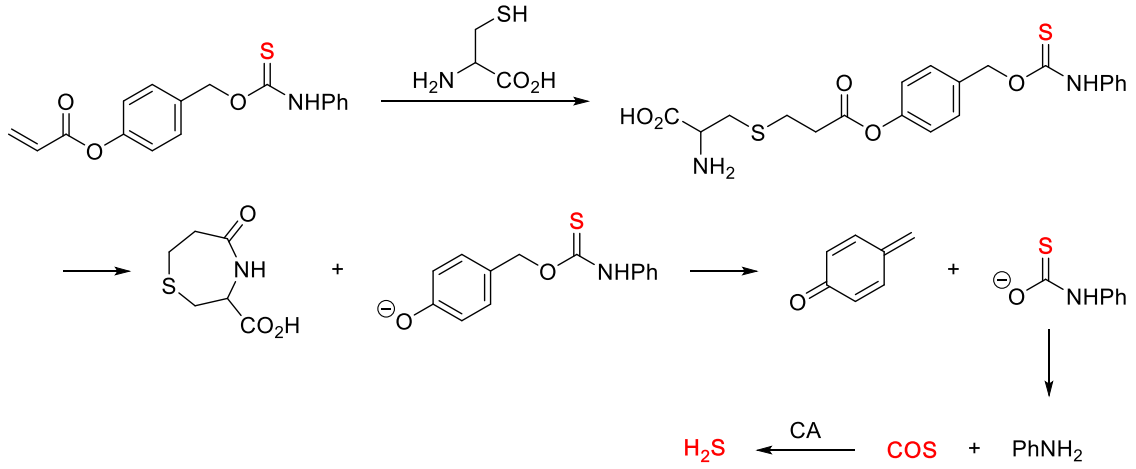

Scheme A.11 Mechanism of cysteine-selective COS/H_2S release from **OA-CysTCM-1** in the presence of carbonic anhydrase (CA)

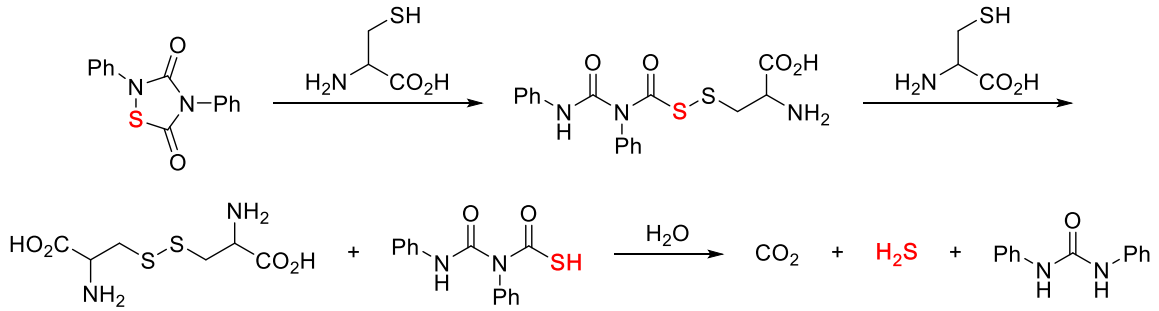

Scheme A.12 Proposed mechanism of H_2S release from 1,2,4-thiadiazolidine-3,5-diones in the presence of cysteine

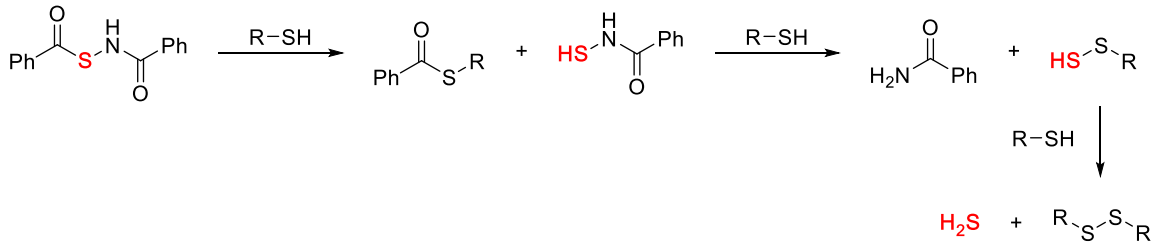

Scheme A.13 Mechanism of H_2S release from "*N*-mercapto donors" in the presence of thiols

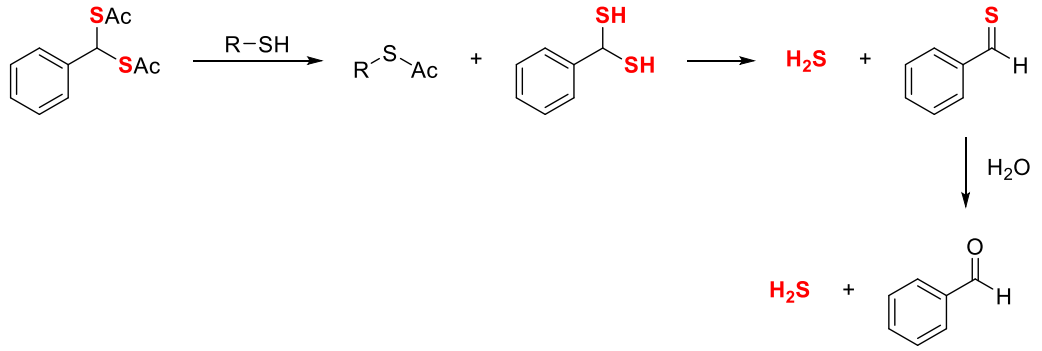

Scheme A.14 Mechanism of H_2S release from acylated geminal dithiols in the presence of thiols

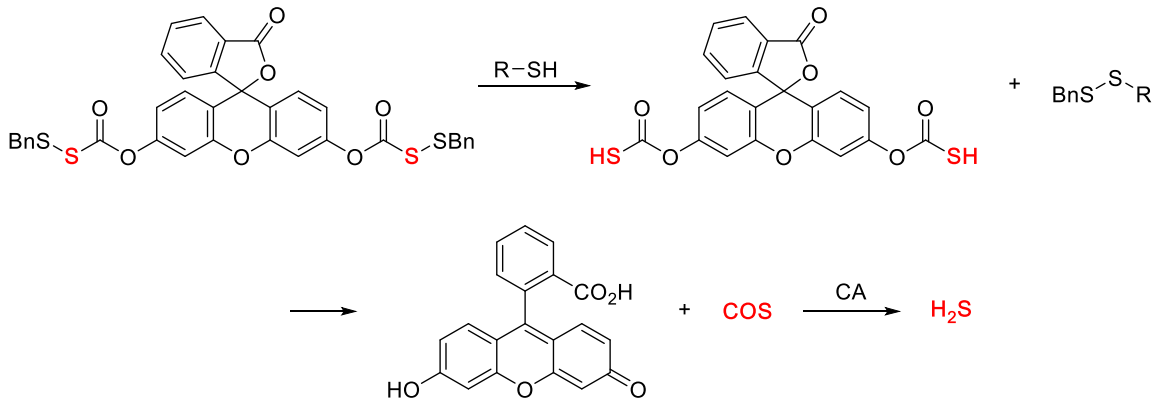

Scheme A.15 Mechanism of COS/H_2S release from **FLD-1** in the presence of thiols and carbonic anhydrase (CA)

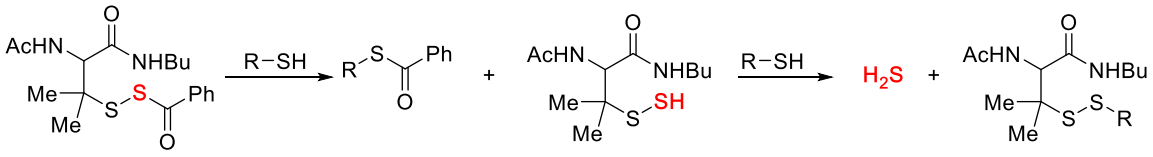

Scheme A.16 Mechanism of H_2S release from acylated persulfides in the presence of thiols

Scheme A.17 Mechanism of H_2S release from organic polysulfides including **DATS** in the presence of thiols. We note the presence of a pendant allyl group likely complicates the mechanism of H_2S release from **DATS**.

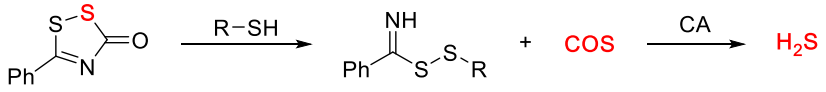

Scheme A.18 Mechanism of thiol-mediated COS/H_2S release from cyclic sulfenylthiocarbamates in the presence of carbonic anhydrase (CA)

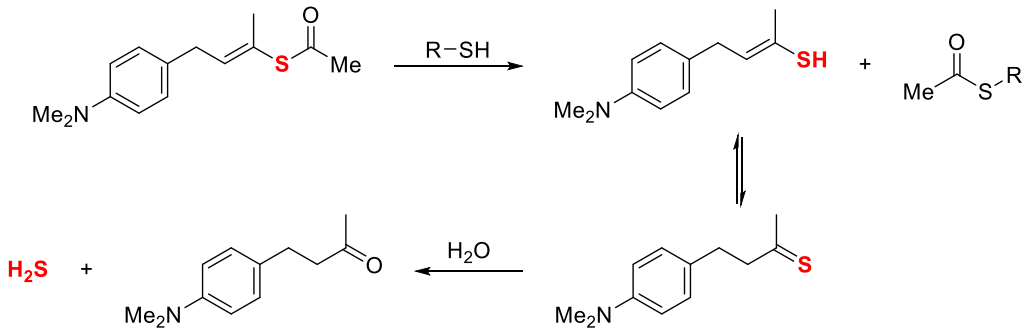

Scheme A.19 Mechanism of H_2S release from protected thioenols in the presence of thiols

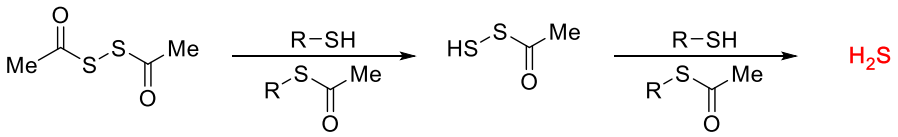

Scheme A.20 Mechanism of H_2S release from dithioperoxyanhydrides in the presence of thiols

Enzyme-Activated Donors

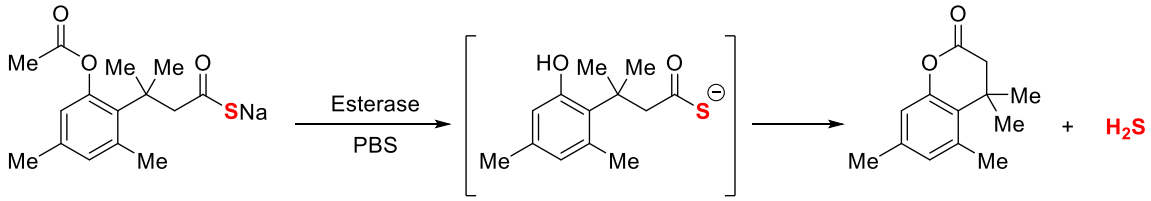

Scheme A.21 Mechanism of H_2S release from **HP-101** in the presence of esterase

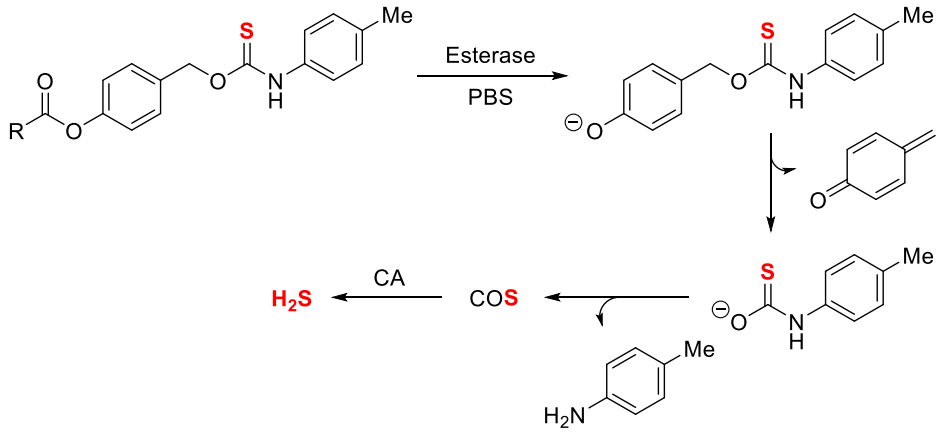

Scheme A.22 Mechanism of H_2S release from **Esterase-TCM-OA** in the presence of esterase and carbonic anhydrase

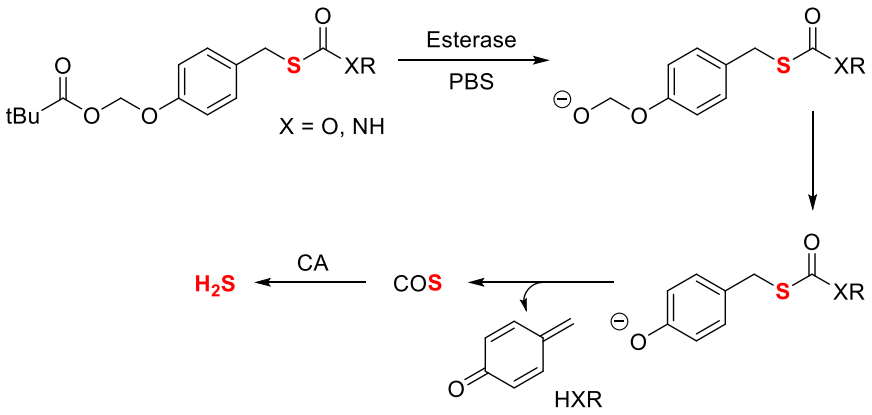

Scheme A.23 Mechanism of H_2S release from **Esterase-TCM-SA** in the presence of esterase and carbonic anhydrase

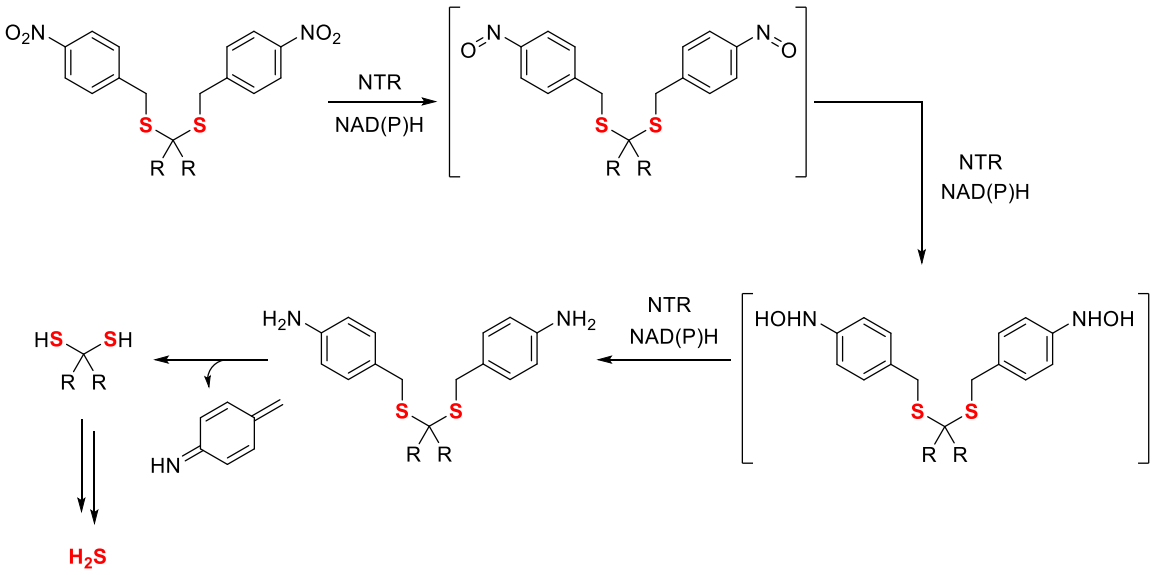

Scheme A.24 Mechanism of H_2S release from **NTR-H2S** in the presence of nitroreductase

H_2O_2-Activated Donors

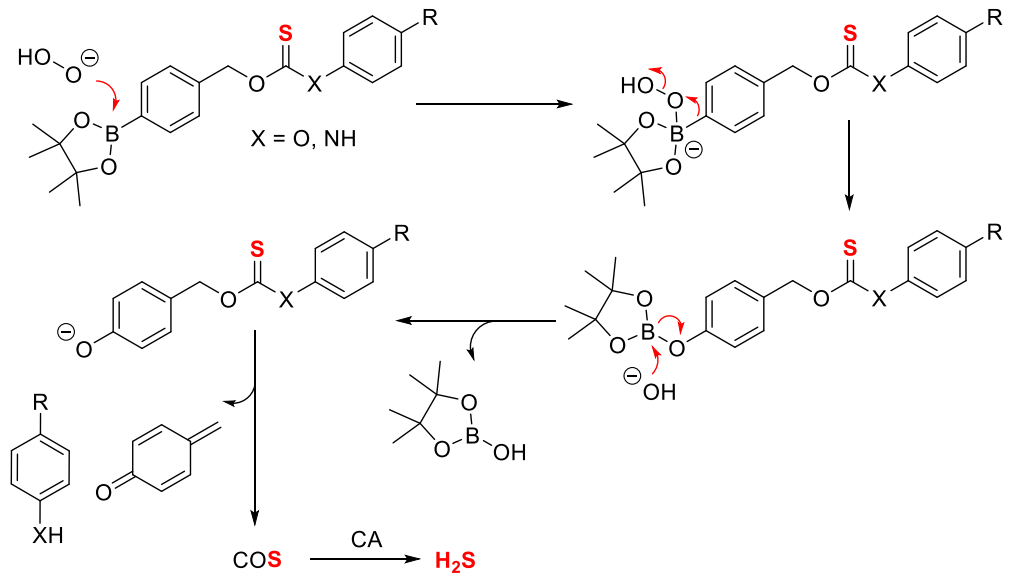

Scheme A.25 Mechanism of H_2S release from H_2O_2-triggered thiocarbamates and thiocarbonates in the presence of carbonic anhydrase

Photolabile Donors

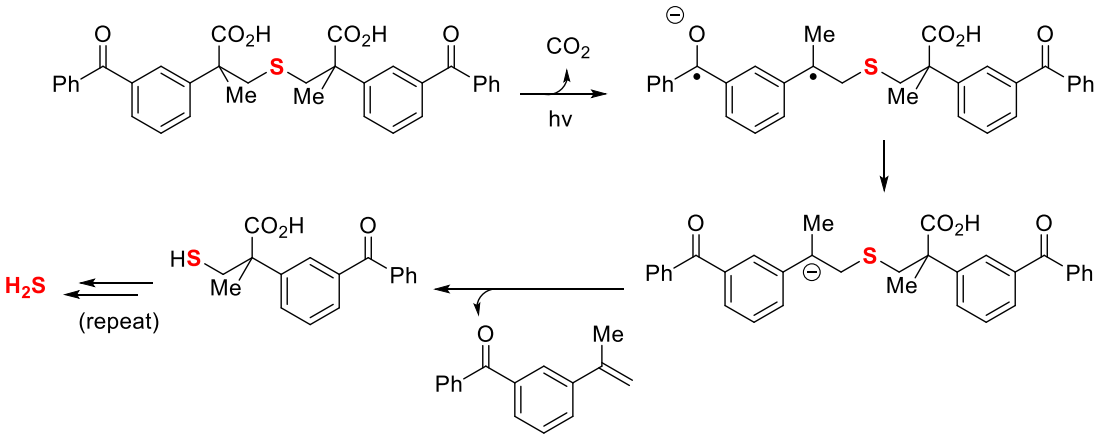

Scheme A.26. Mechanism of H_2S release from photolabile ketoprofenate-caged thioethers

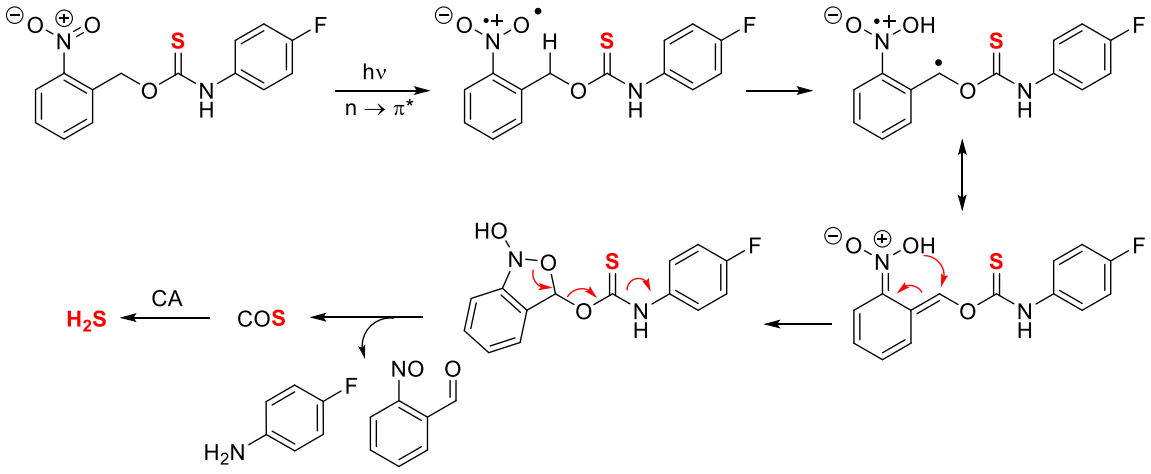

Scheme A.27 Mechanism of H_2S release from ortho-nitrophenyl thiocarbamates **PhotoTCM-1** in the presence of carbonic anhydrase

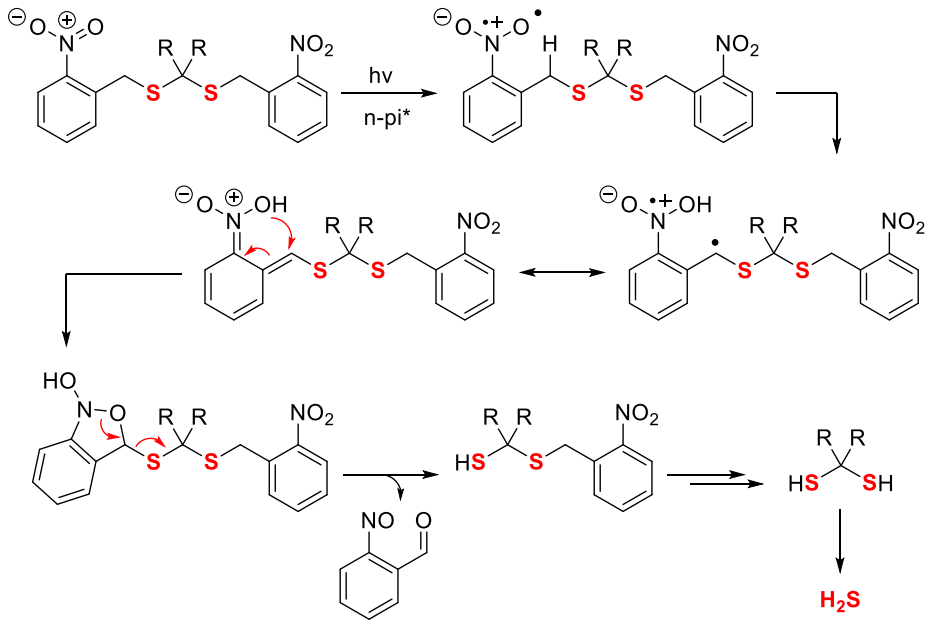

Scheme A.28 Mechanism of H_2S release from ortho-nitrophenyl caged **Photo-gem-dithiol**

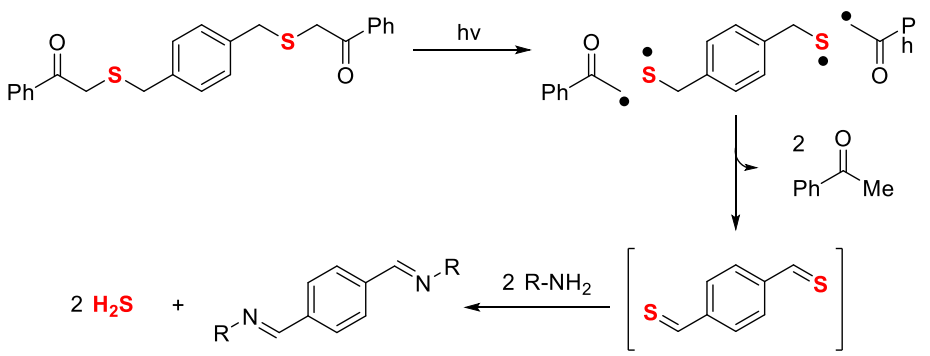

Scheme A.29 Mechanism of H_2S release from photo-caged thiobenzaldehydes in the presence of amines

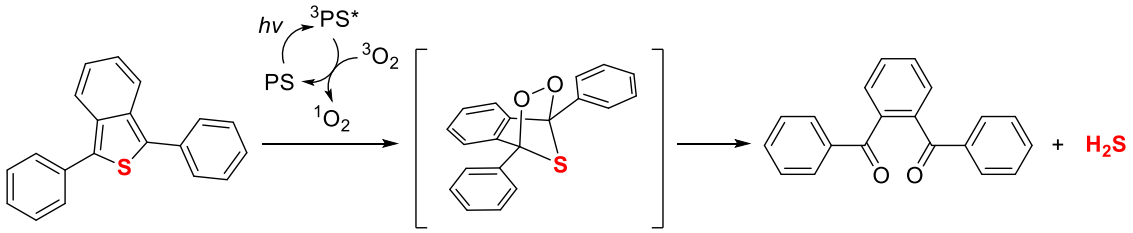

Scheme A.30 Mechanism of H_2S release from **DPBT** in the presence of a photosensitizer (PS) and oxygen. The protons in the generated H_2S originate from the water in the aqueous reaction conditions.

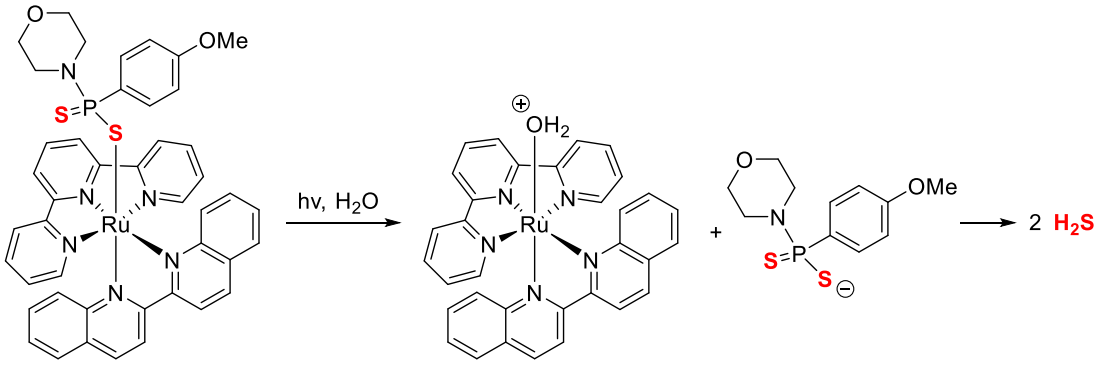

Scheme A.31 Mechanism of H_2S release from **Ru-GYY**

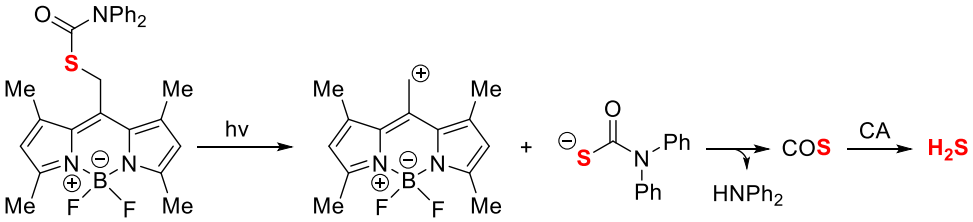

Scheme A.32 Mechanism of H_2S release from **BODIPY-TCM-2** in the presence of CA

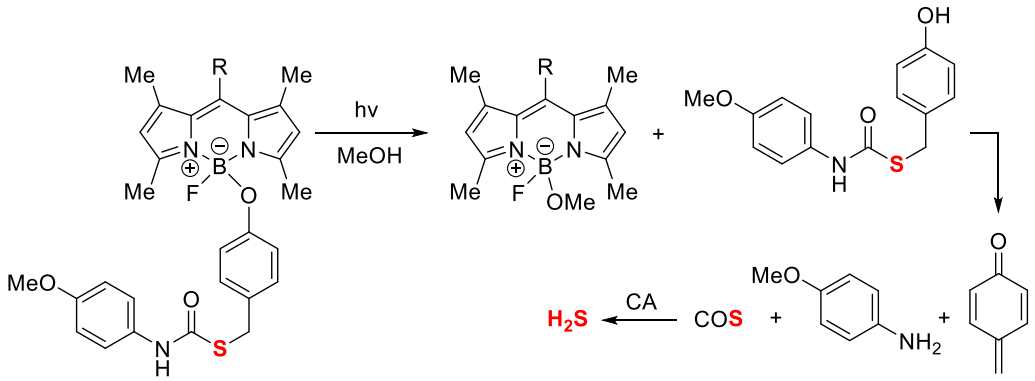

Scheme A.33 Mechanism of H_2S release from **BODIPY-TCM-1** in the presence of CA

APPENDIX B

SUPPLEMENTARY INFORMATION FOR CHAPTER III

Appendix B is the supplementary information for Chapter III of this dissertation. It includes spectra and experimental data relevant to the material in Chapter III.

Synthesis / Spectral Details of Prepared Compounds

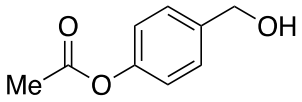

Me-OH was prepared with 4-hydroxybenzyl alcohol and acetyl chloride according to the general synthetic procedure described above. (324 mg, 48% yield). Spectral data is in agreement with those reported in the literature.[268]

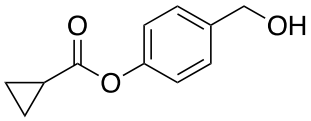

Cp-OH was prepared with 4-hydroxybenzyl alcohol and cyclopropanecarbonyl chloride according to the general synthetic procedure described above. (506 mg, 65% yield). Spectral data is in agreement with those reported in the literature.[269]

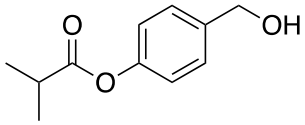

iPr-OH was prepared with 4-hydroxybenzyl alcohol and isobutyryl chloride according to the general synthetic procedure described above. (423 mg, 54% yield). Spectral data is in agreement with those reported in the literature.[270]

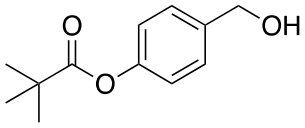

tBu-OH was prepared with 4-hydroxybenzyl alcohol and pivaloyl chloride according to the general synthetic procedure described above. (329 mg, 39% yield). Spectral data is in agreement with those reported in the literature.[271]

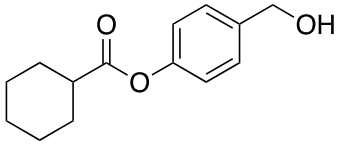

Cy-OH was prepared with 4-hydroxybenzyl alcohol and cyclohexanecarbonyl chloride according to the general synthetic procedure described above. (388 mg, 41% yield). Spectral data is in agreement with those reported in the literature.[270]

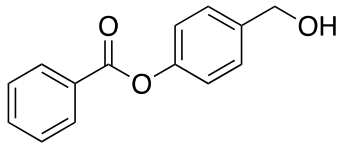

Ph-OH was prepared with 4-hydroxybenzyl alcohol and benzoyl chloride according to the general synthetic procedure described above. (726 mg, 79% yield). Spectral data is in agreement with those reported in the literature.[272]

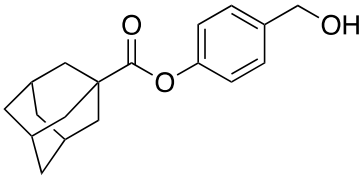

Ad-OH was prepared with 4-hydroxybenzyl alcohol and 1-adamantanecarbonyl chloride according to the general synthetic procedure described above. (416 mg, 36% yield). ^{1}H NMR (500 MHz, $CDCl_3$) δ (ppm): 7.37 (d, *J* = 8.22 Hz, 2H), 7.05 (d, *J* = 8.22 Hz, 2H), 4.69 (d, *J* = 1.65 Hz, 2H), 2.86 (bs, 1H), 2.11 (m, 3H), 2.08 (d, *J* = 3.17 Hz, 6H), 1.79 (d, *J* = 3.51 Hz, 6H). ^{13}C{^{1}H} NMR (125 MHz, $CDCl_3$) δ (ppm): 176.30, 150.52, 138.15, 128.01, 121.67, 64.78, 41.03, 38.76, 34.46, 27.92. IR (cm^{-1}) 3515.75, 2903.27, 2853.32, 1718.00, 1504.69, 1452.47, 1222.53, 1189.10, 1160.28, 1040.92. HRMS m/z $[M + H]^+$ calcd. For $[C_{18}H_{15}O_3]^+$ 279.1021; found 279.1030.

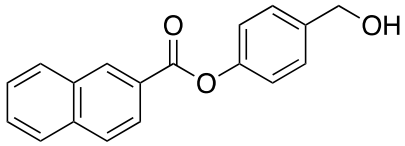

Nap-OH was prepared with 4-hydroxybenzyl alcohol and 2-naphthoyl chloride according to the general synthetic procedure described above. (660 mg, 59% yield). ^{1}H NMR (500 MHz, $CDCl_3$) δ (ppm): 8.83 (s, 1H), 8.23 (dd, *J* = 8.6, 1.7 Hz, 1H), 8.04 (d, *J* = 8.1 Hz, 1H), 7.99 (d, *J* = 8.6 Hz, 1H), 7.96 (d, *J* = 8.1 Hz, 1H), 7.67 (ddd, *J* = 8.1, 6.8, 1.3 Hz, 1H), 7.62 (ddd, *J* = 8.1, 6.8, 1.3 Hz, 1H), 7.50 (d, *J* = 8.6 Hz, 2H), 7.30 (d, *J* = 8.6 Hz, 2H), 4.78 (s, 2H), 1.66 (bs, 1H). $^{13}C\{^{1}H\}$ NMR (125 MHz, $CDCl_3$) δ (ppm): 165.42, 150.48, 138.57, 135.85, 132.51, 131.97, 129.50, 128.67, 128.42, 128.19, 127.86, 126.87, 126.69, 125.46, 121.91, 64.88. IR (cm^{-1}) 3319.86, 3058.22, 2867.44, 2360.09, 2341.52, 1734.43, 1631.12, 1596.86, 1508.04, 1463.36, 1418.26, 1387.99, 1352.95, 1280.24, 1225.79, 1194.70, 1164.29, 1080.76, 1013.92. HRMS m/z $[M + H]^+$ calcd. For $[C_{18}H_{23}O_3]^+$ 287.1647; found 287.1647.

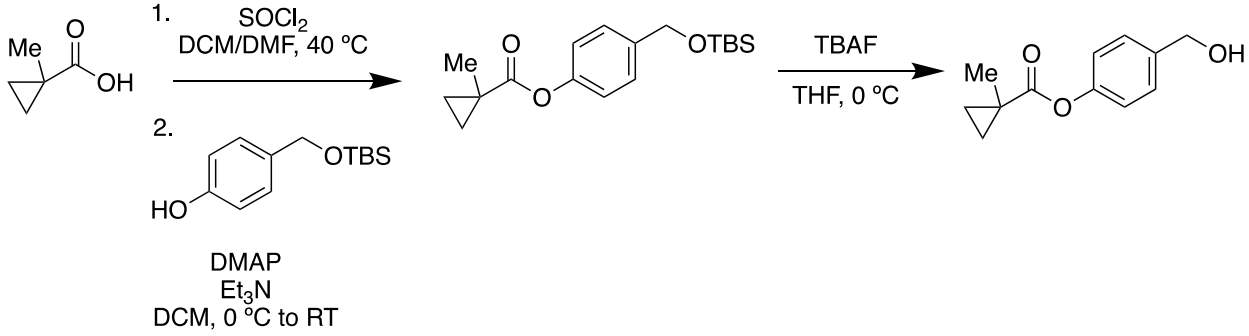

MCp-OH was prepared from the corresponding carboxylic acid. MCp-COOH (1.50 g, 1.0 equiv.) was dissolved in anhydrous dichloromethane (3.0 mL, 5.0 M solution), followed by addition of anhydrous DMF (60 µL, 0.05 equiv.). The reaction mixture was

heated to reflux, and $SOCl_2$ (1.20 mL, 1.1 equiv.) was added dropwise under reflux. The reaction mixture was stirred under reflux for two hours, then concentrated under reduced pressure. The crude reaction mixture was re-dissolved in a minimum of dichloromethane and added dropwise to a stirring solution of 4-(TBS-hydroxymethyl)phenol (2.0 g, 0.56 equiv.), triethylamine (3.51 mL, 1.68 equiv.), and DMAP (500 mg, 0.28 equiv.) in dichloromethane (60 mL, 0.25 M solution). Upon completion (as determined by TLC) the reaction was quenched with 20 mL of brine, and extracted with methylene chloride (3 x 20 mL). The combined organic layers were dried over anhydrous magnesium sulfate, and purified by silica column chromatography to yield 1.03 g (21% yield over two steps). MCp-OTBS (1.03 g, 1.0 equiv.) was dissolved in anhydrous THF (32 mL, 0.1 M solution) under an atmosphere of nitrogen, and cooled to 0 °C. TBAF (3.20 mL 1.0 M in THF, 1.0 equiv.) was added dropwise. The reaction was let stir for 30 minutes, quenched with brine (10 mL), and extracted with ethyl acetate (3 x 20 mL). The combined organic layers were dried over anhydrous $MgSO_4$, concentrated under reduced pressure, and purified by silica column chromatography to yield MCp-OH as a white solid (365 mg, 55% yield). ^{1}H NMR (500 MHz, $CDCl_3$) δ (ppm): 7.37 (d, J = 8.40 Hz, 2H), 7.06 (d, J = 8.40 Hz, 2H), 4.67 (s, 2H), 1.90 (bs, 1H), 1.44 (m, 5H), 0.86 (m, 2H). $^{13}C\{^1H\}$ NMR (125 MHz, $CDCl_3$) δ (ppm): 174.73, 150.38, 138.25, 127.97, 121.65, 64.73, 19.45, 18.81, 17.47. IR (cm^{-1}) 3356.76, 2969.77, 1736.30, 1652.94, 1606.43, 1507.08, 1465.16, 1419.78, 1388.80, 1324.07, 1163.95, 1120.74, 1013.39. HRMS m/z $[M + H]^+$ calcd. For $[C_{12}H_{15}O_3]^+$ 207.1021; found 207.1019.

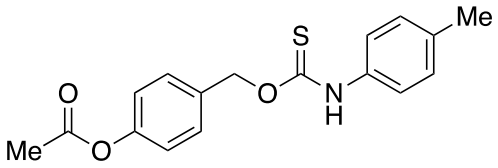

TCM1 was prepared with *p*-tolyl isothiocyanate and Me-OH according to the general synthetic procedure described above. (25 mg, 14% yield). ^{1}H NMR (500 MHz, DMSO-d_6, 60 °C) δ (ppm): 10.99 (s, 1H), 7.69-6.93 (m, 8H), 5.55 (s, 2H), 2.28 (bs, 6H). Broadness is observed in the ^{1}H NMR spectrum due to rotation around the C-N bond of the thiocarbamate. ^{13}C{^{1}H} NMR (125 MHz, DMSO-d_6, 25 °C) δ (ppm) 187.81, 187.20, 169.67, 150.82, 136.45, 135.55, 134.86, 134.57, 134.01, 133.63, 130.23, 129.78, 129.69, 129.35, 123.41, 122.47, 122.38, 71.89, 70.26, 60.23, 21.32, 21.24, 21.00, 20.90, 14.57. Splitting of peaks is observed in the ^{13}C{^{1}H} NMR spectrum due to slow rotation around the C-N bond of the thiocarbamate, yielding rotamers. IR (cm^{-1}) 3195.71, 3170.76, 3100.82, 3030.76, 2950.80, 1753.55, 1593.68, 1540.73, 1507.65, 1455.32, 1405.65, 1365.85, 1342.19, 1218.90, 1206.36, 1186.16, 1173.45, 1162.22. HRMS m/z $[M + H]^+$ calcd. For $[C_{17}H_{18}NO_3S]^+$ 316.1007; found 316.1016.

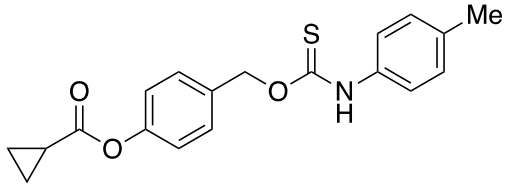

TCM2 was prepared with *p*-tolyl isothiocyanate and Cp-OH according to the general synthetic procedure described above. (65 mg, 39% yield). ^{1}H NMR (500 MHz, DMSO-d_6, 60 °C) δ (ppm): 10.97 (s, 1H), 7.65-6.97 (m, 8H), 5.55 (s, 2H), 2.28 (s, 3H), 1.89 (m,

1H), 1.05 (m, 4H). Broadness is observed in the ^{1}H NMR spectrum due to rotation around the C-N bond of the thiocarbamate. $^{13}C\{^{1}H\}$ NMR (125 MHz, DMSO-d_6, 25 °C) δ (ppm): 187.81, 187.19, 173.35, 150.77, 136.46, 135.55, 134.86, 134.57, 134.02, 133.64, 130.20, 129.78, 129.69, 129.35, 123.42, 122.47, 122.33, 71.88, 70.24, 21.00, 20.90, 13.06, 9.52. Splitting of peaks is observed in the $^{13}C\{^{1}H\}$ NMR spectrum due to slow rotation around the C-N bond of the thiocarbamate, yielding rotamers. IR (cm^{-1}) 3231.59, 3173.53, 3099.77, 3029.41, 2921.09, 1854.61, 1741.51, 1594.89, 1544.77, 1509.09, 1461.52, 1422.56, 1400.67, 1384.26, 1338.06, 1313.36, 1288.42, 1213.37, 1163.87, 1142.12. HRMS m/z $[M + H]^+$ calcd. For $[C_{19}H_{20}NO_3S]^+$ 342.1164; found 342.1174.

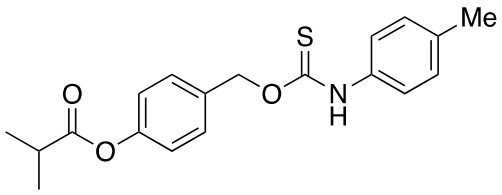

TCM3 was prepared with *p*-tolyl isothiocyanate and iPr-OH according to the general synthetic procedure described above. (52 mg, 31% yield). ^{1}H NMR (500 MHz, DMSO-d_6, 60 °C) δ (ppm): 10.97 (1H, s), 7.67 – 6.94 (bm, 8H), 5.56 (s, 2H), 2.83 (sept, J = 7.84, 1H), 1.25 (d, J = 7.84, 6H). Broadness is observed in the ^{1}H NMR spectrum due to rotation around the C-N bond of the thiocarbamate. $^{13}C\{^{1}H\}$ NMR (125 MHz, DMSO-d_6, 25 °C) δ (ppm): 187.83, 187.21, 175.48, 150.91, 136.47, 135.56, 134.84, 134.57, 134.00, 133.61, 130.23, 130.21, 129.80, 129.67, 129.34, 123.42, 122.47, 122.27, 71.91, 70.25, 33.78, 30.83, 20.98, 19.13. Splitting of peaks is observed in the $^{13}C\{^{1}H\}$ NMR spectrum due to slow rotation around the C-N bond of the thiocarbamate, yielding rotamers. IR (cm^{-1}) 3214.13, 3108.42, 3040.44, 2969.4, 2922.05, 1751.35, 1594.68, 1540.86, 1507.24,

1402.57, 1340.66, 1316.76, 1288.55, 1228.48, 1189.68. HRMS m/z $[M + H]^+$ calcd. For $[C_{19}H_{21}NO_3S]^+$ 344.1320; found 344.1308.

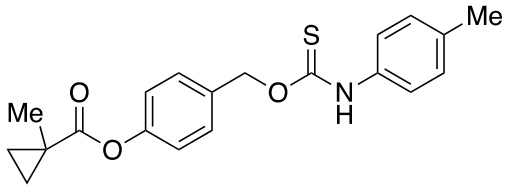

TCM4 was prepared with p-tolyl isothiocyanate and MCp-OH according to the general synthetic procedure described above. (100 mg, 61% yield). ^{1}H NMR (500 MHz, DMSO-d_6, 60 °C) δ (ppm): 10.99 (s, 1H), 7.66-6.99 (m, 8H), 5.54 (s, 2H), 2.28 (s, 3H), 1.38 (s, 3H), 1.34 (q, *J* = 3.84, 2H), 0.92 (q, *J* = 3.84, 2H). Broadness is observed in the ^{1}H NMR spectrum due to rotation around the C-N bond of the thiocarbamate. $^{13}C\{^1H\}$ NMR (125 MHz, DMSO-d_6, 25 °C) δ (ppm): 187.82, 187.18, 174.36, 150.97, 136.46, 135.55, 134.85, 134.56, 133.93, 133.53, 130.13, 129.77, 129.68, 129.34, 123.43, 122.46, 122.34, 71.92, 70.24, 21.00, 20.89, 19.43, 18.90, 17.31. Splitting of peaks is observed in the $^{13}C\{^1H\}$ NMR spectrum due to slow rotation around the C-N bond of the thiocarbamate, yielding rotamers. IR (cm^{-1}) 3208.15, 3172.09, 3102.38, 3034.45, 2969.61, 2924.52, 2868.84, 1739.32, 1592.23, 1541.25, 1508.68, 1449.58, 1421.32, 1398.13, 1334.24, 1315.04, 1287.58, 1211.63, 1189.86, 1166.87, 1123.90, 1013.25. HRMS m/z $[M + H]^+$ calcd. For $[C_{20}H_{22}NO_3S]^+$ 356.1320; found 356.1311.

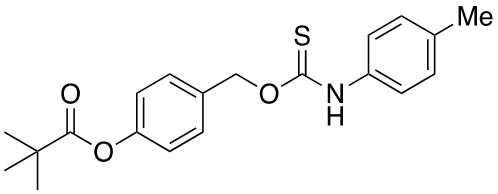

TCM5 was prepared with p-tolyl isothiocyanate and tBu-OH according to the general synthetic procedure described above. (109.4 mg, 64% yield). Spectral data is in agreement with those reported in the literature.[104]

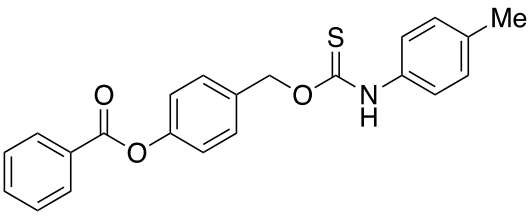

TCM6 was prepared with p-tolyl isothiocyanate and Ph-OH according to the general synthetic procedure described above. (34 mg, 22% yield). ^{1}H NMR (500 MHz, DMSO-d_6, 60 °C) δ (ppm): 11.00 (s, 1H), 8.15 (m, 2H), 7.75 (m, 1H), 7.64 (m, 2H), 7.58-7.11 (m, 8H), 5.59 (s, 2H), 2.28 (s, 3H). Broadness is observed in the ^{1}H NMR spectrum due to rotation around the C-N bond of the thiocarbamate. ^{13}C NMR (125 MHz, DMSO-d_6, 25 °C) δ (ppm): 187.84, 187.21, 165.06, 150.94, 136.47, 135.57, 134.87, 134.58, 134.31, 133.96, 133.91, 130.27, 129.90, 129.85, 129.72, 129.70, 129.62, 129.47, 129.36, 129.31, 123.44, 122.56, 122.50, 71.92, 70.25, 21.01, 20.91. Splitting of peaks is observed in the ^{13}C{^{1}H} NMR spectrum due to slow rotation around the C-N bond of the thiocarbamate, yielding rotamers. IR (cm^{-1}) 3200.22, 3156.21, 3092.37, 3028.96, 2969.84, 2925.83, 1728.56, 1591.53, 1538.83, 1508.72, 1449.12, 1398.19, 1365.23, 1338.94, 1312.68, 1263.16, 1249.22, 1225.59, 1209.75, 1188.14, 1174.53, 1079.50, 1056.59. HRMS m/z $[M + H]^+$ calcd. For $[C_{22}H_{22}NO_3S]^+$ 378.1164; found 378.1165.

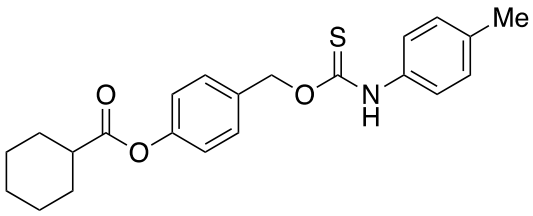

TCM7 was prepared with p-tolyl isothiocyanate and Cy-OH according to the general synthetic procedure described above. (46 mg, 29% yield). ^{1}H NMR (500 MHz, DMSO-d_6, 60 °C) δ (ppm): 10.97 (s, 1H), 7.62 – 7.14 (m, 8H), 5.55 (s, 2H), 2.61 (m, 1H), 2.28 (s, 3H), 2.00 (d, *J* = 12.2, 2H), 1.75 (m, 2H), 1.64 (2, *J* = 13.1, 1H), 1.52 (m, 2H), 1.36 (m, 2H), 1.29 (m, 1H). Broadness is observed in the ^{1}H NMR spectrum due to rotation around the C-N bond of the thiocarbamate. ^{13}C{^{1}H} NMR (125 MHz, DMSO-d_6, 25 °C) δ (ppm): 187.82, 187.20, 174.30, 150.91, 136.46, 135.56, 134.85, 134.57, 133.97, 133.58, 130.22, 129.81, 129.68, 129.61, 129.34, 123.42, 122.47, 122.32, 71.91, 70.25, 42.51, 28.93, 25.74, 25.18, 21.00, 20.90. Splitting of peaks is observed in the ^{13}C{^{1}H} NMR spectrum due to slow rotation around the C-N bond of the thiocarbamate, yielding rotamers. IR (cm^{-1}) 3203.91, 3176.67, 3030.10, 2930.06, 2854.13, 1752.75, 1527.52, 1511.28, 1386.41, 1311.79, 1208.06, 1178.02, 1165.88, 1147.76, 1114.41, 1017.32. HRMS m/z [M + H]$^{+}$ calcd. For [$C_{22}H_{26}NO_3S$]$^{+}$ 384.1633; found 384.1629.

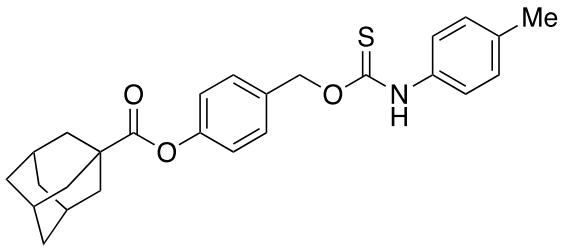

TCM8 was prepared with p-tolyl isothiocyanate and Ad-OH according to the general synthetic procedure described above. (40 mg, 26% yield). ^{1}H NMR (500 MHz, DMSO-

d_6, 60 °C) δ (ppm): 10.98 (s, 1H), 7.57 – 7.05 (m, 8H), 5.55 (s, 2H), 2.28 (s, 3H), 2.06 (bs, 3H), 2.01 (bs, 6H), 1.75 (bs, 6H). Broadness is observed in the ^{1}H NMR spectrum due to rotation around the C-N bond of the thiocarbamate. $^{13}C\{^1H\}$ NMR (125 MHz, DMSO-d_6, 25 °C) δ (ppm): 187.83,187.19, 175.84, 151.07, 136.47, 135.55, 134.86, 134.57, 133.95, 133.54, 130.21, 129.84, 129.68, 129.35, 123.43, 122.47, 122.29, 71.93, 70.25, 60.23, 40.85, 40.53, 38.68, 36.31, 34.85, 30.25, 27.73, 27.62, 21.24, 21.15, 21.00, 20.90, 14.57. Splitting of peaks is observed in the $^{13}C\{^1H\}$ NMR spectrum due to slow rotation around the C-N bond of the thiocarbamate, yielding rotamers. IR (cm^{-1}) 3223.67, 3181.01, 3109.75, 3039.47, 2917.77, 2904.34, 2848.45, 1743.95, 1595.09, 1535.42, 1508.71, 1450.52, 1422.61, 1396.44, 1333.48, 1316.48, 1305.39, 1270.40, 1224.40, 1178.41, 1165.19, 1043.19. HRMS m/z $[M + H]^+$ calcd. For $[C_{26}H_{30}NO_3S]^+$ 436.1946; found 436.1943.

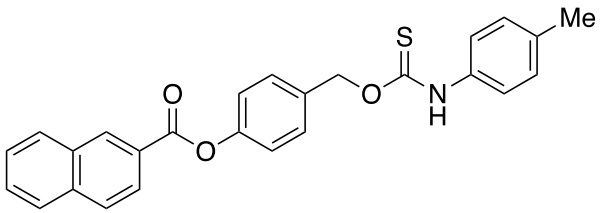

TCM9 was prepared with p-tolyl isothiocyanate and Nap-OH according to the general synthetic procedure described above. (112 mg, 76% yield). ^{1}H NMR (500 MHz, DMSO-d_6, 60 °C) δ (ppm): 11.01 (s, 1H), 8.85 (s, 1H), 8.21 (2, *J* = 8.24, 1H), 8.13 (m, 2H), 8.07 (d, *J* = 8.24, 1H), 7.73 (t, *J* = 7.79, 1H), 7.68 (t, *J* = 7.79, 1H), 7.63-7.09 (m, 8H), 5.61 (s, 2H), 2.29 (s, 3H). Broadness is observed in the ^{1}H NMR spectrum due to rotation around the C-N bond of the thiocarbamate. $^{13}C\{^1H\}$ NMR (125 MHz, DMSO-d_6, 25 °C) δ (ppm): 187.87, 187.23, 165.24, 151.05, 136.48, 135.84, 135.59, 134.88, 134.33, 133.94, 132.58, 132.05, 130.33, 130.02, 129.93, 129.71, 129.52, 129.36, 129.13, 128.26, 127.67,

126.56, 125.50, 123.44, 122.57, 71.94, 70.28, 55.38, 21.00, 20.91, 14.57. Splitting of peaks is observed in the $^{13}C\{^{1}H\}$ NMR spectrum due to slow rotation around the C-N bond of the thiocarbamate, yielding rotamers. IR (cm^{-1}) 3216.92, 3160.40, 3084.34, 3034.41, 2919.03, 2853.89, 1730.67, 1629.73, 1596.74, 1542.65, 1507.24, 1460.72, 1400.09, 1343.64, 1280.39, 1179.23, 1161.82, 1127.63, 1061.28. HRMS m/z $[M + H]^+$ calcd. For $[C_{26}H_{21}NO_3S]^+$ 428.1302; found 428.1290.

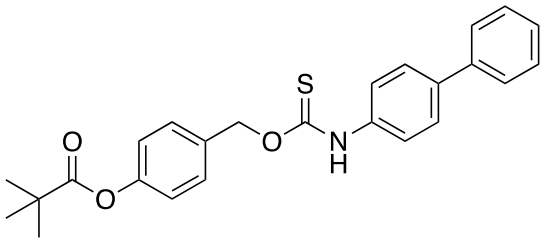

TCM10 was prepared with 4-biphenylyl isothiocyanate and *t*Bu-OH according to the general synthetic procedure described above. (90.9 mg, 45% yield). ^{1}H NMR (500 MHz, DMSO-d_6, 60 °C) δ (ppm): 11.18 (s, 1H), 7.64 (m, 5H), 7.52 (d, J = 8.1 Hz, 2H), 7.45 (t, J = 7.6 Hz, 2H), 7.35 (m, 1H), 7.13 (d, J = 8.8 Hz, 2H), 5.61 (s, 2H), 1.34 (s, 9H). Broadness is observed in the ^{1}H NMR spectrum due to rotation around the C-N bond of the thiocarbamate.$^{13}C\{^{1}H\}$ NMR (125 MHz, DMSO-d_6, 60 °C) δ (ppm): 187.7, 176.8, 151.3, 140.0, 137.2, 133.8, 129.9, 129.4, 127.8, 127.4, 126.9, 123.2, 122.2, 39.1, 27.2. FTIR (ATR, cm^{-1}): 3212.31, 3035.48, 2969.43, 1748.39, 1594.62, 1578.16, 1540.37, 1509.08, 1401.48, 1335.13, 1115.22, 1098.76, 1001.31, 833.74, 755.88, 685.14. HRMS m/z $[M + H^+]$ calc. 420.1633; found 420.1595.

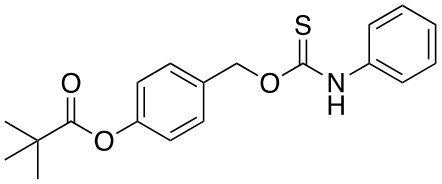

TCM11 was prepared with phenyl isothiocyanate and *t*Bu-OH according to the general synthetic procedure described above. (71.2 mg, 55% yield). ^{1}H NMR (500 MHz, DMSO-d_6, 60 °C) δ (ppm): 11.07 (s, 1H), 7.63-7.42 (m, 4H), 7.33 (m, 2H), 7.16 (m, 1H), 7.35 (m, 1H), 7.12 (d, *J*= 8.7 Hz, 2H), 5.58 (s, 2H), 1.32 (s, 9H). Broadness is observed in the ^{1}H NMR spectrum due to rotation around the C-N bond of the thiocarbamate.^{13}C{^{1}H} NMR (125 MHz, DMSO-d_6, 60 °C) δ (ppm): 187.9, 176.8, 151.3, 138.8, 133.8, 129.9, 129.1, 125.4, 123.1, 122.2, 39.1, 27.3. FTIR (ATR, cm^{-1}): 3218.40, 3125.23, 3061.19, 2973.40, 1746.87, 1595.52, 1545.05, 1494.26, 1406.69, 1309.81, 1202.79, 1163.67, 1117.27, 1013.63, 898.00, 782.7-, 685.16. HRMS m/z [M + H^{+}] calc. 344.1320; found 344.1309.

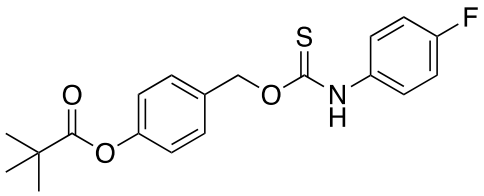

TCM12 was prepared with p-fluorophenyl isothiocyanate and *t*Bu-OH according to the general synthetic procedure described above. (100.1 mg, 58% yield). ^{1}H NMR (500 MHz, DMSO-d_6, 60 °C) δ (ppm): 11.08 (s, 1H), 7.82-7.31 (m, 4H), 7.21-7.06 (m, 4H), 5.57 (s, 2H), 1.33 (s, 9H). Broadness is observed in the ^{1}H NMR spectrum due to rotation around the C-N bond of the thiocarbamate. ^{13}C{^{1}H} NMR (125 MHz, DMSO-d_6, 60 °C) δ (ppm): 176.8, 160.9, 158.9, 151.2, 133.6, 129.9, 125.5, 122.4, 123.1, 115.7, 39.0, 27.2.

^{19}F NMR (460.6 MHz, DMSO-d_6, 60 °C) δ (ppm): -117.17. FTIR (ATR, cm^{-1}): 3181.22, 2971.41, 1747.38, 1596.49, 1537.94, 1504.04, 1393.87, 1336.73, 1275.72, 1186.62, 1151.67, 1069.09, 1014.34, 893.61, 805.78, 684.83. HRMS m/z [M + H$^+$] calc. 362.1226; found 362.1208.

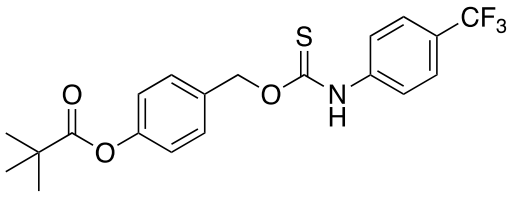

TCM13 was prepared with *p*-trifluoromethylphenyl isothiocyanate and *t*Bu-OH according to the general synthetic procedure described above. (99.9 mg, 51% yield). ^{1}H NMR (500 MHz, DMSO-d_6, 60 °C) δ (ppm): 11.40 (s, 1H), 7.80 (br s, 2H), 7.68 (d, J = 8.4 Hz, 2H), 7.52 (d, J = 8.5 Hz, 2H), 7.13 (d, J = 8.5 Hz, 2H), 5.61 (s, 2H), 1.32 (s, 9H). Broadness is observed in the ^{1}H NMR spectrum due to rotation around the C-N bond of the thiocarbamate. ^{13}C{^{1}H} NMR (125 MHz, DMSO-d_6, 60 °C) δ (ppm): 188.1, 176.8, 151.3, 133.5, 130.0, 126.3, 125.7, 123.4, 122.6, 39.0, 27.2. ^{19}F NMR (460.6 MHz, DMSO-d_6, 60 °C) δ (ppm): -60.6. FTIR (ATR, cm^{-1}): 3185.58, 2969.83, 1746.81, 1601.25, 1544.38, 1510.27, 1461.11, 1396.96, 1317.40, 1164.31, 1110.57, 1067.89, 1014.47, 895.83, 837.74, 730.01. HRMS m/z [M + H$^+$] calc. 412.2294; found 412.1174.

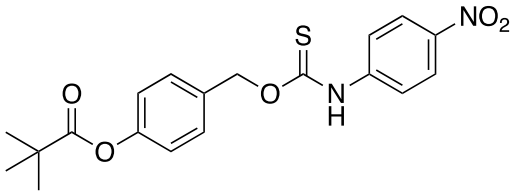

TCM14 was prepared with *p*-nitrophenyl isothiocyanate and *t*Bu-OH according to the general synthetic procedure described above. (67.9l mg, 47% yield). ^{1}H NMR (500 MHz,

DMSO-d_6, 60 °C) δ (ppm): 11.60 (s, 1H), 8.19 (d, J = 9.2 Hz, 2H), 7.85 (br s, 2H), 7.52 (d, J = 6.7 Hz, 2H), 7.13 (d, J = 6.7 Hz, 2H), 5.59 (s, 2H), 1.32 (s, 9H). Broadness is observed in the ^{1}H NMR spectrum due to rotation around the C-N bond of the thiocarbamate. ^{13}C{^{1}H} NMR (125 MHz, DMSO-d_6, 60 °C) δ (ppm): 176.7, 151.3, 143.6, 133.4, 130.1, 124.9, 122.2, 122.0, 39.0, 27.3. FTIR (ATR, cm^{-1}): 3213.46, 3075.42, 2969.58, 1746.40, 1595.02, 1548.26, 1507.20, 1393.72, 1333.09, 1162.50, 1102.61, 1014.04, 893.97, 831.49, 747.03, 681.70. HRMS m/z [M + H$^+$] calc. 389.1171; found 389.1154.

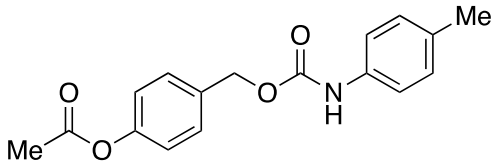

CM1 was prepared with p-tolyl isocyanate and Me-OH according to the general synthetic procedure described above. (65 mg, 36% yield). ^{1}H NMR (500 MHz, $CDCl_3$) δ (ppm) 7.42 (d, J = 8.35, 2H), 7.28 (m, 2H), 7.12 (m, 4H), 6.75 (bs, 1H), 5.19 (s, 2H), 2.32 (m, 6H). ^{13}C NMR (125 MHz, $CDCl_3$) δ (ppm) 169.45, 153.42, 150.59, 135.15, 133.84, 133.13, 129.55, 121.76, 118.87, 66.22, 21.13, 20.77. IR (cm^{-1}) 3326.83, 2922.76, 2360.39, 2341.56, 1762.07, 1704.91, 1597.57, 1524.66, 1508.13, 1451.05, 1406.66, 1368.20, 1314.74, 1295.48, 1191.34, 1164.63, 1049.44, 1016.58. HRMS m/z [M + H]$^+$ calcd. For $[C_{17}H_{18}NO_4]^+$ 300.1236; found 300.1228.

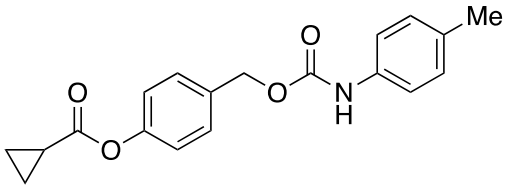

CM2 was prepared with p-tolyl isocyanate and Cp-OH according to the general synthetic procedure described above. (96 mg, 57% yield). ^{1}H NMR (500 MHz, $CDCl_3$) δ (ppm) 7.42 (d, *J* = 8.11, 2H), 7.28 (m, 2H), 7.12 (m, 4H), 6.69 (bs, 1H), 5.19 (s, 2H), 2.33 (s, 3H), 1.87 (m, 1H), 1.19 (m, 2H), 1.05 (m, 2H). ^{13}C NMR (125 MHz, $CDCl_3$) δ (ppm) 173.42, 153.39, 150.74, 135.14, 133.63, 133.13, 129.55, 129.50, 121.76, 118.76, 66.26, 20.76, 13.03, 9.31. IR (cm^{-1}) 3334.74, 3015.89, 2969.69, 2360.04, 2341.58, 1727.03, 1598.07, 1526.98, 1508.92, 1448.66, 1406.77, 1381.64, 1314.94, 1295.88, 1204.23, 1165.01, 1138.93, 1049.63, 1017.09. HRMS m/z $[M + H]^+$ calcd. For $[C_{19}H_{20}NO_4]^+$ 326.1392; found 326.1392.

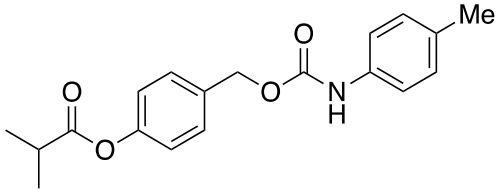

CM3 was prepared with p-tolyl isocyanate and iPr-OH according to the general synthetic procedure described above. (88 mg, 52% yield). ^{1}H NMR (500 MHz, $CDCl_3$) δ (ppm) 7.44 (d, *J* = 8.20, 2H), 7.28 (m, 2H), 7.13 (d, *J* = 8.17, 2H), 7.10 (d, *J* = 8.20, 2H), 6.60 (bs, 1H), 5.20 (s, 2H), 2.83 (hept, *J* = 7.0, 1H), 2.33 (s, 3H), 1.34 (d, *J* = 7.0, 6H). ^{13}C NMR (125 MHz, $CDCl_3$) δ (ppm) 175.50, 153.32, 150.84, 135.08, 133.59, 133.19, 129.56, 129.52, 121.69, 118.86, 66.29, 34.18, 20.76, 18.92. IR (cm^{-1}) 3347.50, 2970.71, 2936.12, 1755.62, 1702.87, 1594.82, 1528.43, 1508.77, 1459.20, 1407.82, 1314.10,

1229.85, 1178.37, 1164.49, 1118.47, 1069.53, 1041.40. HRMS m/z $[M + H]^+$ calcd. For $[C_{19}H_{22}NO_4]^+$ 328.1549; found 328.1565.

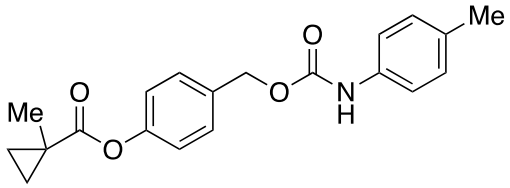

CM4 was prepared with p-tolyl isocyanate and MCp-OH according to the general synthetic procedure described above. (87 mg, 90% yield). ^{1}H NMR (500 MHz, $CDCl_3$) δ (ppm) 7.41 (d, *J* = 8.03, 2H), 7.28 (d, *J* = 8.11, 2H), 7.12 (d, *J* = 8.03, 2H), 7.08 (d, *J* = 8.11, 2H), 6.68 (bs, 1H), 5.18 (s, 2H), 2.33 (s, 3H), 1.45 (bs, 5H), 0.87 (m, 2H). ^{13}C NMR (125 MHz, $CDCl_3$) δ (ppm) 174.55, 153.40, 150.95, 135.14, 133.51, 133.12, 129.55, 129.47, 121.74, 118.87, 66.28, 20.76, 19.43, 18.82, 17.49. IR (cm^{-1}) 3336.98, 3042.16, 2969.35, 1730.15, 1696.57, 1595.43, 1525.80, 1509.41, 1454.78, 1406.03, 1325.66, 1312.51, 1226.40, 1211.00, 1198.55, 1166.74, 1139.45, 1129.51, 1073.47, 1050.49. HRMS m/z $[M + H]^+$ calcd. For $[C_{20}H_{22}NO_4]^+$ 340.1549; found 340.1528.

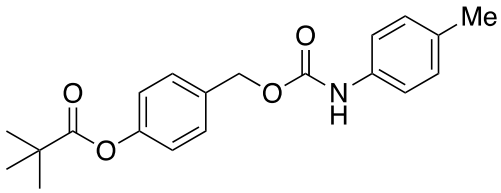

CM5 was prepared with p-tolyl isocyanate and tBu-OH according to the general synthetic procedure described above. (108 mg, 83% yield). Spectral data is in agreement with those reported in the literature.[104]

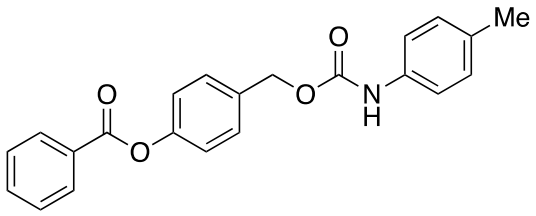

CM6 was prepared with p-tolyl isocyanate and Ph-OH according to the general synthetic procedure described above. (246 mg, 79% yield). ^{1}H NMR (500 MHz, $CDCl_3$) δ (ppm): 8.23 (m, 2H), 7.67 (m, 1H), 7.54 (t, *J* = 7.84, 2H), 7.50 (d, *J* = 8.49, 2H), 7.29 (m, 2H), 7.26 (d, *J* = 8.49, 2H), 7.14 (d, *J* = 8.16, 2H), 6.63 (bs, 1H), 5.24 (s, 2H), 2.33 (s, 3H). ^{13}C{^{1}H} NMR (125 MHz, $CDCl_3$) δ (ppm): 165.09, 150.90, 135.09, 133.86, 133.67, 133.20, 130.20, 129.62, 129.58, 129.44, 128.60, 121.91, 118.90, 66.30, 20.77. IR (cm^{-1}) 3320.43, 2916.58, 1732.04, 1694.16, 1593.59, 1525.22, 1508.19, 1406.42, 1313.55, 1269.13, 1235.09, 1193.82, 1162.28, 1062.11, 1015.89. HRMS m/z $[M + H]^+$ calcd. For $[C_{22}H_{20}NO_4]^+$ 362.1392; found 362.1391.

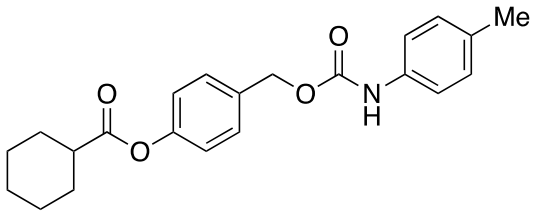

CM7 was prepared with p-tolyl isocyanate and Cy-OH according to the general synthetic procedure described above. (640 mg, 79% yield). ^{1}H NMR (500 MHz, $CDCl_3$) δ (ppm): 7.41 (d, *J* = 8.36, 2H), 7.28 (m, 2H), 7.12 (d, *J* = 8.10, 2H), 7.09 (d, *J* = 8.10, 2H), 6.78 (bs, 1H), 5.18 (s, 2H), 2.59 (m, 1H), 2.33 (s, 3H), 2.09 (m, 2H), 1.85 (m, 2H), 1.73 (m, 1H), 1.62 (m, 2H), 1.38 (m, 3H). ^{13}C{^{1}H} NMR (125 MHz, $CDCl_3$) δ (ppm): 174.51, 153.45, 150.84, 135.20, 133.60, 133.08, 129.53, 129.51, 121.74, 118.88, 66.26, 43.21, 28.96, 25.74, 25.38, 20.77. IR (cm^{-1}) 3357.69, 2963.07, 2934.63, 2858.40, 1740.97,

1701.30, 1594.02, 1526.50, 1508.57, 1461.03, 1407.81, 1314.55, 1301.71, 1227.85, 1211.49, 1191.90, 1179.93, 1010.75. HRMS m/z $[M + H]^+$ calcd. For $[C_{22}H_{26}NO_4]^+$ 368.1862; found 368.1859.

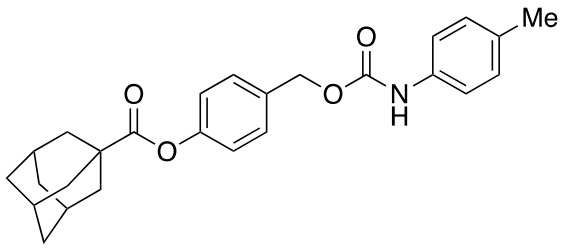

CM8 was prepared with p-tolyl isocyanate and Ad-OH according to the general synthetic procedure described above. (78 mg, 53% yield). ^{1}H NMR (500 MHz, $CDCl_3$) δ (ppm): 7.43 (d, *J* = 8.10, 2H), 7.29 (m, 2H), 7.13 (d, *J* = 8.10, 2H), 7.07 (d, *J* = 8.46, 2H), 6.59 (bs, 1H), 5.20 (s, 2H), 2.33 (s, 3H), 2.11 (bs, 3H), 2.08 (d, *J* = 2.92, 6H), 1.80 (m, 6H). ^{13}C{^{1}H} NMR (125 MHz, $CDCl_3$) δ (ppm): 176.09, 153.35, 151.09, 135.09, 133.41, 133.18, 129.57, 129.51, 121.76, 118.81, 66.33, 41.05, 38.75, 36.46, 27.91, 20.77. IR (cm^{-1}) 3335.00, 2905.92, 2852.06, 2360.58, 2341.57, 1728.80, 1598.69, 1528.20, 1508.60, 1452.54, 1407.35, 1315.33, 1217.92, 1195.02, 1165.11, 1051.05. HRMS m/z $[M + H]^+$ calcd. For $[C_{26}H_{30}NO_4]^+$ 420.2175; found 420.2152.

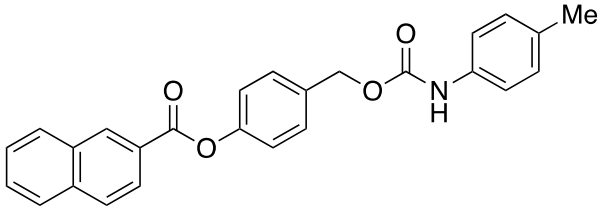

CM9 was prepared with p-tolyl isocyanate and Nap-OH according to the general synthetic procedure described above. (302 mg, 71% yield). ^{1}H NMR (500 MHz, $CDCl_3$) δ (ppm): 8.82 (s, 1H), 8.22 (dt, *J* = 8.67, 1.74, 1.74), 8.03 (d, *J* = 8.18, 1H), 7.98 (d, *J* =

8.67, 1H), 7.95 (d, *J* = 8.18, 1H), 7.66 (m, 1H), 7.61 (m, 1H), 7.52 (m, 2H), 7.30 (m, 3H), 7.14 (d, *J* = 8.12, 2H), 6.63 (bs, 1H), 5.26 (s, 3H), 2.34 (s, 3H). $^{13}C\{^{1}H\}$ NMR (125 MHz, $CDCl_3$) δ (ppm): 165.27, 151.00, 135.86, 135.10, 133.89, 133.21, 132.51, 131.99, 129.65, 129.59, 129.51, 128.69, 128.43, 127.86, 126.88, 126.62, 125.44, 121.97, 118.87, 66.32, 20.77. IR (cm^{-1}) 3275.44, 2915.16, 1731.08, 1697.51, 1631.77, 1598.64, 1406.97, 1353.34, 1314.70, 1281.60, 1260.92, 1218.37, 1197.35, 1129.82, 1065.23. HRMS m/z $[M + H]^+$ calcd. For $[C_{26}H_{22}NO_4]^+$ 412.1549; found 412.1529.

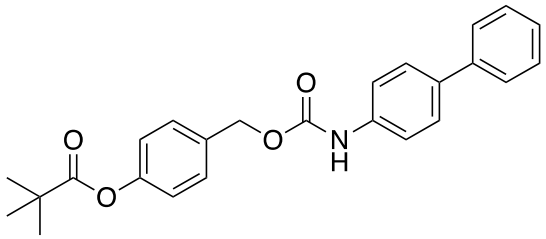

CM10 was prepared with 4-biphenylyl isocyanate and *t*Bu-OH according to the general synthetic procedure described above. (161.9 mg, 56% yield). ^{1}H NMR (500 MHz, $CDCl_3$, rt) δ (ppm): 7.57-7.54 (m, 4H), 7.46-7.40 (m, 6H), 7.34-7.30 (m, 1H), 7.09-7.05 (m, 2H), 5.21 (s, 2H), 1.36 (s, 9H). $^{13}C\{^{1}H\}$ NMR (125 MHz, $CDCl_3$, rt) δ (ppm): 176.9, 151.1, 140.5, 137.0, 136.5, 133.4, 129.6, 128.7, 127.7, 127.0, 126.8, 119.0, 66.5, 39.1, 27.1. FTIR (ATR, cm^{-1}): 3313.48, 2969.35, 1746.36, 1689.12, 1592.73, 1509.58, 1480.26, 1405.51, 1314.67, 1195.27, 1164.21, 1112.53, 1062.14, 896.62, 828.77, 784.19, 695.36. HRMS m/z $[M + H^+]$ calc. 404.1862; found 404.1845.

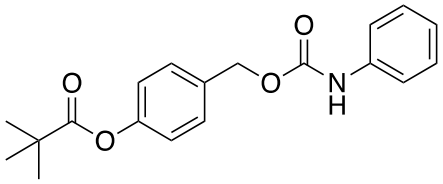

CM11 was prepared with phenyl isocyanate and *t*Bu-OH according to the general synthetic procedure described above. (122.6 mg, 78% yield). ^{1}H NMR (500 MHz, $CDCl_3$, rt) δ (ppm): 7.41-7.37 (m, 4H), 7.32-7.28 (m, 2H), 7.08-7.03 (m, 3H), 6.66 (s, 1H), 5.18 (s, 2H), 1.36 (s, 9H). $^{13}C\{^{1}H\}$ NMR (125 MHz, $CDCl_3$, rt) δ (ppm): 176.9, 151.1, 137.7, 133.4, 129.5, 129.1, 123.6, 121.7, 118.7, 66.4, 39.1, 27.1. FTIR (ATR, cm^{-1}): 3306.13, 2970.18, 1746.49, 1693.12, 1595.72, 1529.13, 1508.09, 1395.71, 1314.76, 1195.33, 1163.48, 1112.67, 1053.18, 1015.91, 896.33, 759.44, 694.14. HRMS m/z [M + H^+] calc. 328.1549; found 328.1553.

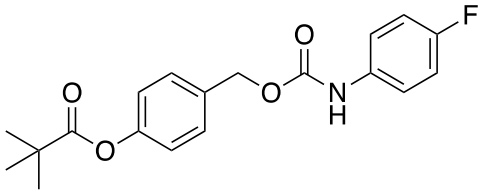

CM12 was prepared with *p*-fluorophenyl isocyanate and *t*Bu-OH according to the general synthetic procedure described above. (124.3 mg, 75% yield). ^{1}H NMR (500 MHz, $CDCl_3$, rt) δ (ppm): 7.41-7.39 (m, 2H), 7.33 (br m, 2H), 7.08-7.05 (m, 2H), 7.01-6.98 (m, 2H), 6.63 (br s, 1H), 5.17 (s, 2H), 1.36 (s, 9H). $^{13}C\{^{1}H\}$ NMR (125 MHz, $CDCl_3$, rt) δ (ppm): 177.0, 151.1, 133.3, 129.6, 121.7, 120.5, 115.8, 115.6, 66.5, 39.1, 27.1. ^{19}F NMR (460.6 MHz, $CDCl_3$, rt) δ (ppm): -119.4. FTIR (ATR, cm^{-1}): 3323.18, 2967.74, 1744.75, 1691.02, 1589.24, 1527.64, 1508.77, 1406.82, 1314.52, 1194.09,

1164.68, 1111.68, 1062.02, 897.11, 827.95, 704.67, 695.28. HRMS m/z [M + Na^+] calc. 368.1274; found 368.1271.

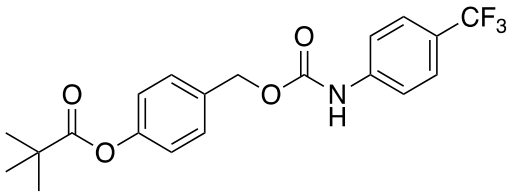

CM13 was prepared with *p*-trifluoromethylphenyl isocyanate and *t*Bu-OH according to the general synthetic procedure described above. (171.7 mg, 90% yield). ^{1}H NMR (500 MHz, $CDCl_3$, rt) δ (ppm): 7.55 (d, *J* = 9.1 Hz, 2H), 7.49 (d, *J* = 7.4 Hz, 2H), 7.41 (d, *J* = 9.1 Hz, 2H), 7.07 (d, *J* = 7.4 Hz, 2H), 6.87 (s, 1H), 5.19 (s, 2H), 1.36 (s, 9H). ^{13}C{^{1}H} NMR (125 MHz, $CDCl_3$, rt) δ (ppm): 177.0, 152.9, 151.2, 140.9, 133.0, 129.7, 126.3, 125.5, 125.2, 123.1, 121.8, 118.1, 66.7, 39.1, 27.1.^{19}F NMR (460.6 MHz, $CDCl_3$, rt) δ (ppm): -62.0. FTIR (ATR, cm^{-1}): 3328.25, 2969.45, 1745.17, 1692.87, 1589.14, 1528.07, 1508.84, 1314.86, 1256.64, 1215.86, 1194.32, 1164.25, 1110.81, 1062.66, 895.70, 831.85, 700.40, 694.55. HRMS m/z [M + H^+] calc. 396.1423; found 396.1410.

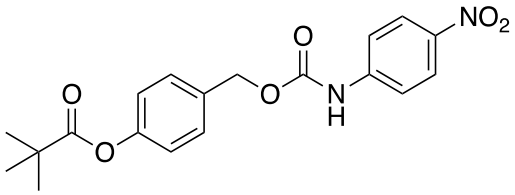

CM14 was prepared with *p*-nitrophenyl isocyanate and *t*Bu-OH according to the general synthetic procedure described above. (142.6 mg, 80% yield). ^{1}H NMR (500 MHz, $CDCl_3$, rt) δ (ppm): 8.19 (d, *J* = 7.3 Hz, 2H), 7.54 (d, *J* = 7.3 Hz, 2H), 7.41 (d, *J* = 8.5 Hz, 2H), 7.08 (d, *J* = 8.5l Hz, 2H), 5.21 (s, 2H), 1.36 (s, 9H). ^{13}C{^{1}H} NMR (125 MHz, $CDCl_3$, rt) δ (ppm): 177.1, 152.5, 151.3, 143.8, 143.1, 132.7, 129.8, 125.2, 121.9, 117.8, 66.1, 39.1,

27.1. FTIR (ATR, cm^{-1}): 3327.31, 2971.82, 1729.89, 1691.69, 1598.33, 1507.95, 1407.53, 1335.48, 1276.09, 1216.16, 1195.58, 1164.38, 1112.36, 1051.41, 1016.71, 897.17, 832.11, 750.35, 689.05. HRMS m/z [M + Na^+] calc. 395.1219; found 395.1212.

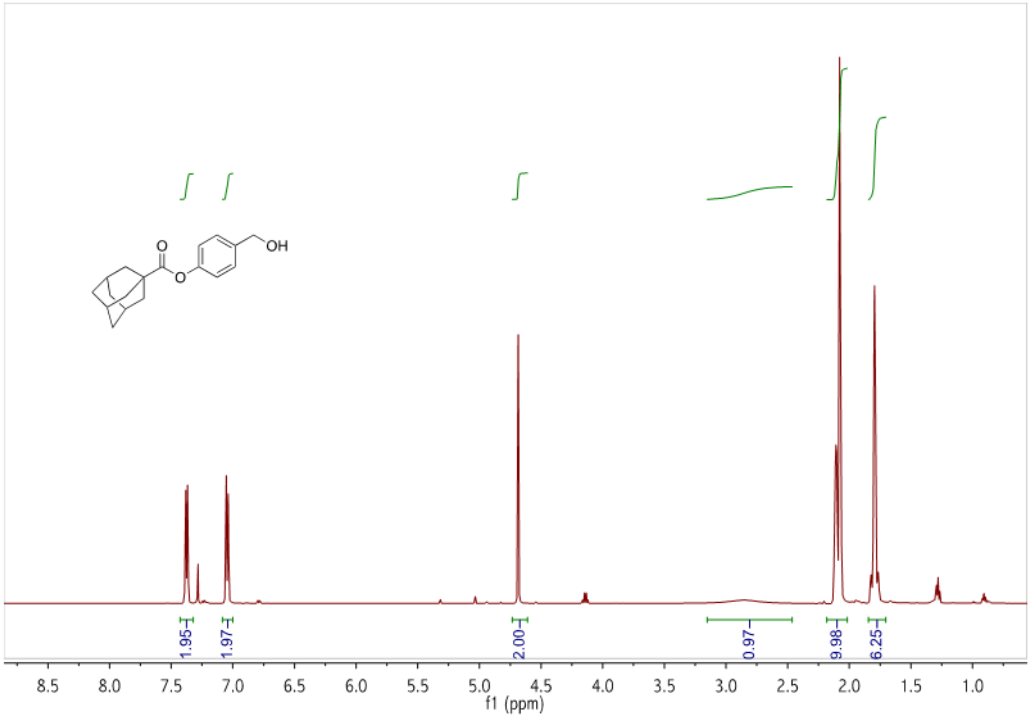

Figure B.1 ^1H (500 MHz, $CDCl_3$) NMR spectrum of **Ad-OH**.

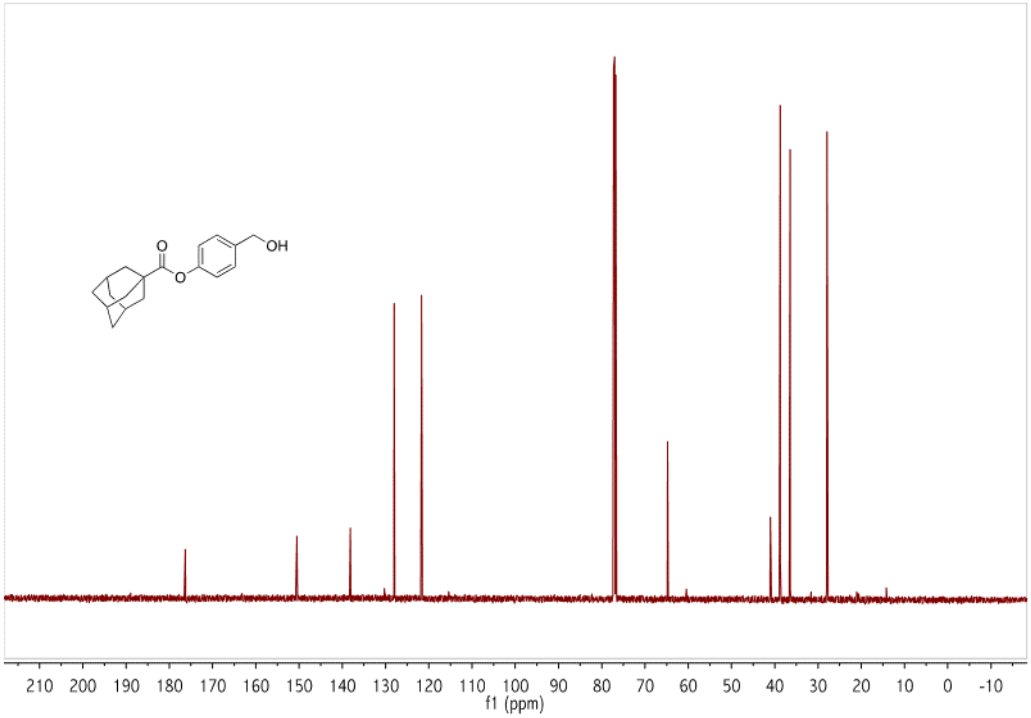

Figure B.2 $^{13}C\{^{1}H\}$ (125 MHz, $CDCl_3$) NMR spectrum of **Ad-OH.**

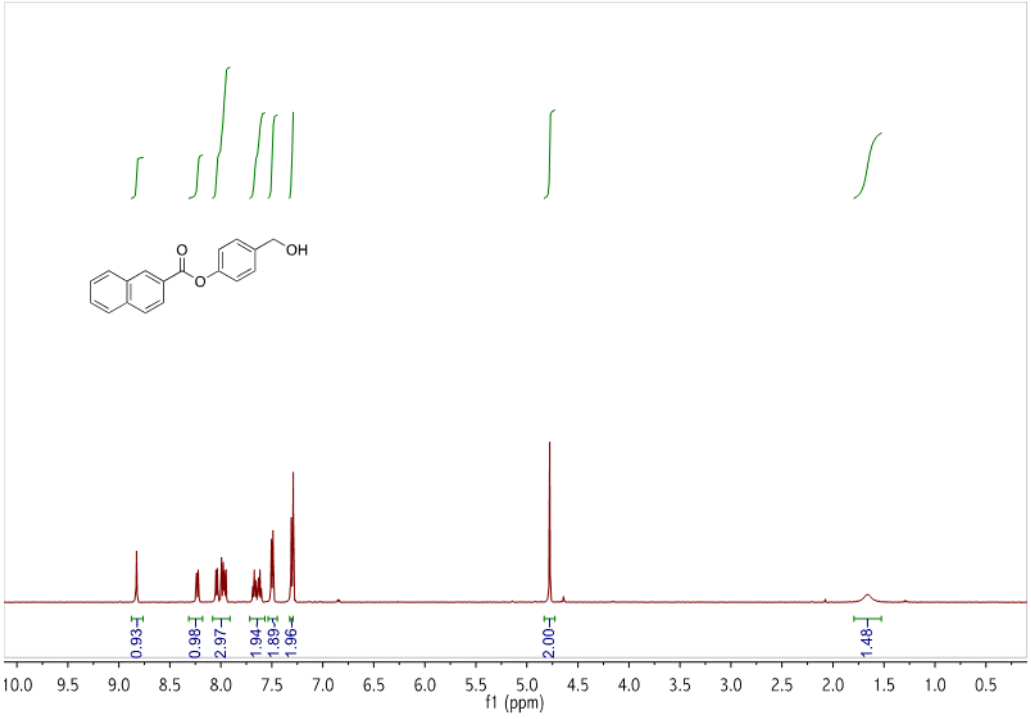

Figure B.3 ^{1}H (500 MHz, $CDCl_3$) NMR spectrum of **Nap-OH.**

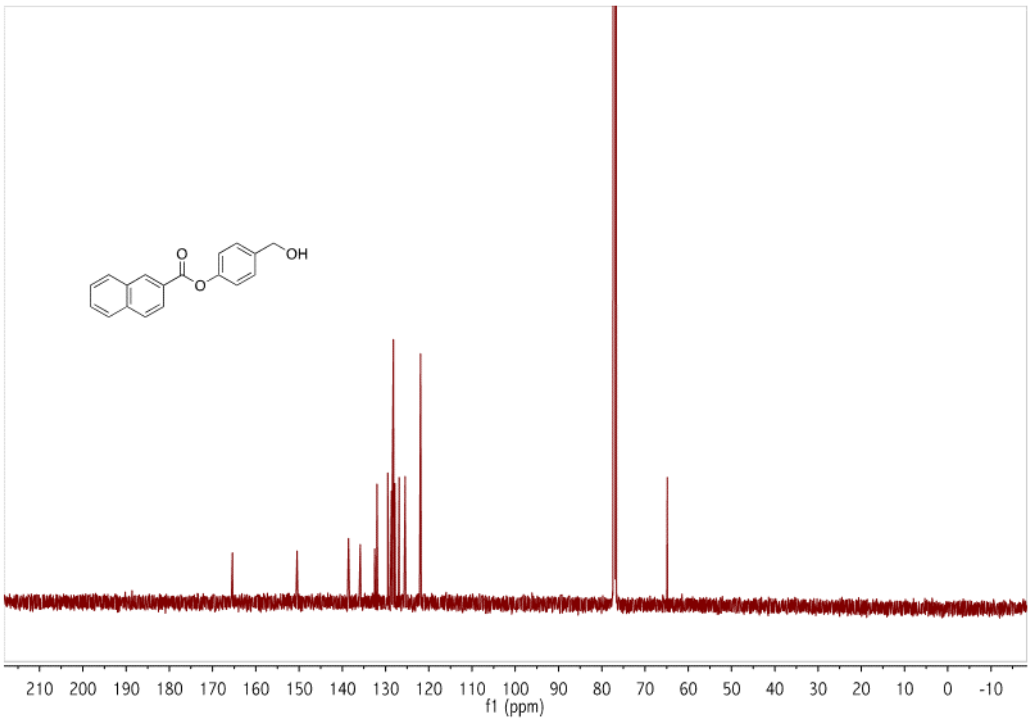

Figure B.4 $^{13}C\{^{1}H\}$ (125 MHz, $CDCl_3$) NMR spectrum of **Nap-OH.**

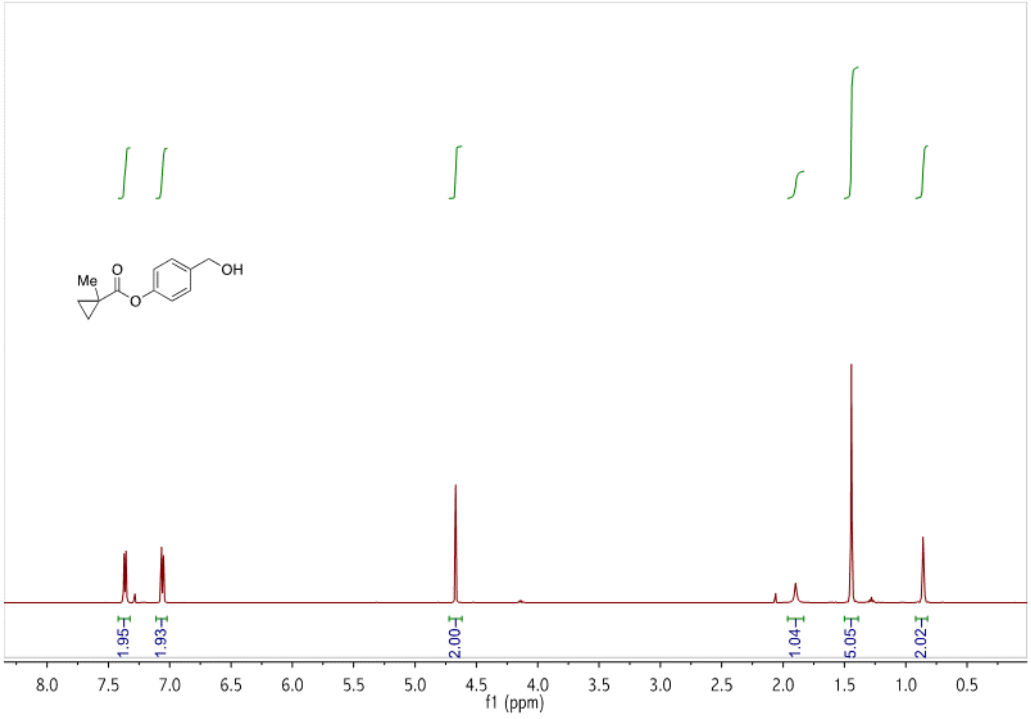

Figure B.5 ^{1}H (500 MHz, $CDCl_3$) NMR spectrum of **MCp-OH.**

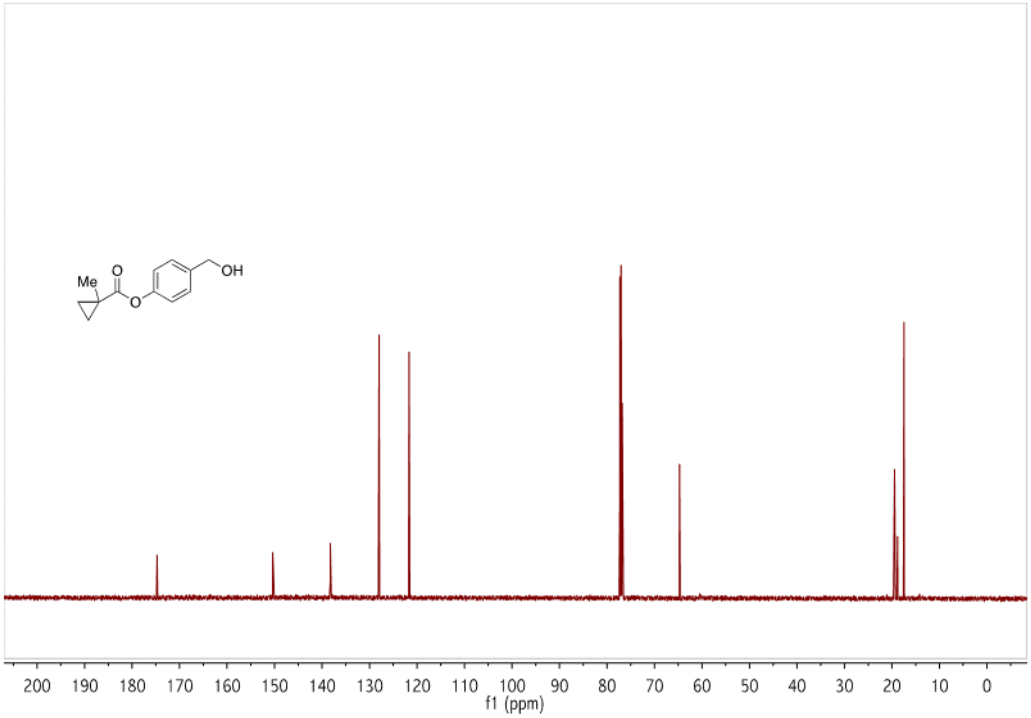

Figure B.6 $^{13}C\{^{1}H\}$ (125 MHz, $CDCl_3$) NMR spectrum of **MCp-OH.**

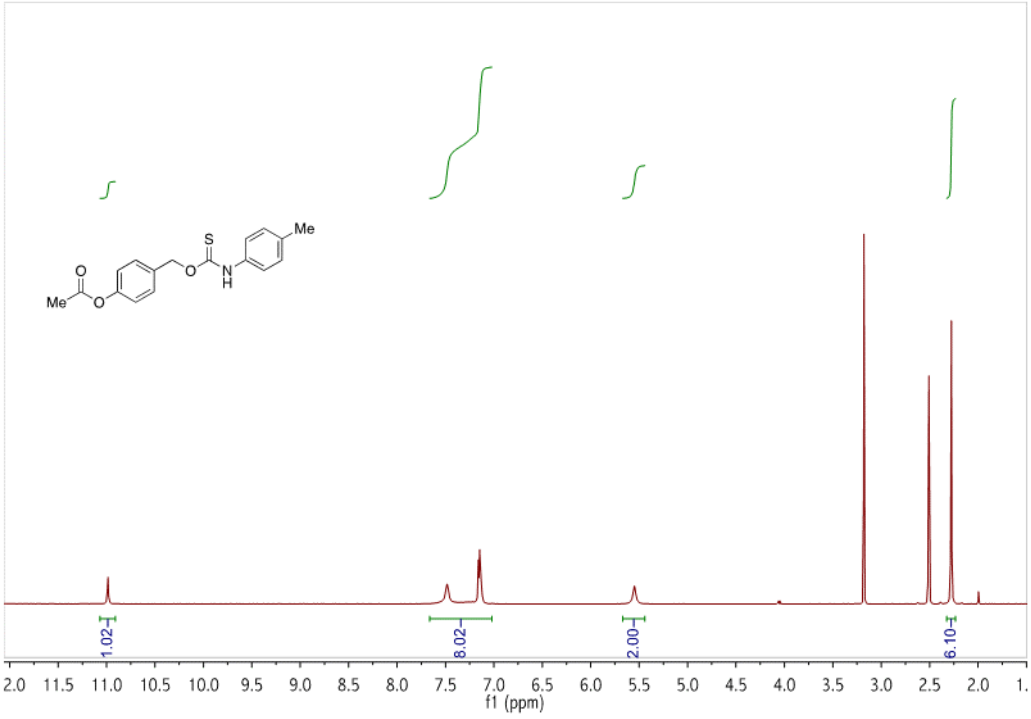

Figure B.7 ^{1}H (500 MHz, DMSO-d_6, 60 °C) NMR spectrum of **TCM1.**

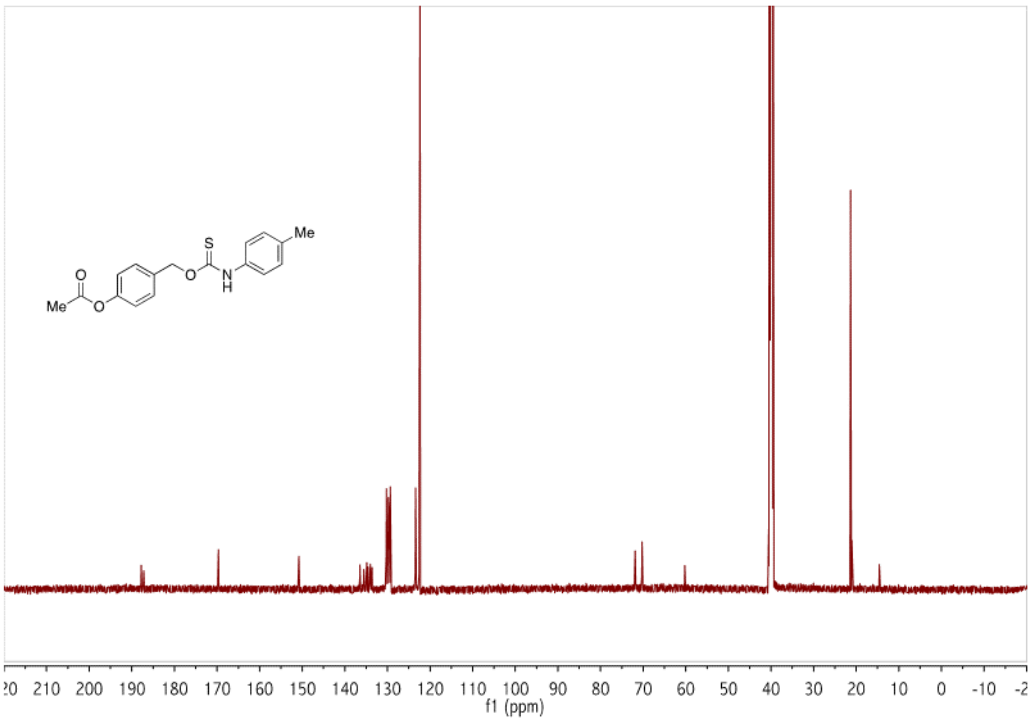

Figure B.8 $^{13}C\{^{1}H\}$ (125 MHz, DMSO-d_6, 25 °C) NMR spectrum of **TCM1.**

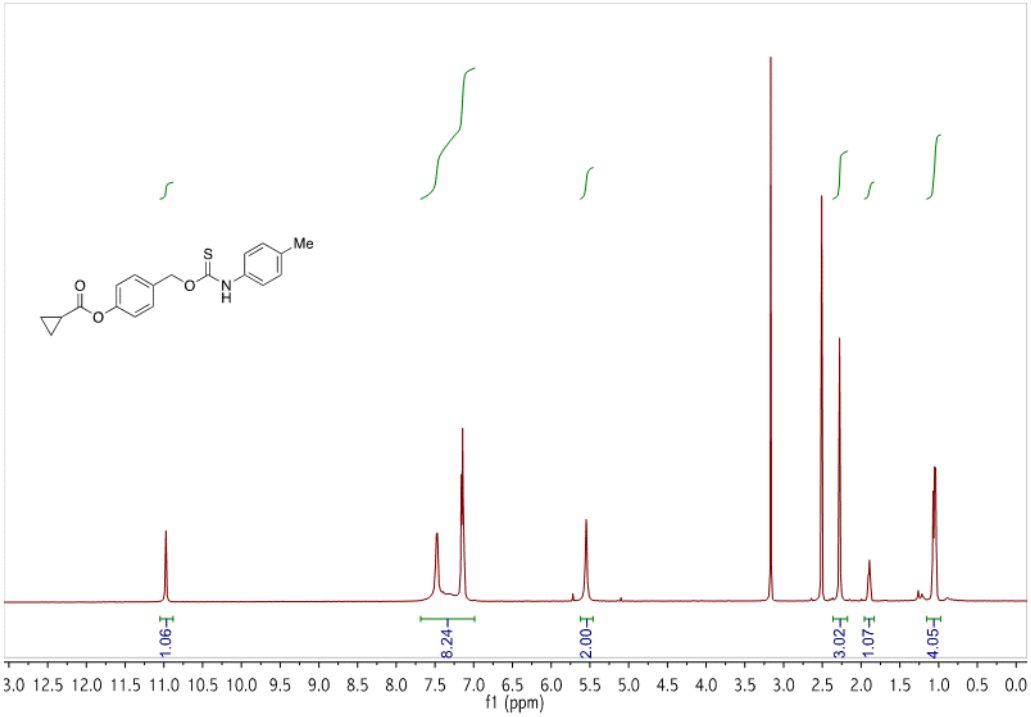

Figure B.9 ^{1}H (500 MHz, DMSO-d_6, 60 °C) NMR spectrum of **TCM2.**

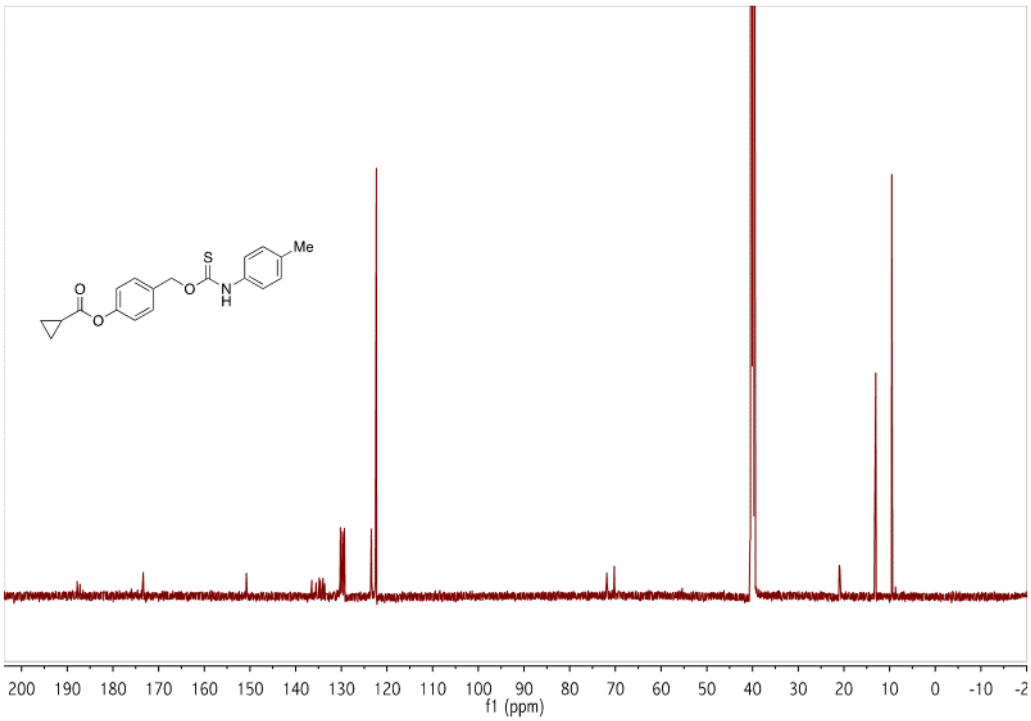

Figure B.10 $^{13}C\{^{1}H\}$ (125 MHz, DMSO-d_6, 25 °C) NMR spectrum of **TCM2.**

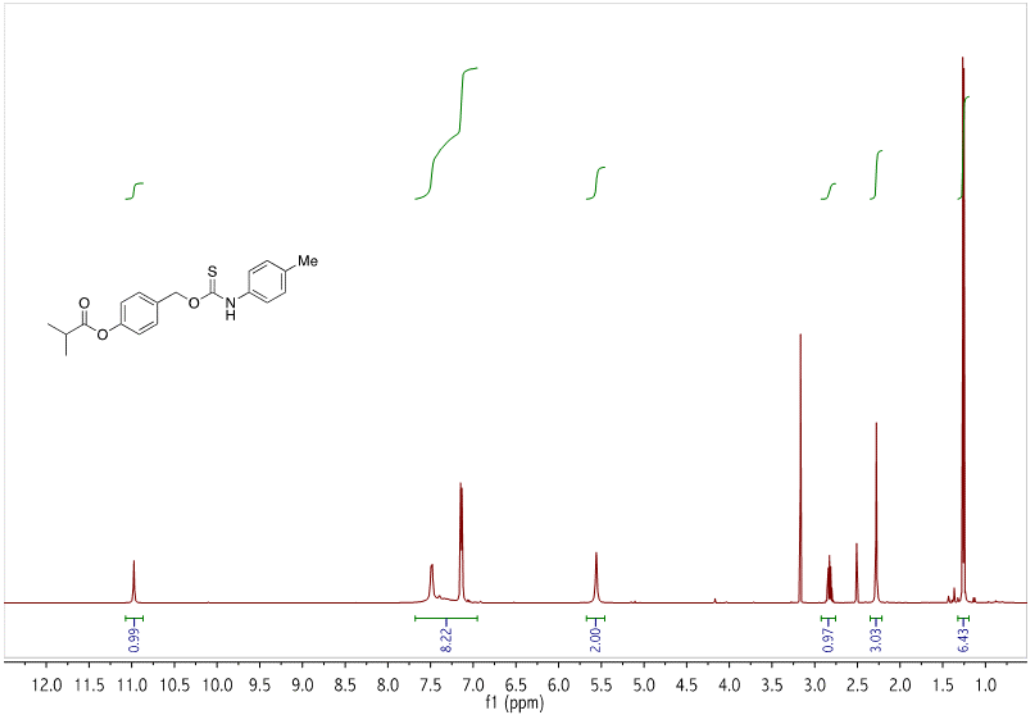

Figure B.11 ^{1}H (500 MHz, DMSO-d_6, 60 °C) NMR spectrum of **TCM3.**

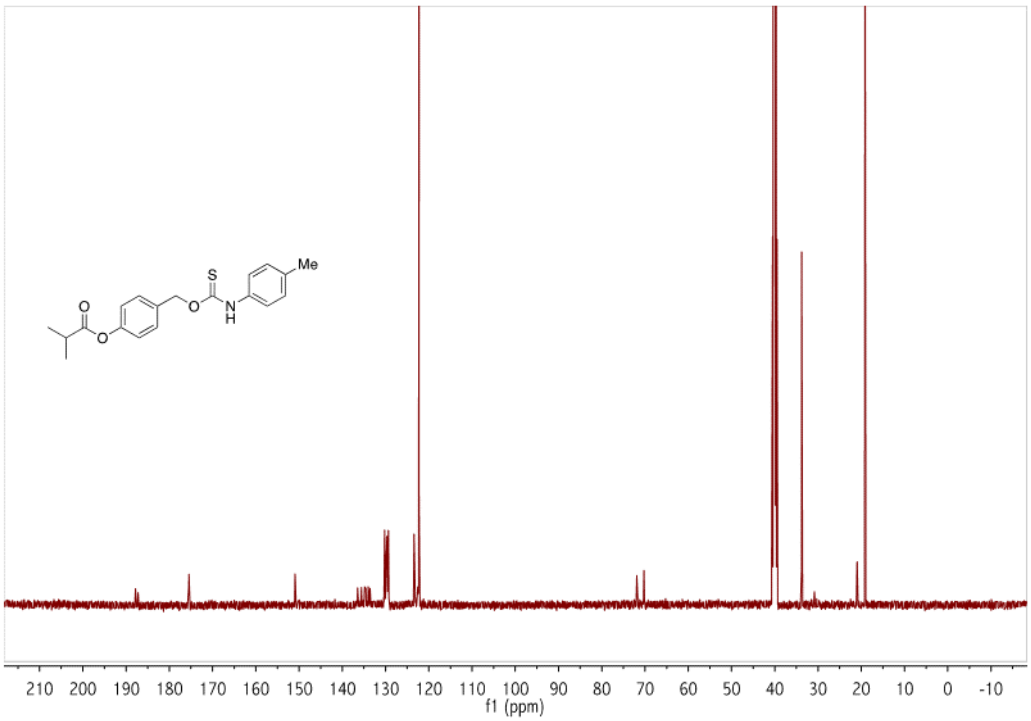

Figure B.12 $^{13}C\{^{1}H\}$ (125 MHz, DMSO-d_6, 25 °C) NMR spectrum of **TCM3.**

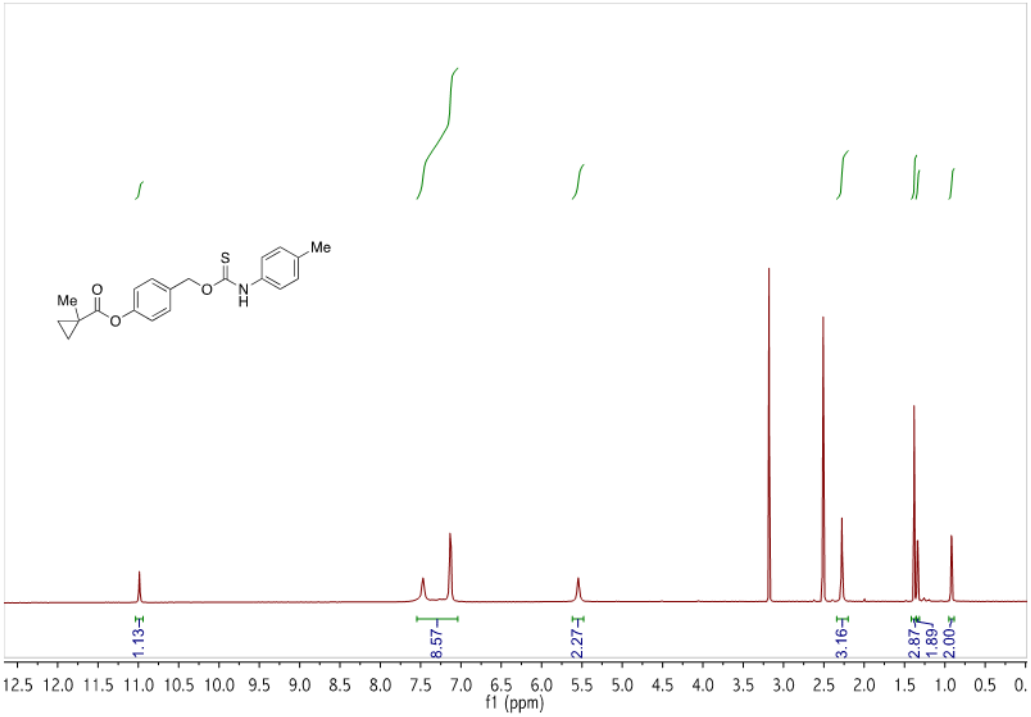

Figure B.13 ^{1}H (500 MHz, DMSO-d_6, 60 °C) NMR spectrum of **TCM4.**

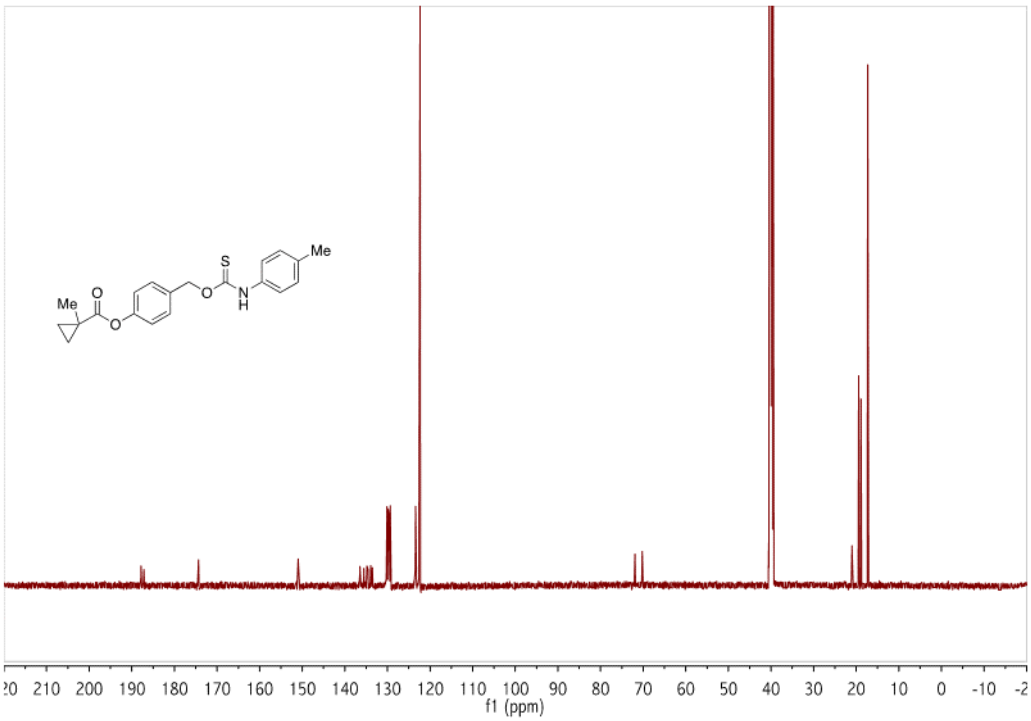

Figure B.14 $^{13}C\{^{1}H\}$ (125 MHz, DMSO-d_6, 25 °C) NMR spectrum of **TCM4.**

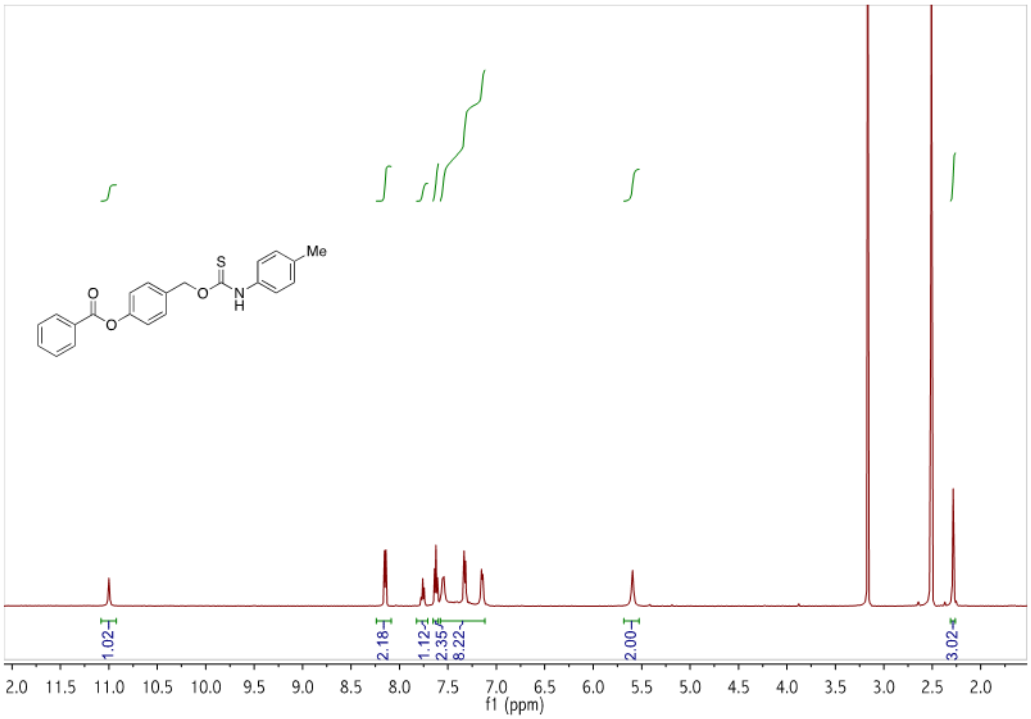

Figure B.15 ^{1}H (500 MHz, DMSO-d_6, 60 °C) NMR spectrum of **TCM6.**

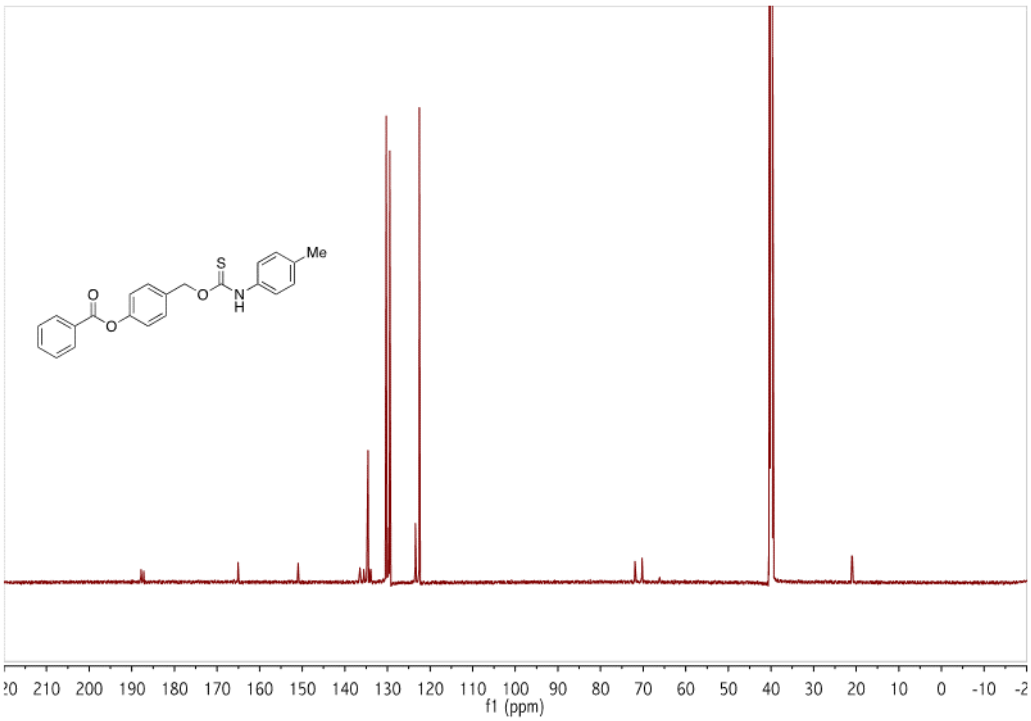

Figure B.16 $^{13}C\{^{1}H\}$ (125 MHz, DMSO-d_6, 25 °C) NMR spectrum of **TCM6.**

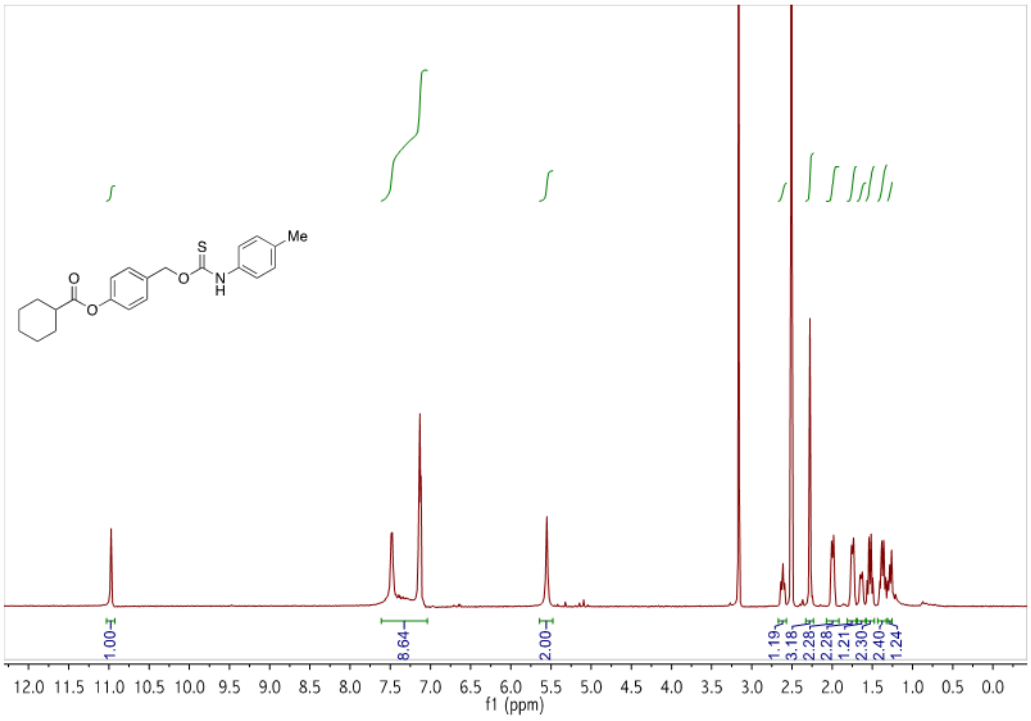

Figure B.17 ^{1}H (500 MHz, DMSO-d_6, 60 °C) NMR spectrum of **TCM7.**

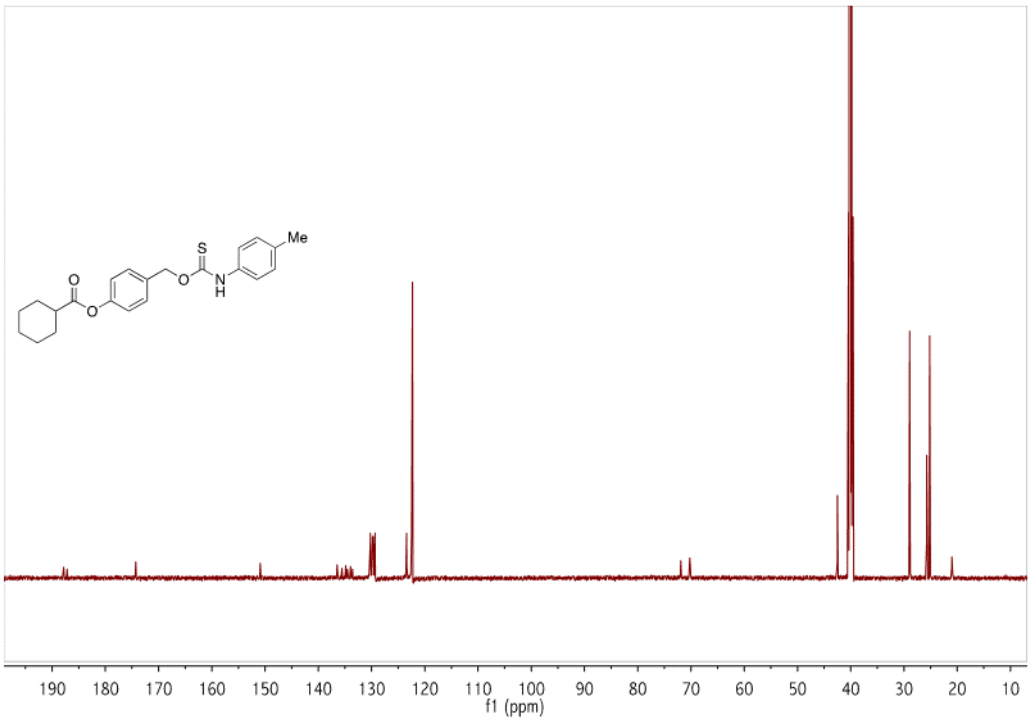

Figure B.18 $^{13}C\{^{1}H\}$ (125 MHz, DMSO-d_6, 25 °C) NMR spectrum of **TCM7.**

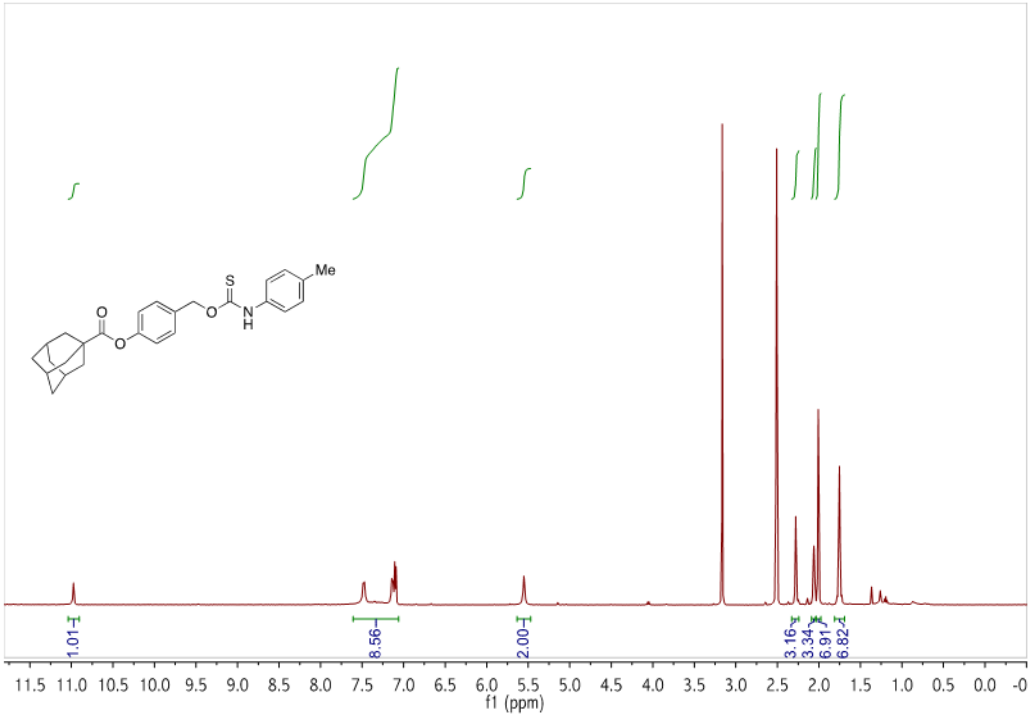

Figure B.19 ^{1}H (500 MHz, DMSO-d_6, 60 °C) NMR spectrum of **TCM8.**

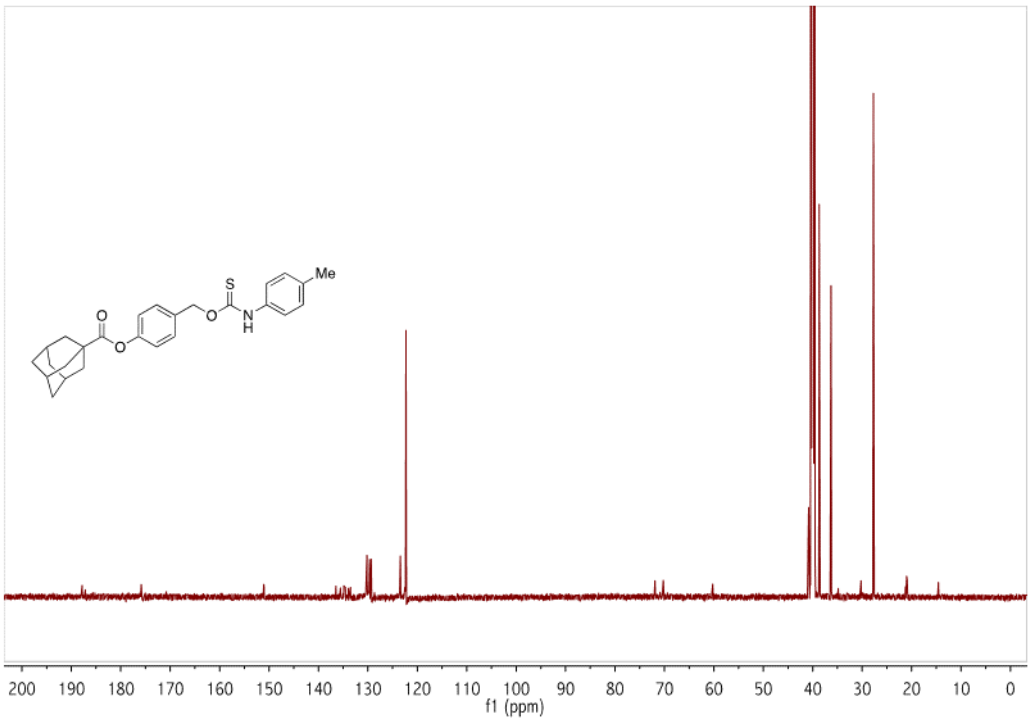

Figure B.20 $^{13}C\{^{1}H\}$ (125 MHz, DMSO-d_6, 25 °C) NMR spectrum of **TCM8.**

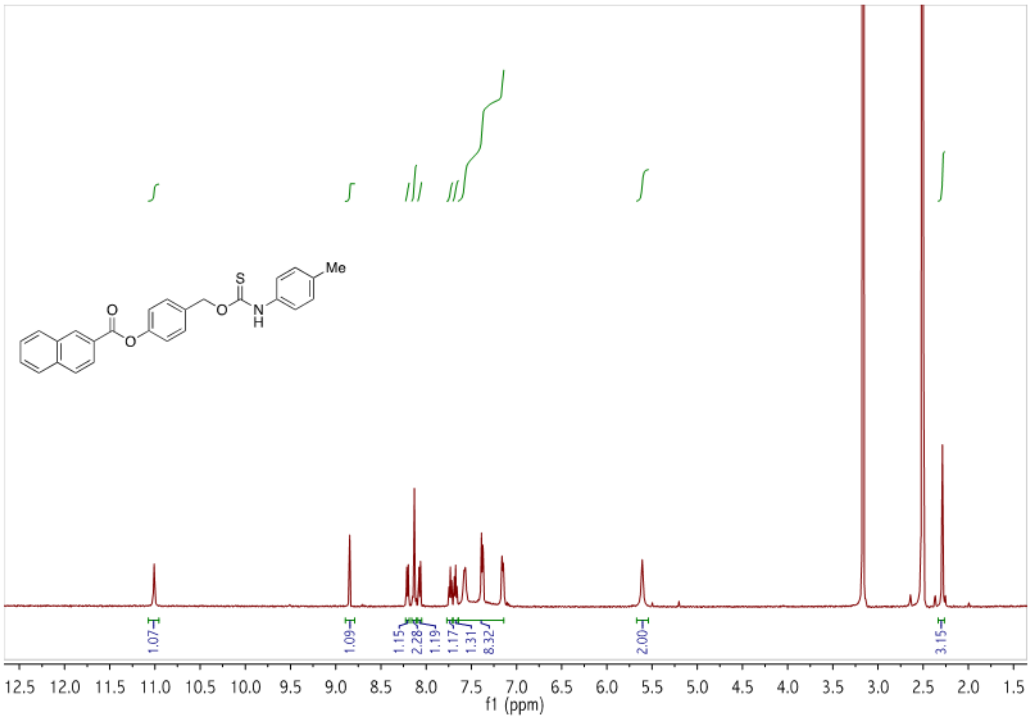

Figure B.21 ^{1}H (500 MHz, DMSO-d_6, 60 °C) NMR spectrum of **TCM9.**

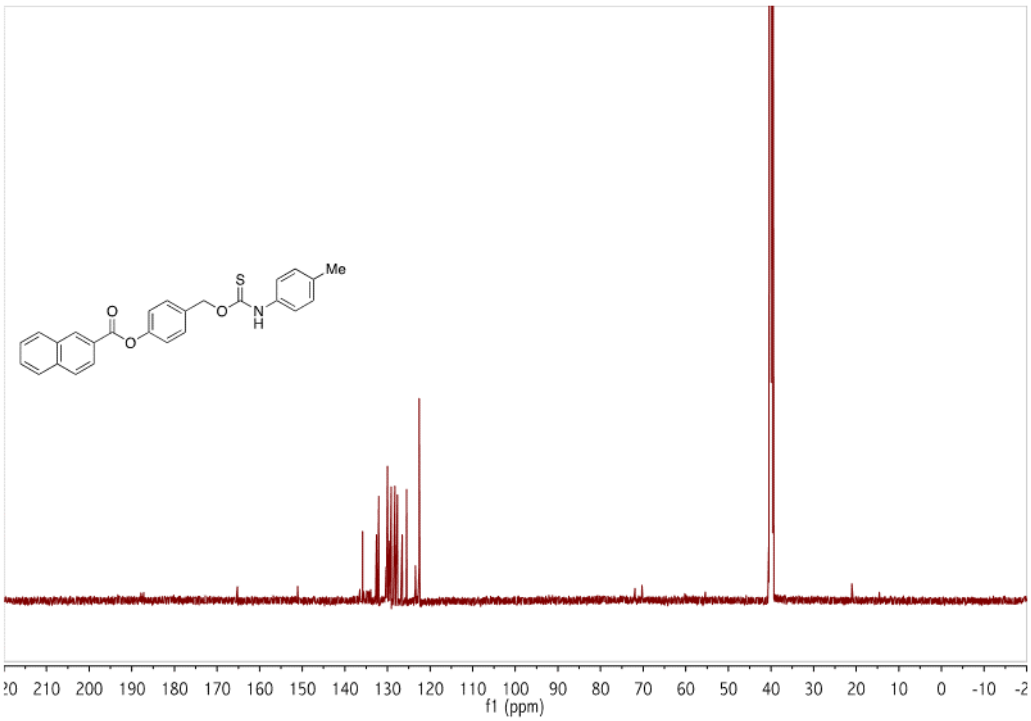

Figure B.22 $^{13}C\{^{1}H\}$ (125 MHz, DMSO-d_6, 25 °C) NMR spectrum of **TCM9.**

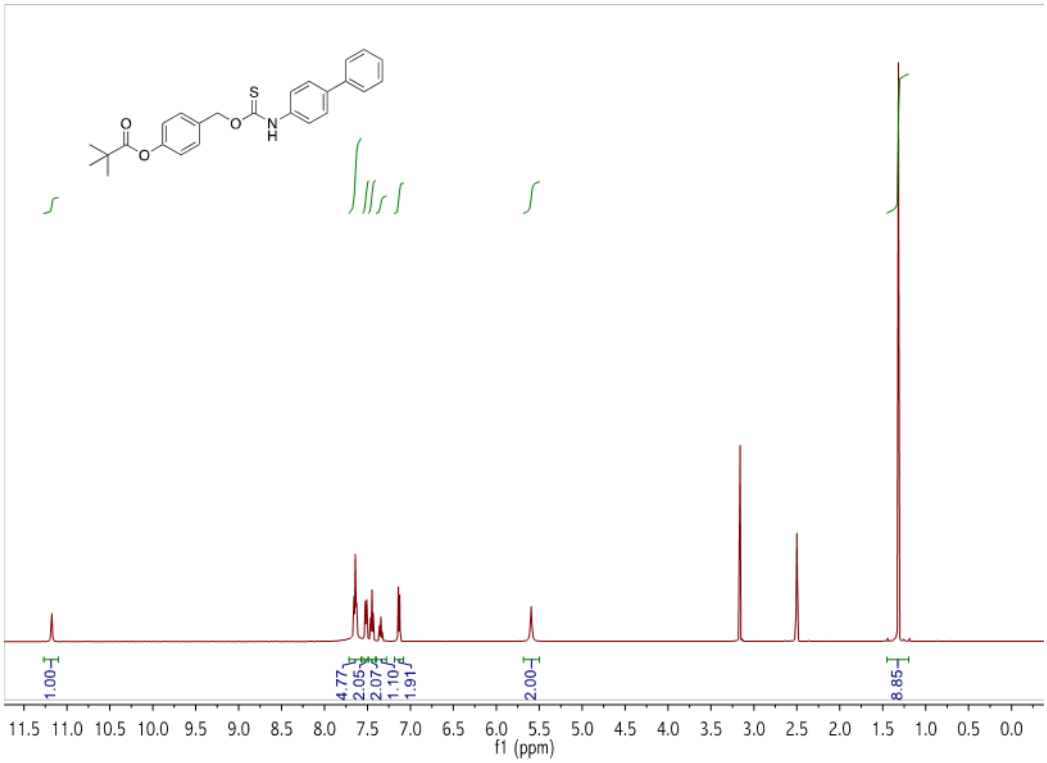

Figure B.23 ^{1}H (500 MHz, DMSO-d_6, 60 °C) NMR spectrum of **TCM10.**

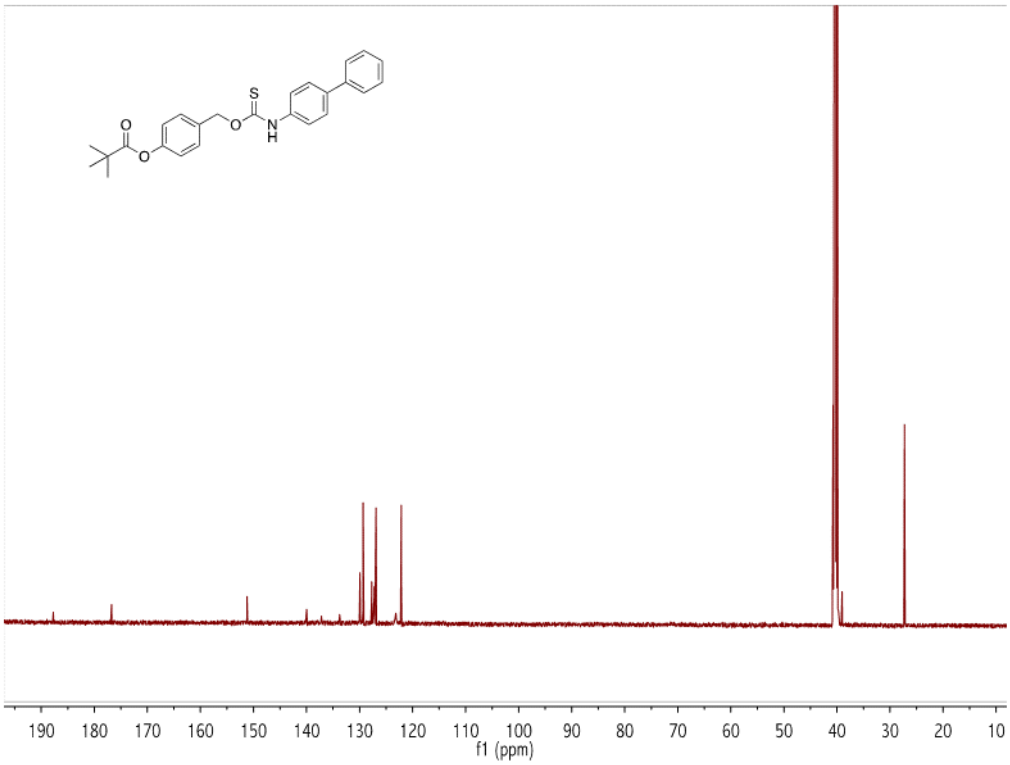

Figure B.24 $^{13}C\{^{1}H\}$ (125 MHz, DMSO-d_6, 60 °C) NMR spectrum of **TCM10.**

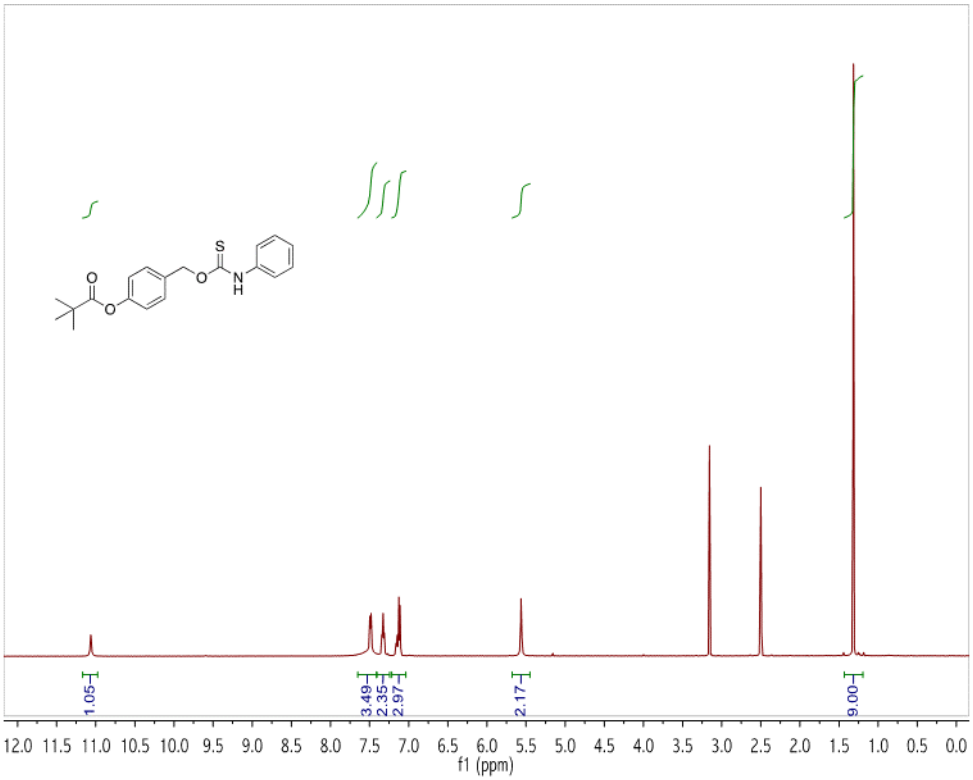

Figure B.25 ^{1}H (500 MHz, DMSO-d_6, 60 °C) NMR spectrum of **TCM11.**

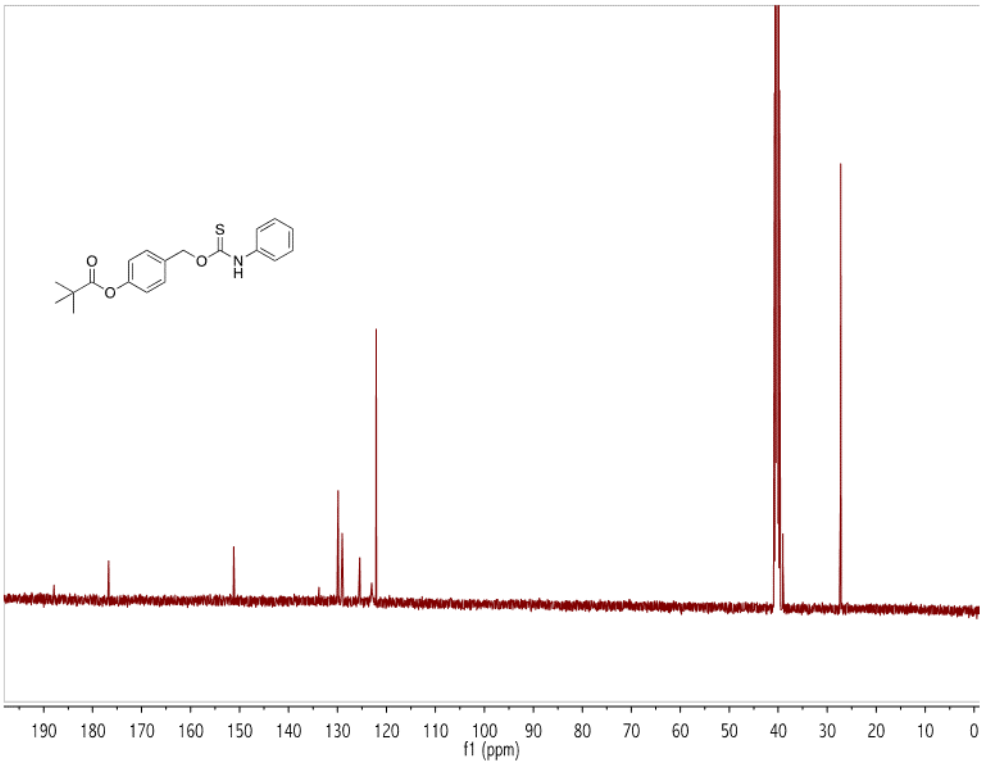

Figure B.26 $^{13}C\{^{1}H\}$ (125 MHz, DMSO-d_6, 60 °C) NMR spectrum of **TCM11.**

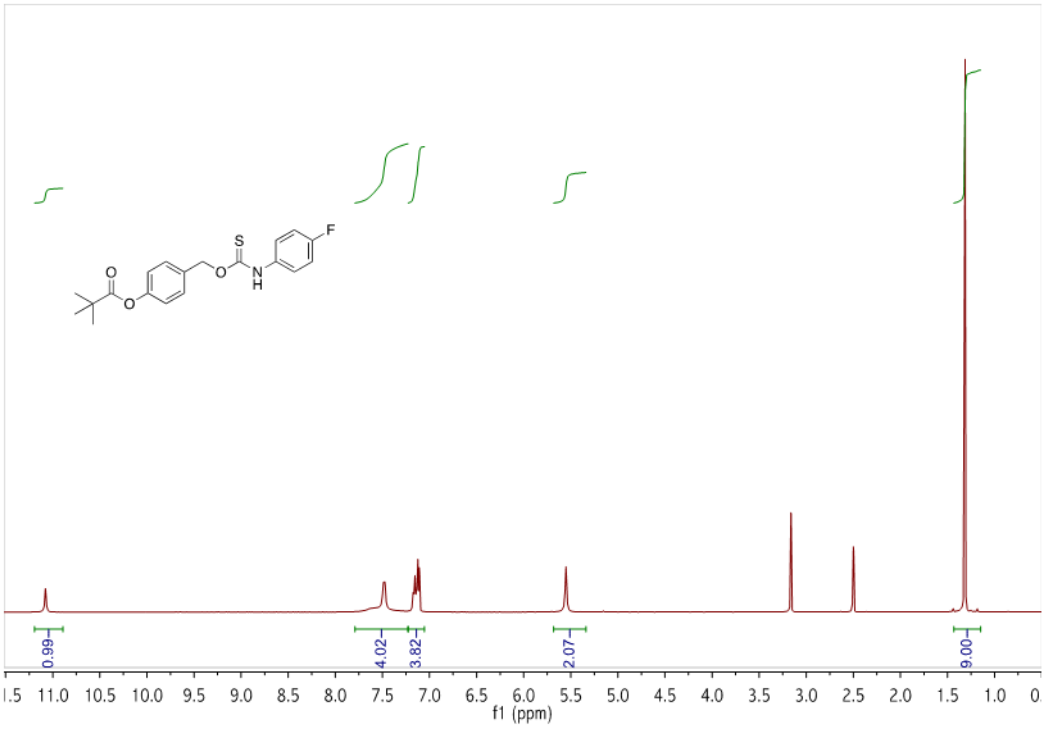

Figure B.27 ^{1}H (500 MHz, DMSO-d_6, 60 °C) NMR spectrum of **TCM12.**

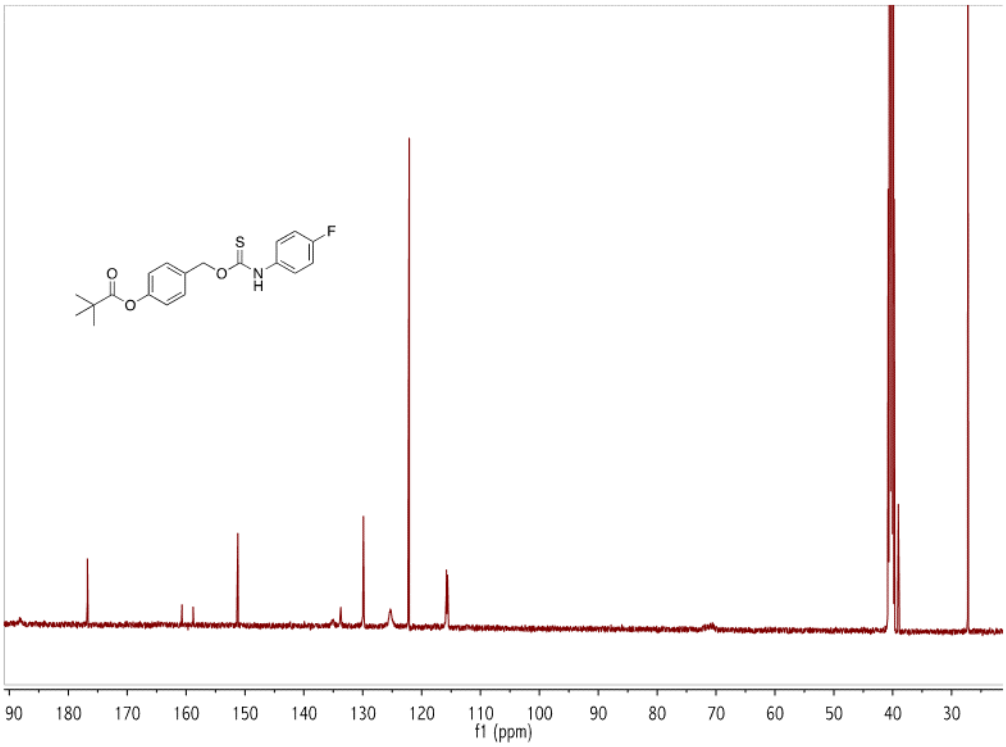

Figure B.28 $^{13}C\{^{1}H\}$ (125 MHz, DMSO-d_6, 60 °C) NMR spectrum of **TCM12.**

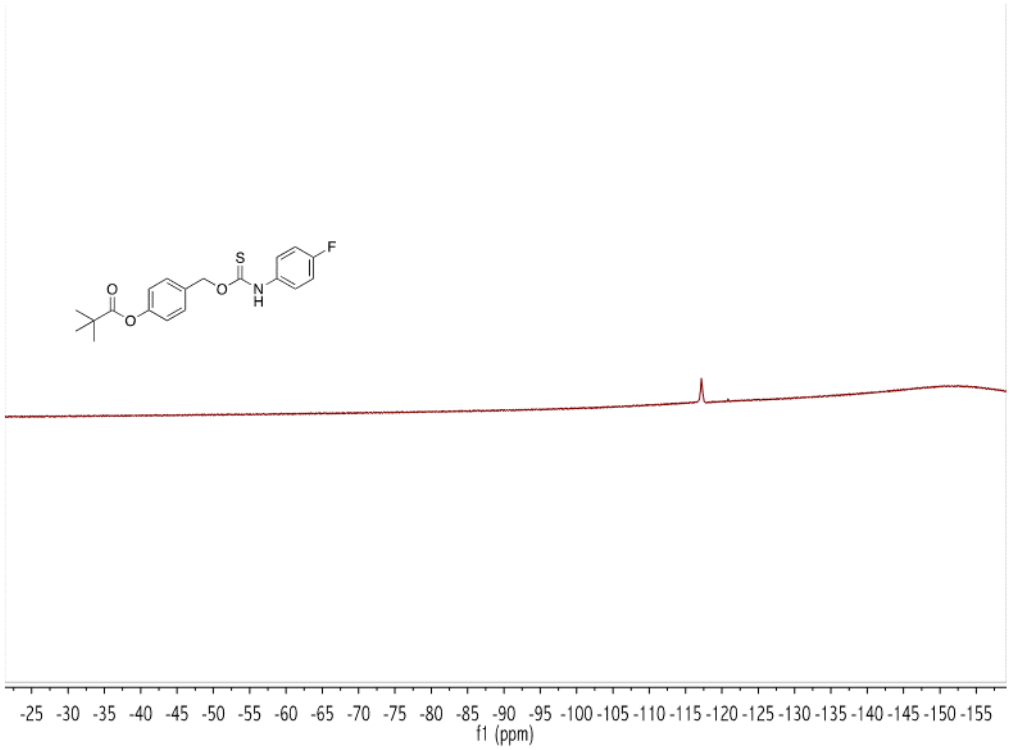

Figure B.29 ^{19}F (470 MHz, DMSO-d_6, 60 °C) NMR spectrum of **TCM12.**

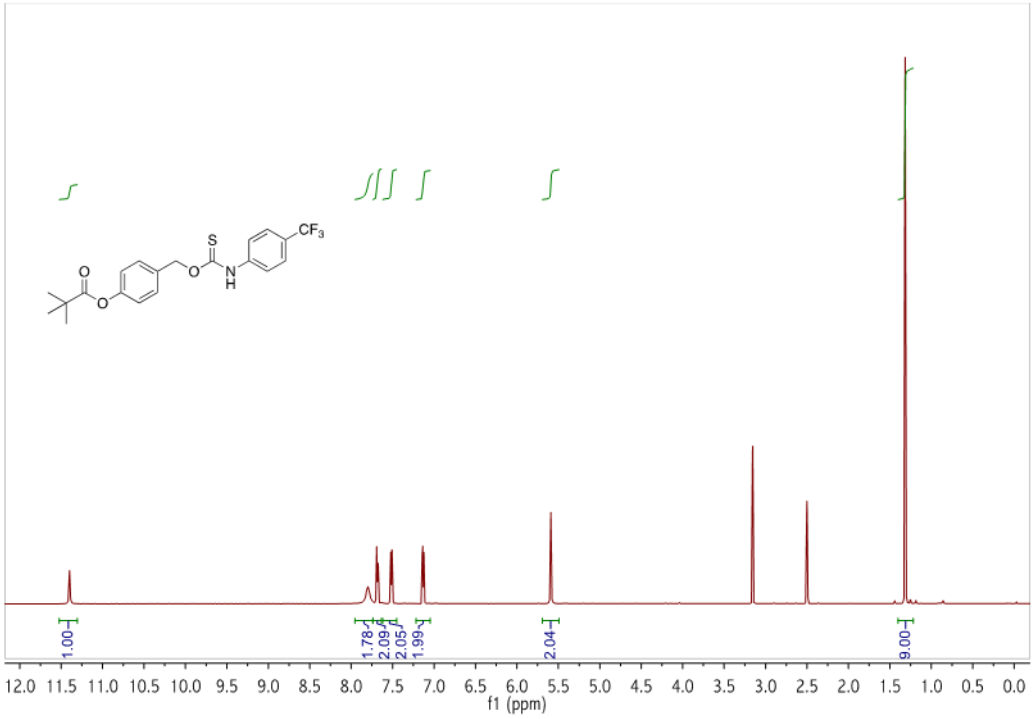

Figure B.30 ^{1}H (500 MHz, DMSO-d_6, 60 °C) NMR spectrum of **TCM13.**

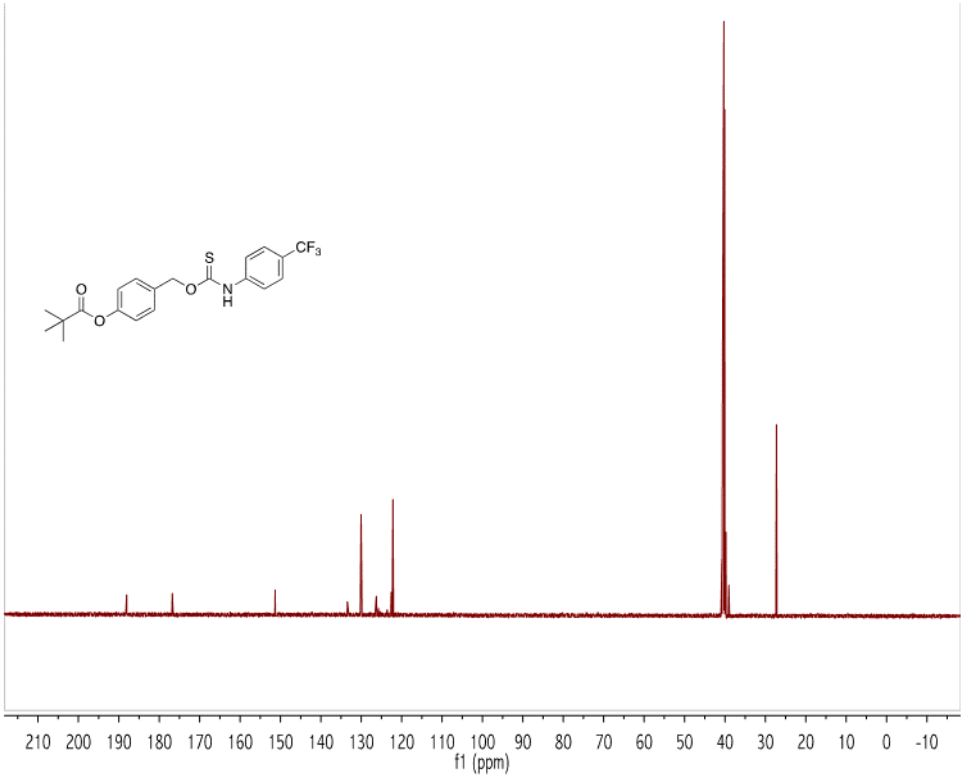

Figure B.31 ^{13}C{^{1}H} (125 MHz, DMSO-d_6, 60 °C) NMR spectrum of **TCM13.**

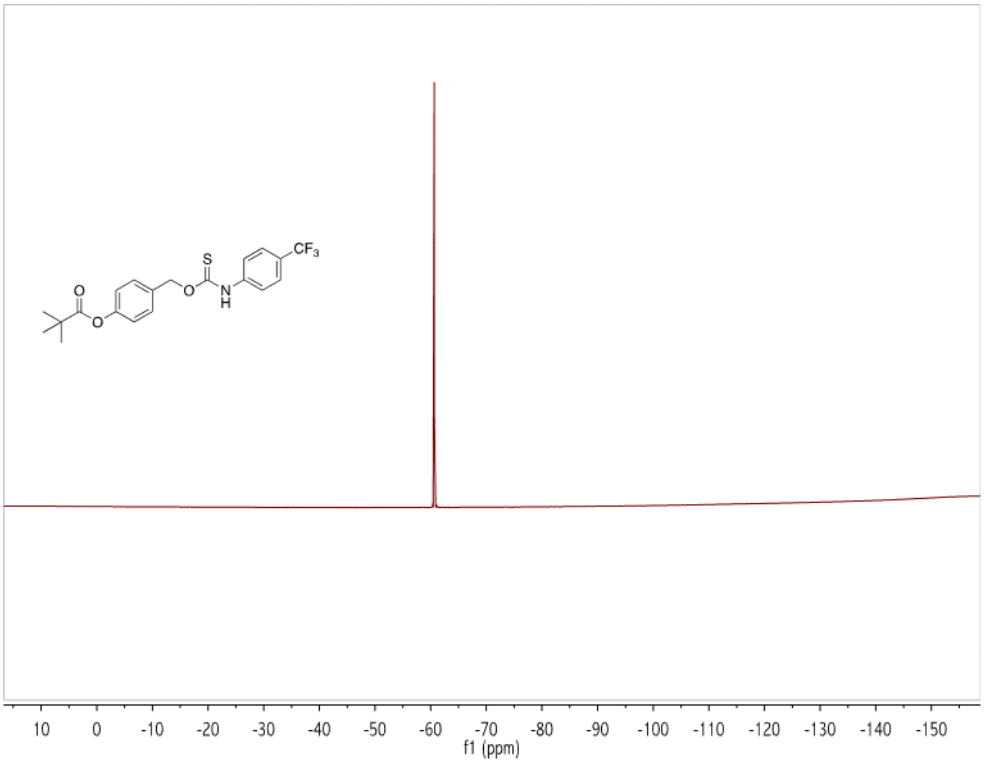

Figure B.32 ^{19}F (470 MHz, DMSO-*d*$_6$, 60 °C) NMR spectrum of **TCM13.**

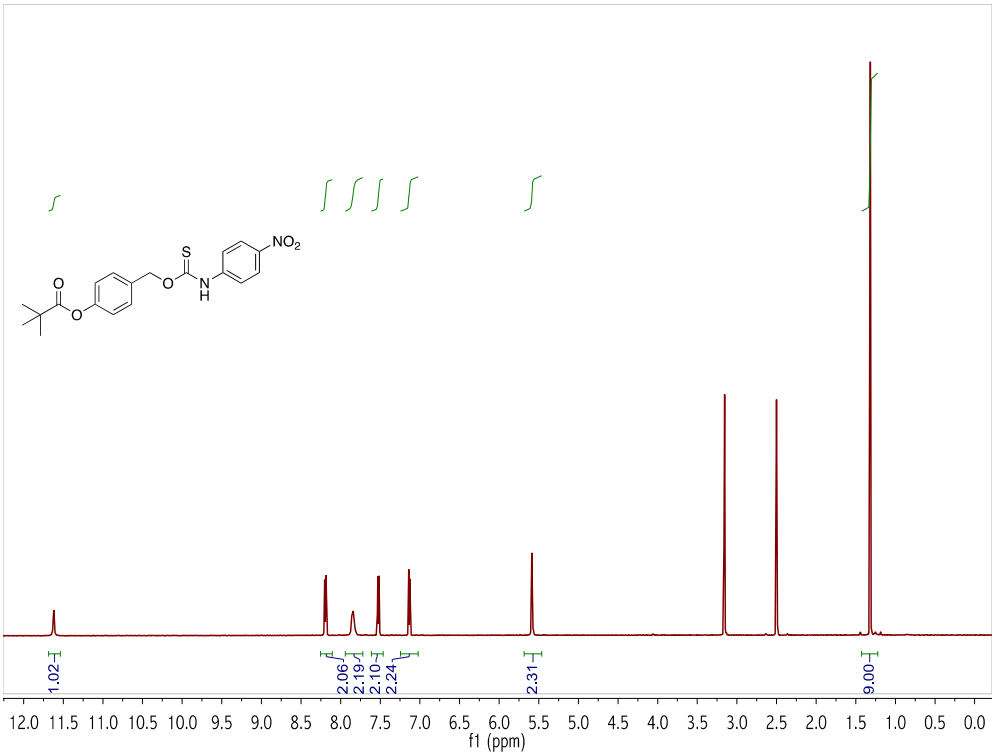

Figure B.33 ^{1}H (500 MHz, DMSO-*d*$_6$, 60 °C) NMR spectrum of **TCM14.**

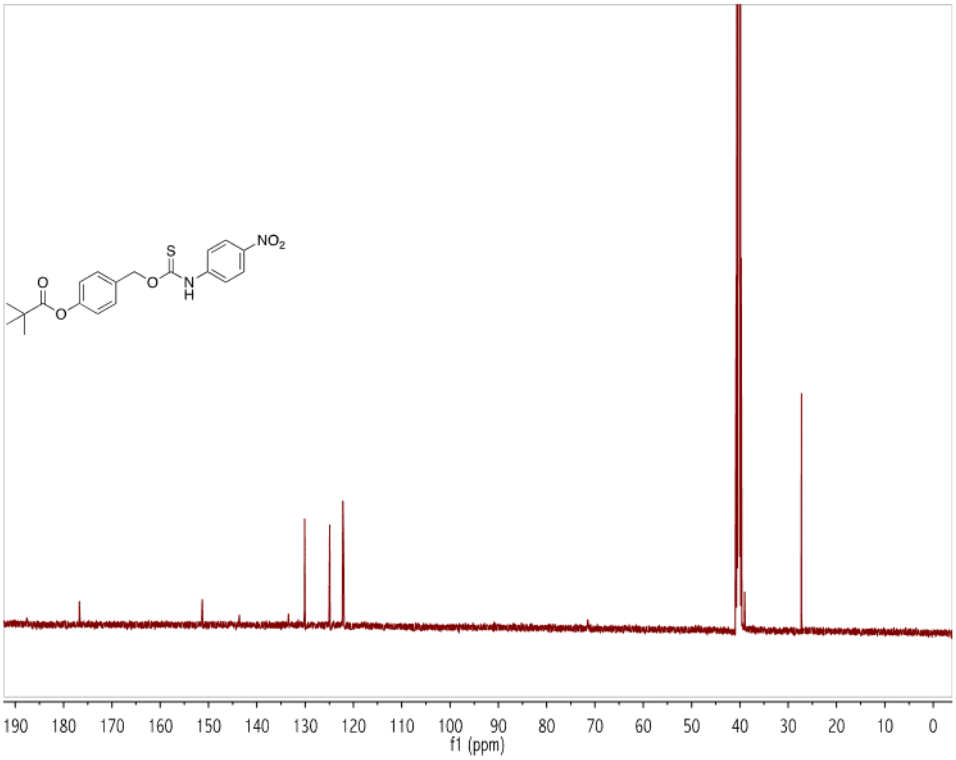

Figure B.34 $^{13}C\{^{1}H\}$ (125 MHz, DMSO-d_6, 60 °C) NMR spectrum of **TCM14.**

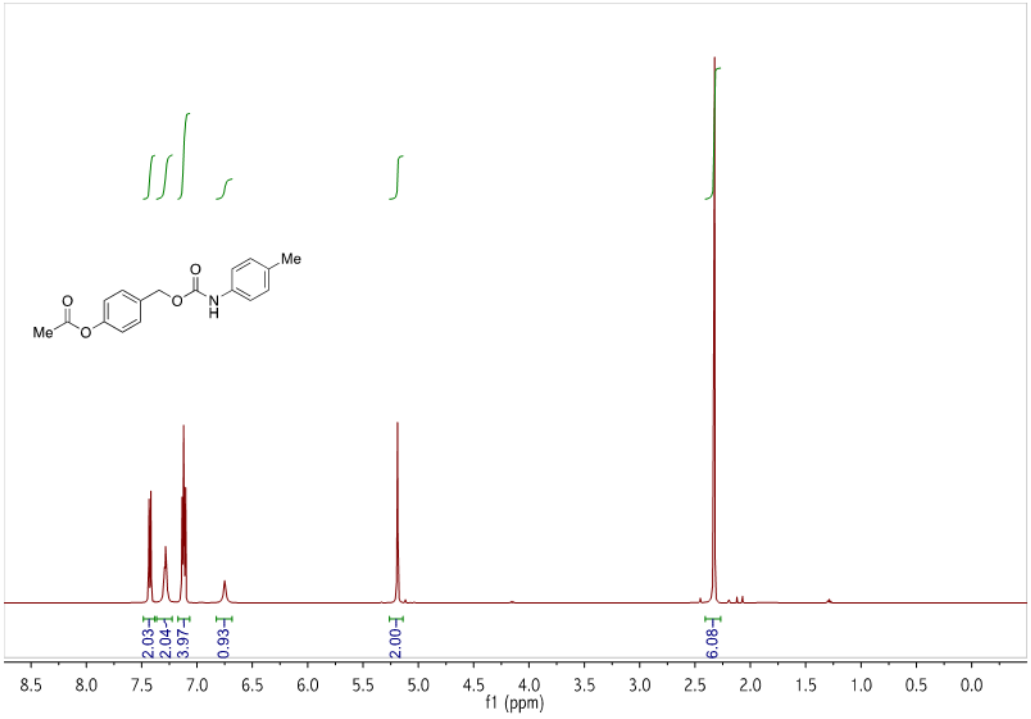

Figure B.35 ^{1}H (500 MHz, $CDCl_3$, RT) NMR spectrum of **CM1.**

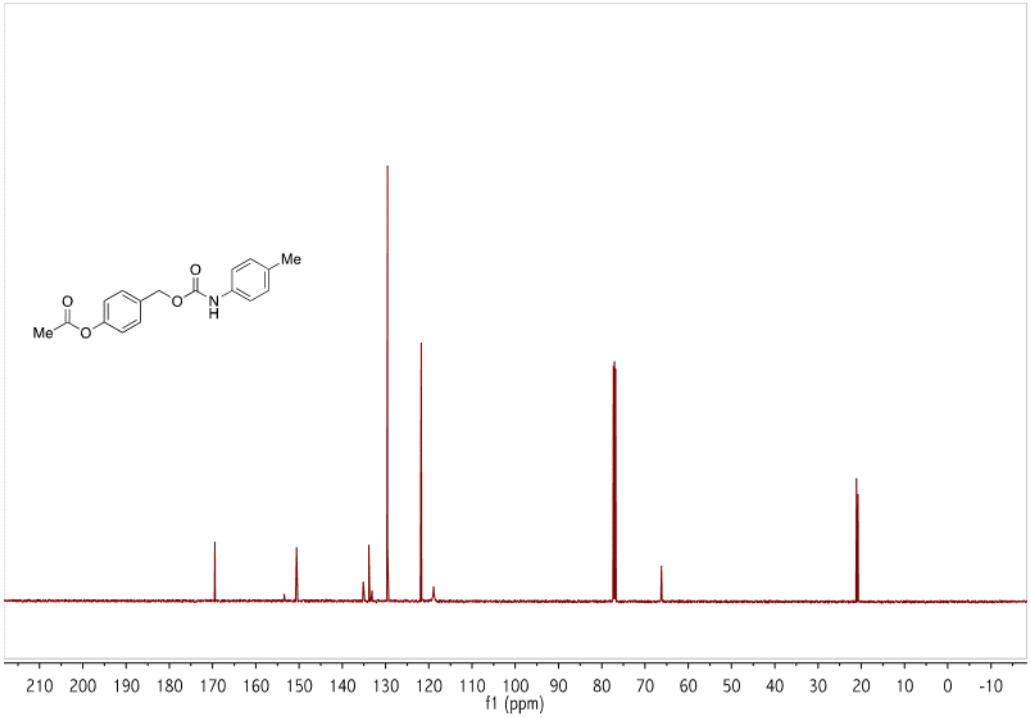

Figure B.36 $^{13}C\{^{1}H\}$ (125 MHz, $CDCl_3$, RT) NMR spectrum of **CM1.**

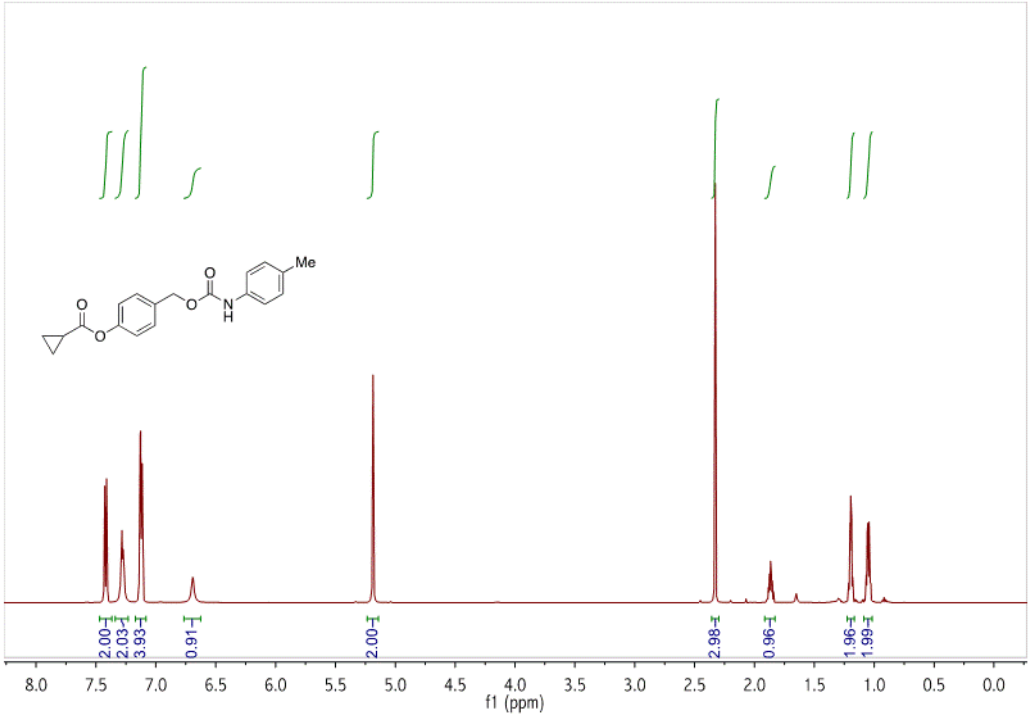

Figure B.37 ^{1}H (500 MHz, $CDCl_3$, RT) NMR spectrum of **CM2.**

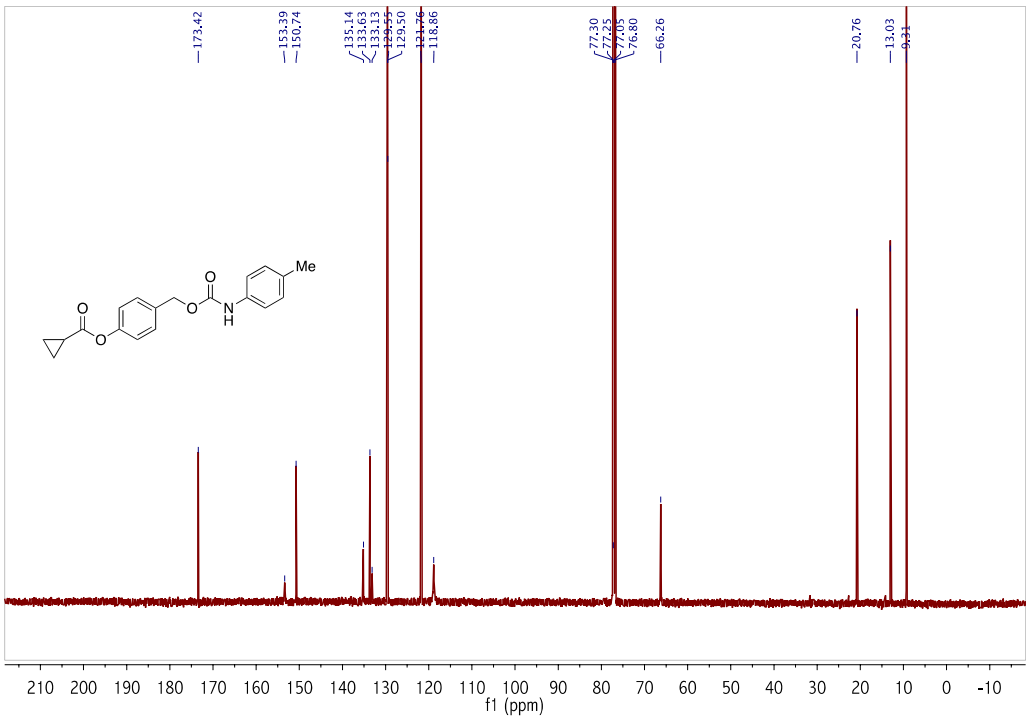

Figure B.38 $^{13}C\{^{1}H\}$ (125 MHz, $CDCl_3$, RT) NMR spectrum of **CM2.**

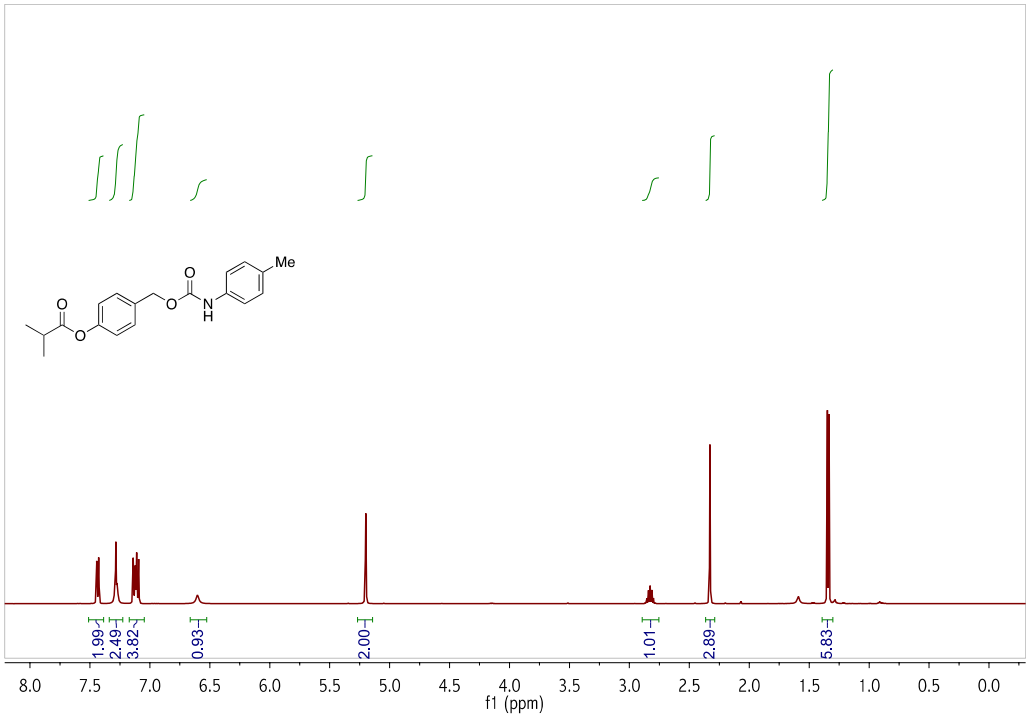

Figure B.39 ^{1}H (500 MHz, $CDCl_3$, RT) NMR spectrum of **CM3.**

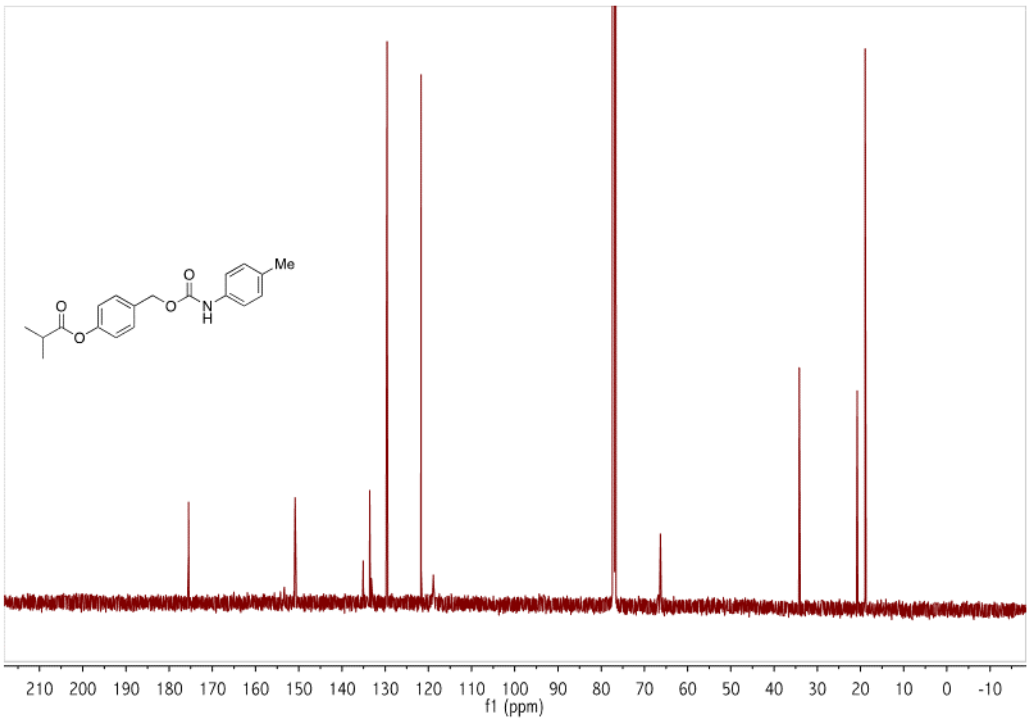

Figure B.40 $^{13}C\{^{1}H\}$ (125 MHz, $CDCl_3$, RT) NMR spectrum of **CM3.**

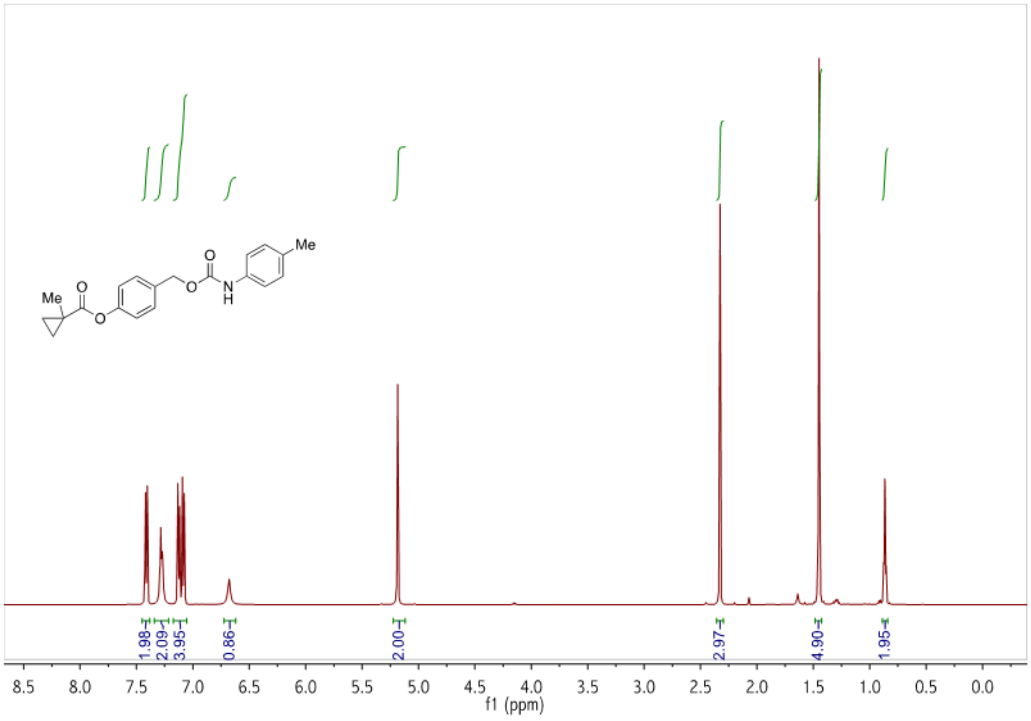

Figure B.41 ^{1}H (500 MHz, $CDCl_3$, RT) NMR spectrum of **CM4.**

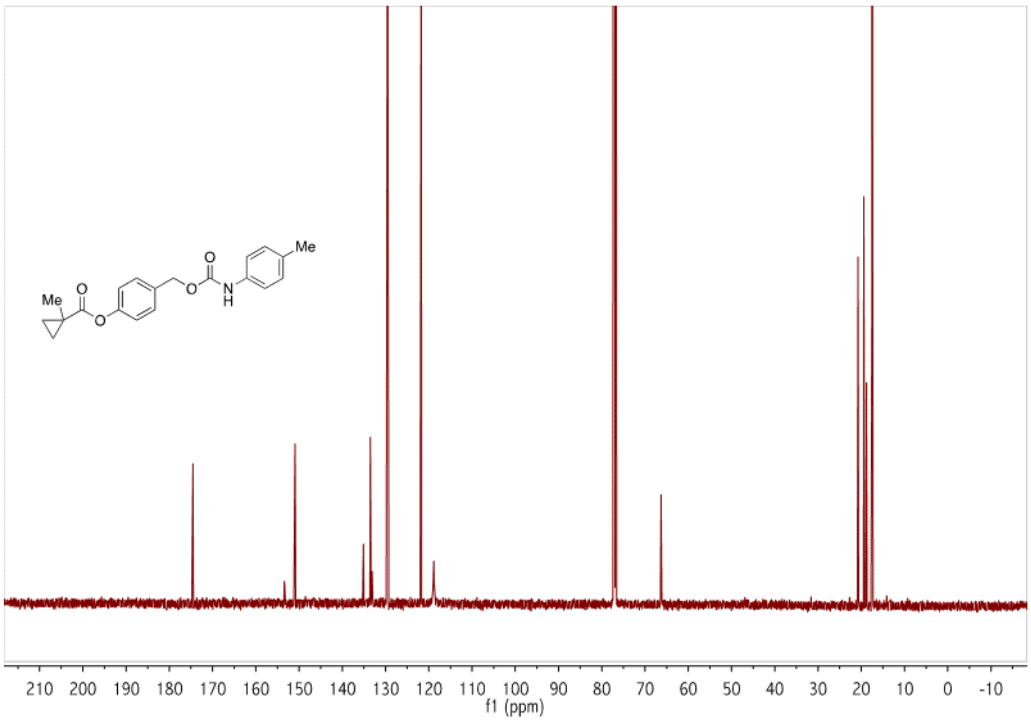

Figure B.42 $^{13}C\{^{1}H\}$ (125 MHz, $CDCl_3$, RT) NMR spectrum of **CM4.**

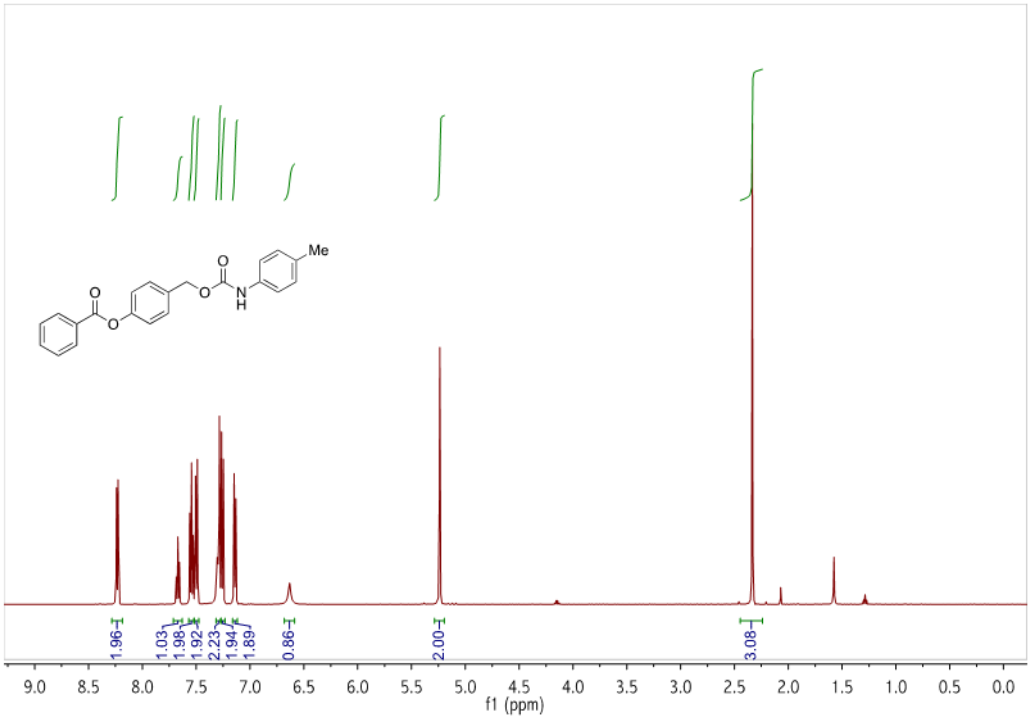

Figure B.43 ^{1}H (500 MHz, $CDCl_3$, RT) NMR spectrum of **CM6.**

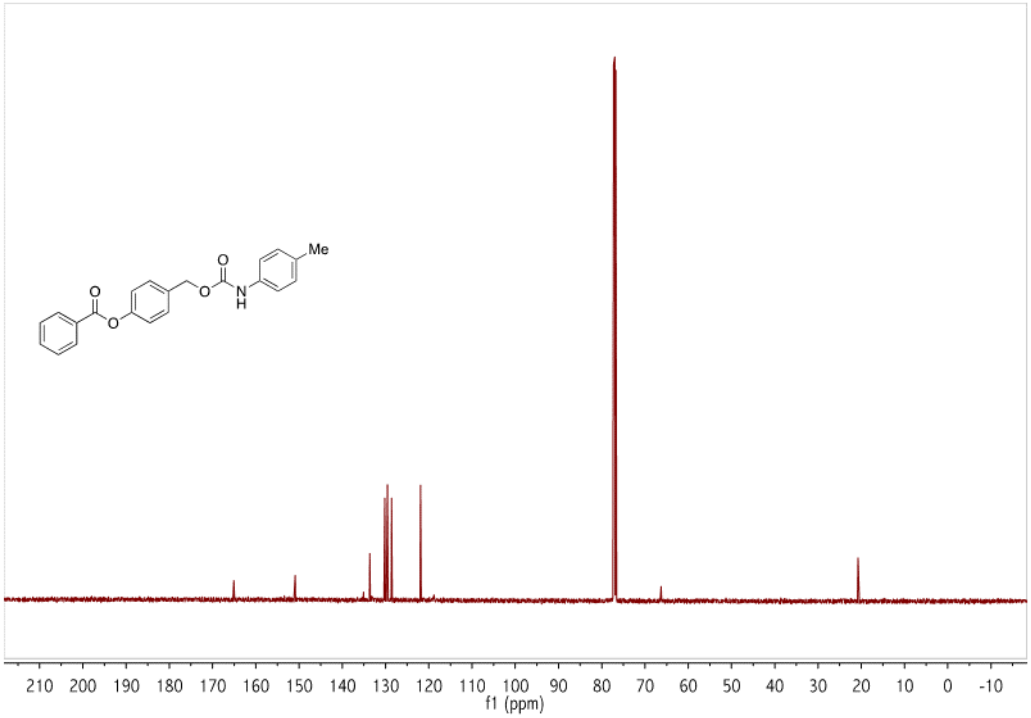

Figure B.44 $^{13}C\{^{1}H\}$ (125 MHz, $CDCl_3$, RT) NMR spectrum of **CM6.**

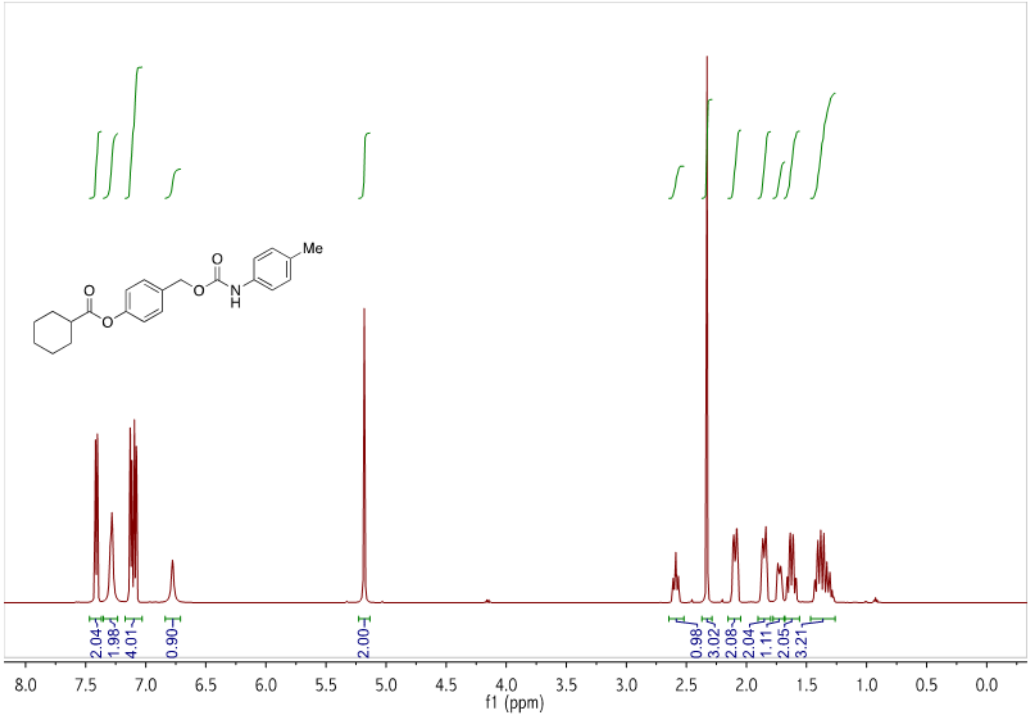

Figure B.45 ^{1}H (500 MHz, $CDCl_3$, RT) NMR spectrum of **CM7.**

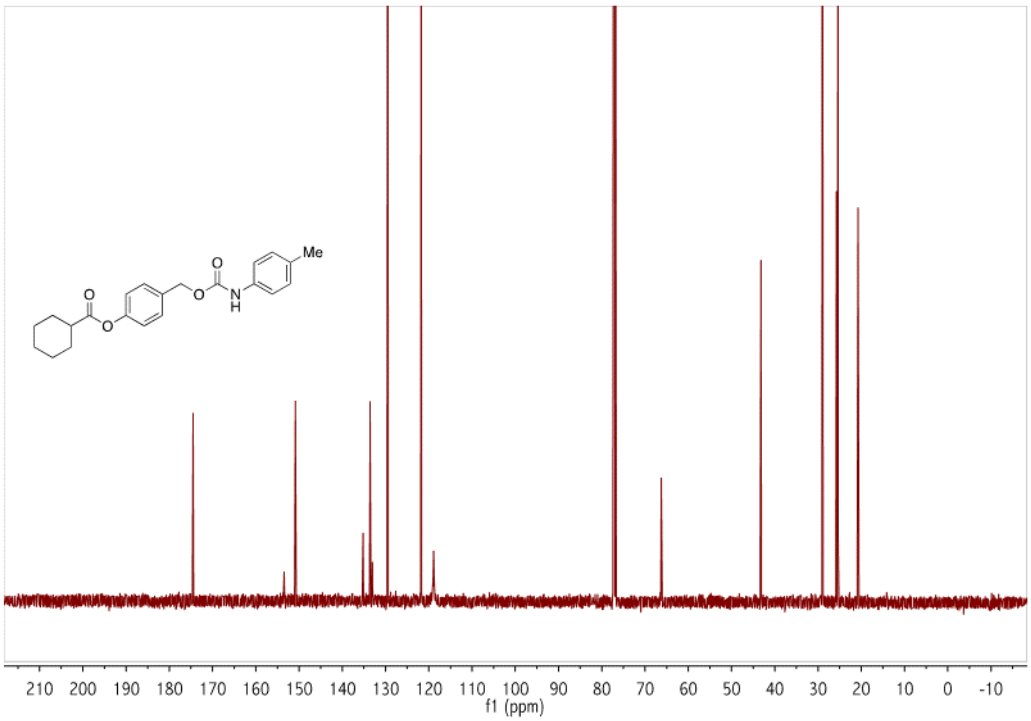

Figure B.46 $^{13}C\{^{1}H\}$ (125 MHz, $CDCl_3$, RT) NMR spectrum of **CM7.**

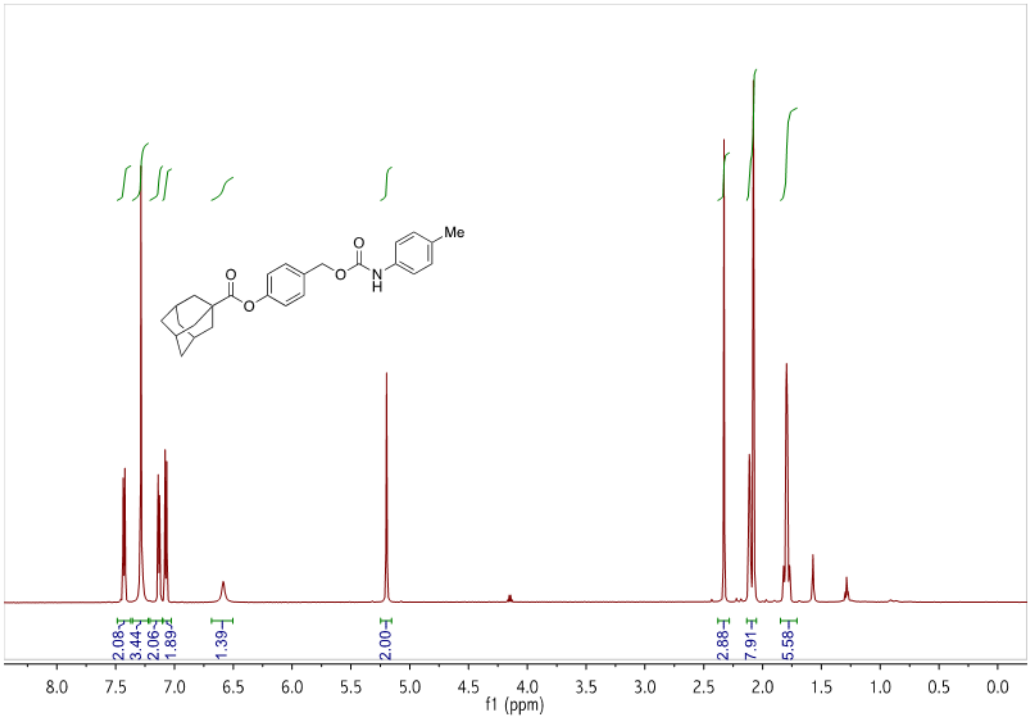

Figure B.47 ^{1}H (500 MHz, $CDCl_3$, RT) NMR spectrum of **CM8.**

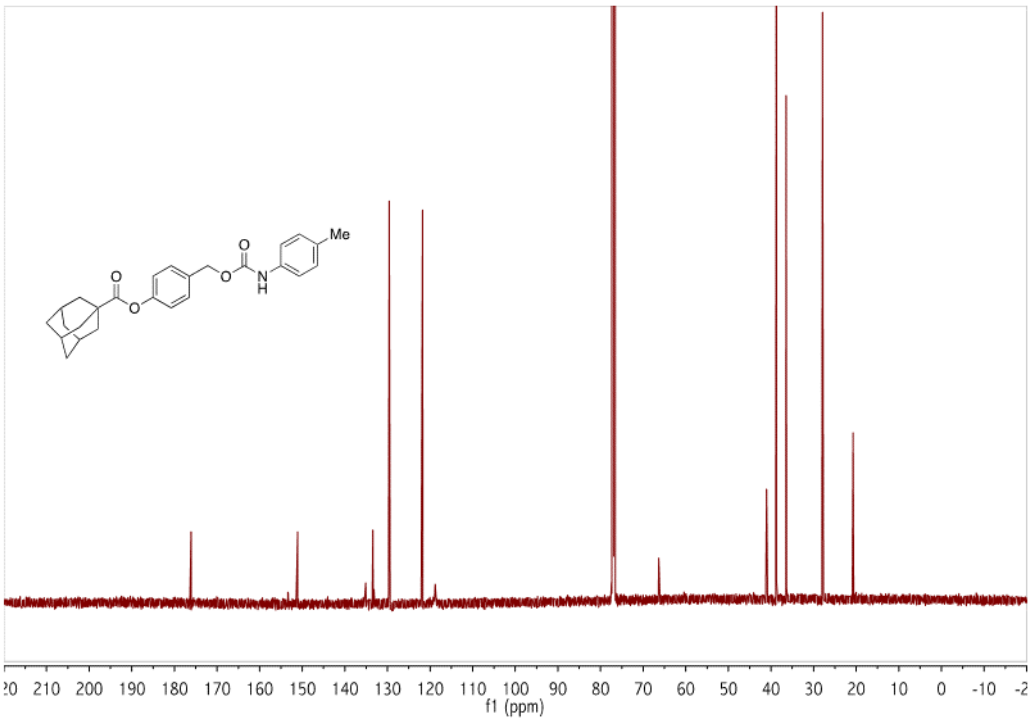

Figure B.48 $^{13}C\{^{1}H\}$ (125 MHz, $CDCl_3$, RT) NMR spectrum of **CM8.**

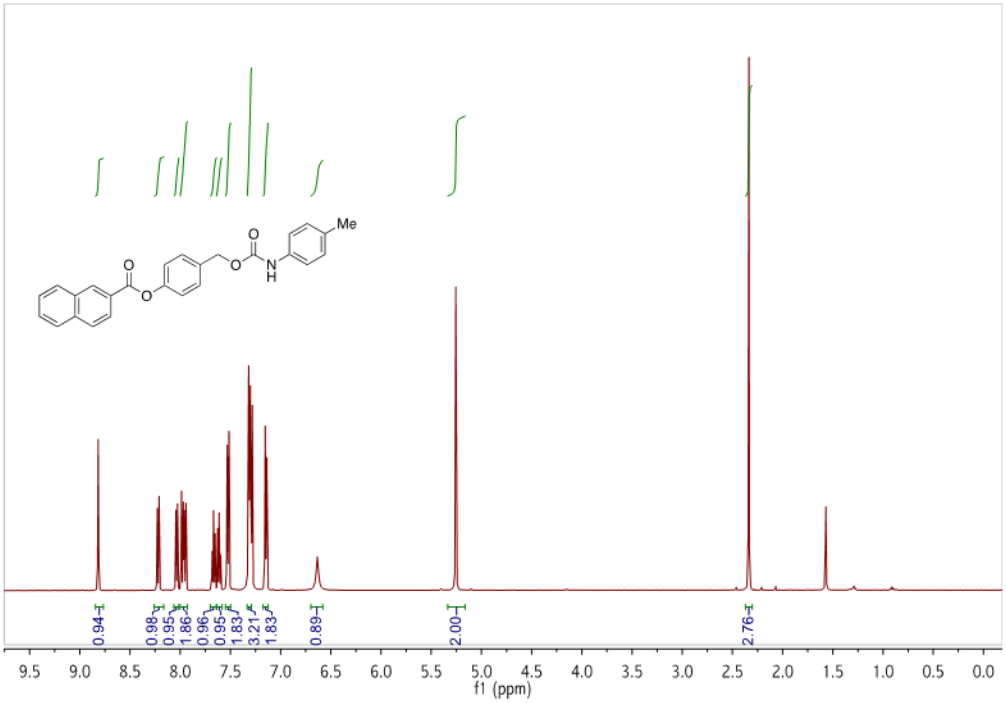

Figure B.49 ^{1}H (500 MHz, $CDCl_3$, RT) NMR spectrum of **CM9.**

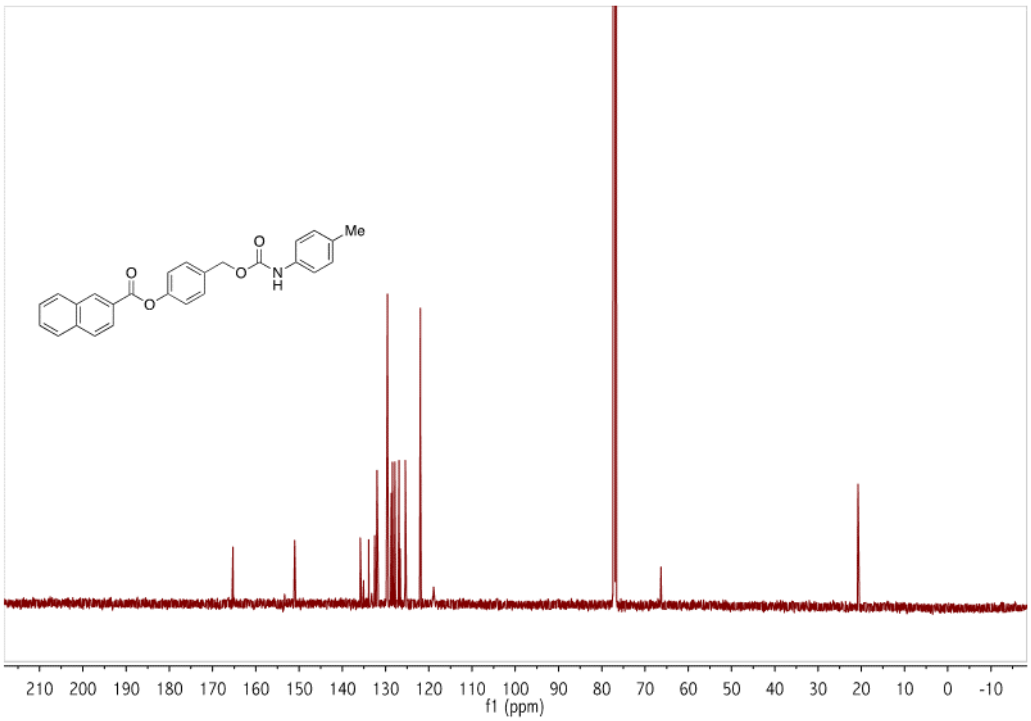

Figure B.50 $^{13}C\{^{1}H\}$ (125 MHz, $CDCl_3$, RT) NMR spectrum of **CM9.**

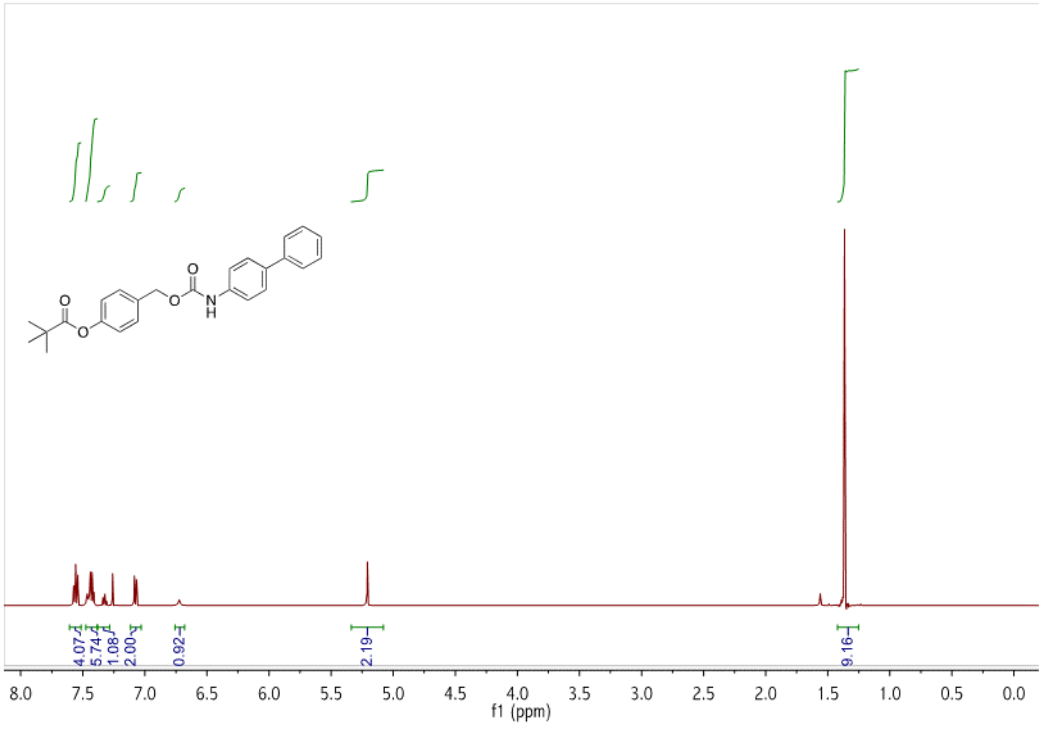

Figure B.51 ^{1}H (500 MHz, $CDCl_3$, RT) NMR spectrum of **CM10.**

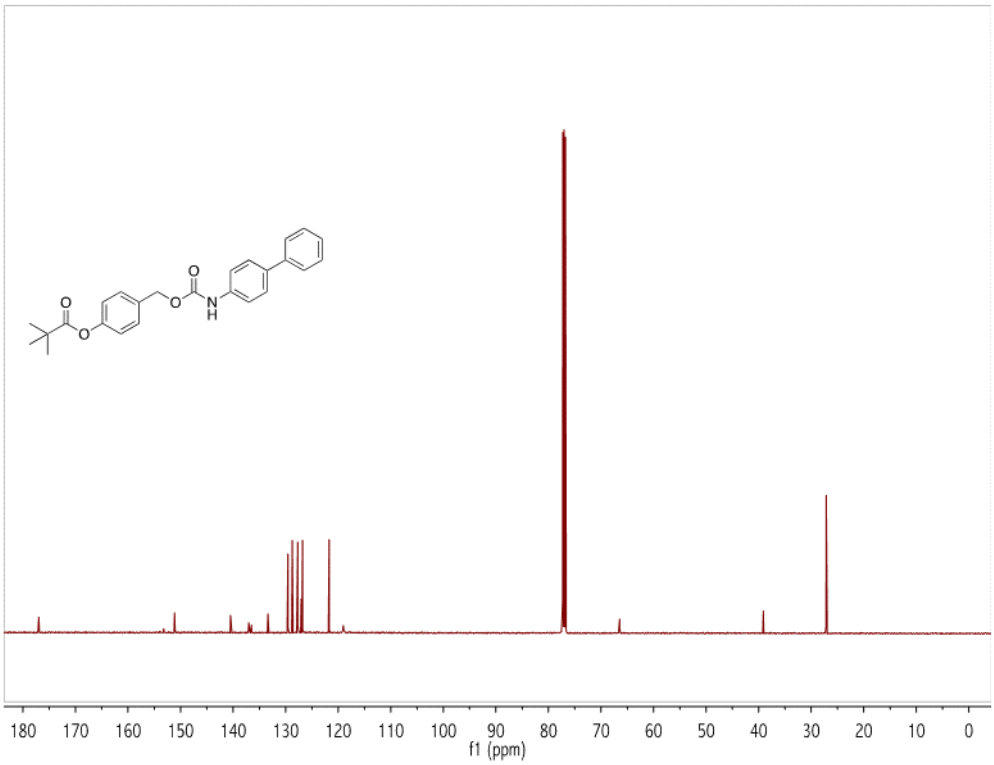

Figure B.52 $^{13}C\{^{1}H\}$ (125 MHz, $CDCl_3$, RT) NMR spectrum of **CM10.**

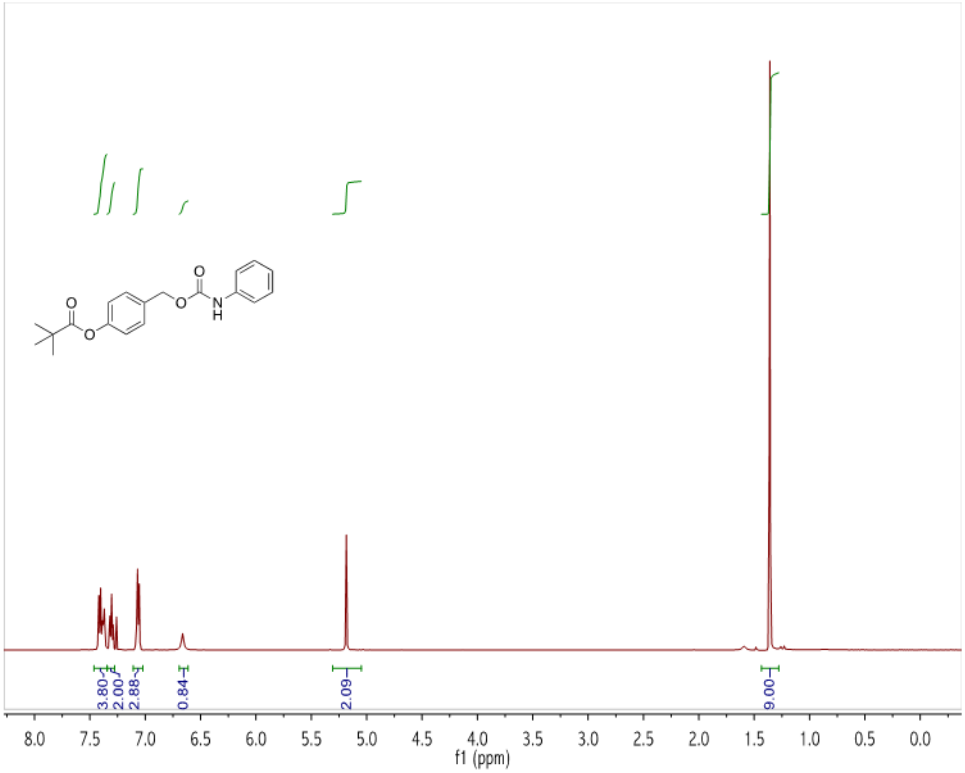

Figure B.53 ^{1}H (500 MHz, $CDCl_3$, RT) NMR spectrum of **CM11.**

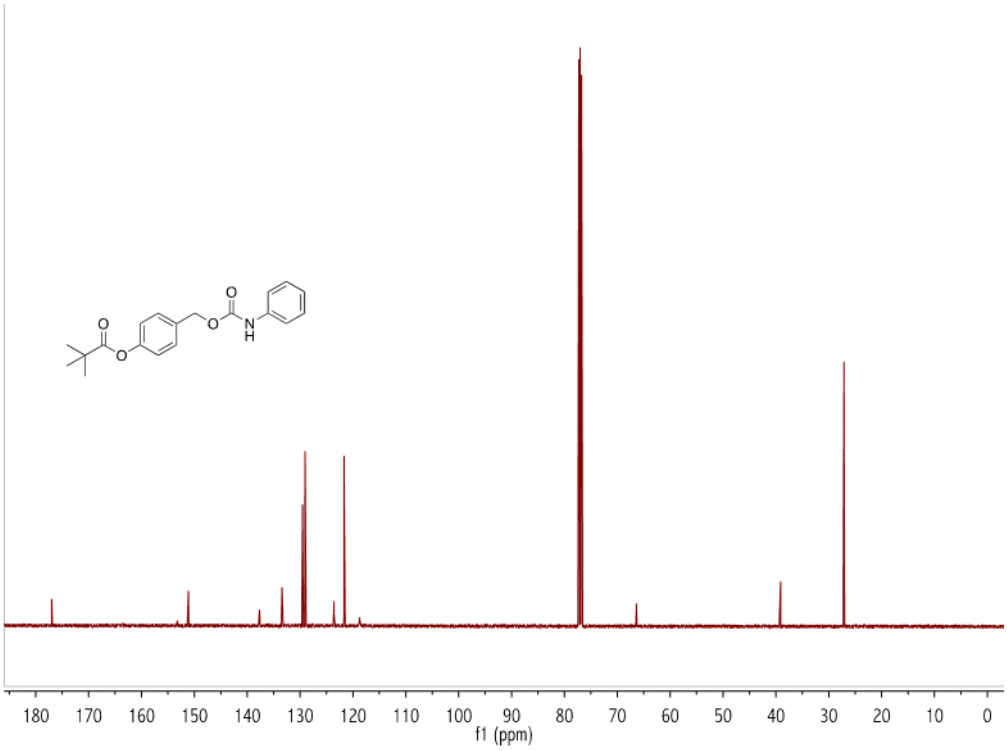

Figure B.54 $^{13}C\{^{1}H\}$ (125 MHz, $CDCl_3$, RT) NMR spectrum of **CM11.**

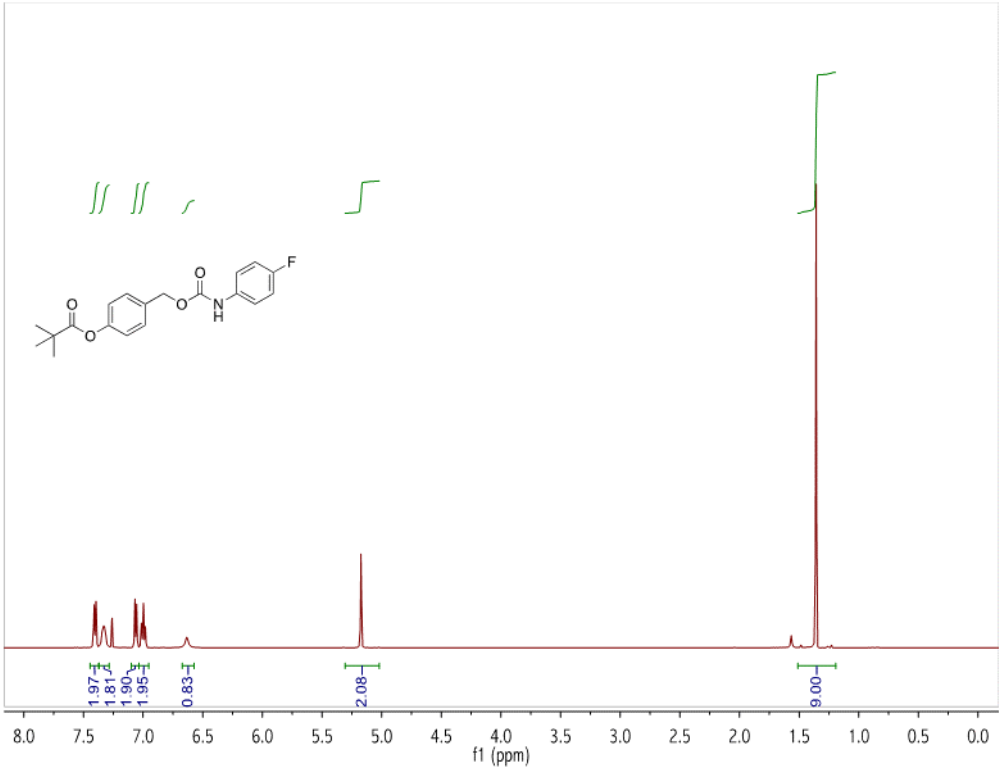

Figure B.55 ^{1}H (500 MHz, $CDCl_3$, RT) NMR spectrum of **CM12.**

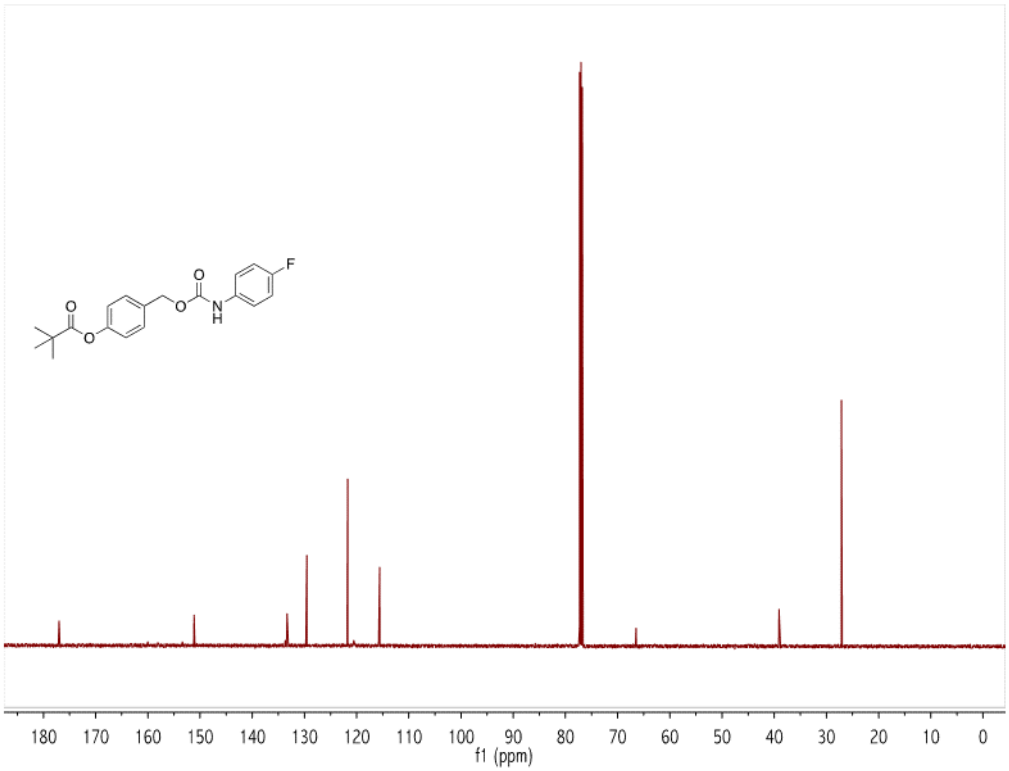

Figure B.56 $^{13}C\{^{1}H\}$ (125 MHz, $CDCl_3$, RT) NMR spectrum of **CM12.**

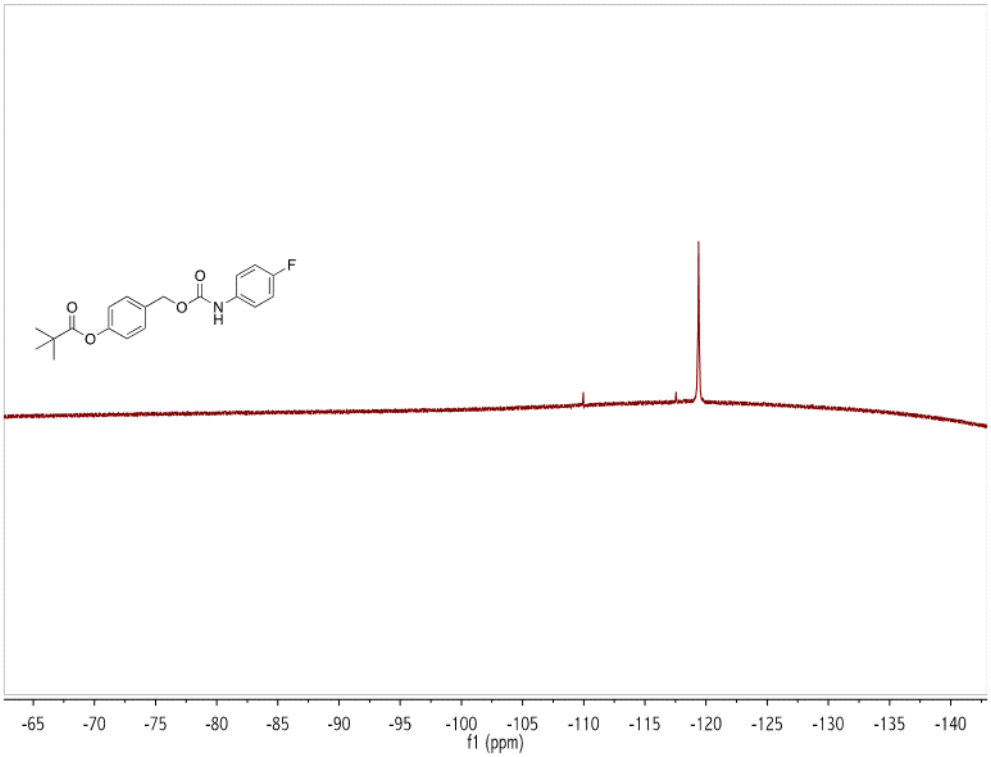

Figure B.57 ^{19}F (470 MHz, $CDCl_3$, RT) NMR spectrum of **CM12.**

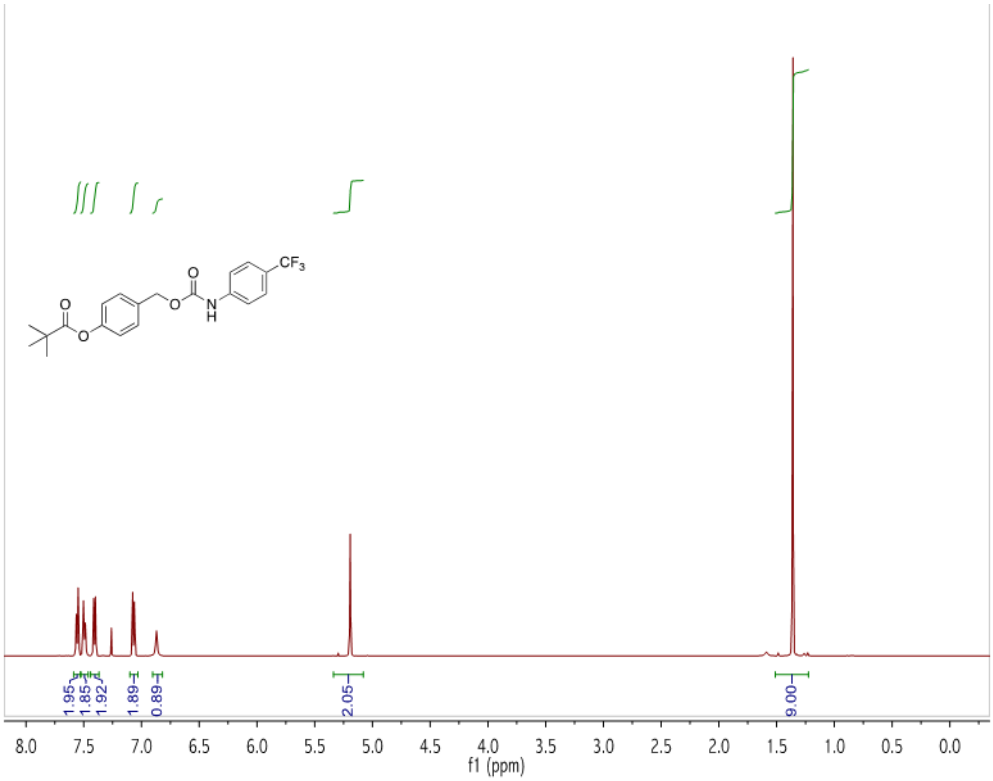

Figure B.58 ^{1}H (500 MHz, $CDCl_3$, RT) NMR spectrum of **CM13.**

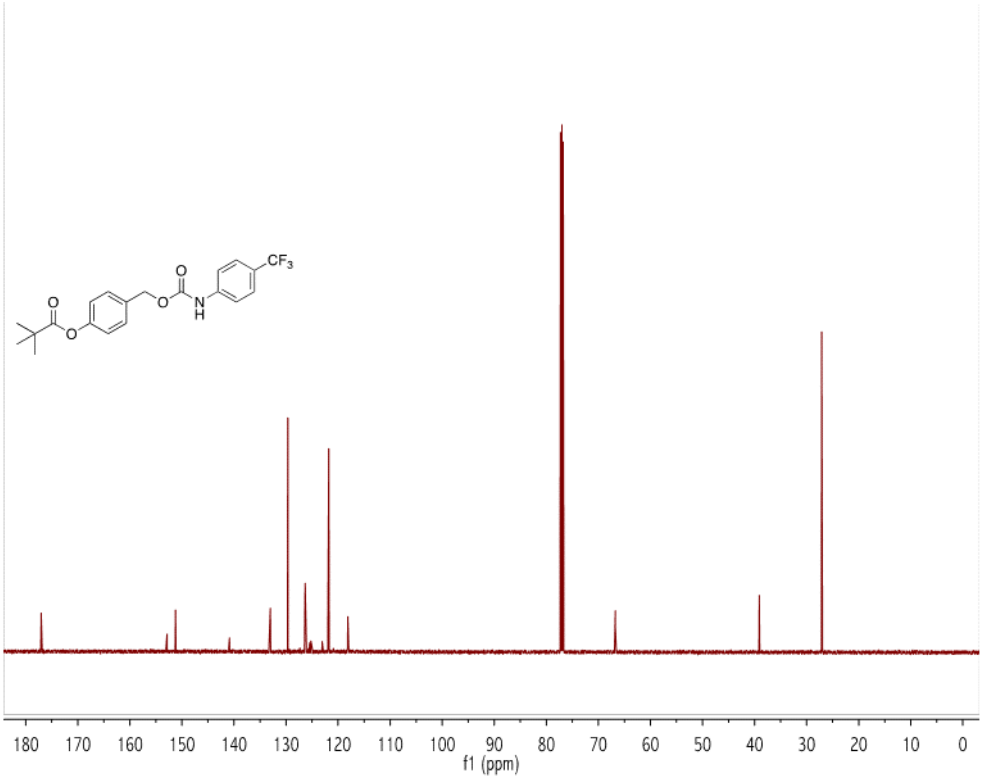

Figure B.59 $^{13}C\{^{1}H\}$ (125 MHz, $CDCl_3$, RT) NMR spectrum of **CM13.**

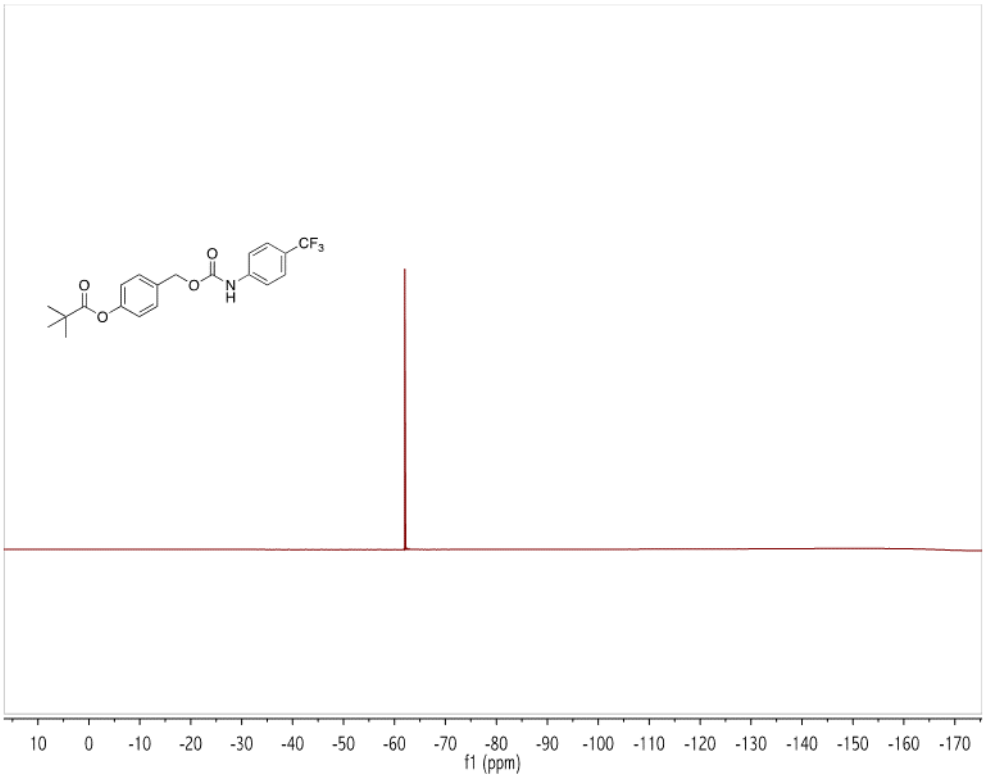

Figure B.60 ^{19}F (470 MHz, $CDCl_3$, RT) NMR spectrum of **CM13.**

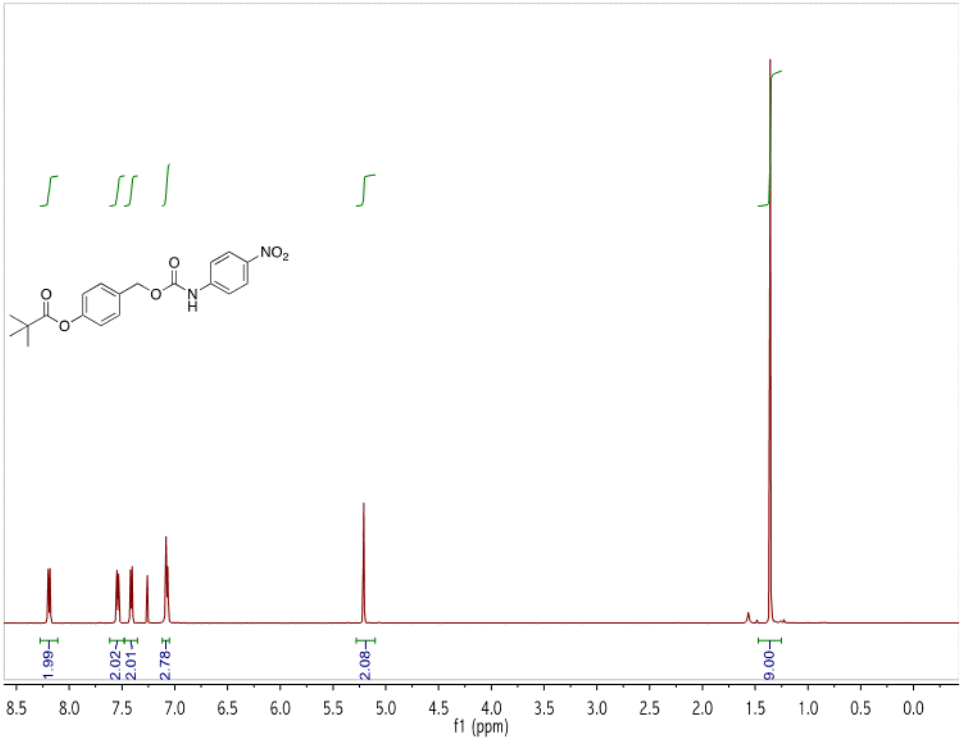

Figure B.61 ^{1}H (500 MHz, $CDCl_3$, RT) NMR spectrum of **CM14.**

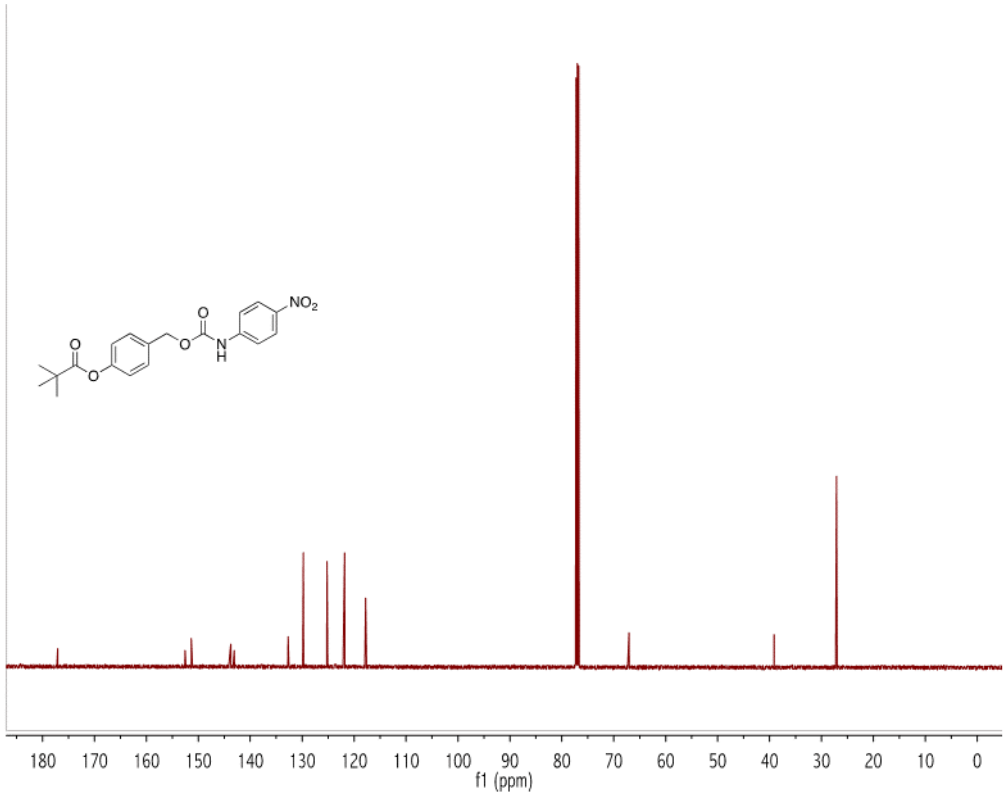

Figure B.62 $^{13}C\{^{1}H\}$ (125 MHz, $CDCl_3$, RT) NMR spectrum of **CM14.**

APPENDIX C

SUPPLEMENTARY INFORMATION FOR CHAPTER 4.1

Appendix C is the supplementary information for Chapter 4.1 of this dissertation. It includes spectra and experimental data relevant to the content in Chapter 4.1.

Synthesis / Spectral Details of Prepared Compounds

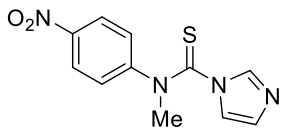

CP-NO2 was prepared according to the general synthetic B procedure described in Chapter 4.1. (40 mg, 26% yield, yellow solid). ^{1}H NMR (500 MHz, $CDCl_3$) δ (ppm): 8.18 (d, *J* = 8.97 Hz, 2H), 7.69 (bs, 1H), 7.23 (d, *J* = 8.97 Hz, 2H), 6.97 (bs, 1H), 6.81 (bs, 1H), 3.85 (s, 3H). ^{13}C{^{1}H} NMR (125 MHz, $CDCl_3$) δ (ppm): 178.88, 148.02, 137.72, 129.97 (q, *J* = 33.22), 129.72, 127.39 (q, *J* = 3.76), 125.02, 123.29 (q, *J* = 272.48), 119.73, 46.60. HRMS m/z $[M + H]^+$ calcd. For $[C_{11}H_{11}O_2N_4S]^+$ 263.0603; found 263.0604.

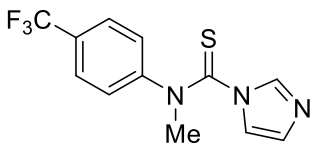

CP-CF3 was prepared according to the general synthetic B procedure described in Chapter 4.1. (625 mg, 81% yield, white solid). ^{1}H NMR (500 MHz, $CDCl_3$) δ (ppm):

7.69 (bs, 1H), 7.60 (d, *J* = 8.70 Hz, 2H), 7.18 (d, *J* = 8.70 Hz, 2H), 6.96 (s, 1H), 6.80 (bs, 1H), 3.84 (s, 3H). $^{13}C\{^{1}H\}$ NMR (125 MHz, $CDCl_3$) δ (ppm): 178.88, 150.30, 146.17, 137.63, 130.01, 125.58, 125.36, 119.70, 46.36. ^{19}F (470 MHz, $CDCl_3$) -62.71 (m). HRMS m/z $[M + H]^+$ calcd. For $[C_{12}H_{11}N_3F_3S]^+$ 286.0626; found 286.0616.

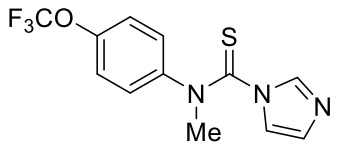

CP-OCF3 was prepared according to the general synthetic procedure A described in Chapter 4.1. (532 mg, 60% yield, yellowish solid). ^{1}H NMR (500 MHz, $CDCl_3$) δ (ppm): 7.72 (s, 1H), 7.18 (d, *J* = 8.94, 2H), 7.10 (d, *J* = 8.94, 2H), 6.94 (s, 1H), 6.80 (bs, 1H), 3.82 (s, 3H). $^{13}C\{^{1}H\}$ NMR (125 MHz, $CDCl_3$) δ (ppm): 170.80, 148.16, 148.14, 143.32, 137.84, 129.51, 126.15, 122.48, 120.23 (q, *J* = 258.34), 119.68, 46.83. ^{19}F (470 MHz, $CDCl_3$) -58.01 (m). HRMS m/z $[M + H]^+$ calcd. For $[C_{12}H_{11}N_3OF_3S]^+$ 302.0575; found 302.0565.

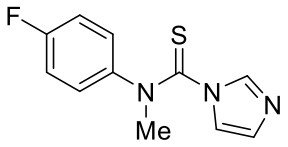

CP-F was prepared according to the general synthetic procedure A described in Chapter 4.1. (1.04 g, 55% yield, pale yellow solid). ^{1}H NMR (500 MHz, $CDCl_3$) δ (ppm): 7.69 (bs, 1H), 7.04 (m, 4H), 6.95 (t, *J* = 1.42, 1H), 6.80 (bs, 1H), 3.81 (s, 3H). $^{13}C\{^{1}H\}$ NMR (125 MHz, $CDCl_3$) δ (ppm): 178.76, 162.31, 160.65, 141.01, 140.99, 137.81, 129.32,

126.43, 126.37, 119.77, 117.33, 117.18, 46.99. ^{19}F (470 MHz, $CDCl_3$) -111.81 (m). HRMS m/z $[M + H]^+$ calcd. For $[C_{11}H_{11}N_3FS]^+$ 236.0658; found 236.0651.

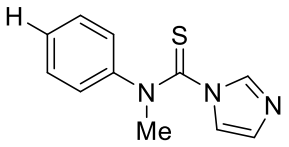

CP-H was prepared according to the general synthetic procedure A described in Chapter 4.1. (606 mg, 75% yield, colorless oil). ^{1}H NMR (500 MHz, $CDCl_3$) δ (ppm): 7.69 (bs, 1H), 7.33 (m, 2H), 7.27 (m, 1H), 7.05 (bs, 1H), 6.76 (bs, 1H), 3.84 (s, 3H). ^{13}C{^{1}H} NMR (125 MHz, $CDCl_3$) δ (ppm): 178.59, 145.02, 137.87, 130.20, 129.09, 128.13, 124.60, 119.87, 46.94. HRMS m/z $[M + H]^+$ calcd. For $[C_{11}H_{12}N_3S]^+$ 218.0752; found 218.0744.

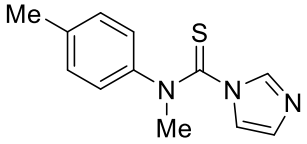

CP-Me was prepared according to the general synthetic procedure A described in Chapter 4.1. (378 mg, 99% yield, pale yellow solid). ^{1}H NMR (500 MHz, $CDCl_3$) δ (ppm): 7.65 (bs, 1H), 7.11 (d, J = 8.15, 2H), 6.98 (t, J = 1.30, 1H), 6.92 (dt, J = 8.15, 1.30, 2H), 6.76 (t, J = 1.30, 1H), 3.81 (s, 3H), 2.30 (s, 3H). ^{13}C{^{1}H} NMR (125 MHz, $CDCl_3$) δ (ppm): 178.49, 142.47, 138.26, 137.80, 130.74, 129.01, 124.29, 119.98, 47.00, 21.03. HRMS m/z $[M + H]^+$ calcd. For $[C_{12}H_{14}N_3S]^+$ 232.0908; found 232.0903.

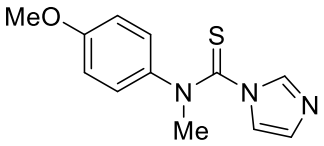

CP-OMe was prepared according to the general synthetic procedure A described in Chapter 4.1. (855.7 mg, 95% yield, brown solid). ^{1}H NMR (500 MHz, $CDCl_3$) δ (ppm): 7.69 (bs, 1H), 6.96 (m, 3H), 6.82 (ddd, *J* = 9.02, 3.50, 2.30, 2H), 6.77 (bs, 1H), 3.81 (s, 3H), 3.76 (s, 3H). $^{13}C\{^{1}H\}$ NMR (125 MHz, $CDCl_3$) δ (ppm): 178.45, 158.94, 137.87, 137.69, 128.97, 125.68, 119.93, 115.27, 55.52, 47.15. HRMS m/z $[M + H]^+$ calcd. For $[C_{12}H_{14}N_3OS]^+$ 248.0858; found 248.0852.

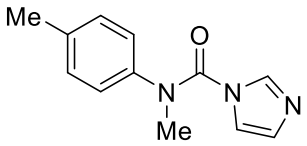

SI-1. N-Me *p*-toluidine (1.04 mL, 8.25 mmol, 1.0 equiv.) was added dropwise to a stirring solution of CDI (2.68 g, 16.50 mmol, 2.0 equiv.) dissolved in anhydrous THF (83 mL, 0.1 M solution) under an atmosphere of N_2. The resulting solution was heated to reflux overnight. The reaction mixture was let cool to room temperature, and the solvent was removed under vacuum. The remaining residue was dissolved in DCM, washed with water, and dried over anhydrous $MgSO_4$ and concentrated to an off-white solid. The crude product was taken forward with no further purification. (1.65 g, 92% yield, white solid). ^{1}H NMR (500 MHz, $CDCl_3$) δ (ppm): 7.60 (bs, 1H), 7.18 (d, *J* = 8.14, 2H), 7.01 (d, *J* = 8.14, 2H), 6.91 (bs, 1H), 6.85 (bs, 1H), 3.47 (s, 3H), 2.35 (s, 3H). $^{13}C\{^{1}H\}$ NMR

(125 MHz, $CDCl_3$) δ (ppm):150.02, 140.18, 138.43, 137.54, 130.97, 128.28, 128.14, 125.74, 118.69, 40.29, 21.07.

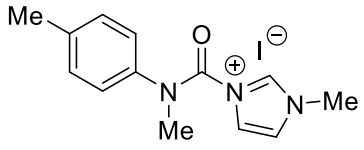

SI-2. SI-1 (2.62 g, 12.17 mmol, 1.0 equiv.) was dissolved in anhydrous MeCN (61 mL, 0.2 M solution) and put under an atmosphere of N_2. MeI (3.03 mL, 48.68 mmol, 4.0 equiv.) was added dropwise, and the reaction mixture was heated to reflux with magnetic stirring overnight. Upon completion, the reaction mixture was let cool and the solvent removed *via* rotary evaporation, to afford the crude product, which was used with no further purification. (4.2 g crude dark reddish-brown solid, 97%). ^{1}H NMR (500 MHz, $CDCl_3$) δ (ppm): 9.76 (bs, 1H), 7.50 (s, 1H), 7.38 (d, *J* = 8.19, 2H), 7.26 (d, *J* = 8.19, 2H), 7.03 (bs, 1H), 4.13 (s, 3H), 3.53 (s, 3H), 2.4 (s, 3H).

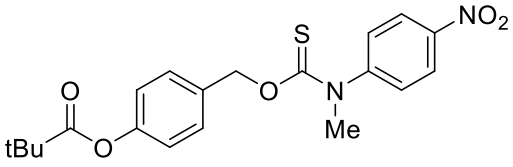

MeTCM-NO_2 was prepared according to the general procedure described in Chapter 4.1. (46 mg, 33% yield, white solid). ^{1}H NMR (500 MHz, DMSO-d_6, 60 °C) δ (ppm): 8.26 (d, *J* = 8.98, 2H), 7.64 (d, *J* = 8.98, 2H), 7.35 (d, *J* = 8.55, 2H), 7.07 (d, *J* = 8.55, 2H), 5.52 (s, 2H), 3.59 (s, 3H), 1.31 (s, 9H). ^{13}C{^{1}H} NMR (125 MHz, $CDCl_3$) δ (ppm):188.41,

176.69, 151.09, 149.92, 146.43, 133.44, 129.39, 128.23, 124.85, 122.03, 72.53, 42.77, 39.02, 27.23. HRMS m/z $[M + H]^+$ calcd. For $[C_{12}H_{14}N_3OS]^+$ 248.0858; found 248.0852.

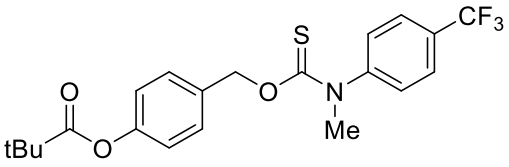

MeTCM-CF$_3$ was prepared according to the general procedure described in Chapter 4.1. (30 mg, 10% yield, white solid). ^{1}H NMR (600 MHz, DMSO-d$_6$, 60 °C) δ (ppm): 7.79 (d, *J* = 8.26, 2H), 7.57 (d, *J* = 8.26, 2H), 7.33 (d, *J* = 8.11, 2H), 7.06 (d, *J* = 8.11, 2H), 5.51 (s, 2H), 3.58 (s, 3H), 1.31 (s, 9H).

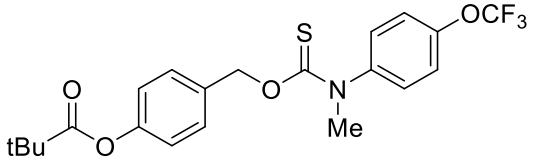

MeTCM-OCF$_3$ was prepared according to the general procedure described in Chapter 4.1. (42 mg, 14% yield, white solid). ^{1}H NMR (600 MHz, DMSO-d$_6$, 60 °C) δ (ppm): 7.46 (m, 2H), 7.40 (m, 2H), 7.3 (bs, 2H), 7.05 (d, *J* = 8.20, 2H), 5.49 (s, 2H), 3.56 (s, 3H), 1.31 (s, 9H). ^{19}F (470 MHz, DMSO-d$_6$, 60 °C) -56.85 (bs).

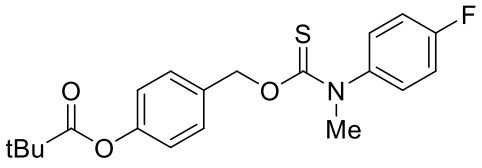

MeTCM-F was prepared according to the general procedure described in Chapter 4.1. (51 mg, 21% yield, white solid). ^{1}H NMR (600 MHz, DMSO-d$_6$, 60 °C) δ (ppm): 7.40 –

7.01 (m, 8H), 5.48 (s, 2H), 3.54 (bs, 3H), 1.31 (s, 9H). ^{19}F (470 MHz, DMSO-d_6, 60 °C) -114.65 (bs).

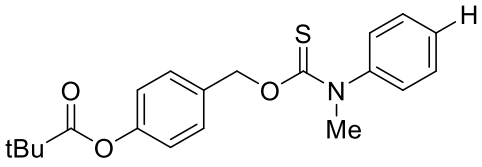

MeTCM-H was prepared according to the general procedure described in Chapter 4.1. (50 mg, 19% yield, white solid). ^{1}H NMR (600 MHz, DMSO-d_6, 60 °C) δ (ppm): 7.43 (t, *J* = 7.61, 2H), 7.35 – 7.25 (m, 5H), 7.04 (d, *J* = 8.05, 2H), 5.47 (s, 2H), 3.56 (s, 3H), 1.31 (s, 9H).

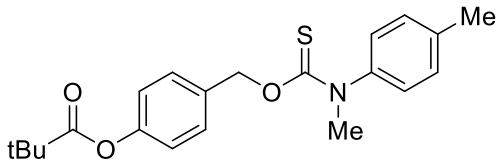

MeTCM-Me was prepared according to the general procedure described in Chapter 4.1. (62 mg, 22% yield, white solid). ^{1}H NMR (600 MHz, DMSO-d_6, 60 °C) δ (ppm): 7.34 – 7.21 (m, 4H), 7.17 (d, *J* = 8.28, 2H), 7.05 (d, *J* = 8.09, 2H), 5.48 (s, 2H), 3.54 (s, 3H), 2.33 (s, 3H), 1.32 (s, 9H).

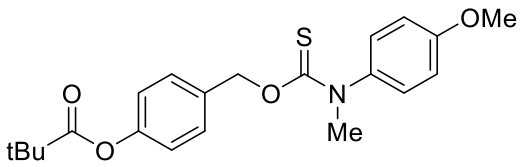

MeTCM-OMe was prepared according to the general procedure described in Chapter 4.1. (24 mg, 9% yield, off-white solid). ^{1}H NMR (600 MHz, DMSO-d_6, 60 °C) δ (ppm): 7.37 – 6.92 (m, 8H), 5.47 (s, 2H), 3.78 (s, 3H), 3.54 (bs, 3H), 1.31 (s, 9H).

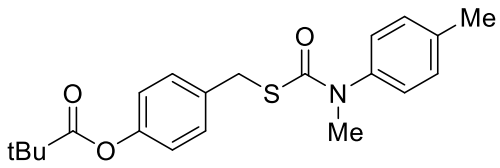

S-alkyl MeTCM, SI-3. 4-(mercaptomethyl)phenyl pivalate (40 mg, 0.18 mmol, 1.0 equiv.) was added to a stirring solution of coupling partner **SI-2** (70.1 mg, 0.20 mmol, 1.1 equiv.) in anhydrous DCM (2 mL, 0.1 M solution). Et_3N (30 µL, 0.21 mmol, 1.2 equiv.) was added, and the reaction mixture was let stir at room temperature for 8 hours. The crude reaction mixture was directly concentrated onto silica and purified *via* silica gel column chromatography (4:1 Hex:EtOAc) to afford the product as a white solid (43 mg, 65% yield, white solid). ^{1}H NMR (500 MHz, $CDCl_3$, 25 °C) δ (ppm): 7.29 (d, J = 8.52, 2H), 7.19 (d, J = 8.20, 2H), 7.14 (d, J = 8.20, 2H), 6.94 (d, J = 8.52, 2H), 4.06 (s, 2H), 3.31 (s, 3H), 2.37 (s, 3H), 1.34 (s, 9H). ^{13}C{^{1}H} NMR (125 MHz, $CDCl_3$) δ (ppm): 177.00, 168.36, 150.04, 135.67, 130.14, 130.01, 128.13, 121.38, 39.05, 38.39, 34.87, 27.13, 21.21. HRMS m/z $[M + H]^+$ calcd. For $[C_{21}H_{26}NO_3S]^+$ 372.1633; found 372.1634.

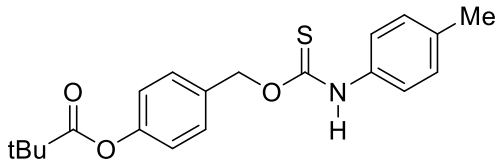

HTCM-Me was prepared according to the literature. Spectral data agreed with those reported.[116]

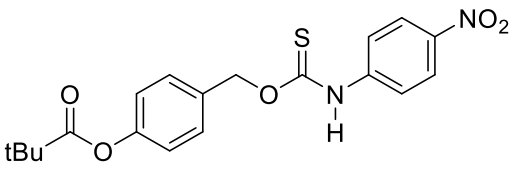

HTCM-NO2 was prepared according to the literature. Spectral data agreed with those reported.[116]

NMR Spectra of Coupling Partners and N-Me Thiocarbamates

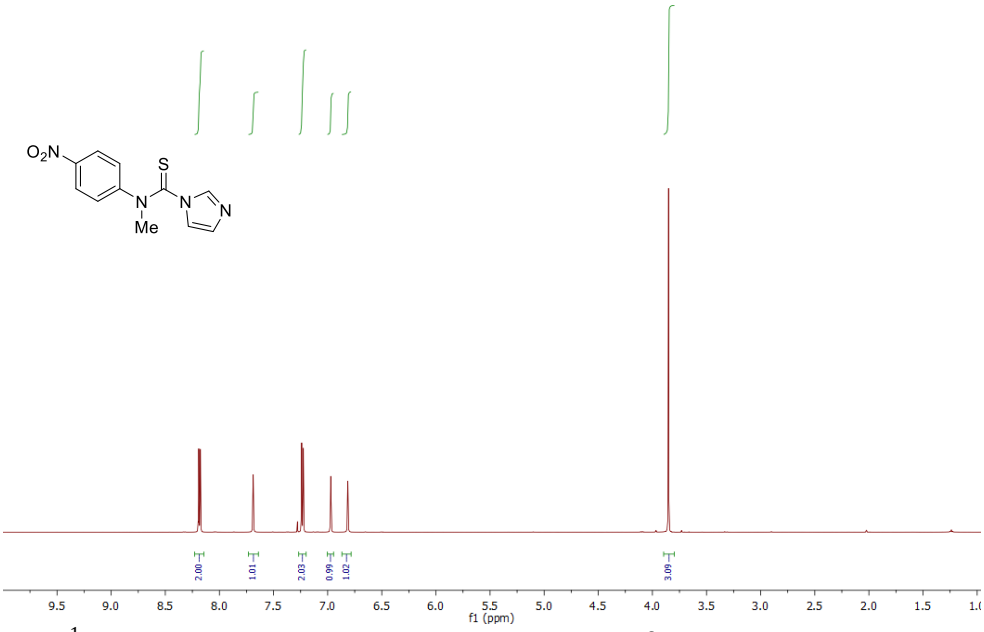

Figure C.1 ^{1}H (500 MHz, $CDCl_3$, RT) NMR spectrum of **CP-NO2.**

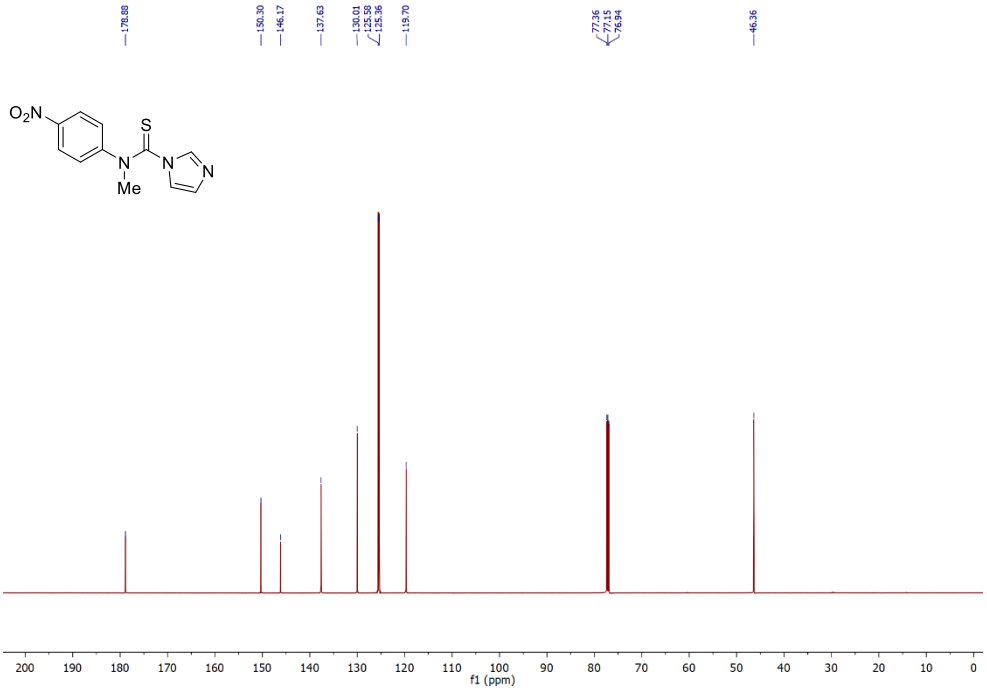

Figure C.2 $^{13}C\{^{1}H\}$ (125 MHz, $CDCl_3$, RT) NMR spectrum of **CP-NO2**.

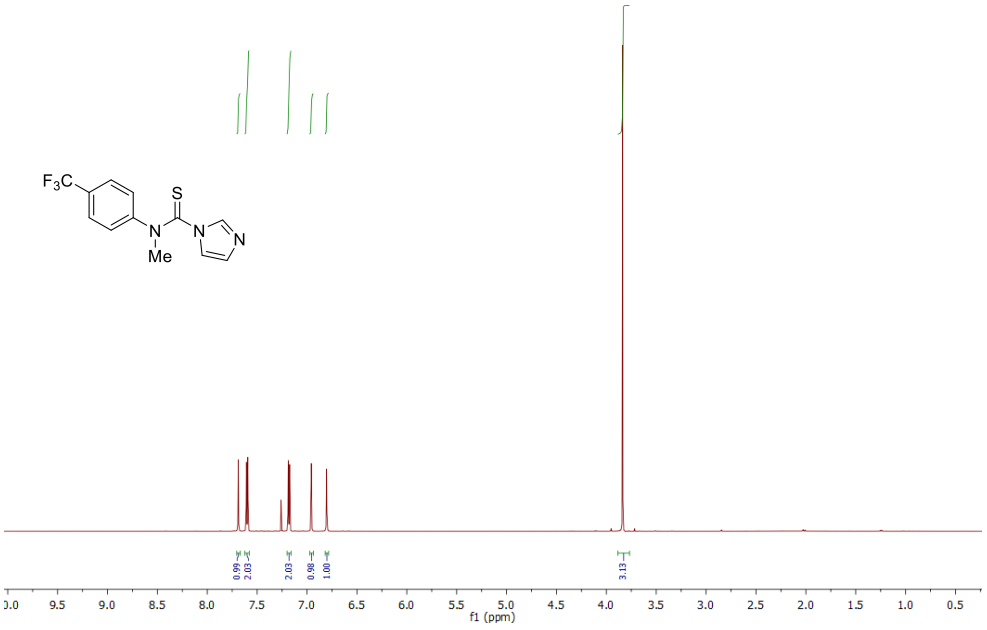

Figure C.3 ^{1}H (500 MHz, $CDCl_3$, RT) NMR spectrum of **CP-CF3.**

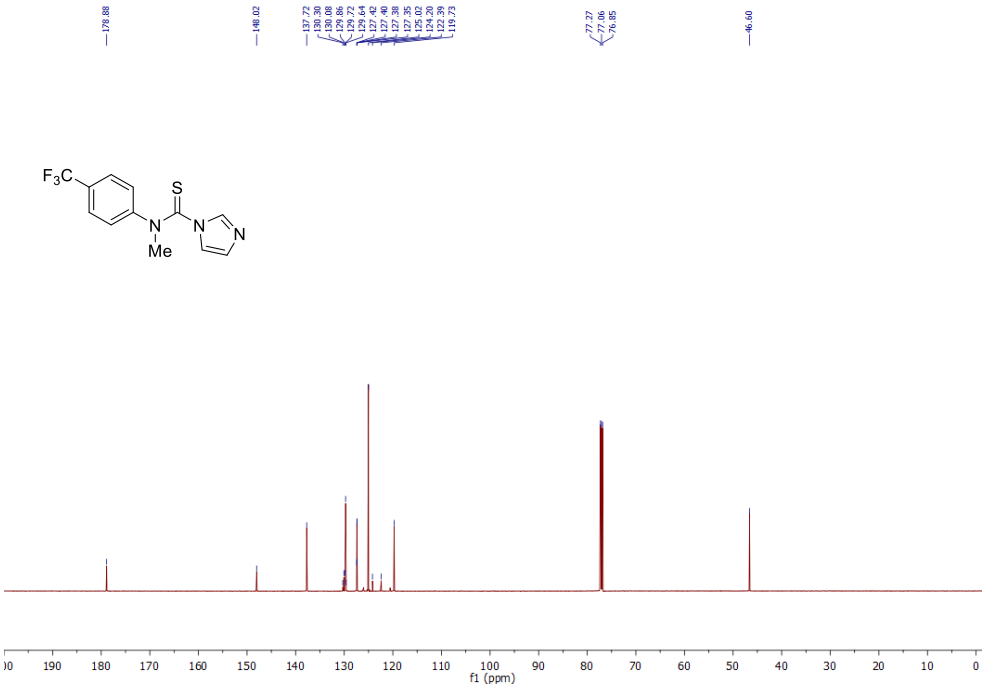

Figure C.4 $^{13}C\{^{1}H\}$ (125 MHz, $CDCl_3$, RT) NMR spectrum of **CP-CF$_3$**.

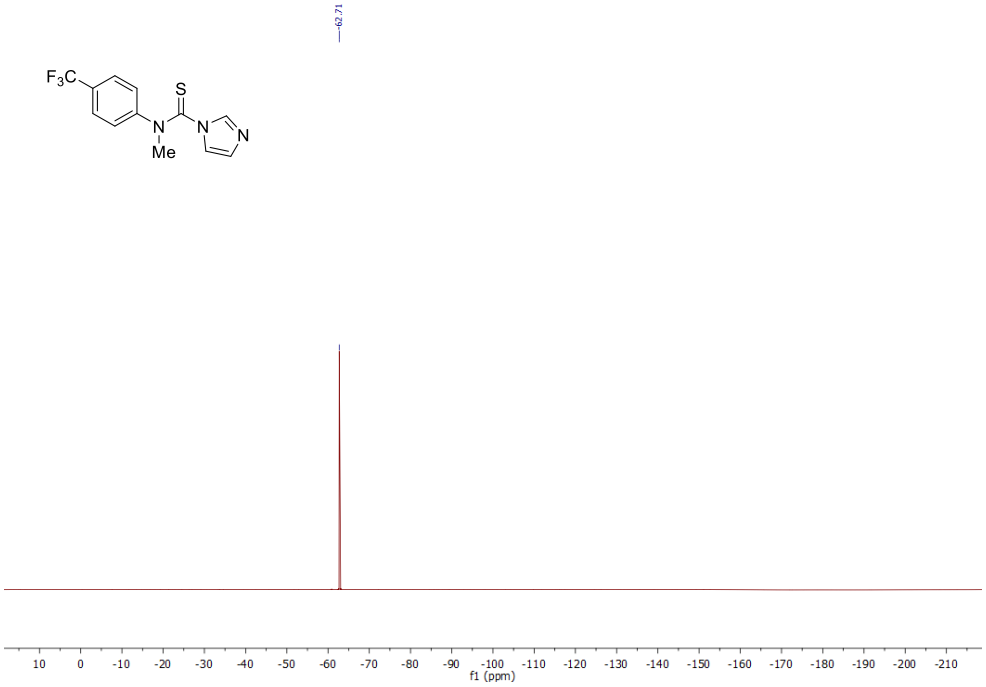

Figure C.5 ^{19}F (470 MHz, $CDCl_3$, RT) NMR spectrum of **CP-CF$_3$.**

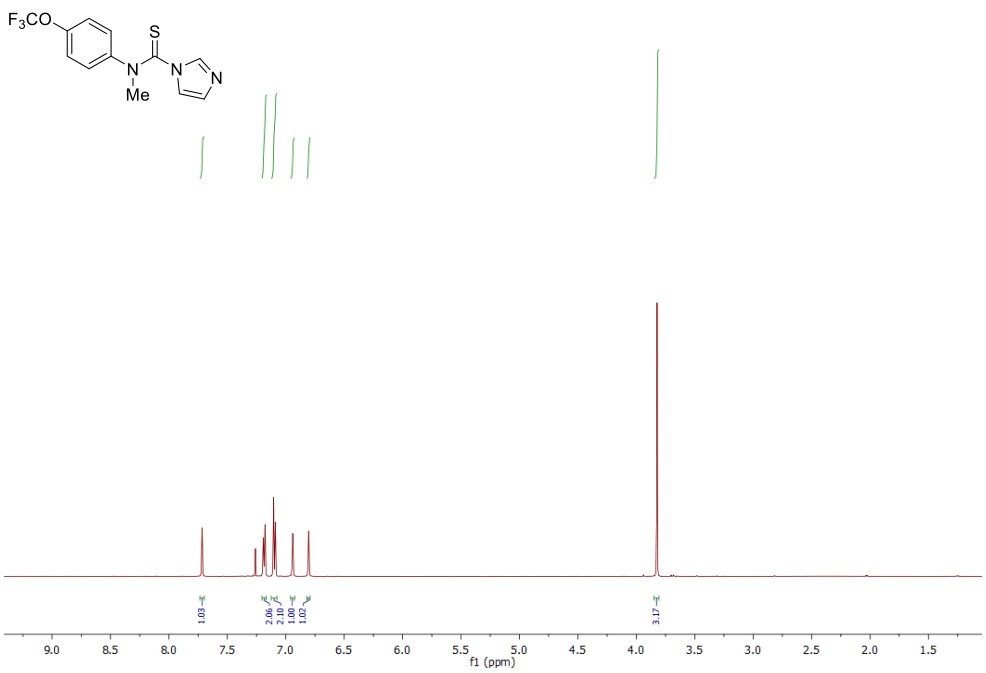

Figure C.6 ^{1}H (500 MHz, $CDCl_3$, RT) NMR spectrum of **CP-OCF$_3$.**

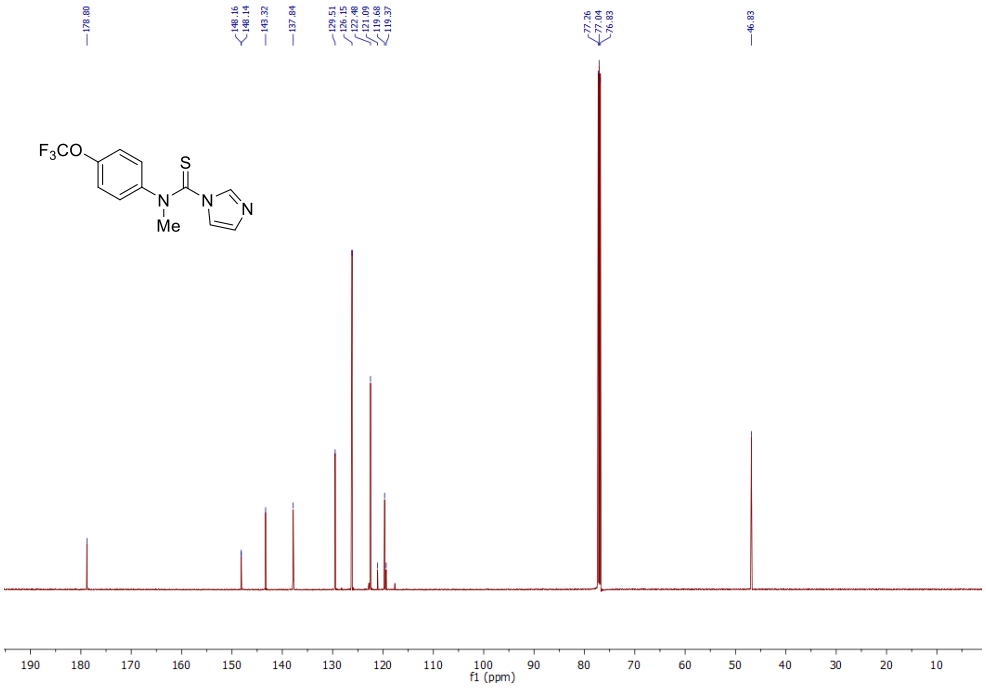

Figure C.7 $^{13}C\{^{1}H\}$ (125 MHz, $CDCl_3$, RT) NMR spectrum of **CP-OCF$_3$**.

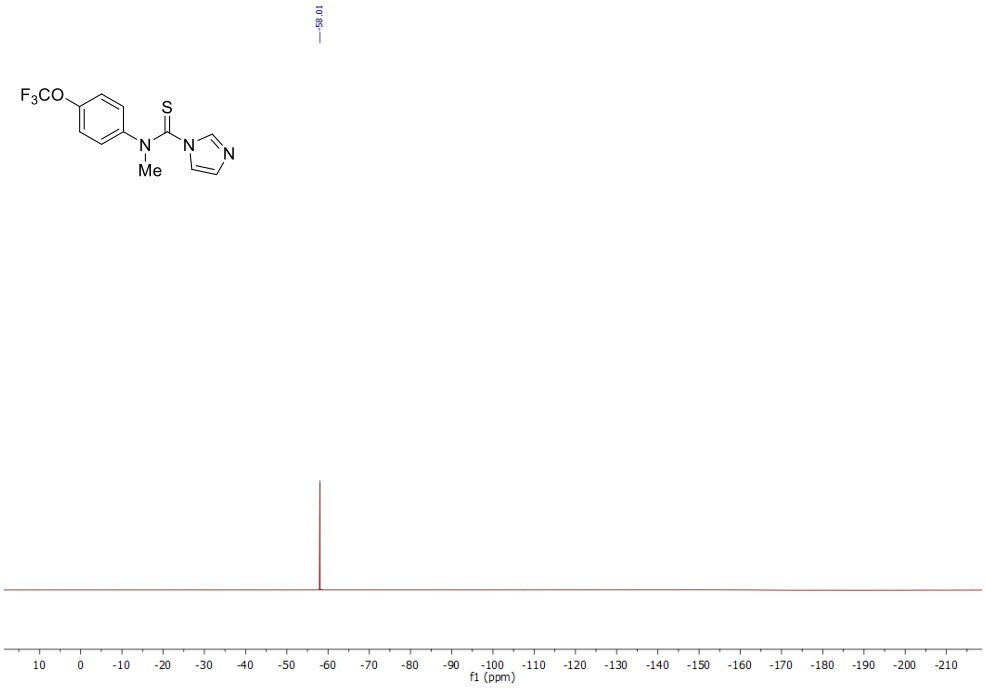

Figure C.8 ^{19}F (470 MHz, $CDCl_3$, RT) NMR spectrum of **CP-OCF$_3$.**

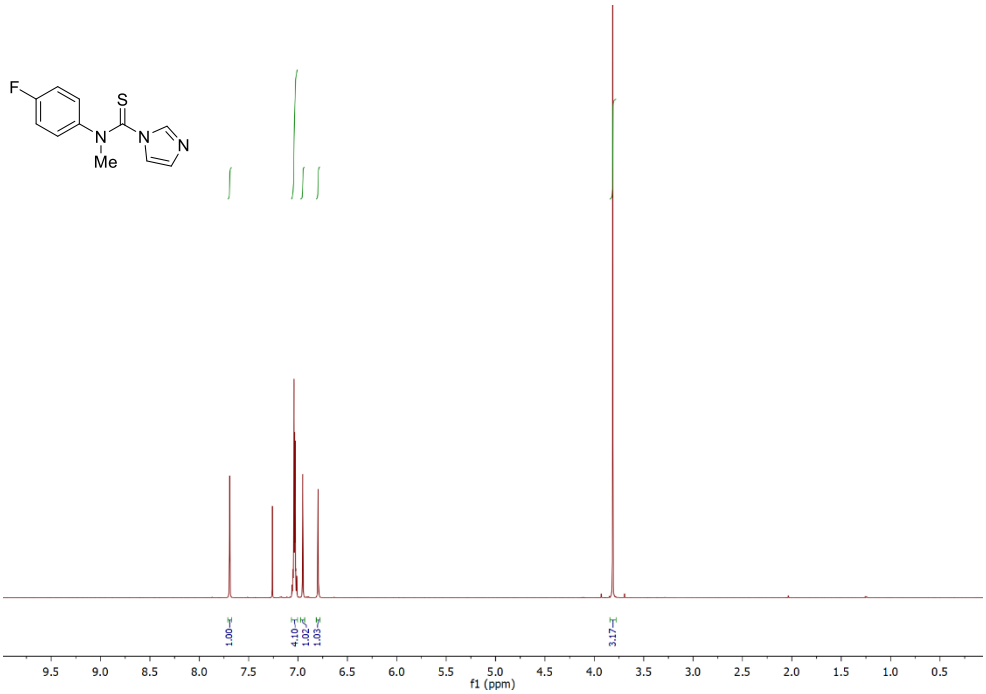

Figure C.9 ^{1}H (500 MHz, $CDCl_3$, RT) NMR spectrum of **CP-F.**

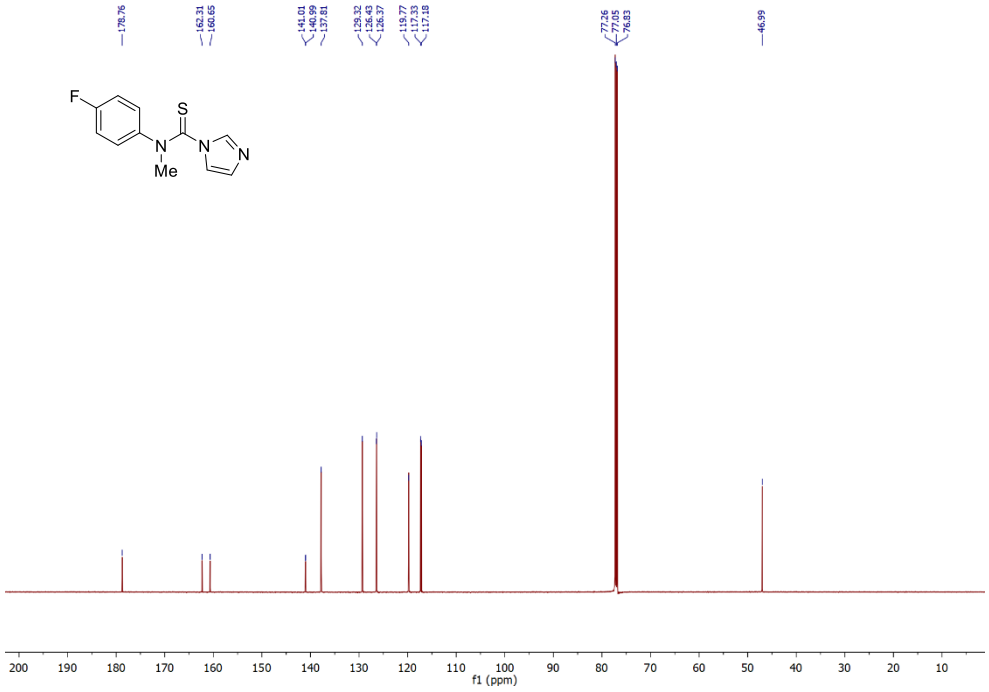

Figure C.10 $^{13}C\{^{1}H\}$ (125 MHz, $CDCl_3$, RT) NMR spectrum of **CP-F.**

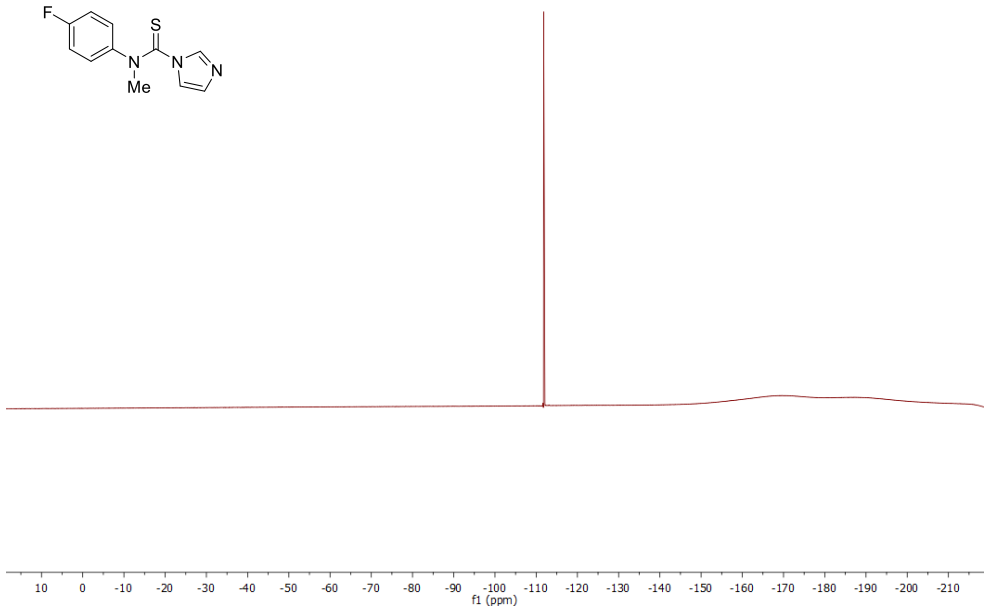

Figure C.11 ^{19}F (470 MHz, $CDCl_3$, RT) NMR spectrum of **CP-F.**

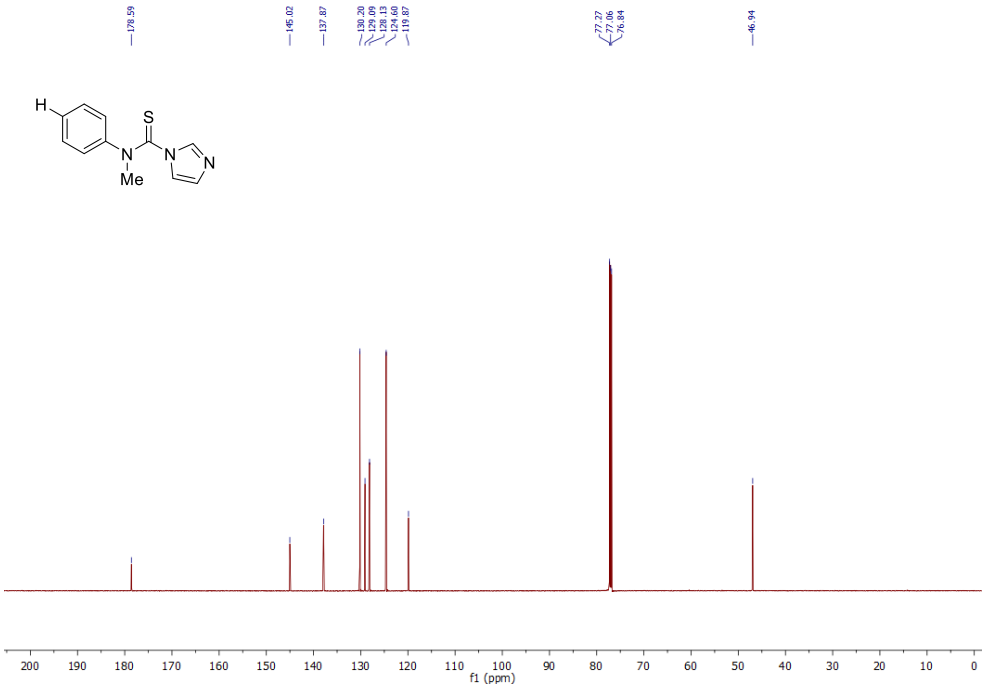

Figure C.12 ^{1}H (500 MHz, $CDCl_3$, RT) NMR spectrum of **CP-H.**

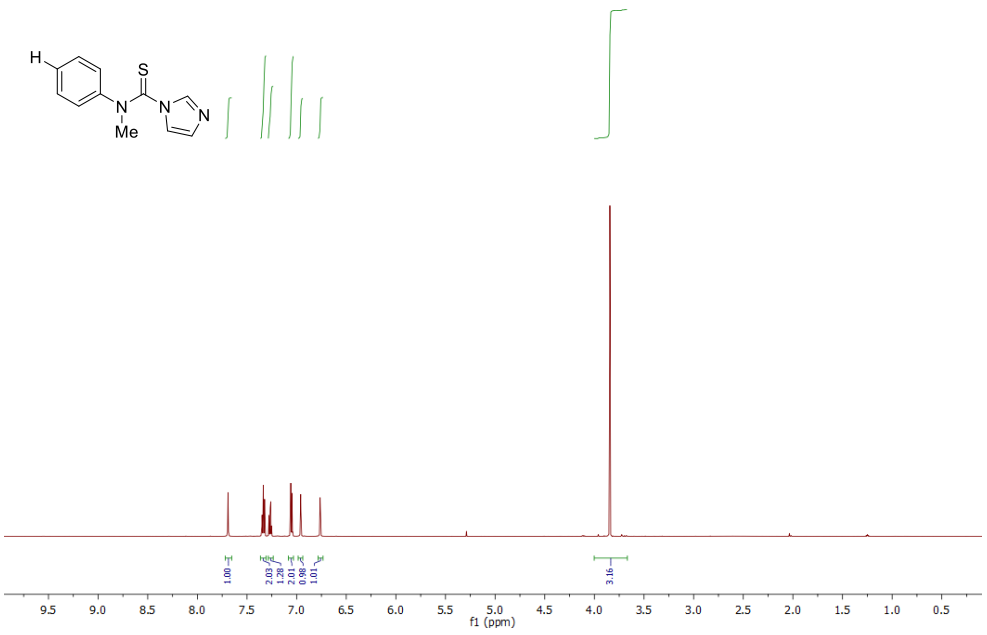

Figure C.13 $^{13}C\{^{1}H\}$ (125 MHz, $CDCl_3$, RT) NMR spectrum of **CP-H.**

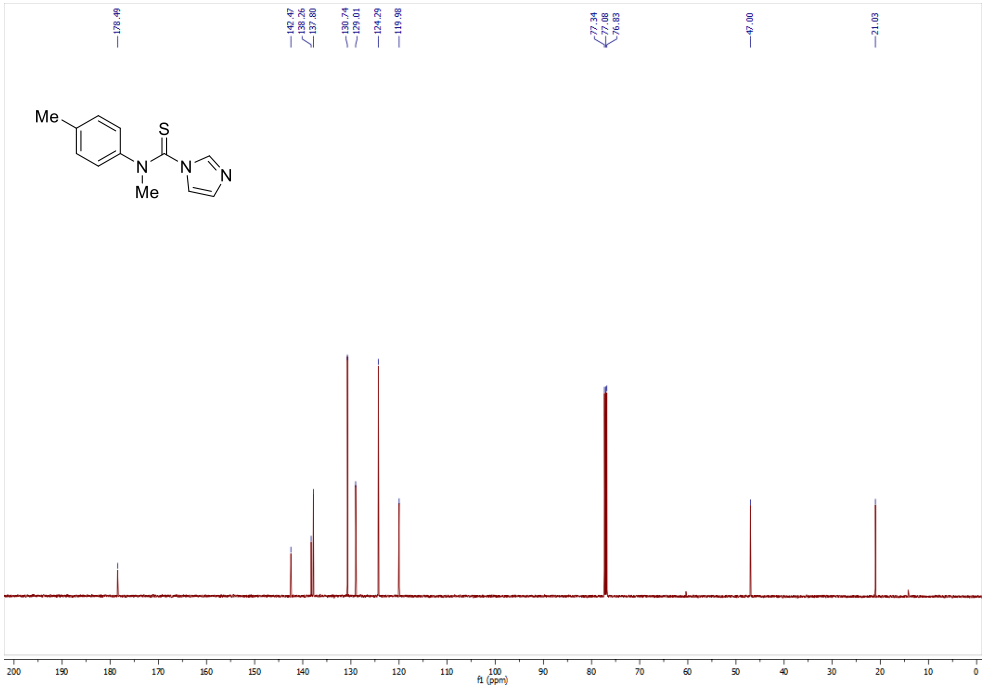

Figure C.14 ^{1}H (500 MHz, $CDCl_3$, RT) NMR spectrum of **CP-Me.**

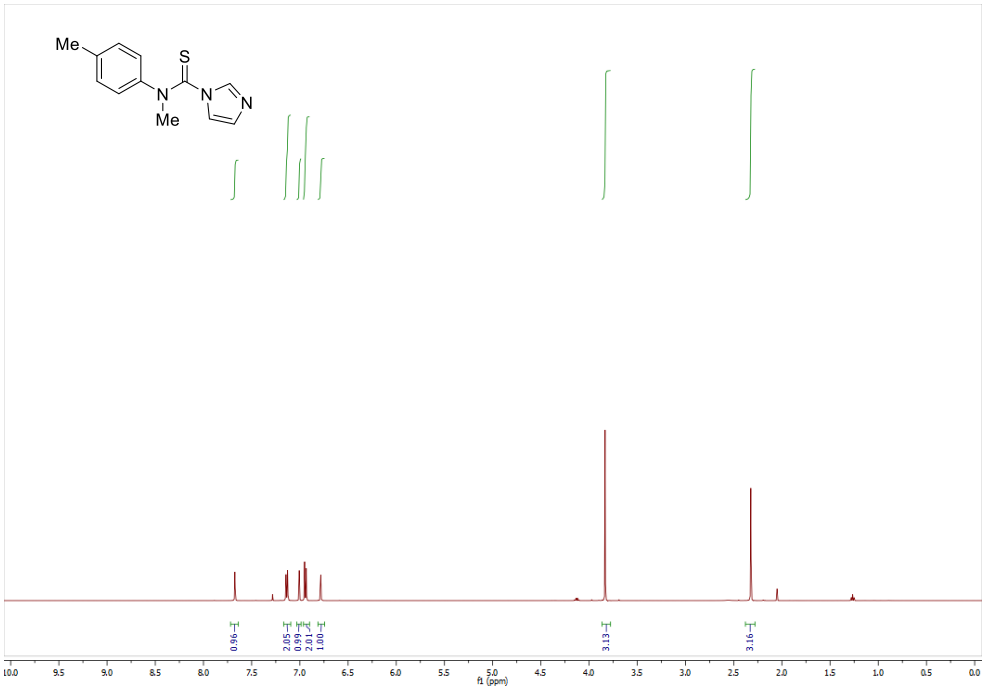

Figure C.15 $^{13}C\{^{1}H\}$ (125 MHz, $CDCl_3$, RT) NMR spectrum of **CP-Me.**

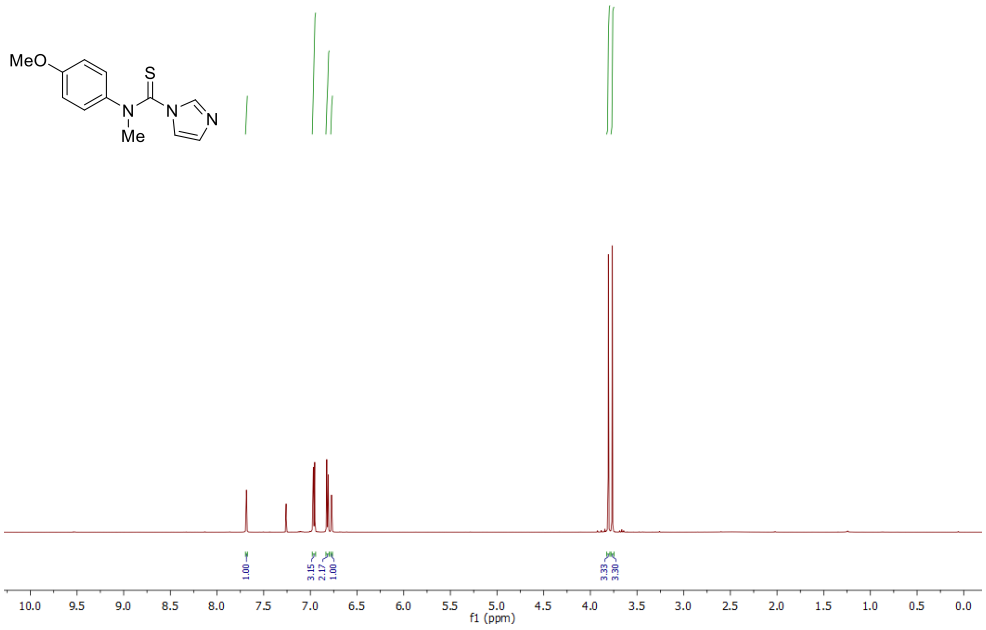

Figure C.16 ^{1}H (500 MHz, $CDCl_3$, RT) NMR spectrum of **CP-OMe.**

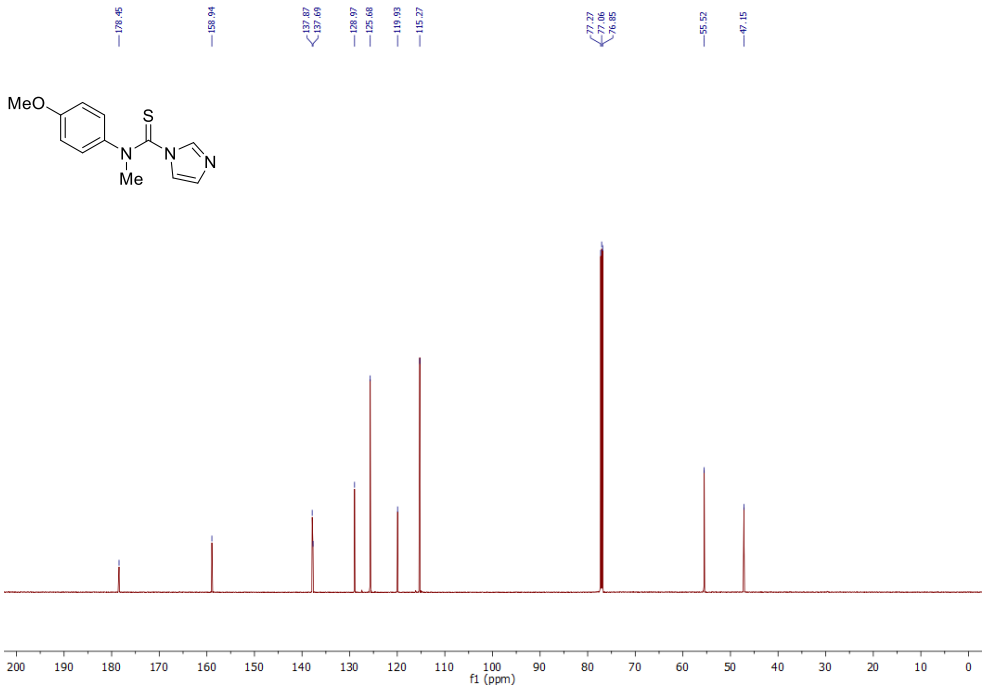

Figure C.17 $^{13}C\{^{1}H\}$ (125 MHz, $CDCl_3$, RT) NMR spectrum of **CP-OMe.**

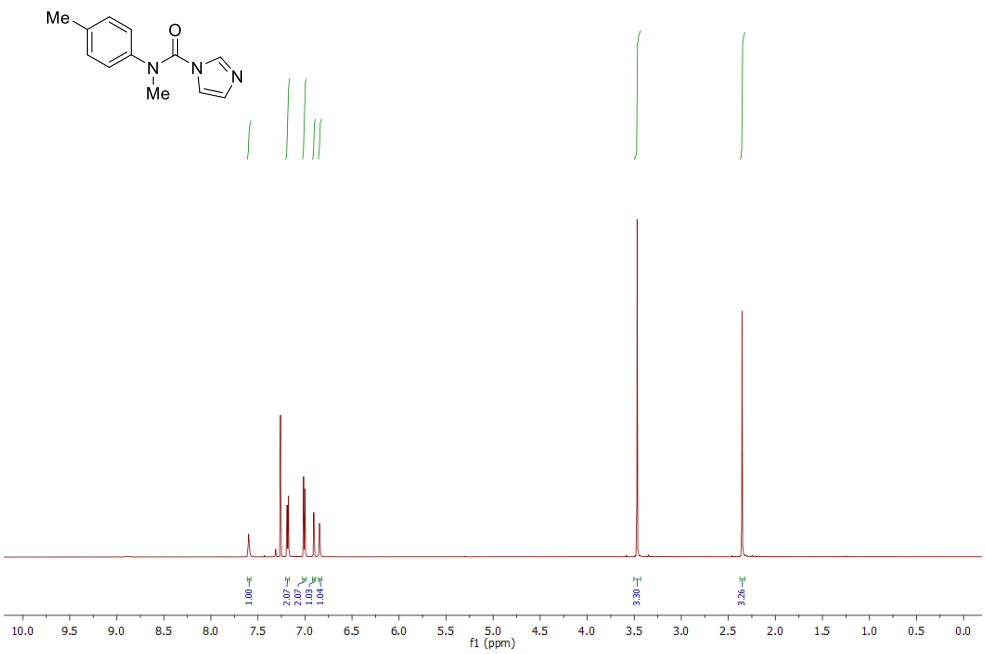

Figure C.18 ^{1}H (500 MHz, $CDCl_3$, RT) NMR spectrum of **SI-I.**

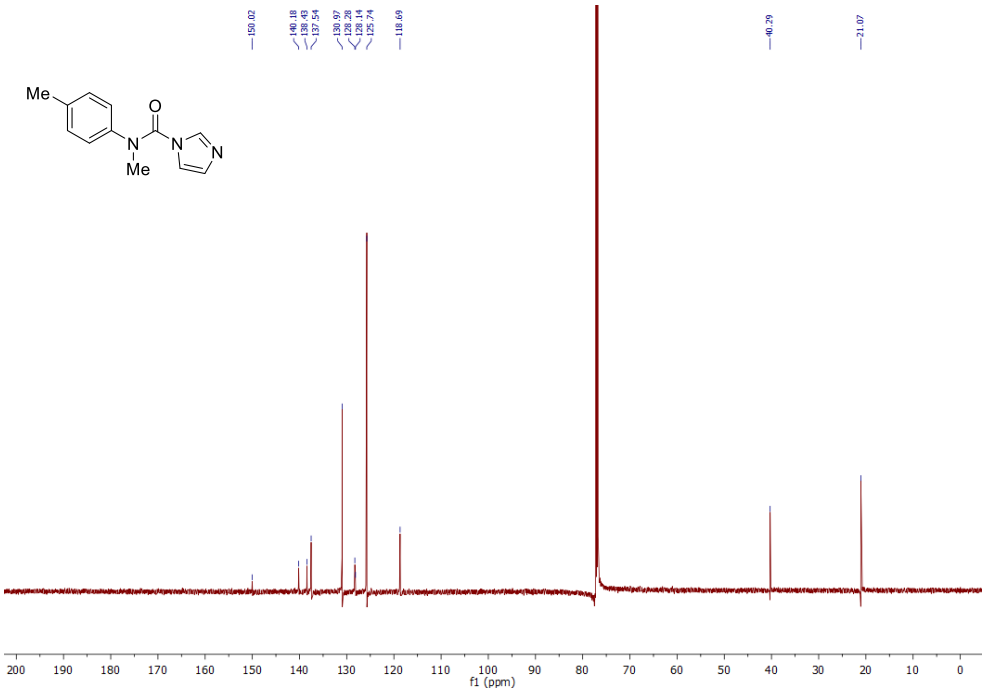

Figure C.19 $^{13}C\{^{1}H\}$ (125 MHz, $CDCl_3$, RT) NMR spectrum of **SI-1.**

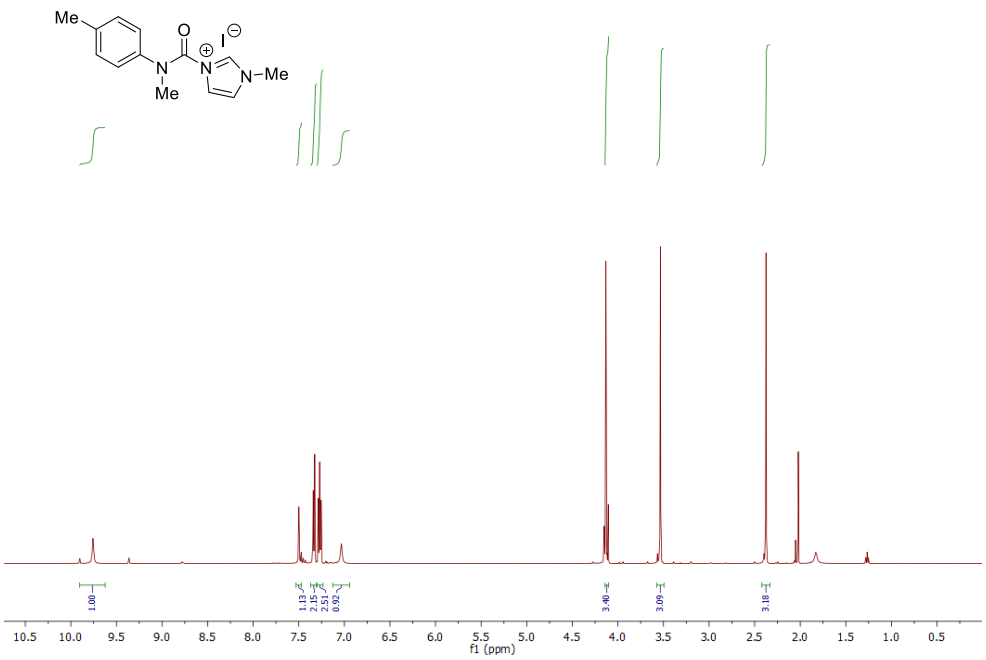

Figure C.20 ^{1}H (500 MHz, $CDCl_3$, RT) NMR spectrum of **SI-2.**

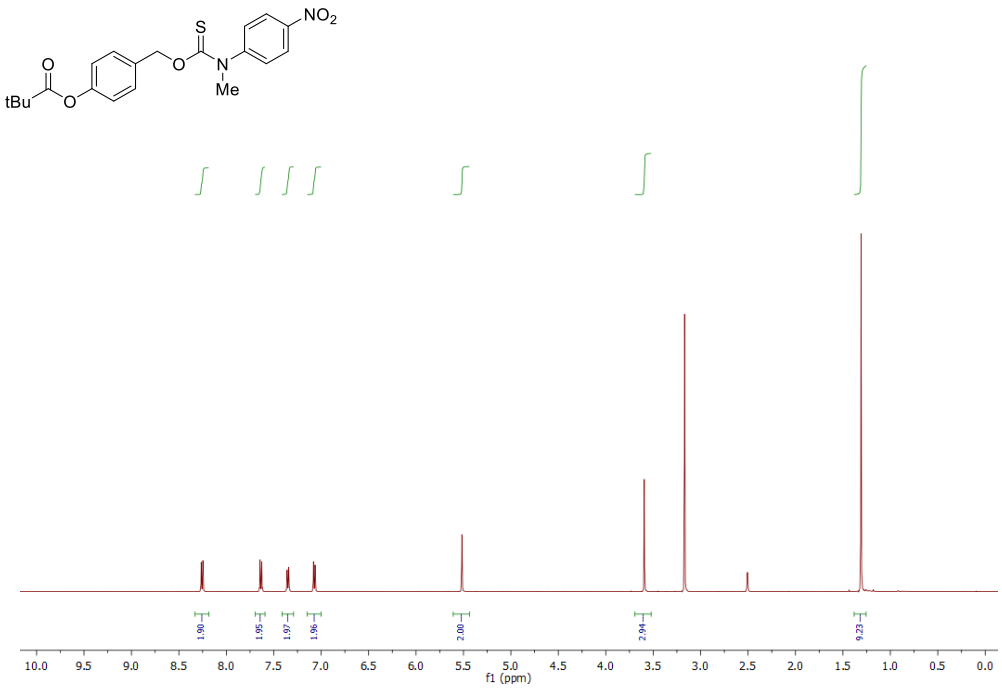

Figure C.21 ^{1}H (500 MHz, DMSO-d_6, 60 °C) NMR spectrum of **MeTCM-NO_2.**

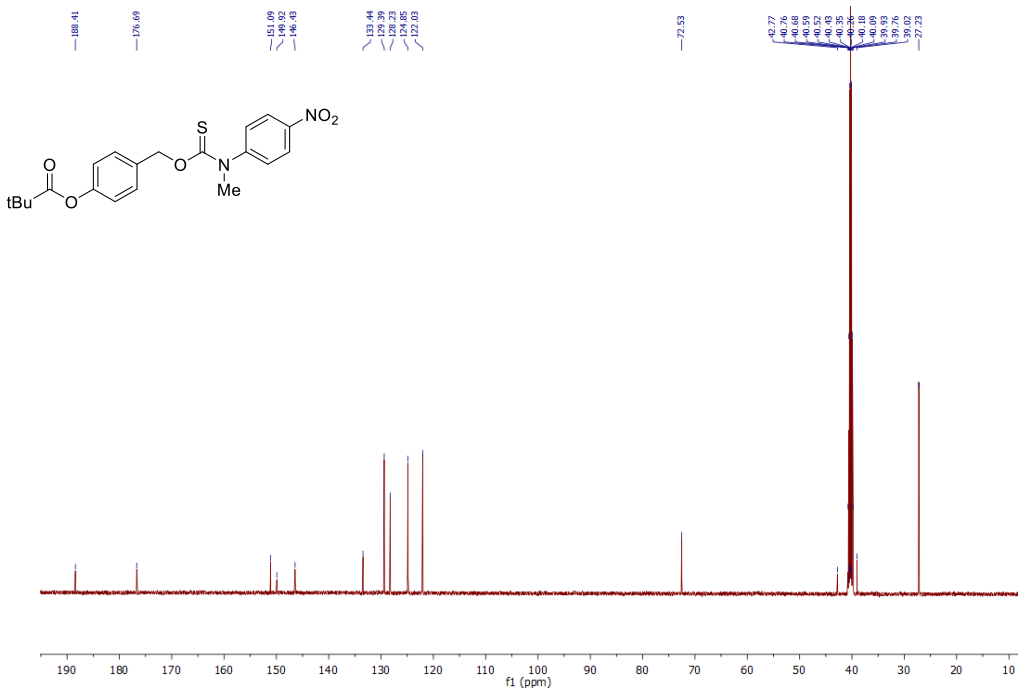

Figure C.22 $^{13}C\{^{1}H\}$ (125 MHz, DMSO-d_6, 60 °C) NMR spectrum of **MeTCM-NO$_2$.**

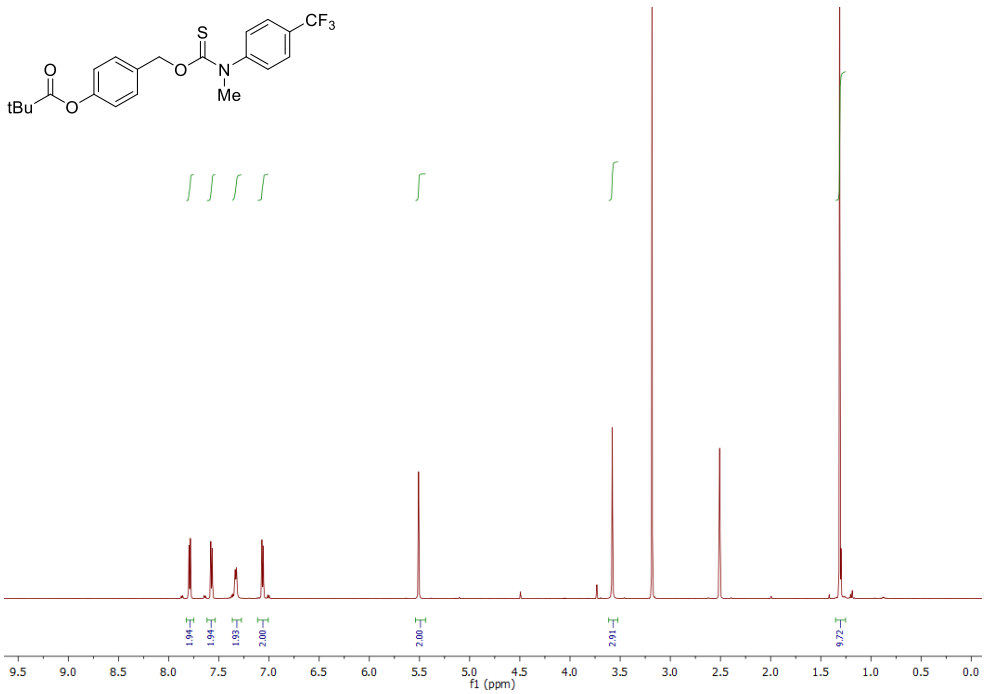

Figure C.23 ^{1}H (600 MHz, DMSO-d_6, 60 °C) NMR spectrum of **MeTCM-CF$_3$.**

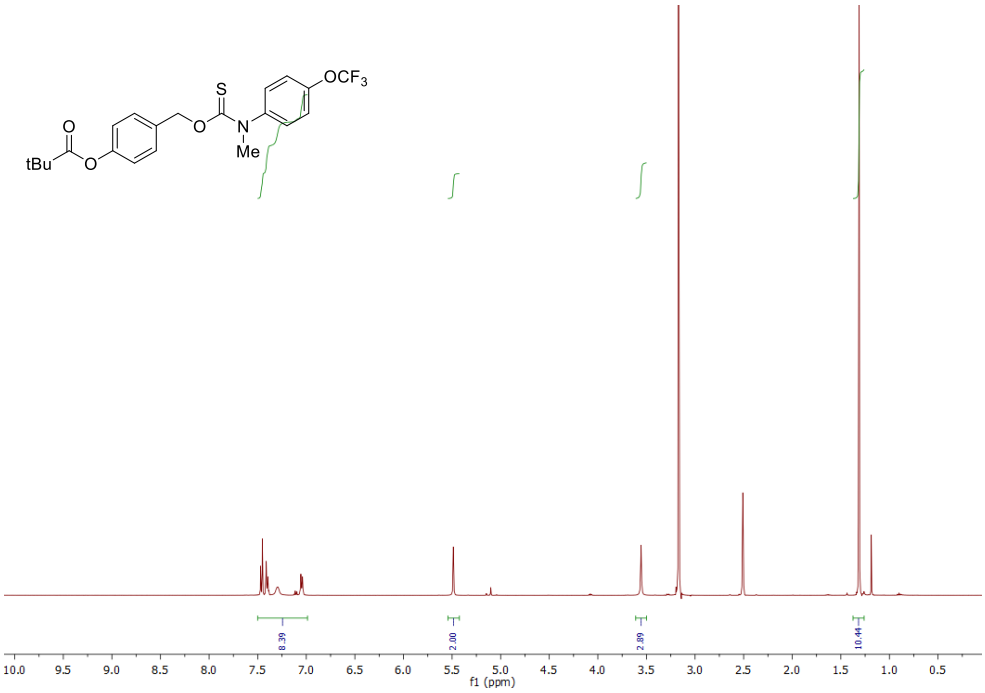

Figure C.24 ^{1}H (600 MHz, DMSO-d_6, 60 °C) NMR spectrum of **MeTCM-OCF$_3$.**

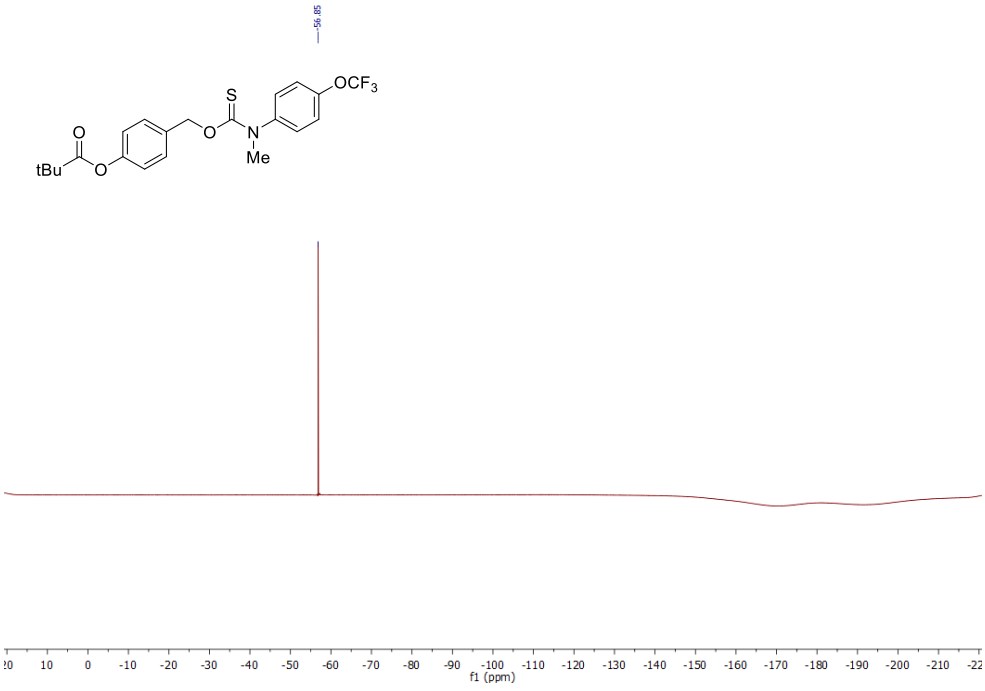

Figure C.25 ^{19}F (470 MHz, DMSO-d_6, 60 °C) NMR spectrum of **MeTCM-OCF$_3$.**

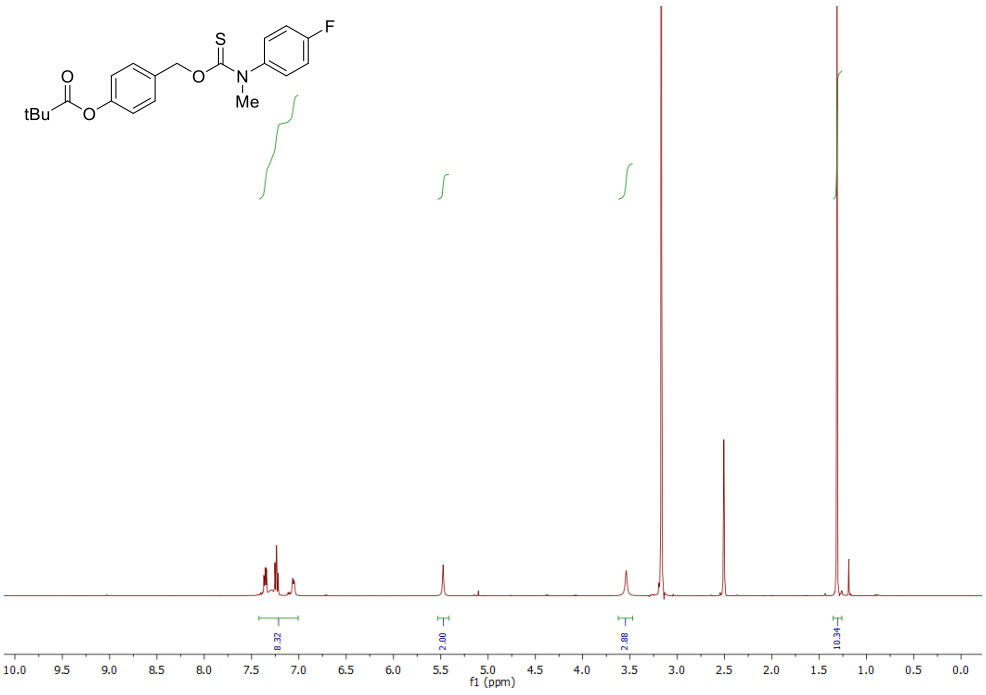

Figure C.26 ^{1}H (600 MHz, DMSO-d_6, 60 °C) NMR spectrum of **MeTCM-F.**

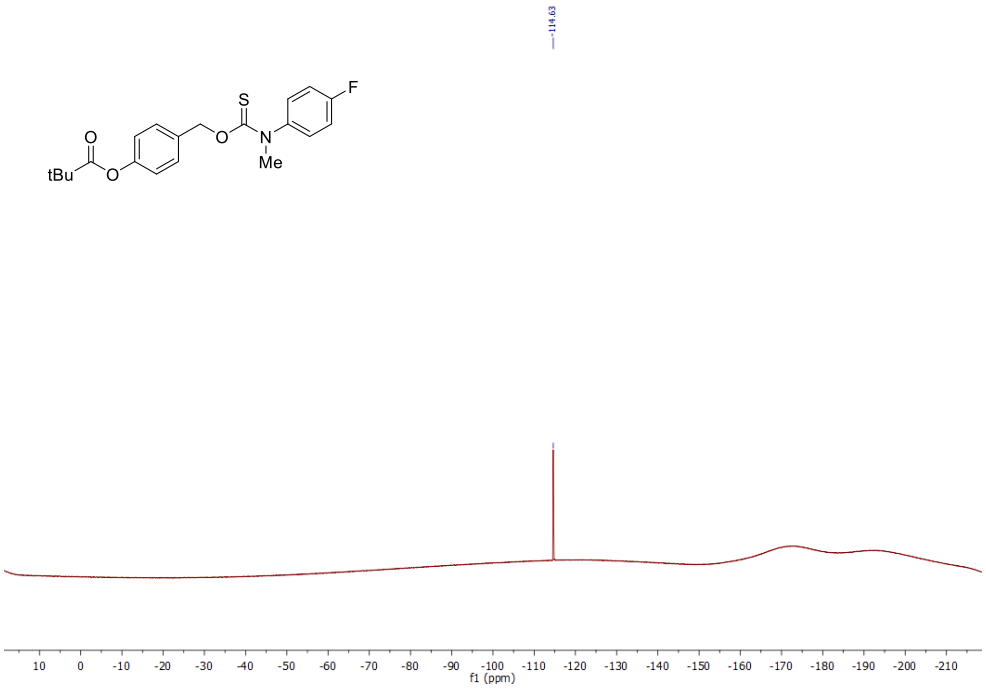

Figure C.27 ^{19}F (470 MHz, DMSO-d_6, 60 °C) NMR spectrum of **MeTCM-F.**

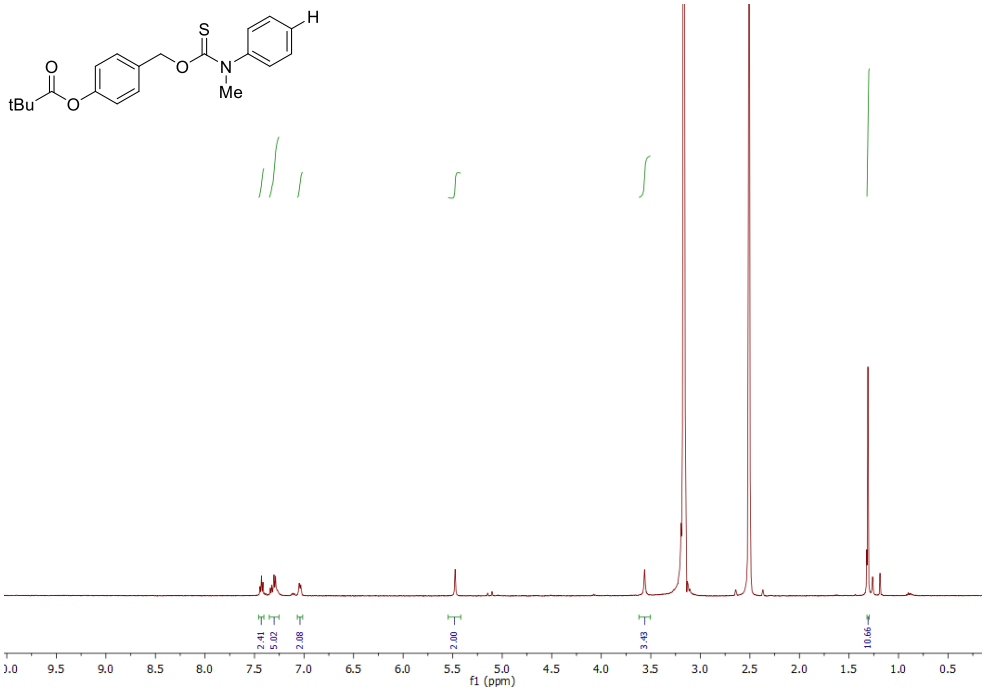

Figure C.28 ^{1}H (600 MHz, DMSO-d$_6$, 60 °C) NMR spectrum of **MeTCM-H.**

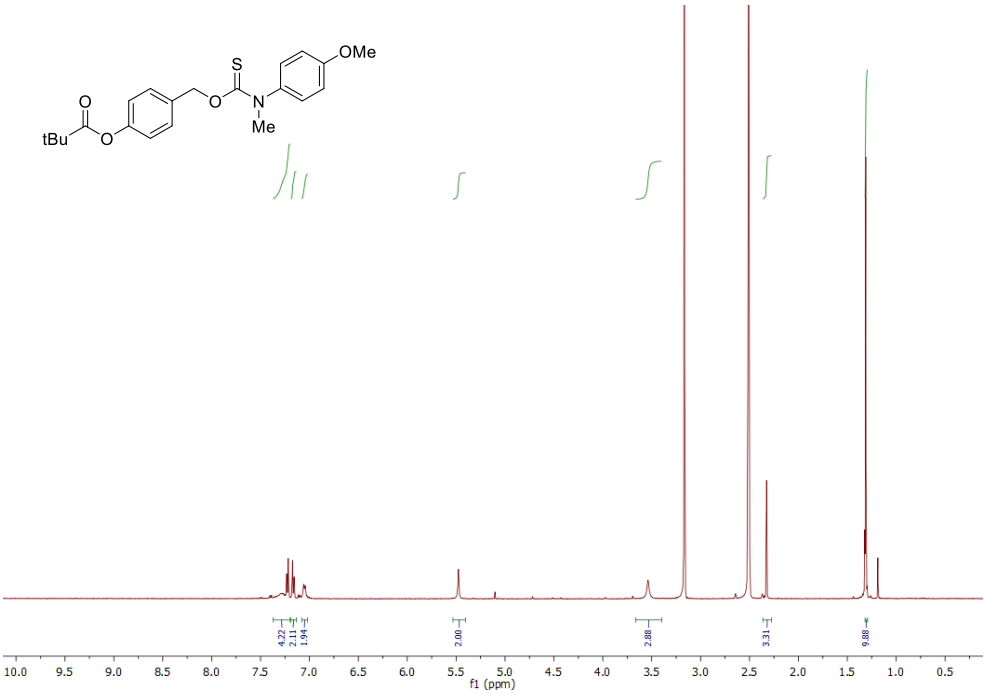

Figure C.29 ^{1}H (600 MHz, DMSO-d$_6$, 60 °C) NMR spectrum of **MeTCM-Me.**

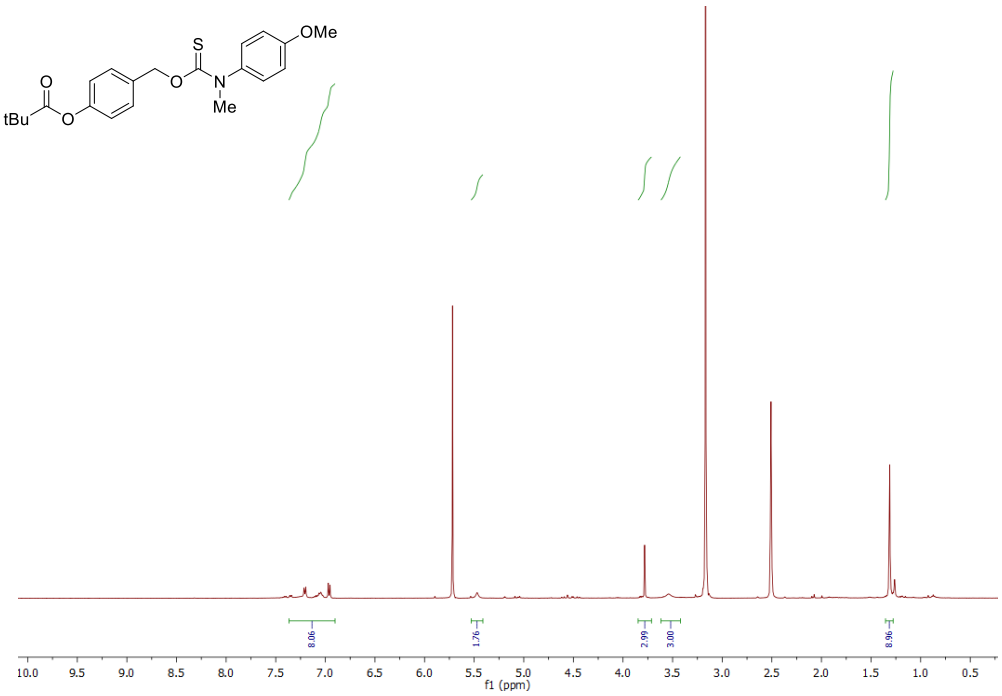

Figure C.30 ^{1}H (600 MHz, DMSO-d_6, 60 °C) NMR spectrum of **MeTCM-OMe.**

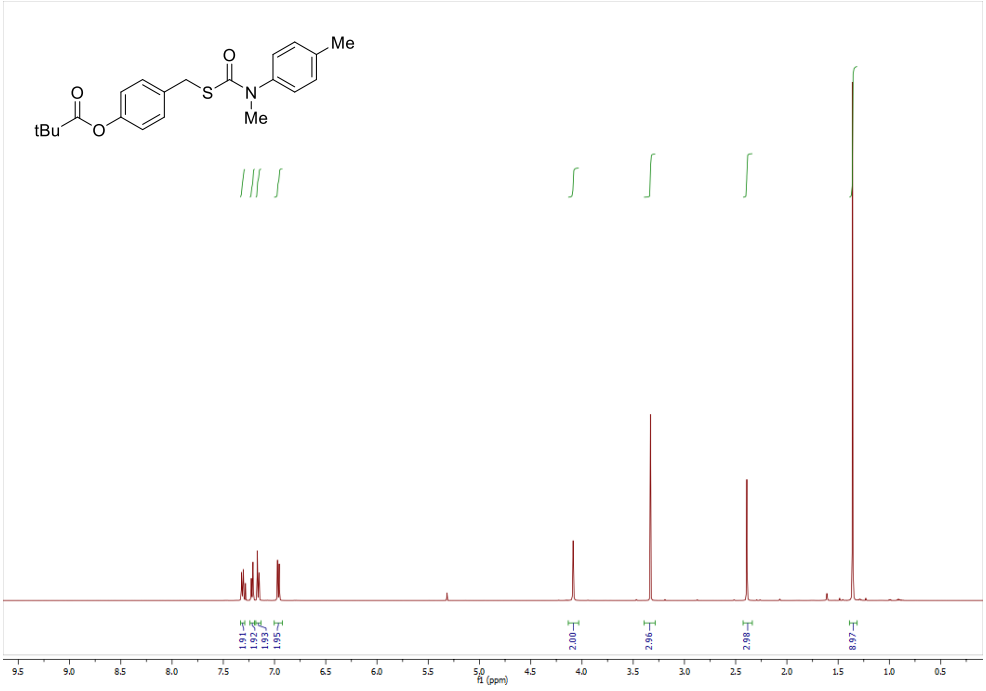

Figure C.31 ^{1}H (500 MHz, $CDCl_3$, 25 °C) NMR spectrum of **S-alkyl MeTCM SI-3**

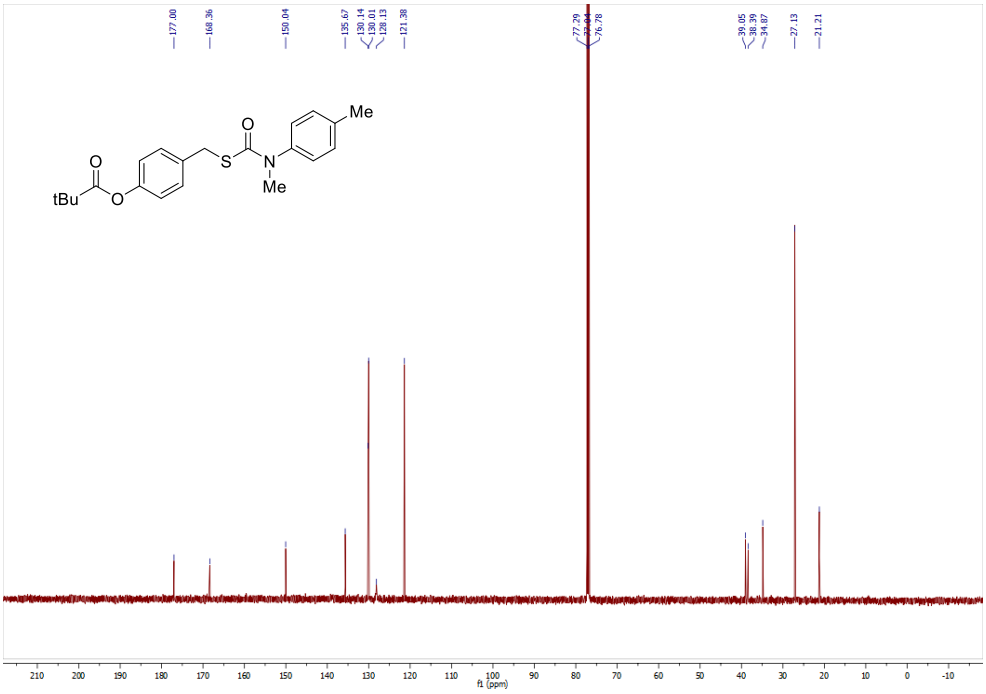

Figure C.32 $^{13}C\{^{1}H\}$ (500 MHz, $CDCl_3$, 25 °C) NMR spectrum of **S-alkyl MeTCM SI-3**

Establishing the Calibration Curve for the Methylene Blue Assay

Solutions containing 0.5 mL of methylene blue cocktail and 0.5 mL PBS (pH 7.4) containing 5% DMSO, 5 U/mL PLE, and 50 μg/mL CA were freshly prepared in disposable 1.5 mL cuvettes. Under inert conditions, a 10 mM stock solution of NaSH (Strem Chemicals) in PBS was prepared and diluted to 1 mM. Immediately after dilution, varying amounts of the 1 mM NaSH stock was added to 1.0 mL solutions for final concentrations of 10, 20, 30, 40, 50, and 60 μM. Solutions were mixed, filtered through a 0.2 micron syringe filter, incubated at room temperature for 1 h, and shielded from light. Absorbance values at 670 nm were measured after 1 hr.

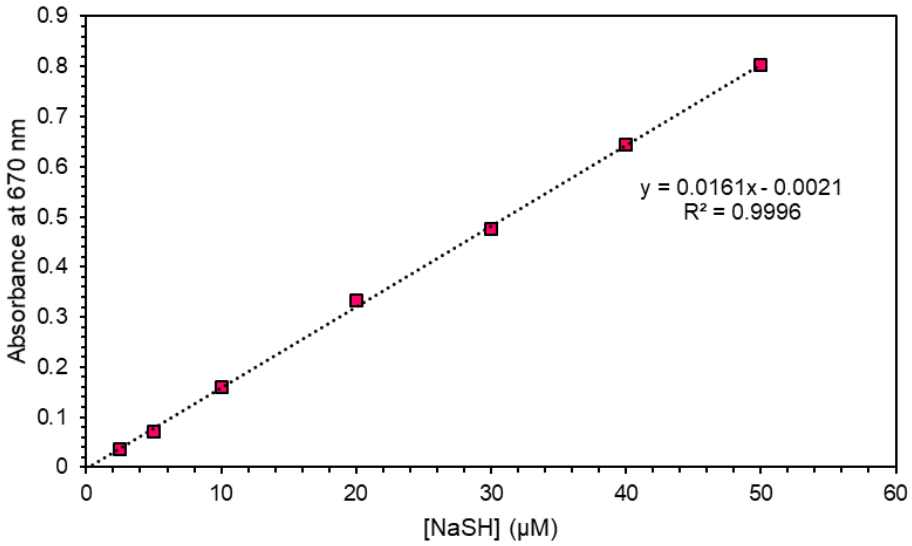

Figure C.33 NaSH calibration curve for the methylene blue assay.

Methylene Blue Assay on S-alkyl N-Me TCM SI-3

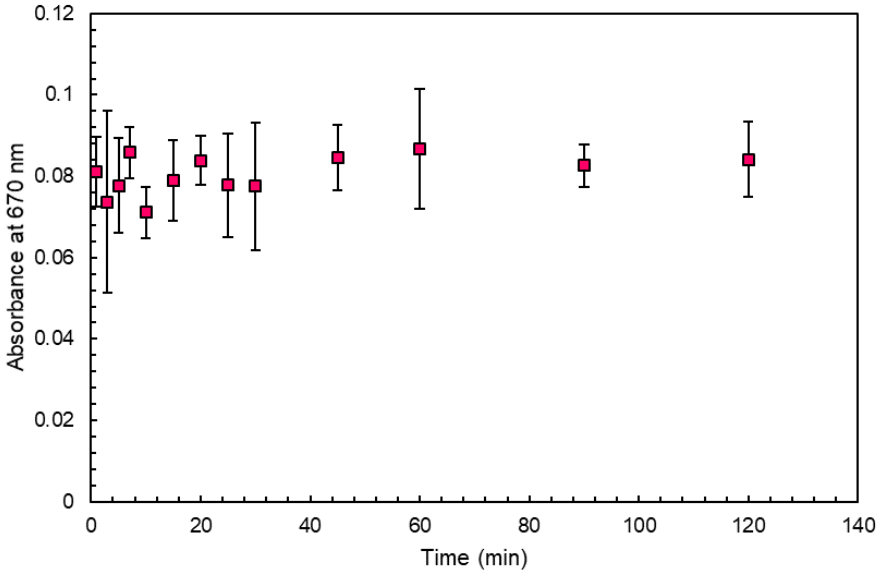

Figure C.34 Methylene assay performed on a 50 µM solution of **SI-3** to determine H_2S release. The standard MBA reaction conditions described in Chapter 4.1 were employed, however the methylene blue aliquots were not filtered through a 0.2 micron syringe filter prior to measuring the absorbance, likely contributing to the large observed error.

Methylene Blue Assay on HTCM-NO_2 in the Absence of Carbonic Anhydrase

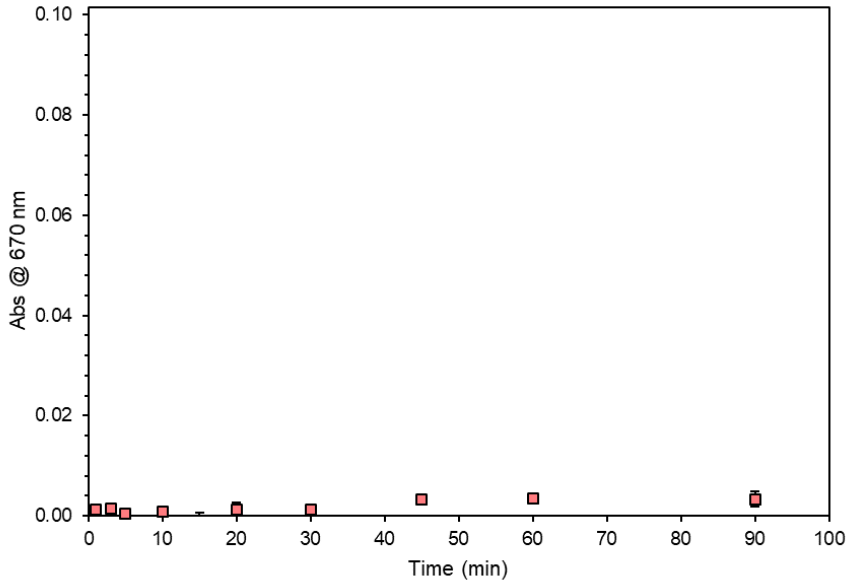

Figure C.35 Methylene assay performed on a 50 μM solution of **HTCM-NO_2** to determine H_2S release. The standard MBA reaction conditions described in Chapter 4.1 were employed, however no carbonic anhydrase was added. The lack of observed response over the course of an hour indicates that the H_2S release observed under the standard reaction conditions does not come from a COS-independent pathway.

Supplementary Computational Data

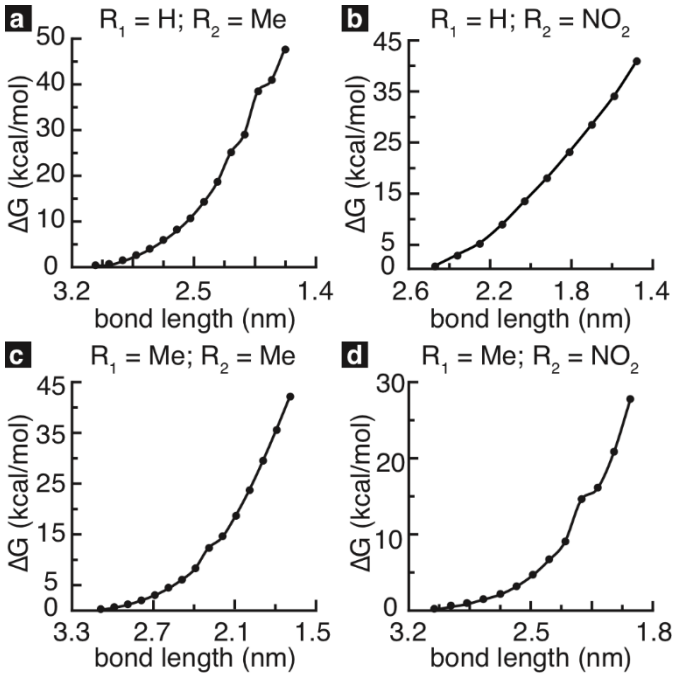

Figure C.36 The change in Gibb's free energy from water and thiocarboxylic acid intermediates beginning at an arbitrary distance was plotted as a function of H_2O-C(=O) bond length. These potential energy surface scans for H_2O attack at the thiocarboxylic acid carbonyl reveal a barrierless transition to the zwitterionic intermediate for which no equilibrium geometry could be recovered. Coupled with the exergonic formation of hyrdolysis byproducts, we expect this reaction to proceed when H_2O attack occurs. Notably, the bond lengths along the potential energy surfaces are arbitrary and the structures are not fully converged; drawing any quantitative confusions would be ill-advised.

APPENDIX D

SUPPLEMENTRAY INFORMATION FOR CHAPTER 4.2

Appendix D is the supplementary information for Chapter 4.2 of this dissertation. It includes spectra and experimental data relevant to the content in Chapter 4.2.

Synthesis / Spectral Details of Prepared Dithiocarbamates

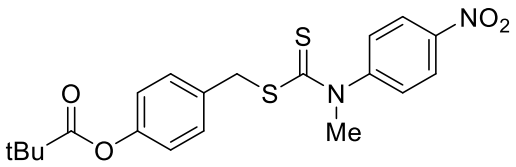

tBu-DTCM was prepared according to the general synthetic procedure outlined in Chapter 4.2, from CP-NO_2 and 4-(mercaptomethyl)phenyl pivalate. (96 mg, 64% yield white solid). ^{1}H NMR (600 MHz, $CDCl_3$) δ 8.33 (d, *J* = 8.9 Hz, 2H), 7.47 (d, *J* = 8.9 Hz, 2H), 7.32 (d, *J* = 8.5 Hz, 2H), 6.98 (d, *J* = 8.5 Hz, 2H), 4.47 (s, 2H), 3.79 (s, 3H), 1.35 (s, 9H). $^{13}C\{^{1}H\}$ NMR (151 MHz, $CDCl_3$) δ 198.79, 177.01, 150.50, 150.13, 147.44, 132.81, 130.37, 128.37, 125.21, 121.62, 45.30, 42.35, 39.07, 27.11. HRMS m/z $[M + H]^+$ calcd. For $[C_{20}H_{23}N_2O_4S_2]^+$ 419.1099; found 419.1092.

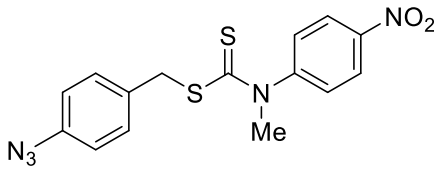

N3-DTCM was prepared according to the general synthetic procedure outlined in Chapter 4.2, from CP-NO_2 and 4-(mercaptomethyl)phenyl azide. (154 mg, 38% yield, off-white solid). ^{1}H NMR (500 MHz, $CDCl_3$) δ 8.33 (d, *J* = 8.9 Hz, 2H), 7.48 (d, *J* = 8.9 Hz, 2H), 7.31 (d, *J* = 8.5 Hz, 2H), 6.95 (d, *J* = 8.5 Hz, 2H), 4.47 (s, 2H), 3.79 (s, 3H). ^{13}C{^{1}H} NMR (126 MHz, $CDCl_3$) δ 198.66, 150.11, 147.46, 139.40, 132.29, 130.76, 128.35, 125.20, 119.16, 45.36, 42.31. HRMS m/z $[M + H]^+$ calcd. For $[C_{15}H_{13}N_5O_2S_2]^+$ 359.0511; found 359.0512.

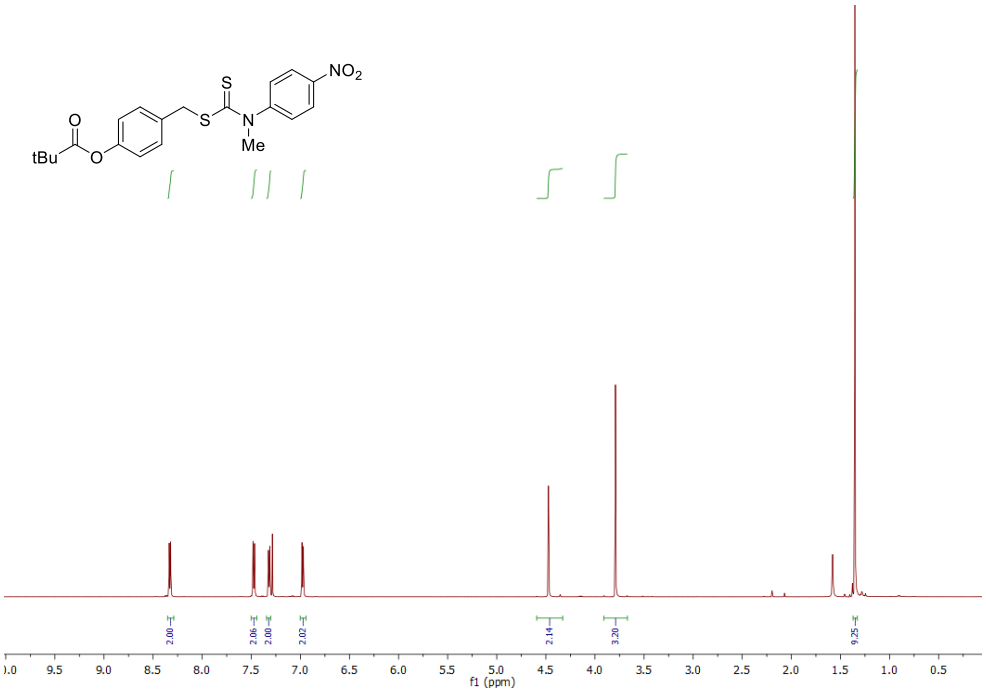

Figure D.1 ^{1}H NMR spectrum of **tBu-DTCM** in $CDCl_3$ taken at 600 MHz.

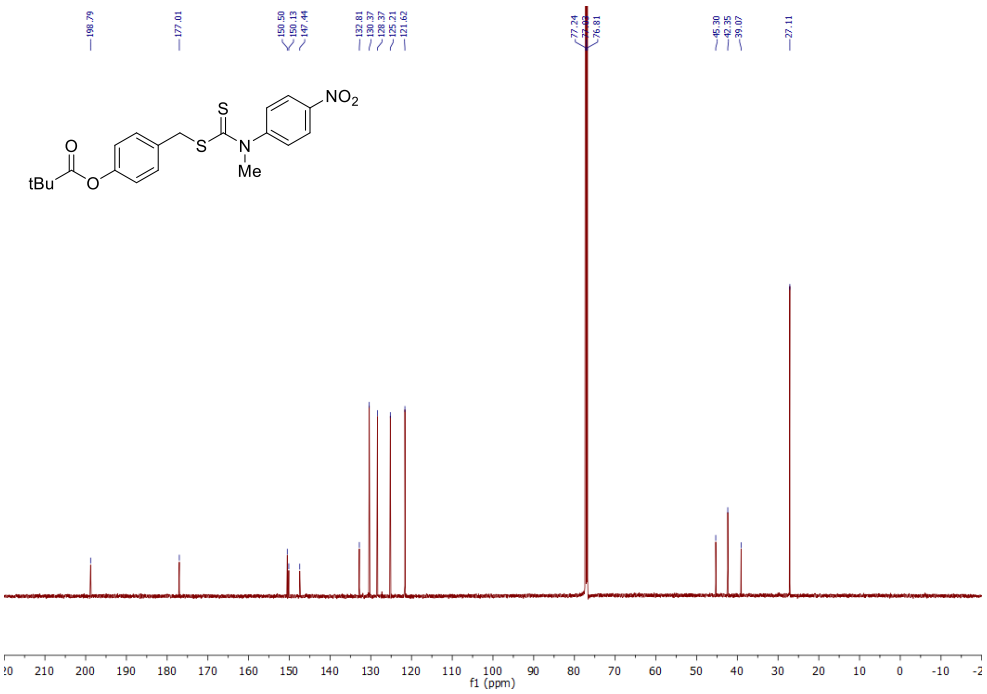

Figure D.2 $^{13}C\{^{1}H\}$ NMR spectrum of **tBu-DTCM** in $CDCl_3$ taken at 151 MHz.

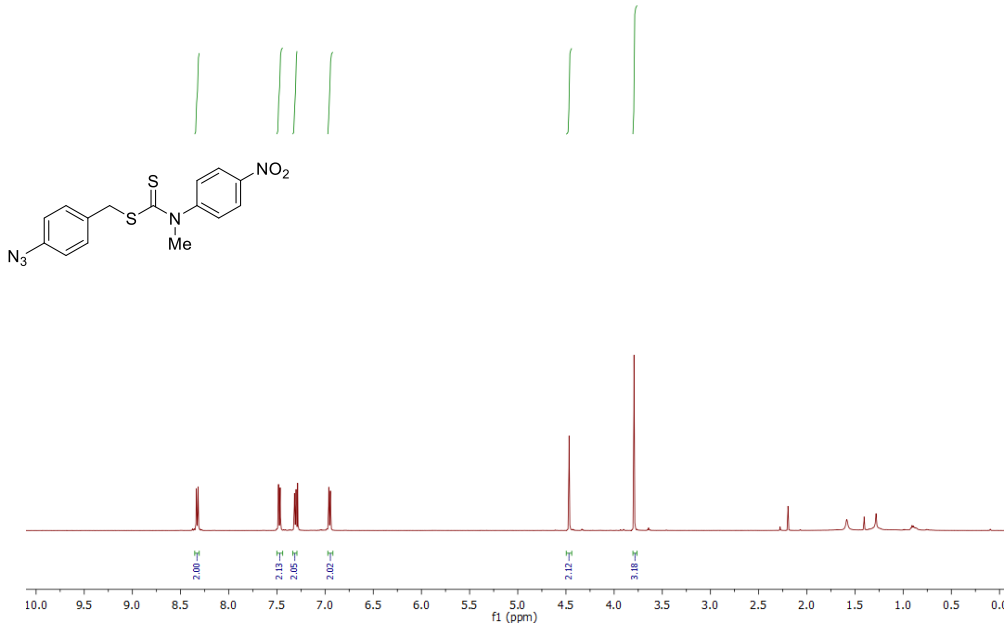

Figure D.3 ^{1}H NMR spectrum of **N3-DTCM** in $CDCl_3$ taken at 500 MHz.

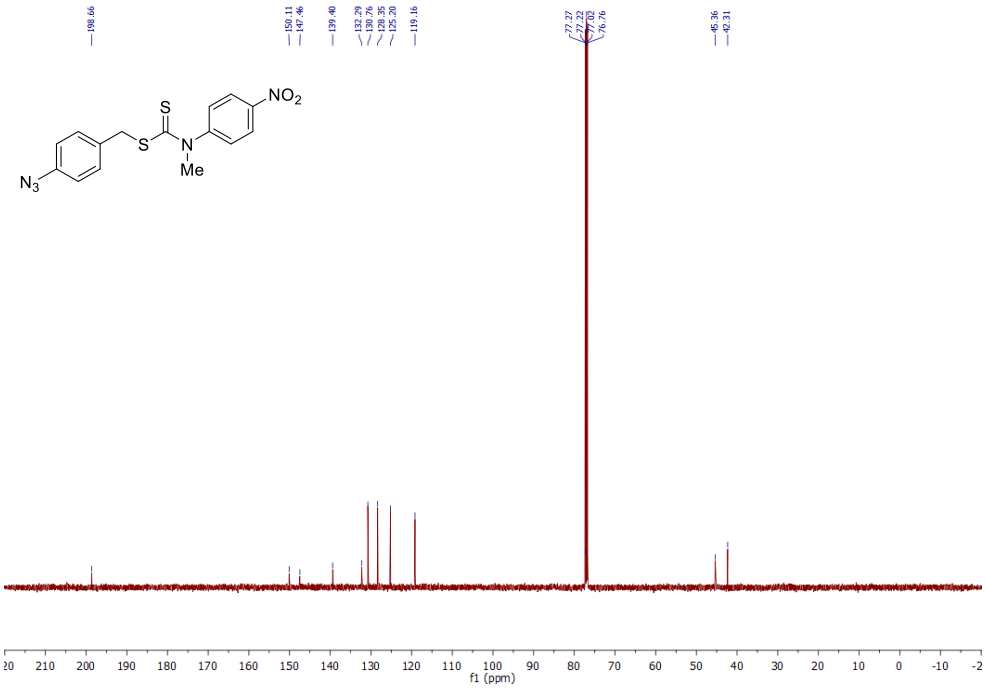

Figure D.4 $^{13}C\{^{1}H\}$ NMR spectrum of **N3-DTCM** in $CDCl_3$ taken at 126 MHz.

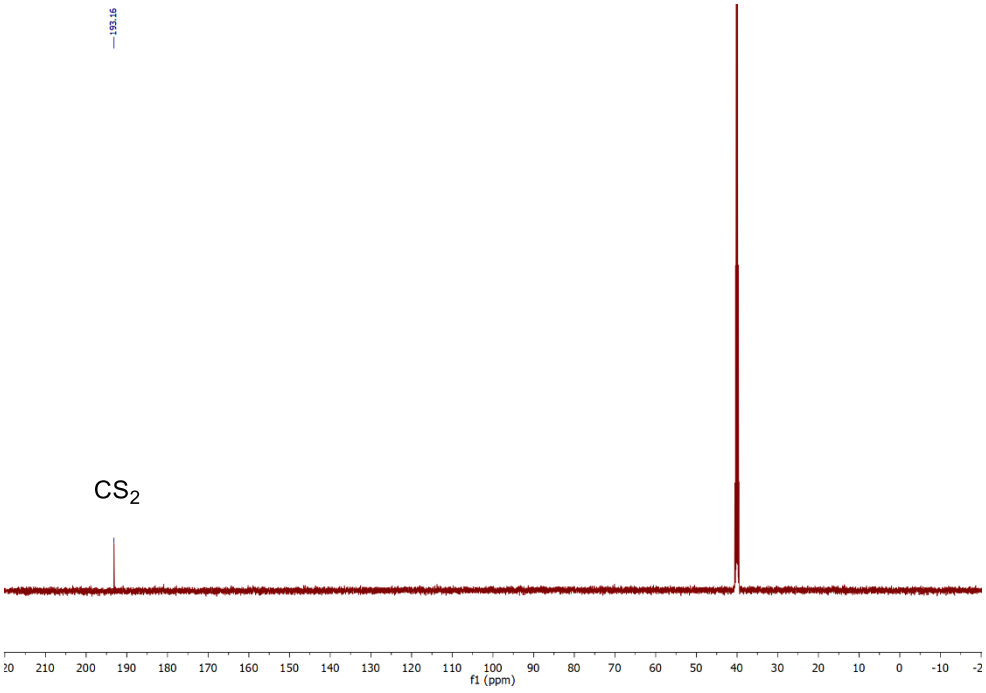

Figure D.5 $^{13}C\{^{1}H\}$ NMR spectrum of **CS_2** in DMSO-d_6 taken at 126 MHz.

APPENDIX E

SUPPLEMENTARY INFORMATION FOR CHAPTER V

Appendix E is the supplementary information for Chapter V of this dissertation. It includes spectra and experimental data relevant to the content in Chapter V.

NMR Spectra of Mem-DTS

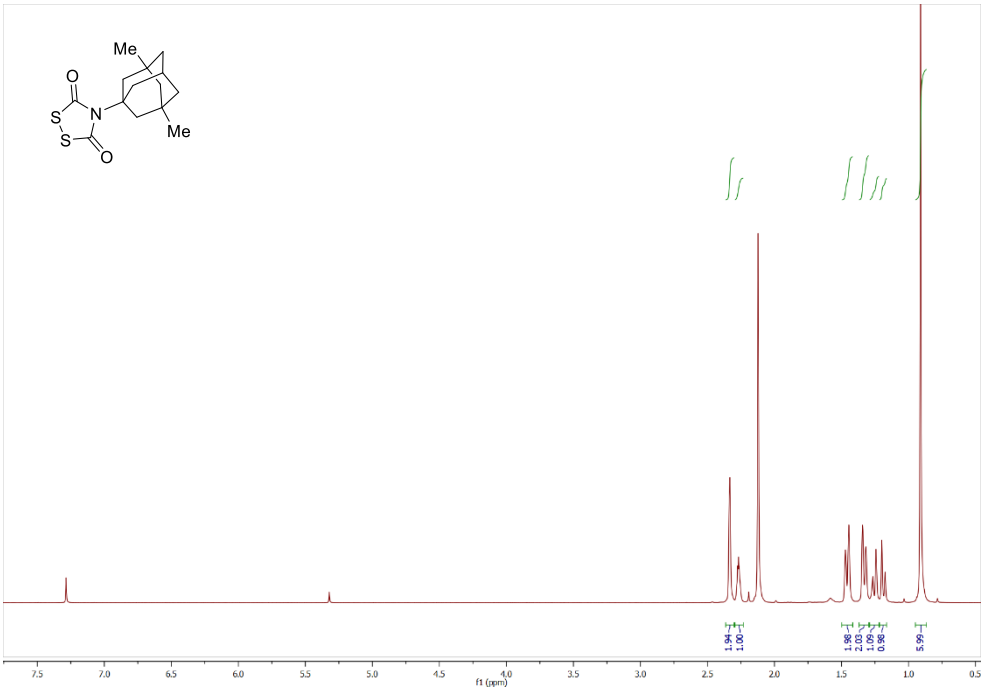

Figure E.1 ^{1}H NMR spectrum of **Mem-DTS** in $CDCl_3$ taken at 500 MHz.

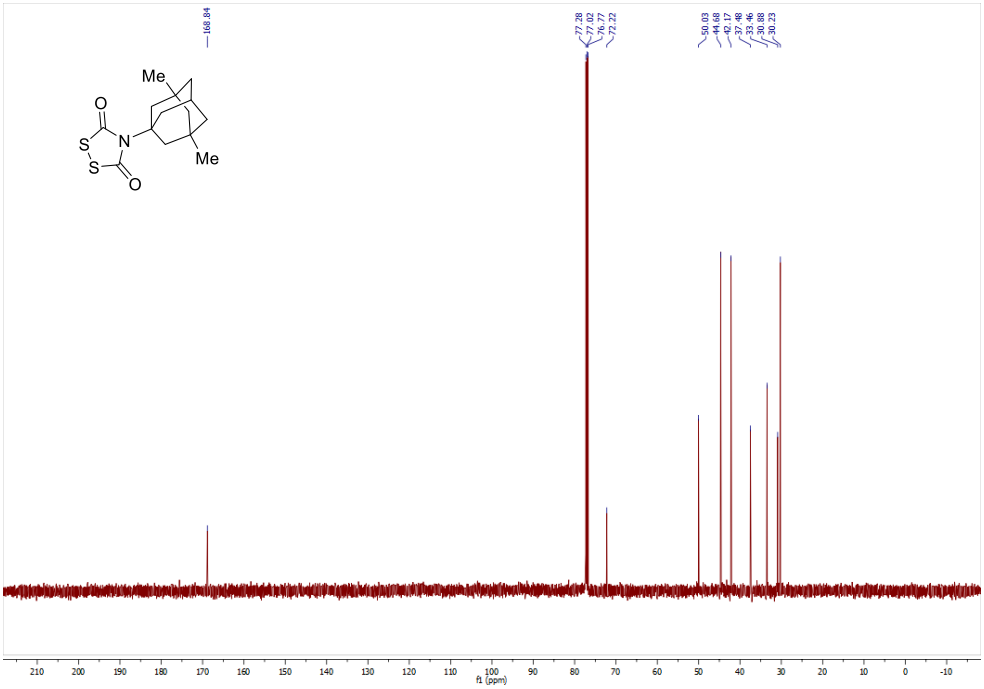

Figure E.2 $^{13}C\{^{1}H\}$ NMR spectrum of **Mem-DTS** in $CDCl_3$ taken at 125 MHz.

Establishing the Calibration Curve for the Methylene Blue Assay

Solutions containing 0.5 mL of methylene blue cocktail and 0.5 mL PBS (pH 7.4) containing 500 µM L-Cys and 50 µg/mL CA were freshly prepared in disposable 1.5 mL cuvettes. Under inert conditions, a 10 mM stock solution of NaSH (Strem Chemicals) in PBS was prepared and diluted to 1 mM. Immediately after dilution, varying amounts of the 1 mM NaSH stock was added to 1.0 mL solutions for final concentrations of 10, 20, 30, 40, 50, and 60 µM. Solutions were mixed, incubated at room temperature for 1 h, and shielded from light. Absorbance values at 670 nm were measured after 1 hr.

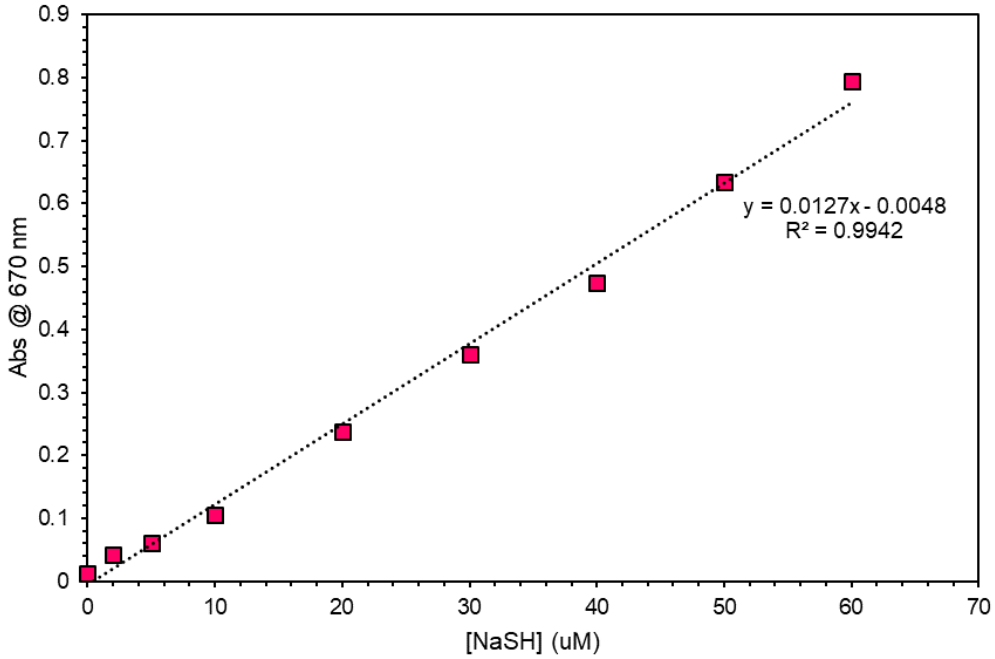

Figure E.3 NaSH Calibration curve for the Methylene Blue Assay on **Mem-DTS.**

APPENDIX F

SUPPLEMENTARY INFORMATION FOR CHAPTER VII

Appendix F is the supplementary information for Chapter VII of this dissertation. It includes spectra and experimental data relevant to the content in Chapter VII.

NMR Spectra of Prepared Compounds

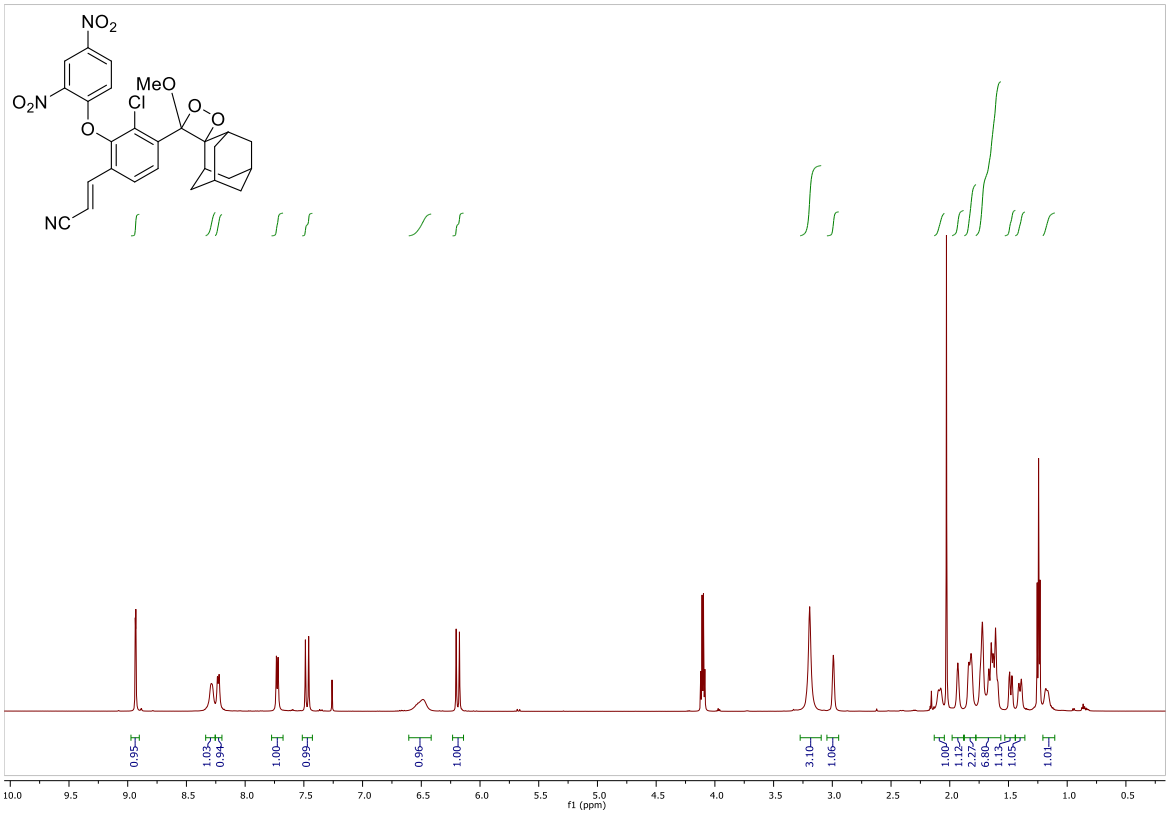

Figure F.1 ^{1}H NMR spectrum of **CL-DNP** in $CDCl_3$ taken at 600 MHz.

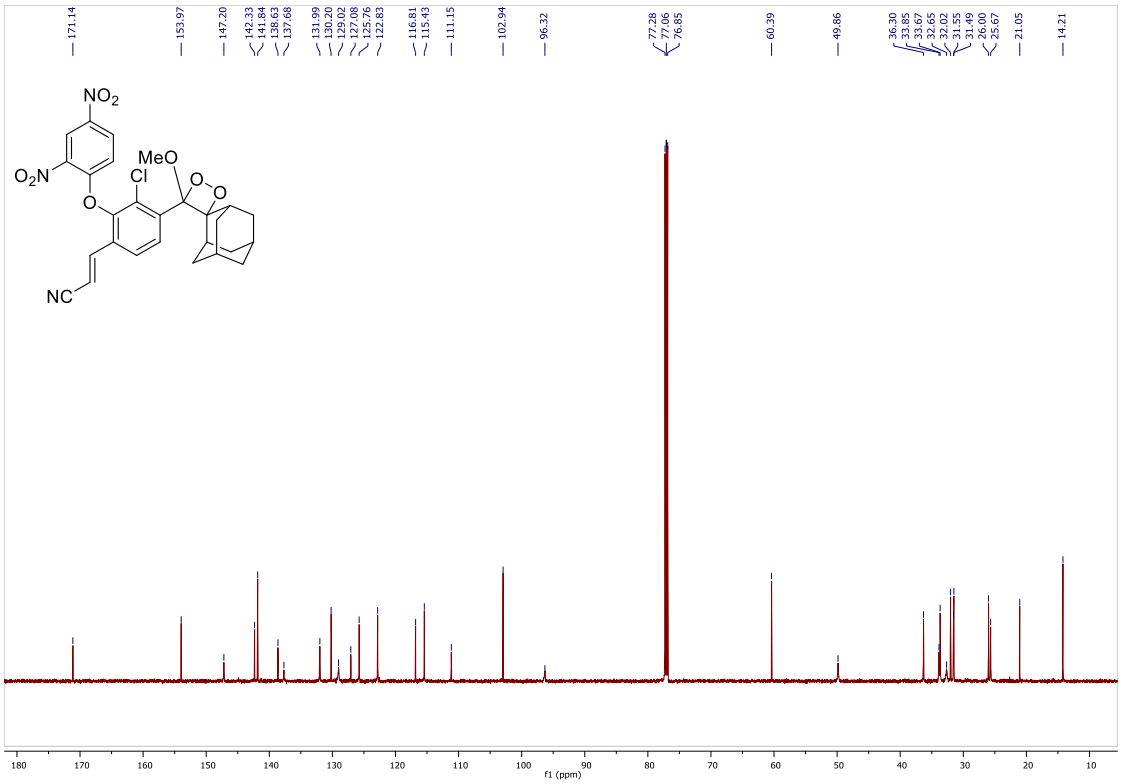

Figure F.2 $^{13}C\{^{1}H\}$ NMR spectrum of **CL-DNP** in $CDCl_3$ taken at 151 MHz.

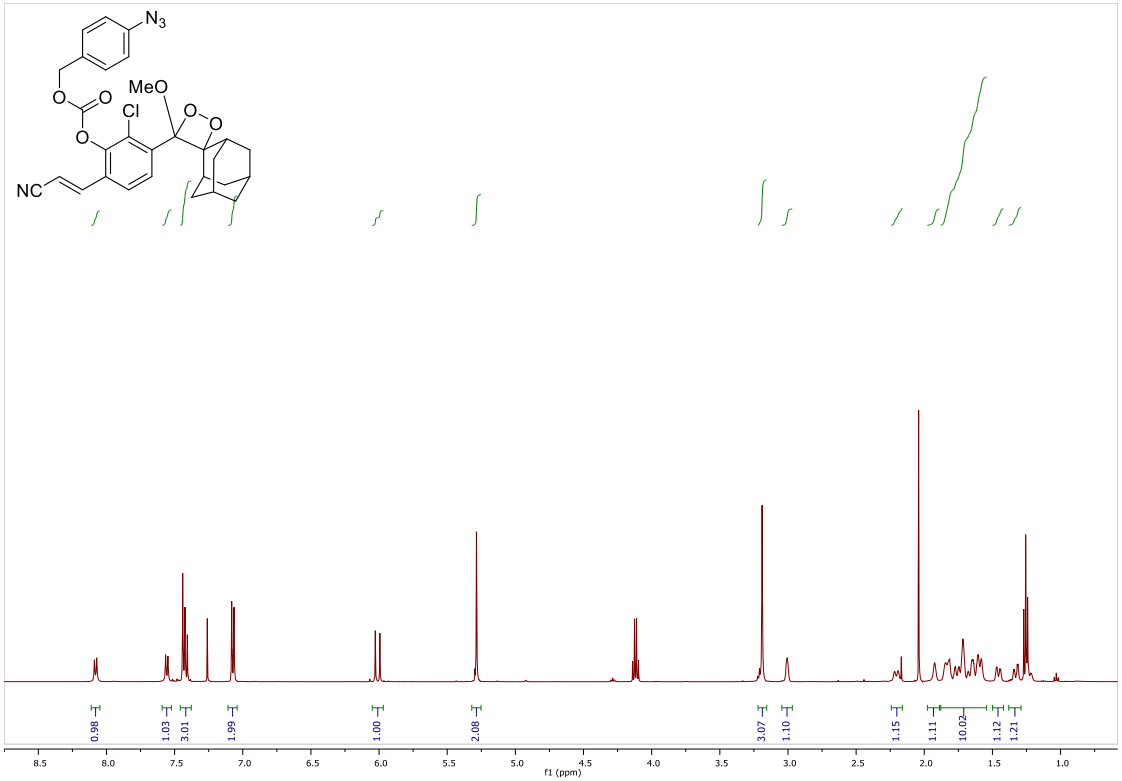

Figure F.3 ^{1}H NMR spectrum of **CL-N3** in $CDCl_3$ taken at 500 MHz.

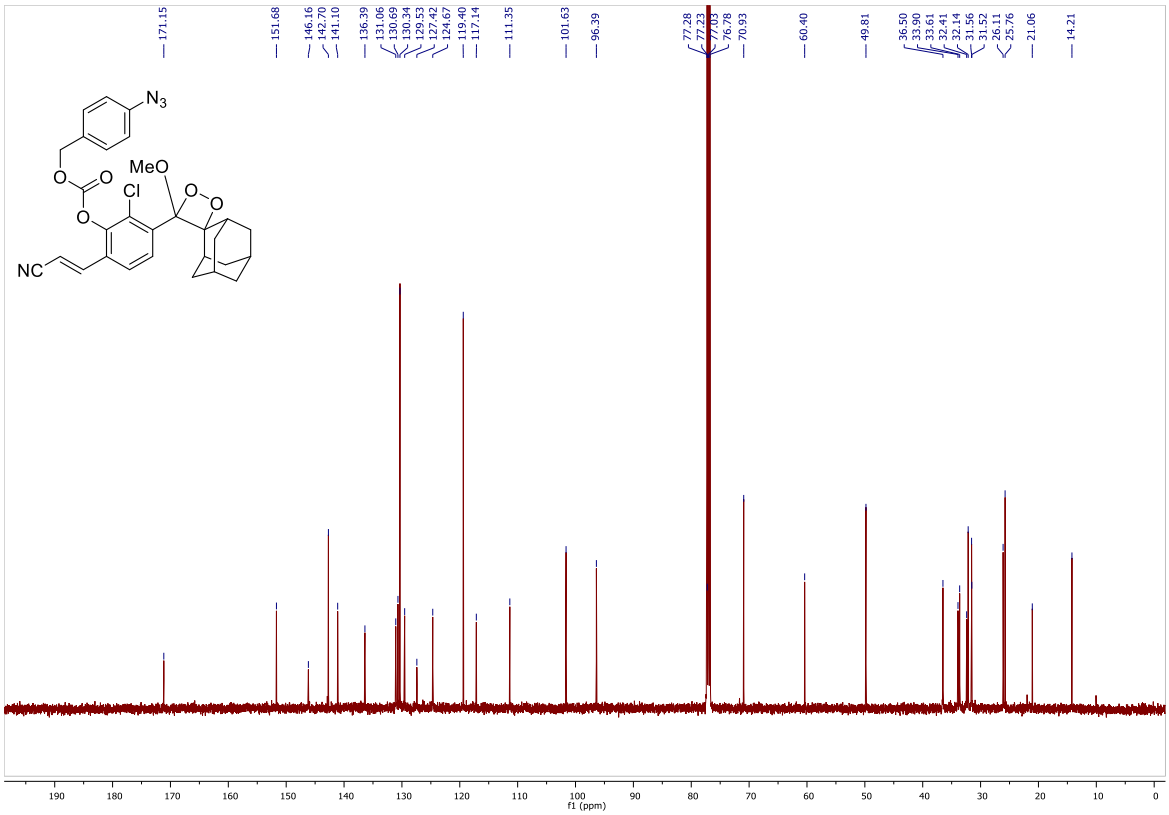

Figure F.4 $^{13}C\{^{1}H\}$ NMR spectrum of **CL-N3** in $CDCl_3$ taken at 126 MHz.

Calculating Normalized Turn-On Response

Data for four blank baseline response trials were collected with 25 µM of either **CL-DNP** or **CL-N3** in either THF or PBS 7.4 with 5% DMSO at 37 °C for 30 minutes, with no analyte added. The same fluorimeter parameters were applied, with excitation slits closed, and the excitation wavelength set to 800 nm. Emission slits were set to 4.0 mm, and the wavelength measured at was 525 nm. Scans were taken every second for at least 30 minutes. The data for each experiment was adjusted so that the minimum measured value for the 30 minute window was set equal to an emission intensity of 0. The adjusted data was integrated over 30 minutes, and used as the baseline turn-on response for calculating the normalized turn-on response. Adjusting for all measurements to be positive ensures that at worst the turn-on response is under-reported, and is likely higher than stated. The tabulated baseline responses are listed in Table F.1.

Experiment	Integrated Response
CL-DNP PBS 7.4 with 5% DMSO	262077.265
CL-DNP THF	288319.194
CL-N3 THF	277440.1992
CL-N3 PBS 7.4 with 5% DMSO	2190880.973
CL-DNP PBS 7.4 with 5% DMSO - 500 s	63127.038

Table F.1 Integrated responses of adjusted blank scans for each probe in each solvent system, integrated over 30 minutes, except for **CL-DNP** PBS 7.4 with 5% DMSO – 500 s, which is integrated over 500 seconds for the L-Lys selectivity study (see figure S7).

Integrated Emission of CL-DNP and CL-N3 in Response to NaSH

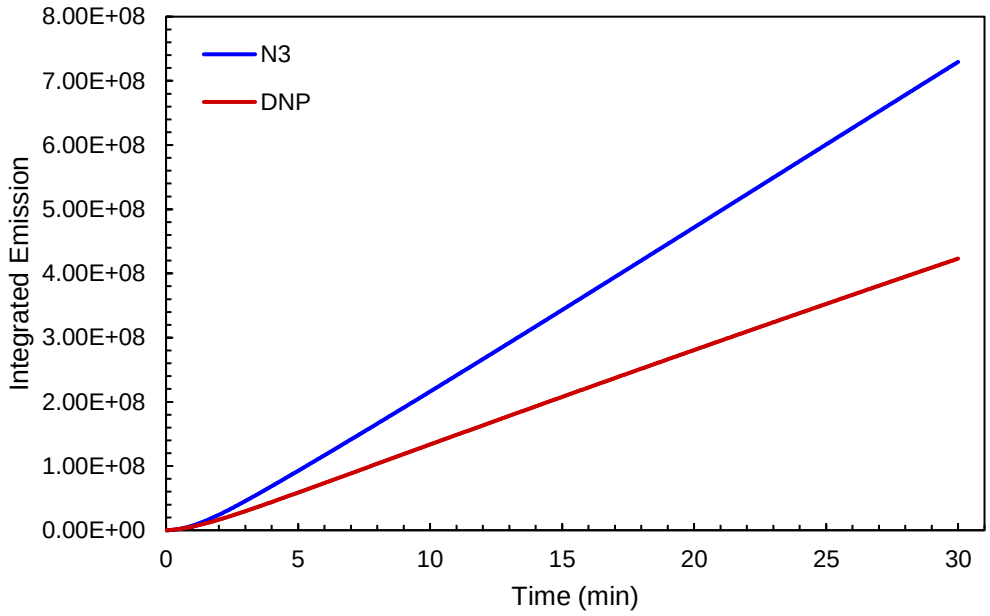

Figure F.5 Integrated emission of **CL-N3** and **CL-DNP** in response to 100 equiv. NaSH in THF at 37 °C. The normalized turn-on response for each probe in this experiment was 2629.4-fold for **CL-N3**, and 1467.5-fold for **CL-DNP**.

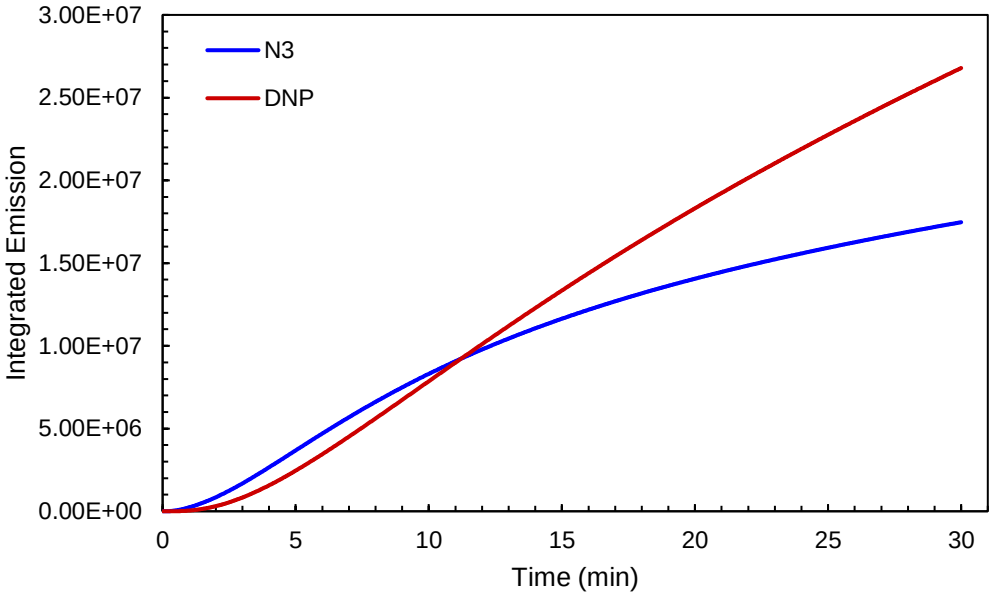

Figure F.6 Integrated emission of **CL-N3** and **CL-DNP** in response to 100 equiv. NaSH in PBS 7.4 with 5% DMSO at 37 °C. The normalized turn-on response for each probe in this experiment was 7.974-fold for **CL-N3**, and 102.2-fold for **CL-DNP**.

Selectivity Studies

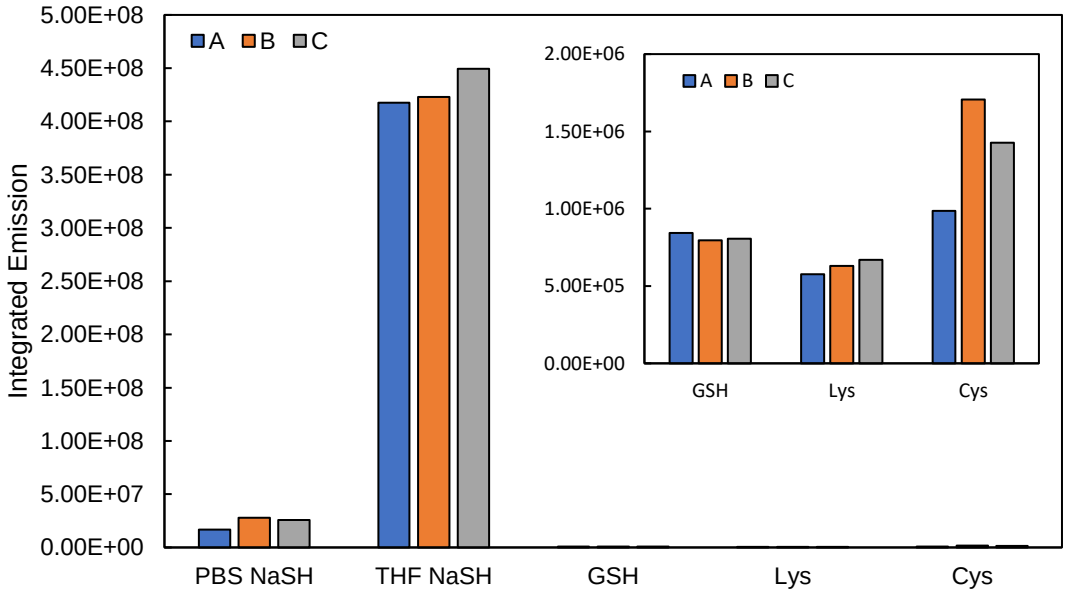

Figure F.7 Integrated emission over 30 minutes of **CL-DNP** in either PBS 7.4 with 5% DMSO or THF, all at 37 °C, with 100 equiv. of analyte added. Three trials were performed for each analyte, and Figure 4a in the text shows the average normalized turn-on response for the three trials. The response curves for the L-Lys experiments crossed the x-axis after about eight minutes, so those curves were integrated over 500 seconds (only the positive values recorded).

	NaSH (PBS)	NaSH (THF)	GSH	L-Lys	L-Cys
A	64.07529812	1448.358265	3.218516321	9.129833565	3.761172155
B	106.4834266	1467.520545	3.037824568	9.996417959	6.511733329
C	98.64365906	1558.771694	3.078243661	10.60451054	5.446087326
Average	89.73	1491.55	3.11	9.91	5.24
StdDev	22.56	59	0.0948	0.741	1.39

Table F.2 Normalized turn-on response for each trial of the selectivity experiments shown in Figure F.7.

CL-DNP Response to Varying NaSH Concentrations

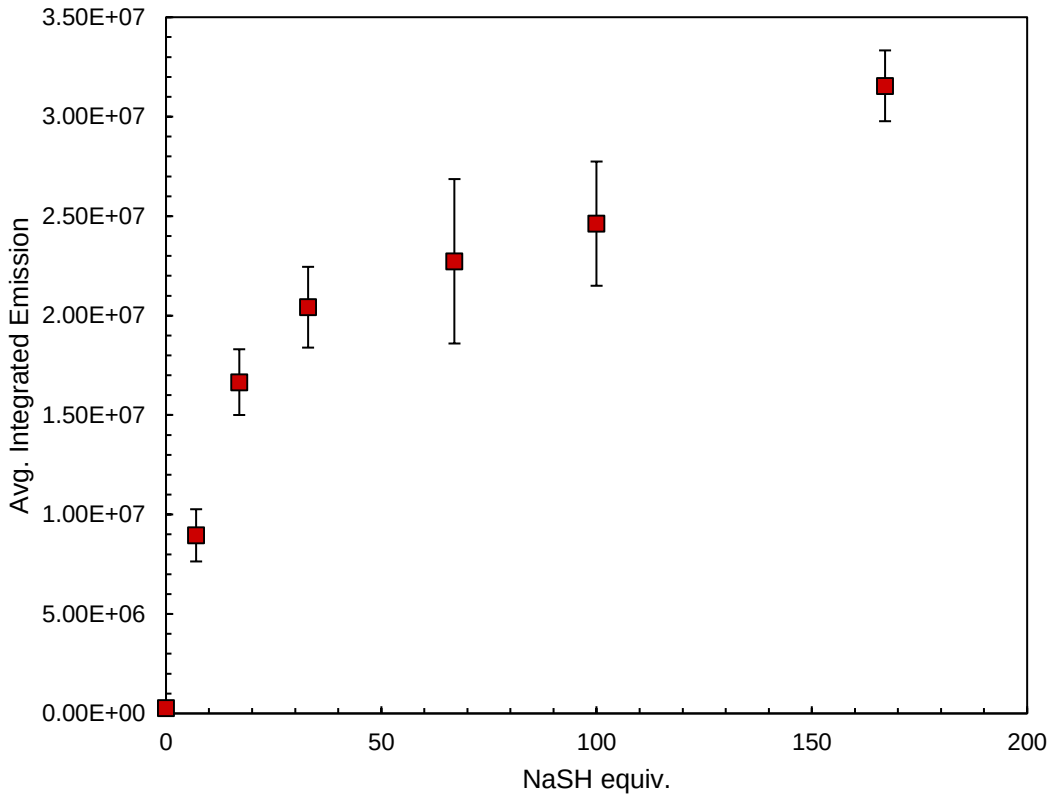

Figure F.8 Average integrated emission over 30 minutes of **CL-DNP** in PBS 7.4 with 5% DMSO at 37 °C, with varying equiv. of NaSH added. Three trials were performed for each analyte, other than the zero equivalents experiment. Figure 4b in the text shows the normalized turn-on response.

NaSH equiv:	0	7	17	33	67	100	167
A	1.01058	30.08493	56.47076	76.26289	68.69561	101.2577	113.0822
B		32.65882	68.54881	71.14107	97.89849	80.20413	126.505
C		39.75468	65.63803	86.36157	93.60619	100.3968	121.5915
Average	1.01058	34.16615	63.55253	77.92184	86.73343	93.95285	120.3929
StdDev		5.007997	6.303317	7.744676	15.76795	11.91452	6.791197

Table F.3 Normalized turn-on response for each trial of the varying NaSH concentration experiments, the average of which is plotted in Figure 7.4b.

APPENDIX G

SUPPLEMENTARY INFORMATION FOR CHAPTER VIII

Appendix G is the supplementary information for Chapter VIII of this dissertation. It includes spectra and experimental data relevant to the content in Chapter VIII.

Synthesis / Spectral Details of Prepared Compounds

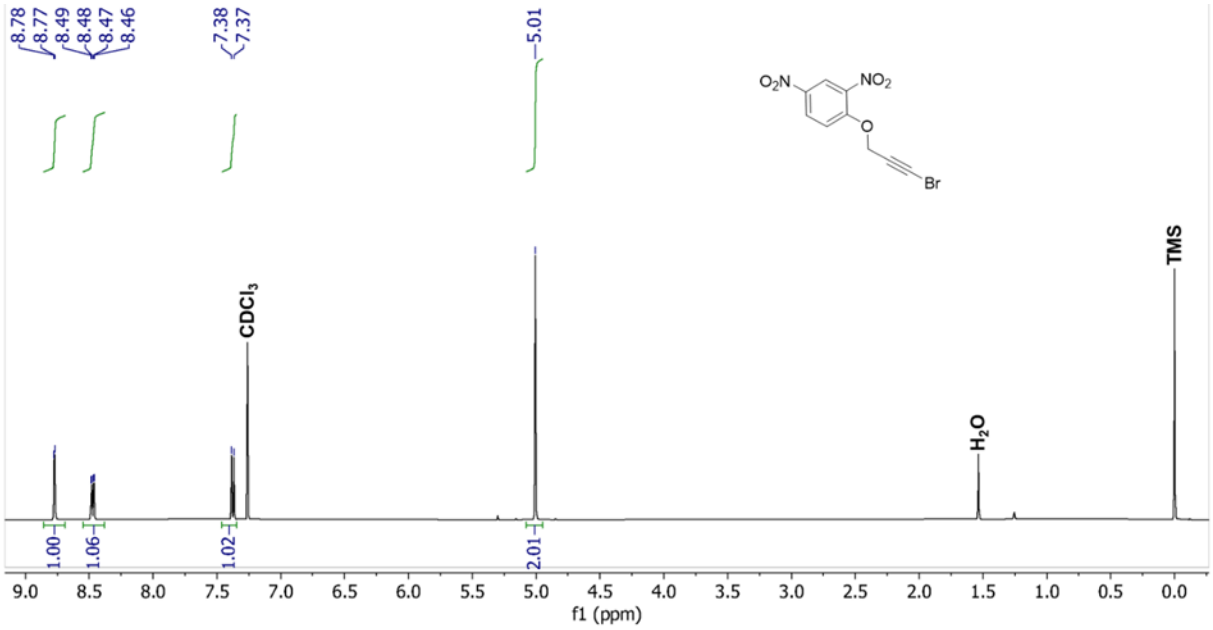

Figure G.1 ^{1}H (500 MHz, $CDCl_3$) NMR spectrum of **DNP-bromoalkyne**.

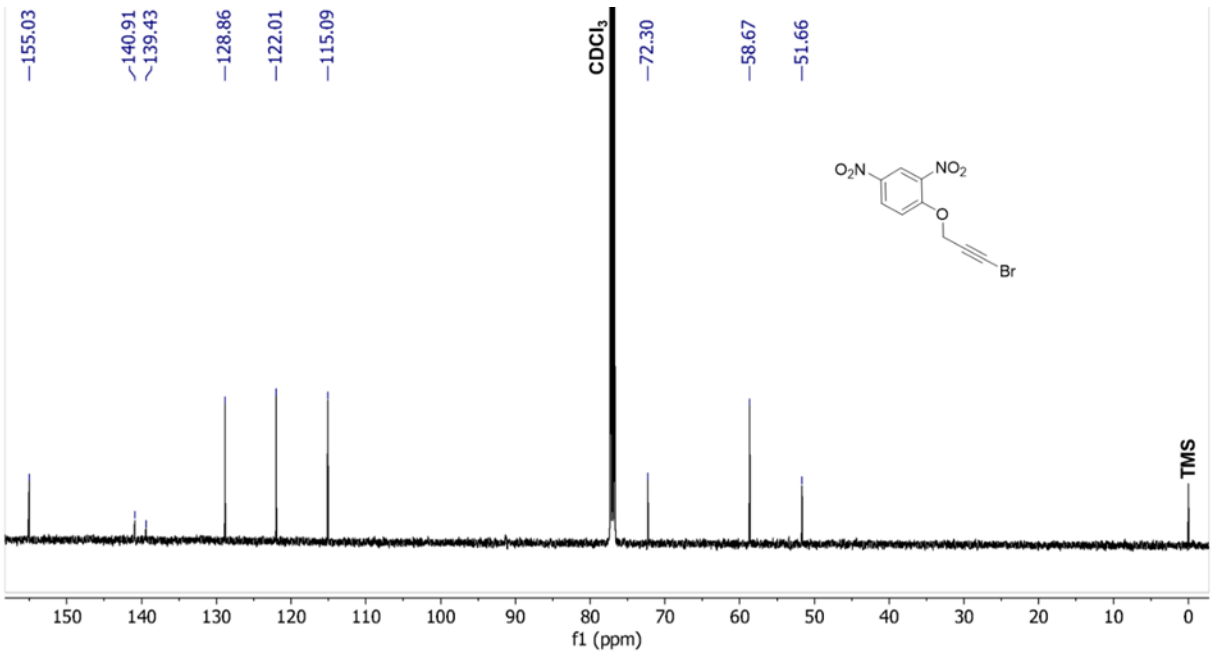

Figure G.2 $^{13}C\{^{1}H\}$ (125 MHz, $CDCl_3$) NMR spectrum of **DNP-bromoalkyne**.

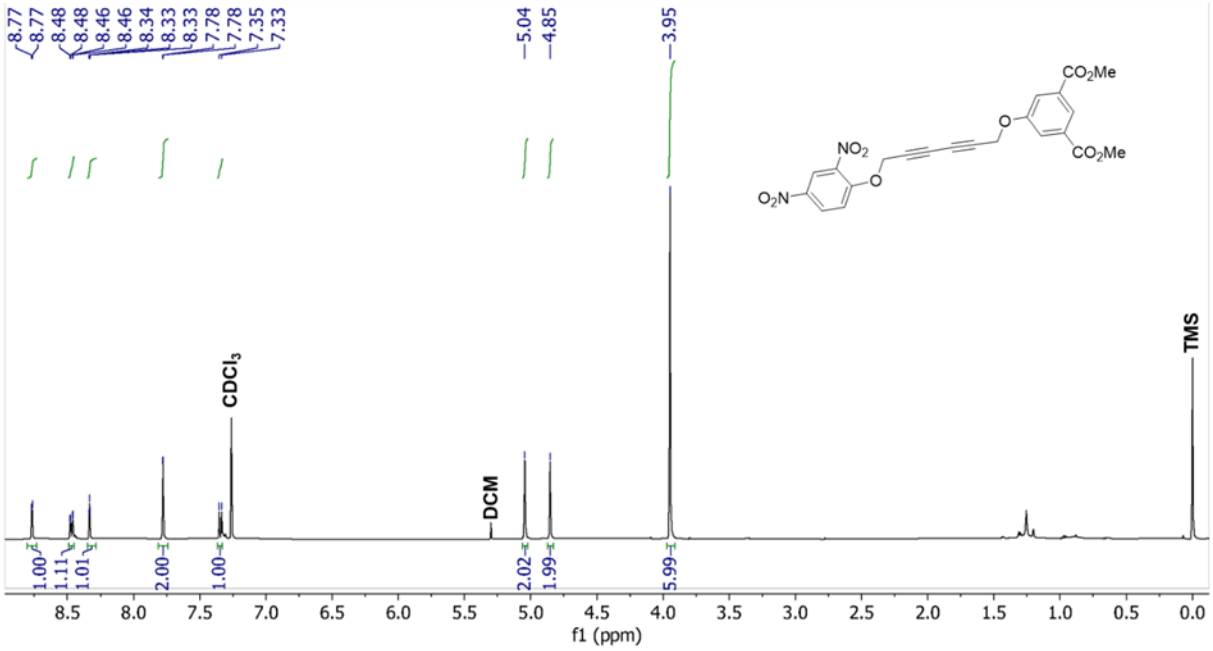

Figure G.3 ^{1}H (500 MHz, $CDCl_3$) NMR spectrum of **AT.**

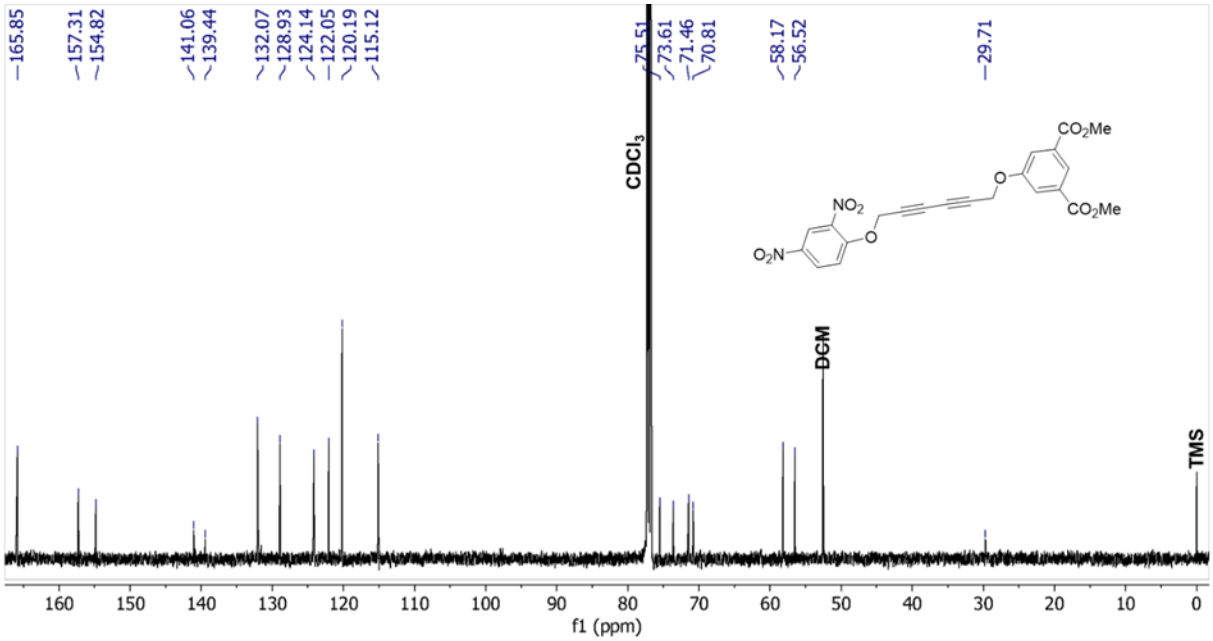

Figure G.4 $^{13}C\{^{1}H\}$ (125 MHz, $CDCl_3$) NMR spectrum of **AT**.

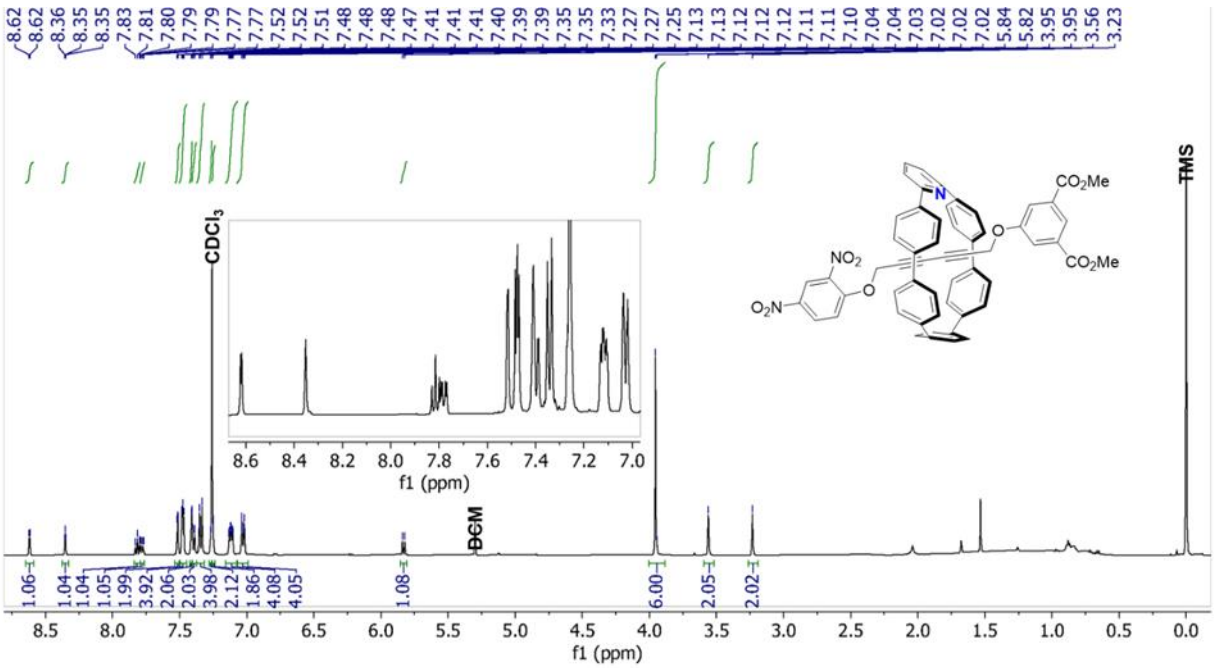

Figure G.5 ^{1}H (500 MHz, $CDCl_3$) NMR spectrum of **AR.**

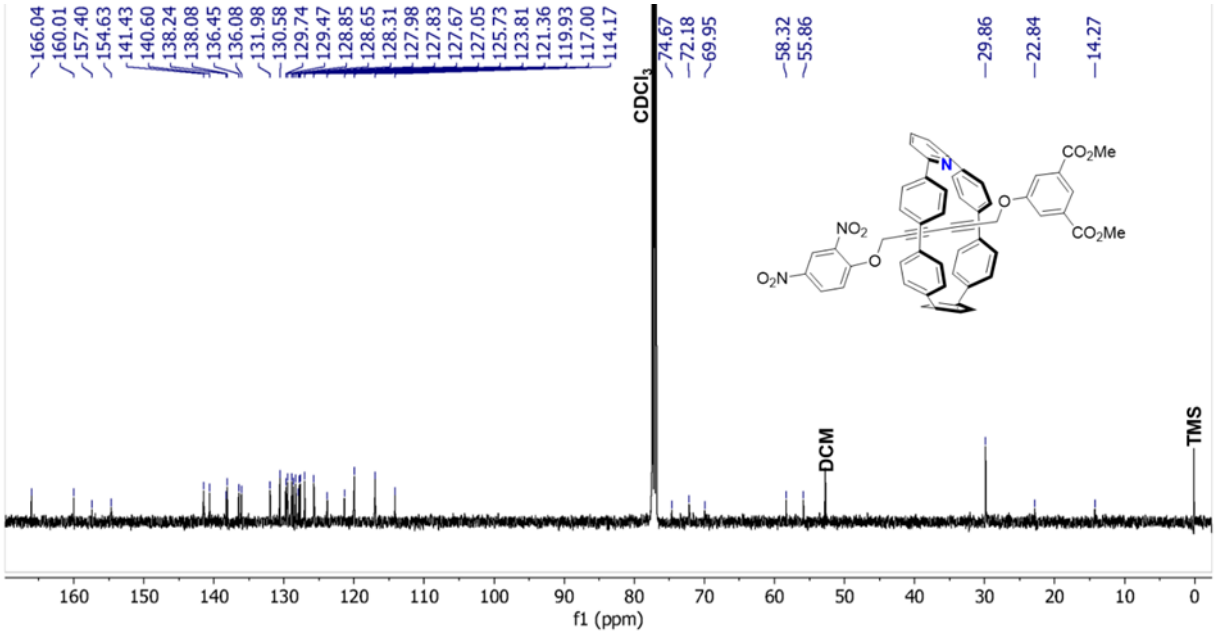

Figure G.6 $^{13}C\{^{1}H\}$ (125 MHz, $CDCl_3$) NMR spectrum of **AR**.

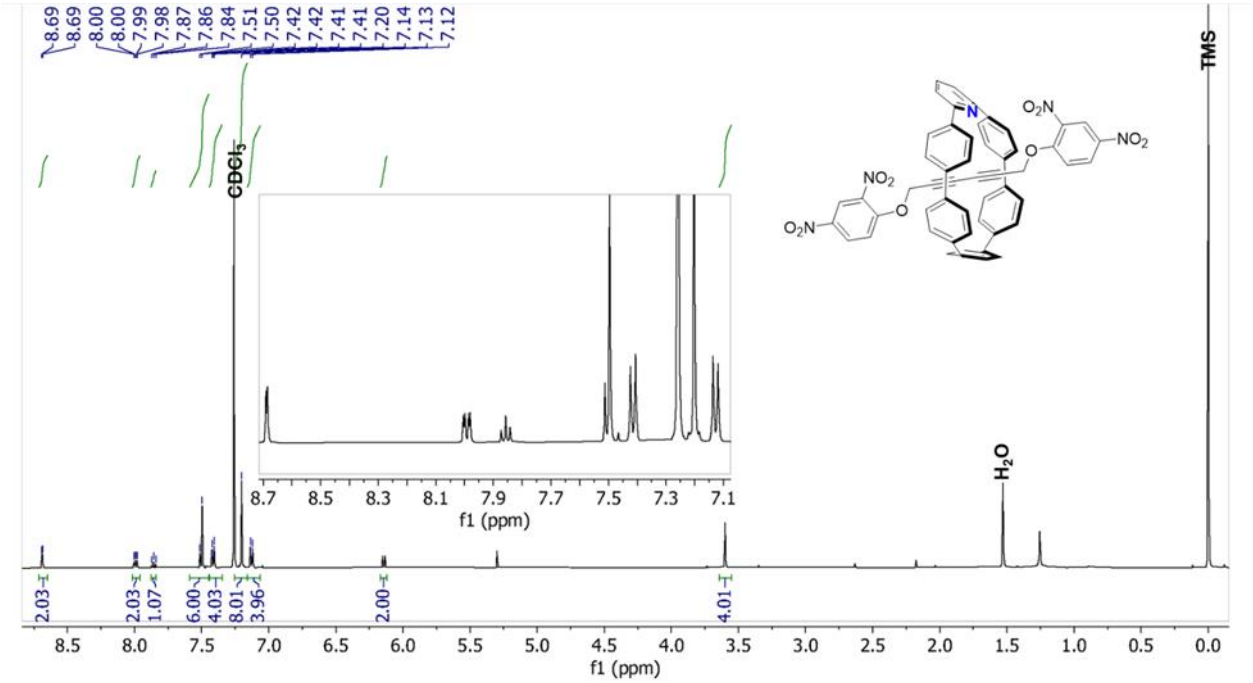

Figure G.7 ^{1}H (500 MHz, $CDCl_3$) NMR spectrum of **SR.**

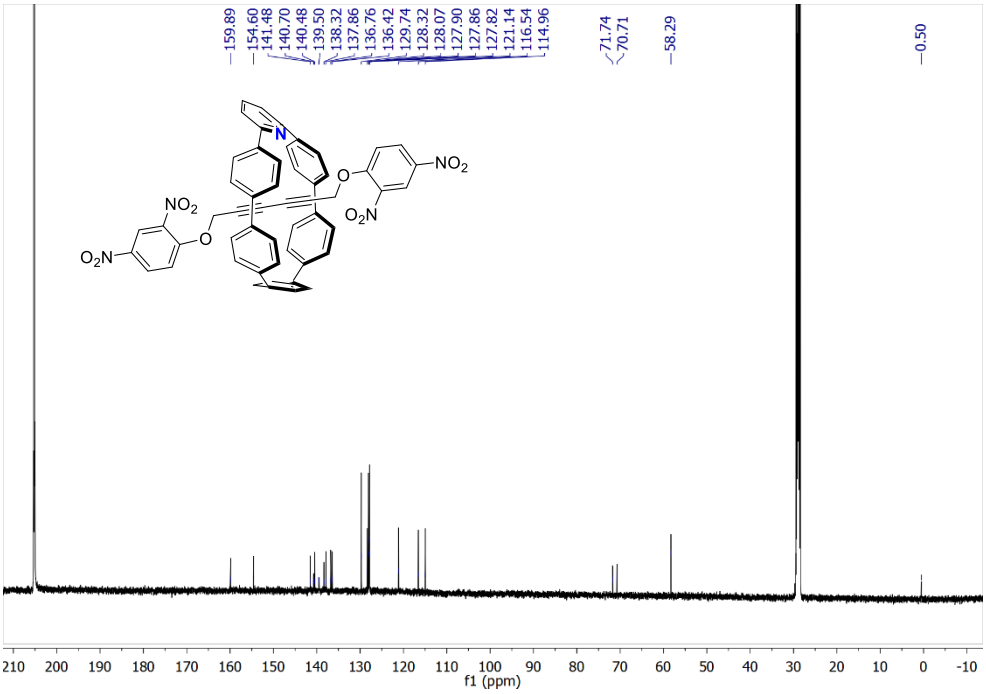

Figure G.8 $^{13}C\{^{1}H\}$ (125 MHz, acetone-d_6) NMR spectrum of **SR**.

Absorbance/Fluorescence of SR in Response to Varying Amounts of TBASH

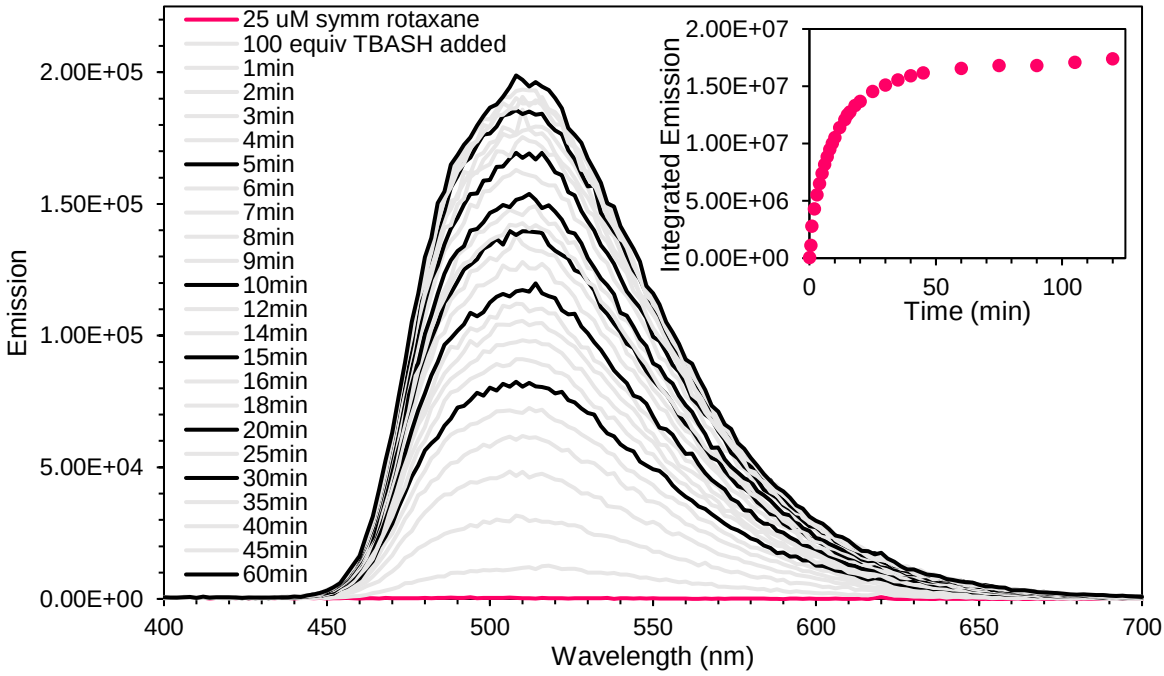

Figure G.9 Fluorescence of **SR** over time with 10 equiv. of TBASH added, exciting at 310 nm.

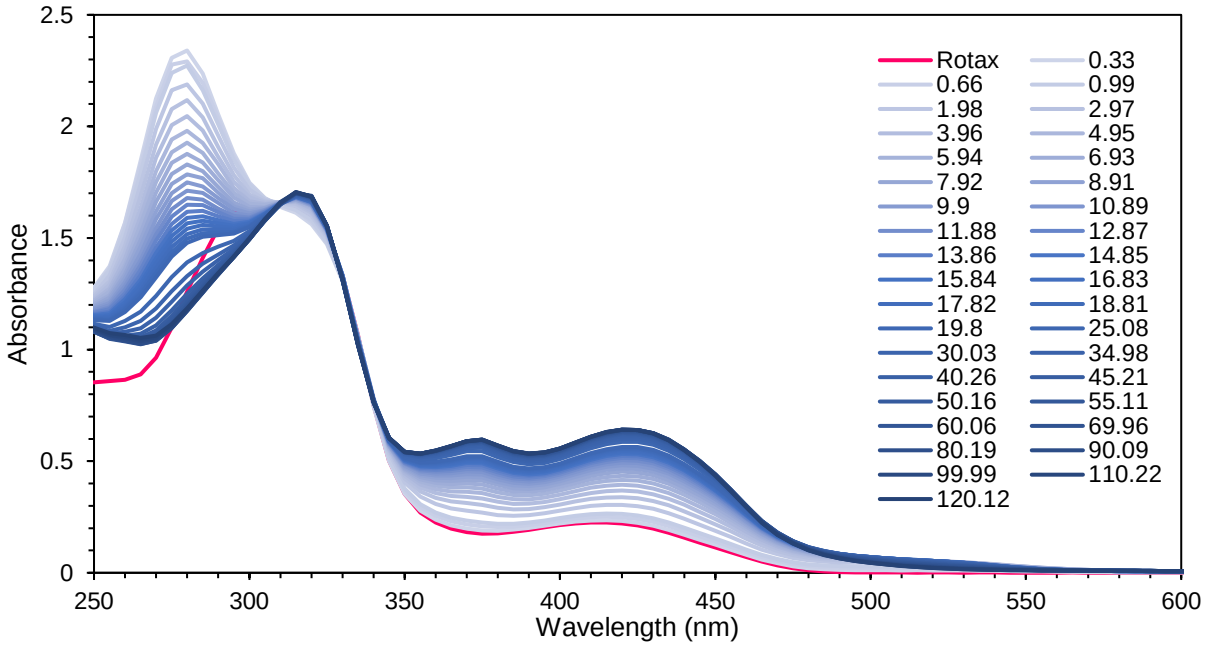

Figure G.10 Absorbance spectrum of **SR** over time with 10 equiv. TBASH added.

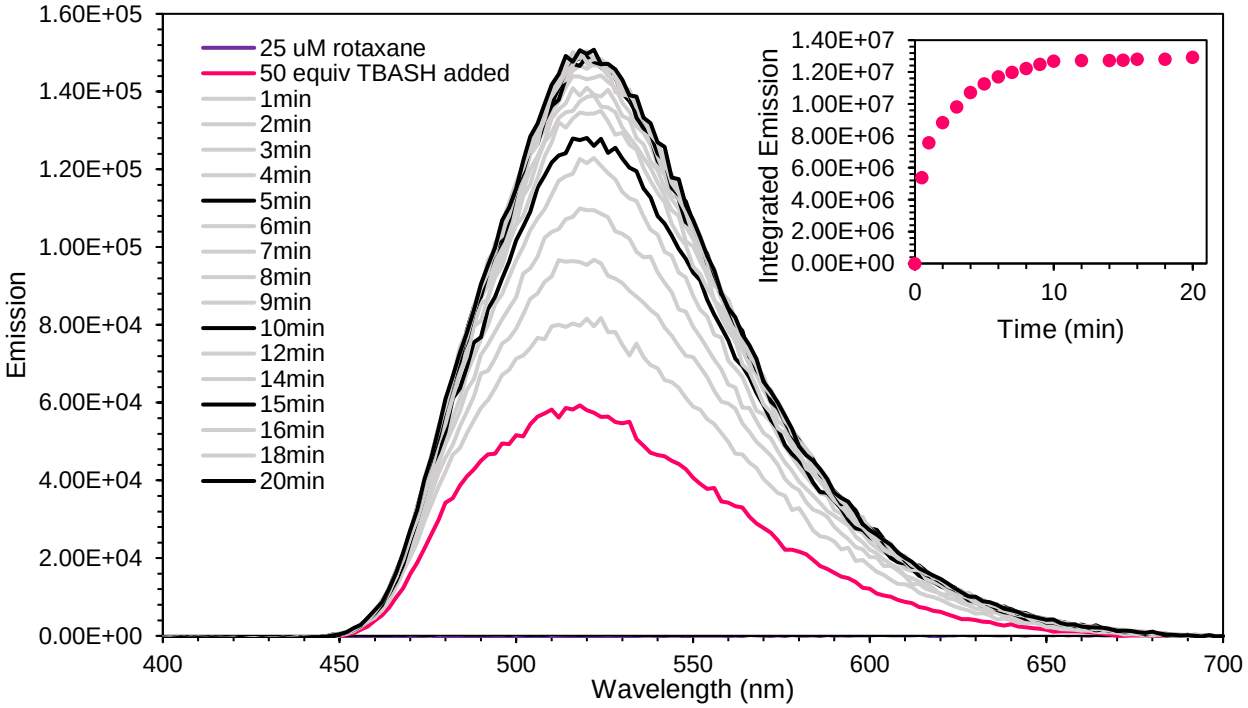

Figure G.11 Fluorescence spectrum of **SR** over time with 50 equiv. TBASH added, exciting at 310 nm.

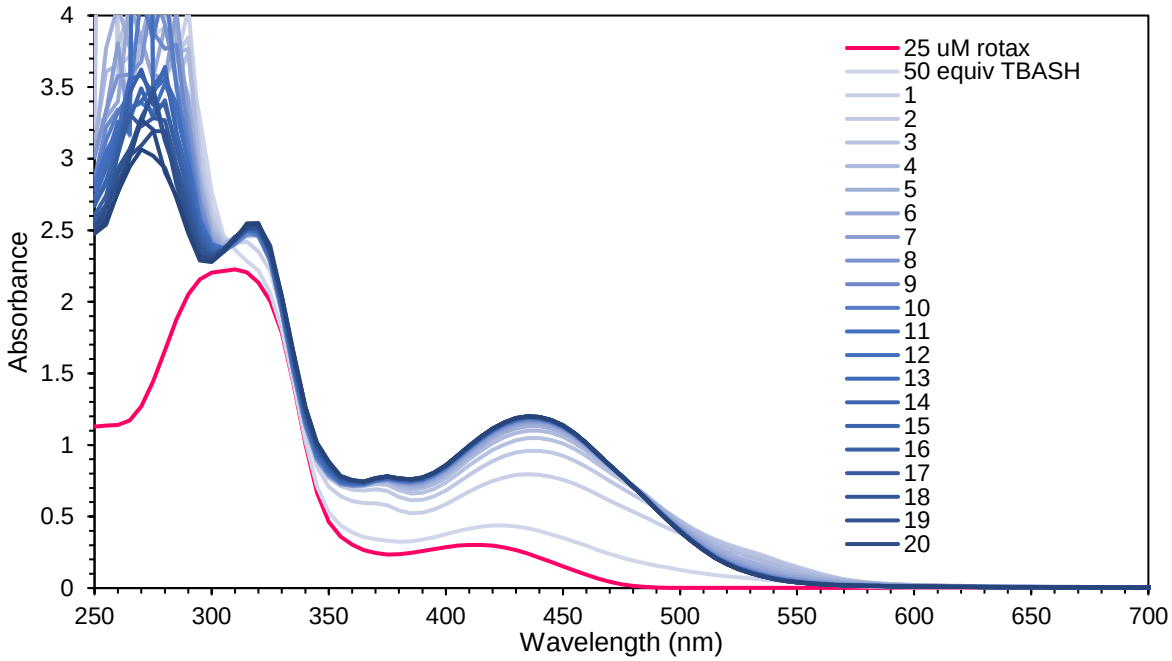

Figure G.12 Absorbance spectrum of **SR** over time with 50 equiv. TBASH added.

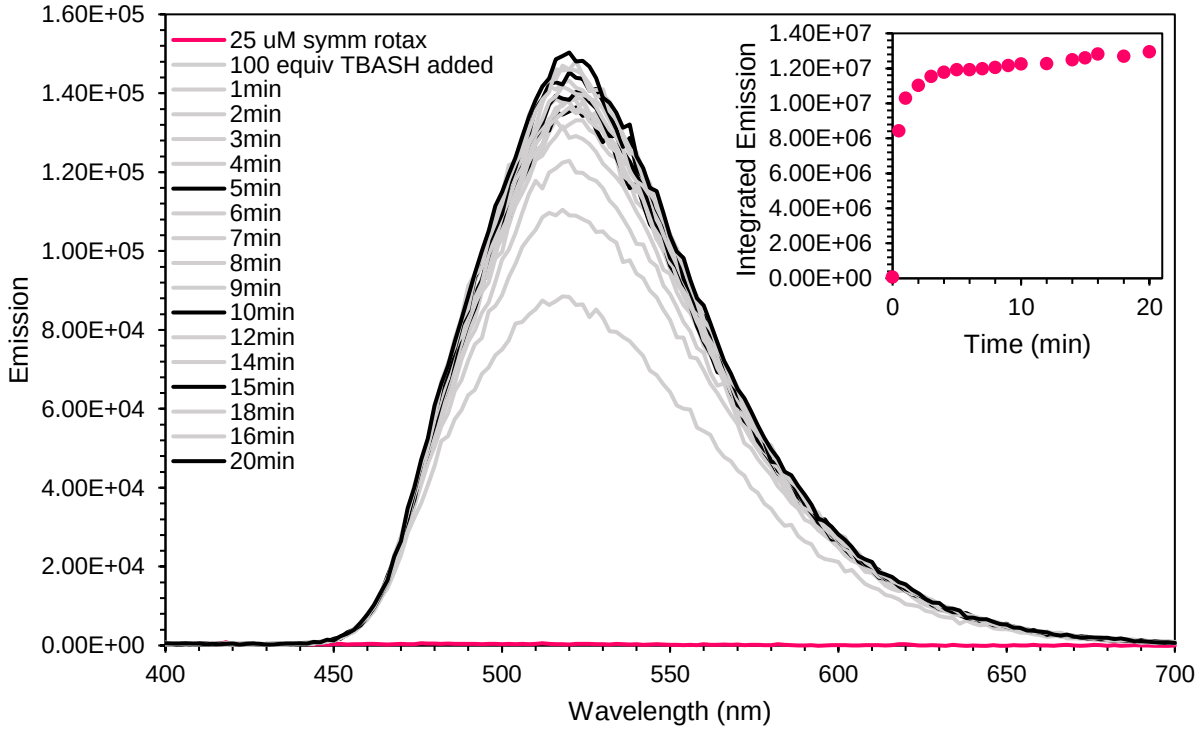

Figure G.13 Fluorescence of **SR** over time with 100 equiv. TBASH added, exciting at 310 nm.

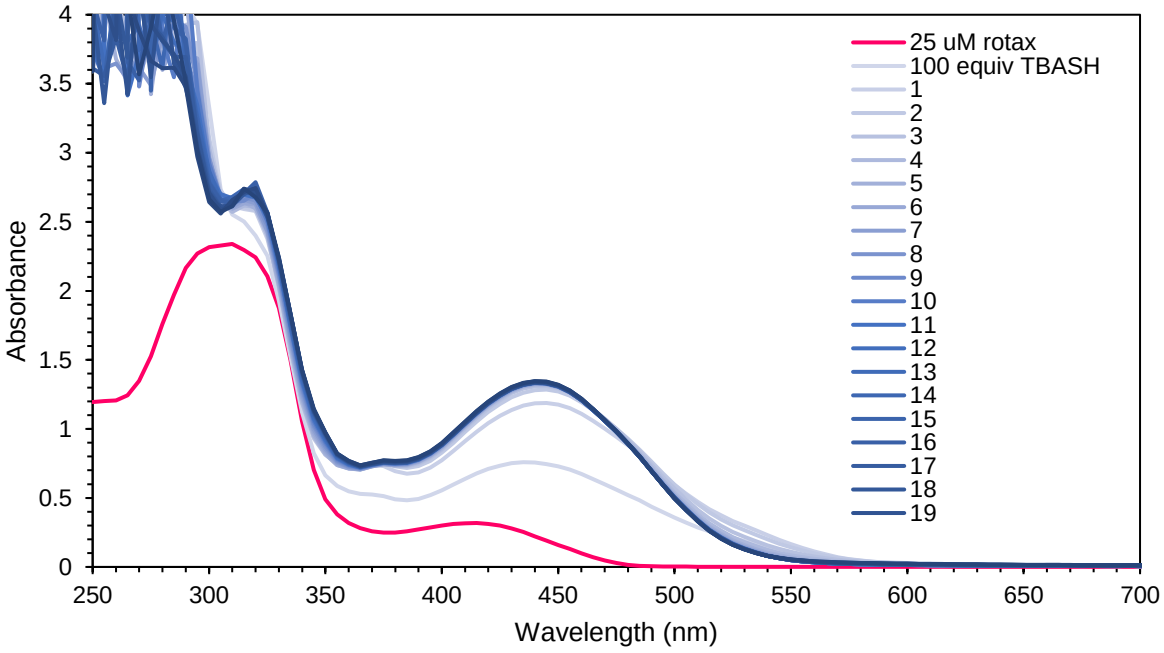

Figure G.14 Absorbance spectrum of **SR** over time with 100 equiv. TBASH added.

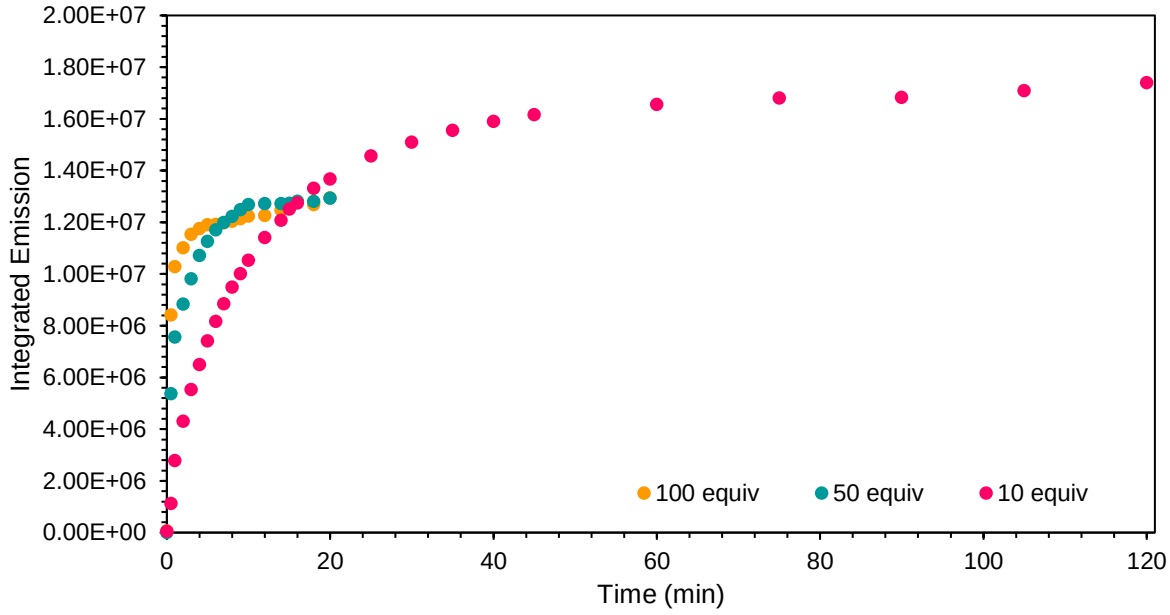

Figure G.15 Comparison of integrated emission *vs.* time for **SR** at varying concentrations of TBASH

*Fluorescence and Absorbance Spectra of **SR** Reacting with PhSNa*

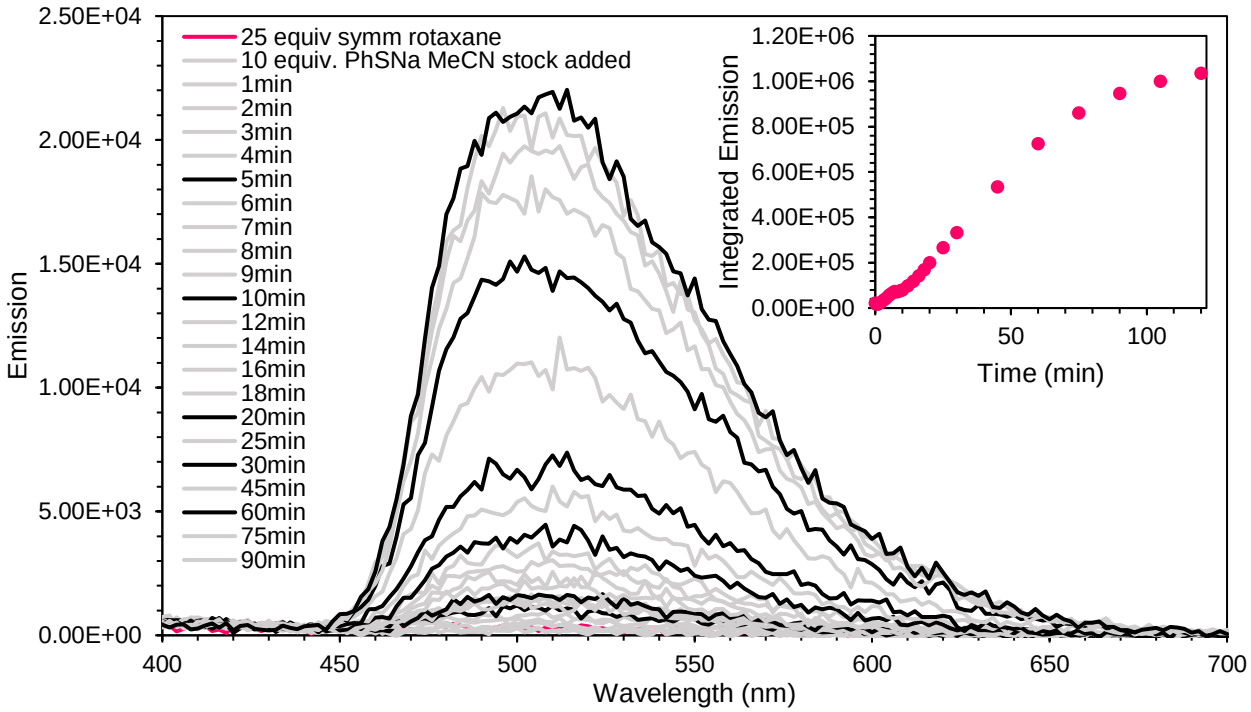

Figure G.16 Fluorescence spectrum of **SR** over time with 10 equiv. of PhSNa added, exciting at 310 nm.

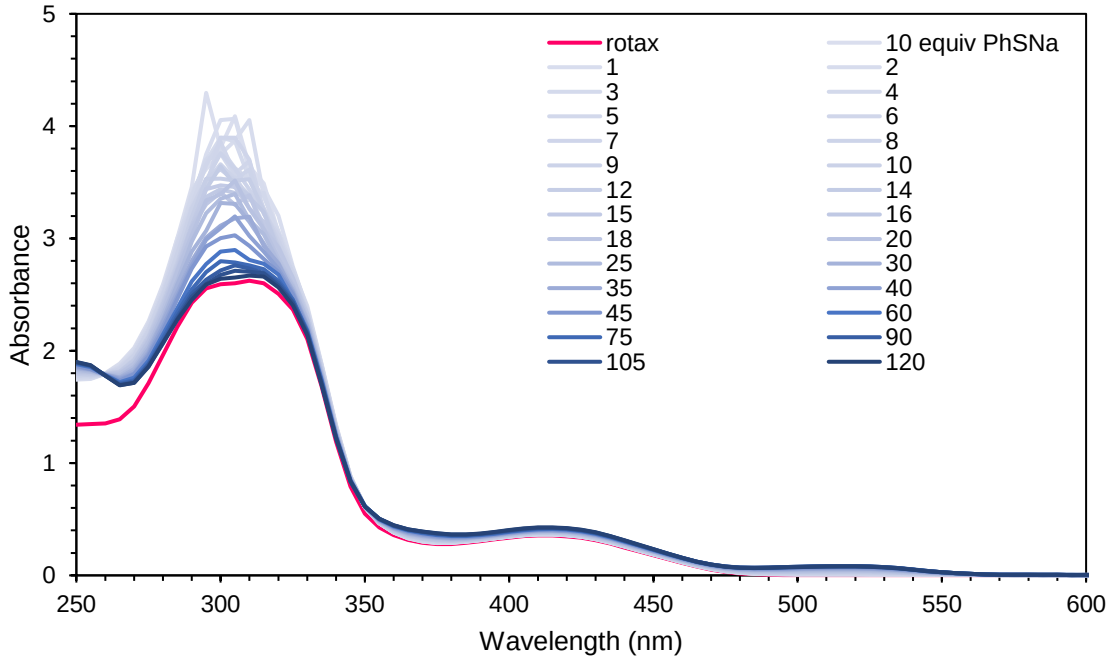

Figure G.17 Absorbance spectrum of **SR** over time with 10 equiv. PhSNa added.

REFERENCES CITED

1. Abe, K.; Kimura, H., The possible role of hydrogen sulfide as an endogenous neuromodulator. *Journal of Neuroscience* **1996,** *16* (3), 1066-1071.

2. Li, L.; Hsu, A.; Moore, P. K., Actions and interactions of nitric oxide, carbon monoxide and hydrogen sulphide in the cardiovascular system and in inflammation - a tale of three gases! *Pharmacology & Therapeutics* **2009,** *123* (3), 386-400.

3. Wang, R., Two's company, three's a crowd: can H2S be the third endogenous gaseous transmitter? *Faseb Journal* **2002,** *16* (13), 1792-1798.

4. Cuevasanta, E.; Moller, M. N.; Alvarez, B., Biological chemistry of hydrogen sulfide and persulfides. *Archives of Biochemistry and Biophysics* **2017,** *617*, 9-25.

5. Hartle, M. D.; Pluth, M. D., A practical guide to working with H2S at the interface of chemistry and biology. *Chemical Society Reviews* **2016,** *45* (22), 6108-6117.

6. Li, Q.; Lancaster, J. R., Chemical foundations of hydrogen sulfide biology. *Nitric Oxide-Biology and Chemistry* **2013,** *35*, 21-34.

7. Ono, K.; Akaike, T.; Sawa, T.; Kumagai, Y.; Wink, D. A.; Tantillo, D. J.; Hobbs, A. J.; Nagy, P.; Xian, M.; Lin, J.; Fukuto, J. M., Redox chemistry and chemical biology of H2S, hydropersulfides, and derived species: Implications of their possible biological activity and utility. *Free Radical Biology and Medicine* **2014,** *77*, 82-94.

8. Szabo, C., A timeline of hydrogen sulfide (H2S) research: From environmental toxin to biological mediator. *Biochemical pharmacology* **2018,** *149*, 5-19.

9. Zhao, Y.; Biggs, T. D.; Xian, M., Hydrogen sulfide (H2S) releasing agents: chemistry and biological applications. *Chemical Communications* **2014,** *50* (80), 11788-11805.

10. Calvert, J. W.; Coetzee, W. A.; Lefer, D. J., Novel Insights Into Hydrogen Sulfide-Mediated Cytoprotection. *Antioxidants & redox signaling* **2010,** *12* (10), 1203-1217.

11. Cao, X.; Ding, L.; Xie, Z. Z.; Yang, Y.; Whiteman, M.; Moore, P. K.; Bian, J. S., A Review of Hydrogen Sulfide Synthesis, Metabolism, and Measurement: Is Modulation of Hydrogen Sulfide a Novel Therapeutic for Cancer? *Antioxidants & redox signaling* **2019,** *31* (1), 1-38.

12. Durante, W., Hydrogen Sulfide Therapy in Diabetes-Accelerated Atherosclerosis: A Whiff of Success. *Diabetes* **2016,** *65* (10), 2832-2834.

13. Kasinath, B. S.; Feliers, D.; Lee, H. J., Hydrogen sulfide as a regulatory factor in kidney health and disease. *Biochemical pharmacology* **2018,** *149*, 29-41.

14. Kolluru, G. K.; Shen, X. G.; Bir, S. C.; Kevil, C. G., Hydrogen sulfide chemical biology: Pathophysiological roles and detection. *Nitric Oxide-Biology and Chemistry* **2013,** *35*, 5-20.

15. Cao, X.; Cao, L.; Ding, L.; Bian, J. S., A New Hope for a Devastating Disease: Hydrogen Sulfide in Parkinson's Disease. *Molecular Neurobiology* **2018,** *55* (5), 3789-3799.

16. Panthi, S.; Manandhar, S.; Gautam, K., Hydrogen sulfide, nitric oxide, and neurodegenerative disorders. *Translational Neurodegeneration* **2018,** *7*.

17. Shefa, U.; Kim, M. S.; Jeong, N. Y.; Jung, J., Antioxidant and Cell-Signaling Functions of Hydrogen Sulfide in the Central Nervous System. *Oxidative Medicine and Cellular Longevity* **2018,** *2018*.

18. Chen, Y. H.; Wang, R., The message in the air: Hydrogen sulfide metabolism in chronic respiratory diseases. *Respiratory Physiology & Neurobiology* **2012,** *184* (2), 130-138.

19. Donnarumma, E.; Trivedi, R. K.; Lefer, D. J., Protective Actions of H2S in Acute Myocardial Infarction and Heart Failure. *Comprehensive Physiology* **2017,** *7* (2), 583-602.

20. Wu, D. D.; Wang, J.; Li, H.; Xue, M. Z.; Ji, A. L.; Li, Y. Z., Role of Hydrogen Sulfide in Ischemia-Reperfusion Injury. *Oxidative Medicine and Cellular Longevity* **2015,** *2015*.

21. Yu, X. H.; Cui, L. B.; Wu, K.; Zheng, X. L.; Cayabyab, F. S.; Chen, Z. W.; Tang, C. K., Hydrogen sulfide as a potent cardiovascular protective agent. *Clinica Chimica Acta* **2014,** *437*, 78-87.

22. Kondo, K.; Bhushan, S.; King, A. L.; Prabhu, S. D.; Hamid, T.; Koenig, S.; Murohara, T.; Predmore, B. L.; Gojon, G.; Gojon, G.; Wang, R.; Karusula, N.; Nicholson, C. K.; Calvert, J. W.; Lefer, D. J., H2S Protects Against Pressure Overload-Induced Heart Failure via Upregulation of Endothelial Nitric Oxide Synthase. *Circulation* **2013,** *127* (10), 1116-+.

23. Kohn, C. D., G.; Huang, Y.; Gollasch, M., Hydrogen Sulfide: Potent Regulator of Vascular Tone and Stimulator of Angiogenesis *Int. J. Biomed. Sci.* **2012,** *8* (2), 81-86.

24. Wang, G. G.; Li, W.; Chen, Q. Y.; Jiang, Y. X.; Lu, X. H.; Zhao, X., Hydrogen sulfide accelerates wound healing in diabetic rats. *International Journal of Clinical and Experimental Pathology* **2015,** *8* (5), 5097-5104.

25. Zheng, D. C., Z.; Chen, J.; Zhuang, X.; Feng, J.; Li, J., Exogenous hydrogen sulfide exerts proliferation, anti-apoptosis, migration effects and accelerates cell cycle progression in multiple myeloma cells via activating the Akt pathway. *Oncology Reports* **2016,** *36* (4), 1909-1916.

26. Alshorafa, A. K. H.; Guo, Q.; Zeng, F. Q.; Chen, M. C.; Tan, G. Z.; Tang, Z. Q.; Yin, R. F., Psoriasis Is Associated with Low Serum Levels of Hydrogen Sulfide, a Potential Anti-inflammatory Molecule. *Tohoku Journal of Experimental Medicine* **2012,** *228* (4), 325-332.

27. Yang, G. D.; Sun, X. F.; Wang, R., Hydrogen sulfide-induced apoptosis of human aorta smooth muscle cells via the activation of mitogen-activated protein kinases and caspase-3. *Faseb Journal* **2004,** *18* (12), 1782-+.

28. Gemici, B.; Wallace, J. L., Anti-inflammatory and Cytoprotective Properties of Hydrogen Sulfide. In *Hydrogen Sulfide in Redox Biology, Pt B*, Cadenas, E.; Packer, L., Eds. 2015; Vol. 555, pp 169-193.

29. Wallace, J. L., Hydrogen sulfide-releasing anti-inflammatory drugs. *Trends in Pharmacological Sciences* **2007,** *28* (10), 501-505.

30. Wallace, J. L.; Blackler, R. W.; Chan, M. V.; Da Silva, G. J.; Elsheikh, W.; Flannigan, K. L.; Gamaniek, I.; Manko, A.; Wang, L.; Motta, J. P.; Buret, A. G., Anti-Inflammatory and Cytoprotective Actions of Hydrogen Sulfide: Translation to Therapeutics. *Antioxidants & redox signaling* **2015,** *22* (5), 398-410.

31. Wu, D.; Hu, Q. X.; Liu, X. H.; Pan, L. L.; Xiong, Q. H.; Zhu, Y. Z., Hydrogen sulfide protects against apoptosis under oxidative stress through SIRT1 pathway in H9c2 cardiomyocytes. *Nitric Oxide-Biology and Chemistry* **2015,** *46*, 204-212.

32. Giggenbach, W., Optical Spectra of Highly Alkaline Sulfide Solutions and the Second Dissociation Constant of Hydrogen Sulfide. *Inorganic Chemistry* **1971,** *10* (7), 1333-1338.

33. DeLeon, E. R.; Stoy, G. F.; Olson, K. R., Passive loss of hydrogen sulfide in biological experiments. *Analytical Biochemistry* **2012,** *421* (1), 203-207.

34. Whiteman, M.; Li, L.; Rose, P.; Tan, C. H.; Parkinson, D. B.; Moore, P. K., The Effect of Hydrogen Sulfide Donors on Lipopolysaccharide-Induced Formation of Inflammatory Mediators in Macrophages. *Antioxidants & redox signaling* **2010,** *12* (10), 1147-1154.

35. Bora, P.; Chauhan, P.; Pardeshi, K. A.; Chakrapani, H., Small molecule generators of biologically reactive sulfur species. *Rsc Advances* **2018,** *8* (48), 27359-27374.

36. Dillon, K. M.; Powell, C. R.; Matson, J. B., Self-Immolative Prodrugs: Effective Tools for the Controlled Release of Sulfur Signaling Species. *Synlett* **2019,** *30* (5), 525-531.

37. Papapetropoulos, A.; Whiteman, M.; Cirino, G., Pharmacological tools for hydrogen sulphide research: a brief, introductory guide for beginners. *British Journal of Pharmacology* **2015,** *172* (6), 1633-1637.

38. Powell, C. R.; Dillon, K. M.; Matson, J. B., A review of hydrogen sulfide (H2S) donors: Chemistry and potential therapeutic applications. *Biochemical pharmacology* **2018,** *149*, 110-123.

39. Song, Z. J.; Ng, M. Y.; Lee, Z. W.; Dai, W.; Hagen, T.; Moore, P. K.; Huang, D.; Deng, L. W.; Tan, C. H., Hydrogen sulfide donors in research and drug development. *Medchemcomm* **2014,** *5* (5), 557-570.

40. Szabo, C.; Papapetropoulos, A., International Union of Basic and Clinical Pharmacology. CII: Pharmacological Modulation of H2S Levels: H2S Donors and H2S Biosynthesis Inhibitors. *Pharmacological Reviews* **2017,** *69* (4), 497-564.

41. Wu, D.; Hu, Q. X.; Zhu, Y. Z., Therapeutic application of hydrogen sulfide donors: the potential and challenges. *Frontiers of Medicine* **2016,** *10* (1), 18-27.

42. Steiger, A. K.; Pardue, S.; Kevil, C. G.; Pluth, M. D., Self-Immolative Thiocarbamates Provide Access to Triggered H2S Donors and Analyte Replacement Fluorescent Probes. *Journal of the American Chemical Society* **2016,** *138* (23), 7256-9.

43. Lehrman, L., Thioacetamide as a source of hydrogen sulfide in qualitative analysis. *Journal of Chemical Education* **1955,** *32* (9), 474-475.

44. Martelli, A.; Testai, L.; Citi, V.; Marino, A.; Pugliesi, I.; Barresi, E.; Nesi, G.; Rapposelli, S.; Taliani, S.; Da Settimo, F.; Breschi, M. C.; Calderone, V., Arylthioamides as H2S Donors: L-Cysteine-Activated Releasing Properties and Vascular Effects in Vitro and in Vivo. *Acs Medicinal Chemistry Letters* **2013,** *4* (10), 904-908.

45. Zhou, Z.; von Wantoch Rekowski, M.; Coletta, C.; Szabo, C.; Bucci, M.; Cirino, G.; Topouzis, S.; Papapetropoulos, A.; Giannis, A., Thioglycine and L-thiovaline: biologically active H_2S-donors. *Bioorganic & Medicinal Chemistry Letters* **2012,** *20* (8), 2675-8.

46. Lecher, H. Z.; Greenwood, R. A.; Whitehouse, K. C.; Chao, T. H., The Phosphonation of Aromatic Compounds with Phosphorus Pentasulfide. *Journal of the American Chemical Society* **1956,** *78* (19), 5018-5022.

47. Pedersen, B. S.; Scheibye, S.; Nilsson, N. H.; Lawesson, S. O., Studies on organophosphorus compounds XX. syntheses of thioketones. *Bulletin des Sociétés Chimiques Belges* **1978,** *87* (3), 223-228.

48. Li, L.; Whiteman, M.; Guan, Y. Y.; Neo, K. L.; Cheng, Y.; Lee, S. W.; Zhao, Y.; Baskar, R.; Tan, C. H.; Moore, P. K., Characterization of a novel, water-soluble hydrogen sulfide-releasing molecule (GYY4137): new insights into the biology of hydrogen sulfide. *Circulation* **2008,** *117* (18), 2351-2360.

49. Park, C. M.; Zhao, Y.; Zhu, Z.; Pacheco, A.; Peng, B.; Devarie-Baez, N. O.; Bagdon, P.; Zhang, H.; Xian, M., Synthesis and evaluation of phosphorodithioate-based hydrogen sulfide donors. *Molecular Biosystems* **2013,** *9* (10), 2430-2434.

50. Feng, W.; Teo, X. Y.; Novera, W.; Ramanujulu, P. M.; Liang, D.; Huang, D.; Moore, P. K.; Deng, L. W.; Dymock, B. W., Discovery of New H_2S Releasing Phosphordithioates and 2,3-Dihydro-2-phenyl-2-sulfanylenebenzo[d][1,3,2]oxazaphospholes with Improved Antiproliferative Activity. *Journal of Medicinal Chemistry* **2015,** *58* (16), 6456-6480.

51. Kang, J.; Li, Z.; Organ, C. L.; Park, C. M.; Yang, C. T.; Pacheco, A.; Wang, D.; Lefer, D. J.; Xian, M., pH-Controlled Hydrogen Sulfide Release for Myocardial Ischemia-Reperfusion Injury. *Journal of the American Chemical Society* **2016,** *138* (20), 6336-6339.

52. Sagi, A.; Weinstain, R.; Karton, N.; Shabat, D., Self-immolative polymers. *Journal of the American Chemical Society* **2008,** *130* (16), 5434-5435.

53. Zhao, Y.; Steiger, A. K.; Pluth, M. D., Colorimetric Carbonyl Sulfide (COS) / Hydrogen Sulfide (H_2S) Donation from gamma-Ketothiocarbamate Donor Motifs. *Angewandte Chemie-International Edition* **2018,** *57* (40), 13101-13105.

54. Gilbert, A. K.; Zhao, Y.; Otteson, C. E.; Pluth, M. D., Development of Acid-Mediated H_2S/COS Donors that Respond to a Specific pH Window *The Journal of Organic Chemistry* **2019**, in press.

55. Barresi, E.; Nesi, G.; Citi, V.; Piragine, E.; Piano, I.; Taliani, S.; Da Settimo, F.; Rapposelli, S.; Testai, L.; Breschi, M. C.; Gargini, C.; Calderone, V.; Martelli, A., Iminothioethers as Hydrogen Sulfide Donors: From the Gasotransmitter Release to the Vascular Effects. *J. Med. Chem.* **2017,** *60* (17), 7512-7523.

56. Martelli, A.; Testai, L.; Citi, V.; Marino, A.; Bellagambi, F. G.; Ghimenti, S.; Breschi, M. C.; Calderone, V., Pharmacological characterization of the vascular effects of aryl isothiocyanates: is hydrogen sulfide the real player? *Vascul Pharmacol* **2014,** *60* (1), 32-41.

57. Lin, Y.; Yang, X.; Lu, Y.; Liang, D.; Huang, D., Isothiocyanates as H_2S Donors Triggered by Cysteine: Reaction Mechanism and Structure and Activity Relationship. *Organic Letters* **2019,** *21*, 5911-5980.

58. Dawson, P. E.; Muir, T. W.; Clark-Lewis, I.; Kent, S. B., Synthesis of proteins by native chemical ligation. *Science* **1994,** *266* (5186), 776-779.

59. Cerda, M. M.; Zhao, Y.; Pluth, M. D., Thionoesters: A Native Chemical Ligation-Inspired Approach to Cysteine-Triggered H_2S Donors. *Journal of the American Chemical Society* **2018,** *140* (39), 12574-12579.

60. Cerda, M. M.; Newton, T. D.; Zhao, Y.; Collins, B. K.; Hendon, C. H.; Pluth, M. D., Dithioesters: simple, tunable, cysteine-selective H_2S donors. *Chemical Science* **2019,** *10* (6), 1773-1779.

61. Kim, N. H.; Moon, H.; Kim, J. H.; Huh, Y.; Kim, Y. J.; Kim, B. M.; Kim, D., A benzothioate native chemical ligation-based cysteine-selective fluorescent probe. *Dyes and Pigments* **2019,** *171*, 107764.

62. Zhao, Y.; Kang, J.; Park, C. M.; Bagdon, P. E.; Peng, B.; Xian, M., Thiol-activated gem-dithiols: a new class of controllable hydrogen sulfide donors. *Organic Letters* **2014,** *16* (17), 4536-4539.

63. Zhu, Y.; Romero, E. L.; Ren, X.; Sanca, A. J.; Du, C.; Liu, C.; Karim, Z. A.; Alshbool, F. Z.; Khasawneh, F. T.; Zhou, J.; Zhong, D.; Geng, B., Clopidogrel as a donor probe and thioenol derivatives as flexible promoieties for enabling H_2S biomedicine. *Nature Communications* **2018,** *9* (1), 3952.

64. Zhao, Y.; Wang, H.; Xian, M., Cysteine-activated hydrogen sulfide (H_2S) donors. *Journal of the American Chemical Society* **2011,** *133* (1), 15-17.

65. Zhao, Y.; Yang, C.; Organ, C.; Li, Z.; Bhushan, S.; Otsuka, H.; Pacheco, A.; Kang, J.; Aguilar, H. C.; Lefer, D. J.; Xian, M., Design, Synthesis, and Cardioprotective Effects of N-Mercapto-Based Hydrogen Sulfide Donors. *Journal of Medicinal Chemistry* **2015,** *58* (18), 7501-7511.

66. Zhao, Y.; Bhushan, S.; Yang, C.; Otsuka, H.; Stein, J. D.; Pacheco, A.; Peng, B.; Devarie-Baez, N. O.; Aguilar, H. C.; Lefer, D. J.; Xian, M., Controllable hydrogen sulfide donors and their activity against myocardial ischemia-reperfusion injury. *ACS Chemical Biology* **2013,** *8* (6), 1283-1290.

67. Foster, J. C.; Powell, C. R.; Radzinski, S. C.; Matson, J. B., S-aroylthiooximes: a facile route to hydrogen sulfide releasing compounds with structure-dependent release kinetics. *Organic Letters* **2014,** *16* (6), 1558-1561.

68. Kang, J.; Ferrell, A. J.; Chen, W.; Wang, D.; Xian, M., Cyclic Acyl Disulfides and Acyl Selenylsulfides as the Precursors for Persulfides (RSSH), Selenylsulfides (RSeSH), and Hydrogen Sulfide (H_2S). *Organic Letters* **2018,** *20* (3), 852-855.

69. Hamsath, A.; Wang, Y.; Yang, C. T.; Xu, S.; Canedo, D.; Chen, W.; Xian, M., Acyl Selenyl Sulfides as the Precursors for Reactive Sulfur Species (Hydrogen Sulfide, Polysulfide, and Selenyl Sulfide). *Organic Letters* **2019,** *21* (14), 5685-5688.

70. Roger, T.; Raynaud, F.; Bouillaud, F.; Ransy, C.; Simonet, S.; Crespo, C.; Bourguignon, M. P.; Villeneuve, N.; Vilaine, J. P.; Artaud, I.; Galardon, E., New biologically active hydrogen sulfide donors. *ChemBioChem* **2013,** *14* (17), 2268-2271.

71. Park, C. M.; Weerasinghe, L.; Day, J. J.; Fukuto, J. M.; Xian, M., Persulfides: current knowledge and challenges in chemistry and chemical biology. *Molecular Biosystems* **2015,** *11* (7), 1775-1785.

72. Pluth, M.; Bailey, T.; Hammers, M.; Hartle, M.; Henthorn, H.; Steiger, A., Natural Products Containing Hydrogen Sulfide Releasing Moieties. *Synlett* **2015,** *26* (19), 2633-2643.

73. Benavides, G. A.; Squadrito, G. L.; Mills, R. W.; Patel, H. D.; Isbell, T. S.; Patel, R. P.; Darley-Usmar, V. M.; Doeller, J. E.; Kraus, D. W., Hydrogen sulfide mediates the vasoactivity of garlic. *Proceedings of the National Academy of Sciences, USA* **2007,** *104* (46), 17977-17982.

74. Liang, D.; Wu, H.; Wong, M. W.; Huang, D., Diallyl Trisulfide Is a Fast H_2S Donor, but Diallyl Disulfide Is a Slow One: The Reaction Pathways and Intermediates of Glutathione with Polysulfides. *Organic Letters* **2015,** *17* (17), 4196-4199.

75. Cai, Y. R.; Hu, C. H., Computational Study of H2S Release in Reactions of Diallyl Polysulfides with Thiols. *Journal of Physical Chemistry B* **2017,** *121* (26), 6359-6366.

76. Yao, H.; Luo, S.; Liu, J.; Xie, S.; Liu, Y.; Xu, J.; Zhu, Z.; Xu, S., Controllable thioester-based hydrogen sulfide slow-releasing donors as cardioprotective agents. *Chemical Communications* **2019,** *55* (44), 6193-6196.

77. Cerda, M. M.; Hammers, M. D.; Earp, M. S.; Zakharov, L. N.; Pluth, M. D., Applications of Synthetic Organic Tetrasulfides as H_2S Donors. *Organic Letters* **2017,** *19* (9), 2314-2317.

78. Bolton, S. G.; Cerda, M. M.; Gilbert, A. K.; Pluth, M. D., Effects of sulfane sulfur content in benzyl polysulfides on thiol-triggered H2S release and cell proliferation. *Free Radical Biology and Medicine* **2019,** *131*, 393-398.

79. Toohey, J. I., Sulfur signaling: is the agent sulfide or sulfane? *Anal Biochem* **2011,** *413* (1), 1-7.

80. Ercole, F.; Whittaker, M. R.; Halls, M. L.; Boyd, B. J.; Davis, T. P.; Quinn, J. F., Garlic-inspired trisulfide linkers for thiol-stimulated H_2S release. *Chemical Communications* **2017,** *53* (57), 8030-8033.

81. Zhao, Y.; Cerda, M. M.; Pluth, M. D., Fluorogenic hydrogen sulfide (H_2S) donors based on sulfenyl thiocarbonates enable H_2S tracking and quantification. *Chemical Science* **2019,** *10* (6), 1873-1878.

82. Zhao, Y.; Steiger, A. K.; Pluth, M. D., Cysteine-activated hydrogen sulfide (H_2S) delivery through caged carbonyl sulfide (COS) donor motifs. *Chemical Communications* **2018,** *54* (39), 4951-4954.

83. Severino, B.; Corvino, A.; Fiorino, F.; Luciano, P.; Frecentese, F.; Magli, E.; Saccone, I.; Di Vaio, P.; Citi, V.; Calderone, V.; Servillo, L.; Casale, R.; Cirino, G.; Vellecco, V.; Bucci, M.; Perissutti, E.; Santagada, V.; Caliendo, G., 1,2,4-Thiadiazolidin-3,5-diones as novel hydrogen sulfide donors. *European Journal of Medicinal Chemistry* **2018,** *143*, 1677-1686.

84. Ai, X. Z.; Mu, J.; Xing, B. G., Recent Advances of Light-Mediated Theranostics. *Theranostics* **2016,** *6* (13), 2439-2457.

85. Chen, H. Z.; Zhao, Y. L., Applications of Light-Responsive Systems for Cancer Theranostics. *ACS Applied Materials & Interfaces* **2018,** *10* (25), 21021-21034.

86. Devarie-Baez, N. O.; Bagdon, P. E.; Peng, B.; Zhao, Y.; Park, C. M.; Xian, M., Light-Induced Hydrogen Sulfide Release from "Caged" gem-Dithiols. *Organic Letters* **2013,** *15* (11), 2786-2789.

87. Zheng, Y. Y.; Ji, X. Y.; Ji, K. L.; Wang, B. H., Hydrogen sulfide prodrugs-a review. *Acta Pharmaceutica Sinica B* **2015,** *5* (5), 367-377.

88. Li, Z. H.; Li, D. A.; Wang, L.; Lu, C. J.; Shan, P. F.; Zou, X. L.; Li, Z. Y., Photocontrollable water-soluble polymeric hydrogen sulfide (H_2S) donor. *Polymer* **2019,** *168*, 16-20.

89. Chen, W. S.; Chen, M.; Zang, Q. G.; Wang, L. Q.; Tang, F. Y.; Han, Y. J.; Yang, C. J.; Deng, L.; Liu, Y. N., NIR light controlled release of caged hydrogen sulfide based on upconversion nanoparticles. *Chemical Communications* **2015,** *51* (44), 9193-9196.

90. Fukushima, N.; Ieda, N.; Sasakura, K.; Nagano, T.; Hanaoka, K.; Suzuki, T.; Miyata, N.; Nakagawa, H., Synthesis of a photocontrollable hydrogen sulfide donor using ketoprofenate photocages. *Chemical Communications* **2014,** *50* (5), 587-589.

91. Fukushima, N.; Ieda, N.; Kawaguchi, M.; Sasakura, K.; Nagano, T.; Hanaoka, K.; Miyata, N.; Nakagawa, H., Development of photo-controllable hydrogen sulfide donor applicable in live cells. *Bioorganic & Medicinal Chemistry Letters* **2015,** *25* (2), 175-178.

92. Xiao, Z. Y.; Bonnard, T.; Shakouri-Motlagh, A.; Wylie, R. A. L.; Collins, J.; White, J.; Heath, D. E.; Hagemeyer, C. E.; Connal, L. A., Triggered and Tunable Hydrogen Sulfide Release from Photogenerated Thiobenzaldehydes. *Chemistry-a European Journal* **2017,** *23* (47), 11294-11300.

93. Yi, S. Y.; Moon, Y. K.; Kim, S.; Kim, S.; Park, G.; Kim, J. J.; You, Y., Visible light-driven photogeneration of hydrogen sulfide. *Chemical Communications* **2017,** *53* (86), 11830-11833.

94. Woods, J. J.; Cao, J.; Lippert, A. R.; Wilson, J. J., Characterization and Biological Activity of a Hydrogen Sulfide-Releasing Red Light-Activated Ruthenium(II) Complex. *Journal of the American Chemical Society* **2018,** *140* (39), 12383-12387.

95. Luo, X. J.; Wu, J. B.; Lv, T.; Lai, Y. S.; Zhang, H. H.; Lu, J. J.; Zhang, Y. H.; Huang, Z. J., Synthesis and evaluation of novel O_2-derived diazeniumdiolates as photochemical and real-time monitoring nitric oxide delivery agents. *Organic Chemistry Frontiers* **2017,** *4* (12), 2445-2449.

96. Venkatesh, Y.; Das, J.; Chaudhuri, A.; Karmakar, A.; Maiti, T. K.; Singh, N. D. P., Light triggered uncaging of hydrogen sulfide (H_2S) with real-time monitoring. *Chemical Communications* **2018,** *54* (25), 3106-3109.

97. Zhao, Y.; Bolton, S. G.; Pluth, M. D., Light-Activated COS/H2S Donation from Photocaged Thiocarbamates. *Organic Letters* **2017,** *19* (9), 2278-2281.

98. Zheng, Y. Q.; Yu, B. C.; Ji, K. L.; Pan, Z. X.; Chittavong, V.; Wang, B. H., Esterase-Sensitive Prodrugs with Tunable Release Rates and Direct Generation of Hydrogen Sulfide. *Angewandte Chemie-International Edition* **2016,** *55* (14), 4514-4518.

99. Fukami, T.; Yokoi, T., The Emerging Role of Human Esterases. *Drug Metabolism and Pharmacokinetics* **2012,** *27* (5), 466-477.

100. Brown, J. M.; William, W. R., Exploiting tumour hypoxia in cancer treatment. *Nature Reviews Cancer* **2004,** *4* (6), 437-447.

101. Wilson, W. R.; Hay, M. P., Targeting hypoxia in cancer therapy. *Nature Reviews Cancer* **2011,** *11* (6), 393-410.

102. Shukla, P.; Khodade, V. S.; SharathChandra, M.; Chauhan, P.; Mishra, S.; Siddaramappa, S.; Pradeep, B. E.; Singh, A.; Chakrapani, H., "On demand" redox buffering by H_2S contributes to antibiotic resistance revealed by a bacteria-specific H_2S donor. *Chemical Science* **2017,** *8* (7), 4967-4972.

103. Chauhan, P.; Bora, P.; Ravikumar, G.; Jos, S.; Chakrapani, H., Esterase Activated Carbonyl Sulfide/Hydrogen Sulfide (H_2S) Donors. *Org. Lett.* **2017,** *19* (1), 62-65.

104. Steiger, A. K.; Marcatti, M.; Szabo, C.; Szczesny, B.; Pluth, M. D., Inhibition of Mitochondrial Bioenergetics by Esterase-Triggered COS/H_2S Donors. *ACS Chem. Biol.* **2017,** *12* (8), 2117-2123.

105. Chengelis, C. P.; Neal, R. A., Studies of carbonyl sulfide toxicity: Metabolism by carbonic anhydrase. *Toxicology and Applied Pharmacology* **1980,** *55* (1), 198-202.

106. Steiger, A. K.; Zhao, Y.; Pluth, M. D., Emerging Roles of Carbonyl Sulfide in Chemical Biology: Sulfide Transporter or Gasotransmitter? *Antioxid. Redox Signal.* **2018,** *28* (16), 1516-1532.

107. Haritos, V. S.; Dojchinov, G., Carbonic anhydrase metabolism is a key factor in the toxicity of CO2 and COS but not CS2 toward the flour beetle Tribolium castaneum Coleoptera : Tenebrionidae. *Comp. Biochem. Physiol. C-Toxicol. Pharmacol.* **2005,** *140* (1), 139-147.

108. Kernohan, J. C., The activity of bovine carbonic anhydrase in imidazole buffers. *Biochimica et Biophysica Acta (BBA) - Specialized Section on Enzymological Subjects* **1964,** *81* (2), 346-356.

109. Lindskog, S., Structure and mechanism of carbonic anhydrase. *Pharmacology & Therapeutics* **1997,** *74* (1), 1-20.

110. Maren, T. H., Carbonic Anhydrase - Chemistry, Physiology, and Inhibition. *Physiol. Rev.* **1967,** *47* (4), 595-+.

111. Steiger, A. K.; Pardue, S.; Kevil, C. G.; Pluth, M. D., Self-Immolative Thiocarbamates Provide Access to Triggered H_2S Donors and Analyte Replacement Fluorescent Probes. *J. Am. Chem. Soc.* **2016,** *138* (23), 7256-7259.

112. Zhao, Y.; Pluth, M., Hydrogen Sulfide Donors Activated by Reactive Oxygen Species. *Free Radical Biology and Medicine* **2016,** *100*, S28-S28.

113. Zhao, Y.; Henthorn, H. A.; Pluth, M. D., Kinetic Insights into Hydrogen Sulfide Delivery from Caged-Carbonyl Sulfide Isomeric Donor Platforms. *J. Am. Chem. Soc.* **2017,** *139* (45), 16365-16376.

114. Sharma, A. K.; Nair, M.; Chauhan, P.; Gupta, K.; Saini, D. K.; Chakrapani, H., Visible-Light-Triggered Uncaging of Carbonyl Sulfide for Hydrogen Sulfide (H_2S) Release. *Organic Letters* **2017,** *19* (18), 4822-4825.

115. Stacko, P.; Muchova, L.; Vitek, L.; Klan, P., Visible to NIR Light Photoactivation of Hydrogen Sulfide for Biological Targeting. *Organic Letters* **2018,** *20* (16), 4907-4911.

116. Levinn, C. M.; Steiger, A. K.; Pluth, M. D., Esterase-Triggered Self-Immolative Thiocarbamates Provide Insights into COS Cytotoxicity. *ACS chemical biology* **2019,** *14* (2), 170-175.

117. Tian, L.; Yang, Y. L.; Wysocki, L. M.; Arnold, A. C.; Hu, A.; Ravichandran, B.; Sternson, S. M.; Looger, L. L.; Lavis, L. D., Selective esterase-ester pair for targeting small molecules with cellular specificity. *Proc. Natl. Acad. Sci. USA* **2012,** *109* (13), 4756-4761.

118. Steiger, A. K.; Yang, Y.; Royzen, M.; Pluth, M. D., Bio-orthogonal "click-and-release" donation of caged carbonyl sulfide (COS) and hydrogen sulfide (H2S). *Chemical Communications* **2017,** *53* (8), 1378-1380.

119. Siegel, L. M., A direct microdetermination for sulfide. *Analytical Biochemistry* **1965,** *11* (1), 126-132.

120. Henthorn, H. A.; Pluth, M. D., Mechanistic Insights into the H_2S-Mediated Reduction of Aryl Azides Commonly Used in H_2S Detection. *J. Am. Chem. Soc.* **2015,** *137* (48), 15330-6.

121. Hammers, M. D.; Taormina, M. J.; Cerda, M. M.; Montoya, L. A.; Seidenkranz, D. T.; Parthasarathy, R.; Pluth, M. D., A Bright Fluorescent Probe for H2S Enables Analyte-Responsive, 3D Imaging in Live Zebrafish Using Light Sheet Fluorescence Microscopy. *Journal of the American Chemical Society* **2015,** *137* (32), 10216-23.

122. Montoya, L. A.; Pluth, M. D., Selective turn-on fluorescent probes for imaging hydrogen sulfide in living cells. *Chemical communications* **2012,** *48* (39), 4767-9.

123. Zhao, Y.; Steiger, A. K.; Pluth, M. D., Colorimetric Carbonyl Sulfide (COS)/Hydrogen Sulfide (H2S) Donation from gamma-Ketothiocarbamate Donor Motifs. *Angewandte Chemie-International Edition* **2018,** *57* (40), 13101-13105.

124. Polhemus, D. J.; Calvert, J. W.; Butler, J.; Lefer, D. J., The cardioprotective actions of hydrogen sulfide in acute myocardial infarction and heart failure. *Scientifica* **2014,** *2014*, 768607.

125. Wang, R., Physiological implications of hydrogen sulfide: a whiff exploration that blossomed. *Physiological Reviews* **2012,** *92*, 791-896.

126. Powell, C. R.; Dillon, K. M.; Matson, J. B., A review of hydrogen sulfide (H_2S) donors: Chemistry and potential therapeutic applications. *Biochemical pharmacology* **2018,** *149*, 110-123.

127. Zhao, Y.; Henthorn, H. A.; Pluth, M. D., Kinetic Insights into Hydrogen Sulfide Delivery from Caged-Carbonyl Sulfide Isomeric Donor Platforms. *Journal of the American Chemical Society* **2017,** *139* (45), 16365-16376.

128. Zhao, Y.; Pluth, M. D., Hydrogen Sulfide Donors Activated by Reactive Oxygen Species. *Angewandte Chemie-International Edition* **2016,** *55* (47), 14638-14642.

129. Powell, C. R.; Foster, J. C.; Okyere, B.; Theus, M. H.; Matson, J. B., Therapeutic Delivery of H2S via COS: Small Molecule and Polymeric Donors with Benign Byproducts. *Journal of the American Chemical Society* **2016,** *138* (41), 13477-13480.

130. Zhao, Y.; Steiger, A. K.; Pluth, M. D., Cysteine-activated hydrogen sulfide (H2S) delivery through caged carbonyl sulfide (COS) donor motifs. *Chemical communications* **2018,** *54* (39), 4951-4954.

131. Zhao, Y.; Bolton, S. G.; Pluth, M. D., Light-Activated COS/H2S Donation from Photocaged Thiocarbamates. *Organic letters* **2017,** *19* (9), 2278-2281.

132. Balazy, M.; Abu-Yousef, I. A.; Harpp, D. N.; Park, J., Identification of carbonyl sulfide and sulfur dioxide in porcine coronary artery by gas chromatography/mass spectrometry, possible relevance to EDHF. *Biochemical and Biophysical Research Communications* **2003,** *311* (3), 728-734.

133. Kamboures, M. A.; Blake, D. R.; Cooper, D. M.; Newcomb, R. L.; Barker, M.; Larson, J. K.; Meinardi, S.; Nussbaum, E.; Rowland, F. S., Breath sulfides and pulmonary function in cystic fibrosis. *Proceedings of the National Academy of Sciences of the United States of America* **2005,** *102* (44), 15762-15767.

134. Sehnert, S. S.; Jiang, L.; Burdick, J. F.; Risby, T. H., Breath biomarkers for detection of human liver diseases: preliminary study. *Biomarkers* **2002,** *7* (2), 174-187.

135. Studer, S. M.; Orens, J. B.; Rosas, I.; Krishnan, J. A.; Cope, K. A.; Yang, S.; Conte, J. V.; Becker, P. B.; Risby, T. H., Patterns and significance of exhaled-breath biomarkers in lung transplant recipients with acute allograft rejection. *Journal of Heart and Lung Transplantation* **2001,** *20* (11), 1158-1166.

136. Haritos, V. S.; Dojchinov, G., Carbonic anhydrase metabolism is a key factor in the toxicity of CO2 and COS but not CS2 toward the flour beetle Tribolium castaneum [Coleoptera: Tenebrionidae]. *Comparative biochemistry and physiology. Toxicology & pharmacology : CBP* **2005,** *140* (1), 139-47.

137. Barton, P.; Laws, A. P.; Page, M. I., Structure-Activity-Relationships in the Esterase-Catalyzed Hydrolysis and Transesterification of Esters and Lactones. *J Chem Soc Perk T 2* **1994,** (9), 2021-2029.

138. Kistiakowsky, G. B.; Mangelsdorf, P. C., The Kinetics of Ester Hydrolysis by Liver Esterase. *Journal of the American Chemical Society* **1956,** *78* (13), 2964-2969.

139. Chauhan, P.; Bora, P.; Ravikumar, G.; Jos, S.; Chakrapani, H., Esterase Activated Carbonyl Sulfide/Hydrogen Sulfide (H2S) Donors. *Organic letters* **2017,** *19* (1), 62-65.

140. Lin, V. S.; Lippert, A. R.; Chang, C. J., Cell-trappable fluorescent probes for endogenous hydrogen sulfide signaling and imaging H2O2-dependent H2S production. *Proceedings of the National Academy of Sciences of the United States of America* **2013,** *110* (18), 7131-5.

141. Lin, V. S.; Chang, C. J., Fluorescent probes for sensing and imaging biological hydrogen sulfide. *Current Opinion in Chemical Biology* **2012,** *16* (5-6), 595-601.

142. Schindelin, J.; Arganda-Carreras, I.; Frise, E.; Kaynig, V.; Longair, M.; Pietzsch, T.; Preibisch, S.; Rueden, C.; Saalfeld, S.; Schmid, B.; Tinevez, J. Y.; White, D. J.; Hartenstein, V.; Eliceiri, K.; Tomancak, P.; Cardona, A., Fiji: an open-source platform for biological-image analysis. *Nature Methods* **2012,** *9* (7), 676-682.

143. Szabo, G.; Veres, G.; Radovits, T.; Gero, D.; Modis, K.; Miesel-Groschel, C.; Horkay, F.; Karck, M.; Szabo, C., Cardioprotective effects of hydrogen sulfide. *Nitric Oxide-Biology and Chemistry* **2011,** *25* (2), 201-210.

144. Gong, Q. H.; Shi, X. R.; Hong, Z. Y.; Pan, L. L.; Liu, X. H.; Zhu, Y. Z., A New Hope for Neurodegeneration: Possible Role of Hydrogen Sulfide. *Journal of Alzheimers Disease* **2011,** *24*, 173-182.

145. Hu, L. F.; Lu, M.; Tiong, C. X.; Dawe, G. S.; Hu, G.; Bian, J. S., Neuroprotective effects of hydrogen sulfide on Parkinson's disease rat models. *Aging Cell* **2010,** *9* (2), 135-46.

146. Vandini, E.; Ottani, A.; Zaffe, D.; Calevro, A.; Canalini, F.; Cavallini, G. M.; Rossi, R.; Guarini, S.; Giuliani, D., Mechanisms of Hydrogen Sulfide against the Progression of Severe Alzheimer's Disease in Transgenic Mice at Different Ages. *Pharmacology* **2019,** *103* (1-2), 50-60.

147. Muniraj, N.; Stamp, L. K.; Badiei, A.; Hegde, A.; Cameron, V.; Bhatia, M., Hydrogen sulfide acts as a pro-inflammatory mediator in rheumatic disease. *International Journal of Rheumatic Diseases* **2017,** *20* (2), 182-189.

148. Benedetti, F.; Curreli, S.; Krishnan, S.; Davinelli, S.; Cocchi, F.; Scapagnini, G.; Gallo, R. C.; Zella, D., Anti-inflammatory effects of H2S during acute bacterial infection: a review. *Journal of Translational Medicine* **2017,** *15*.

149. Winyard, M. W. P. G., Hydrogen sulfide and inflammation: the good, thebad, the ugly and the promising. *Expert Review of Clinical Pharmacology* **2011,** *4*, 13-32.

150. Yang, G.; Wu, L. Y.; Wang, R., Pro-apoptotic effect of endogenous H2S on human aorta smooth muscle cells. *Faseb Journal* **2006,** *20* (1), 553-+.

151. Shi, S.; Li, Q. S.; Li, H.; Zhang, L.; Xu, M.; Cheng, J. L.; Peng, C. H.; Xu, C. Q.; Tian, Y., Anti-apoptotic action of hydrogen sulfide is associated with early JNK inhibition. *Cell Biology International* **2009,** *33* (10), 1095-1101.

152. Zheng, D.; Chen, Z.; Chen, J. F.; Zhuang, X. M.; Feng, J. Q.; Li, J., Exogenous hydrogen sulfide exerts proliferation, anti-apoptosis, migration effects and accelerates cell cycle progression in multiple myeloma cells via activating the Akt pathway. *Oncology Reports* **2016,** *36* (4), 1909-1916.

153. Levinn, C. M.; Cerda, M. M.; Pluth, M. D., Activatable Small-Molecule Hydrogen Sulfide Donors. *Antioxidants & redox signaling* **2020,** *32* (2), 96-109.

154. Levinn, C. M.; Cerda, M. M.; Pluth, M. D., Development and Application of Carbonyl Sulfide-Based Donors for H2S Delivery. *Accounts of Chemical Research* **2019,** *52* (9), 2723-2731.

155. Gilbert, A. K.; Zhao, Y.; Otteson, C. E.; Pluth, M. D., Development of Acid-Mediated H2S/COS Donors That Respond to a Specific pH Window. *Journal of Organic Chemistry* **2019,** *84* (22), 14469-14475.

156. Levinn, C. M.; Steiger, A. K.; Pluth, M. D., Esterase-Triggered Self-Immolative Thiocarbamates Provide Insights into COS Cytotoxicity. *Acs Chemical Biology* **2019,** *14* (2), 170-175.

157. Chauhan, P.; Jos, S.; Chakrapani, H., Reactive Oxygen Species-Triggered Tunable Hydrogen Sulfide Release. *Organic Letters* **2018,** *20* (13), 3766-3770.

158. MacLellan, P.; Clayden, J., Enantioselective synthesis of tertiary thiols by intramolecular arylation of lithiated thiocarbamates. *Chemical Communications* **2011,** *47* (12), 3395-3397.

159. Siegel, L. M., A DIRECT MICRODETERMINATION FOR SULFIDE. *Analytical Biochemistry* **1965,** *11* (1), 126-&.

160. Kumar, M.; Francisco, J. S., Hydrogen Sulfide Induced Carbon Dioxide Activation by Metal-Free Dual Catalysis. *Chemistry-a European Journal* **2016,** *22* (13), 4359-4363.

161. DeMartino, A.; Zigler, D. F.; Fukuto, J. M.; Ford, P. C., Carbon disulfide. Just toxic or also bioregulatory and/or therapeutic? *Chemical Society Reviews* **2017,** *46* (1), 21-39.

162. Buszewski, B.; Ulanowska, A.; Ligor, T.; Jackowski, M.; Klodzinska, E.; Szeliga, J., Identification of volatile organic compounds secreted from cancer tissues and bacterial cultures. *Journal of Chromatography B-Analytical Technologies in the Biomedical and Life Sciences* **2008,** *868* (1-2), 88-94.

163. Phillips, M., DETECTION OF CARBON-DISULFIDE IN BREATH AND AIR - A POSSIBLE NEW RISK FACTOR FOR CORONARY-ARTERY DISEASE. *International Archives of Occupational and Environmental Health* **1992,** *64* (2), 119-123.

164. Phillips, M.; Sabas, M.; Greenberg, J., INCREASED PENTANE AND CARBON-DISULFIDE IN THE BREATH OF PATIENTS WITH SCHIZOPHRENIA. *Journal of Clinical Pathology* **1993,** *46* (9), 861-864.

165. DeMartino, A. W.; Souza, M. L.; Ford, P. C., Uncaging carbon disulfide. Delivery platforms for potential pharmacological applications: a mechanistic approach. *Chemical Science* **2017,** *8* (10), 7186-7196.

166. Ensafi, A. A.; Mansour, H. R.; Majlesi, R., Determination of trace amount of carbon disulfide in water by the spectrophotometric reaction-rate method. *Analytical Sciences* **2003,** *19* (12), 1679-1681.

167. Wei, H. J.; Li, X.; Tang, X. Q., Therapeutic benefits of H2S in Alzheimer's disease. *Journal of Clinical Neuroscience* **2014,** *21* (10), 1665-1669.

168. 2020 Alzheimer's disease facts and figures. *Alzheimers. Dement.* **2020,** *16* (3), 391-460.

169. Burns, A.; Iliffe, S., Alzheimer's disease. *Bmj-British Medical Journal* **2009,** *338*.

170. Morrison, L. D.; Smith, D. D.; Kish, S. J., Brain S-Adenosylmethionine levels are severely decreased in Alzheimer's disease. *Journal of Neurochemistry* **1996,** *67* (3), 1328-1331.

171. Di Meco, A.; Li, J. G.; Barrero, C.; Merali, S.; Pratico, D., Elevated levels of brain homocysteine directly modulate the pathological phenotype of a mouse model of tauopathy. *Molecular Psychiatry* **2019,** *24* (11), 1696-1706.

172. Tang, X. Q.; Shen, X. T.; Huang, Y. E.; Chen, R. Q.; Ren, Y. K.; Fang, H. R.; Zhuang, Y. Y.; Wang, C. Y., Inhibition of Endogenous Hydrogen Sulfide Generation is Associated with Homocysteine-Induced Neurotoxicity: Role of ERK1/2 Activation. *Journal of Molecular Neuroscience* **2011,** *45* (1), 60-67.

173. Giuliani, D.; Ottani, A.; Zaffe, D.; Galantucci, M.; Strinati, F.; Lodi, R.; Guarini, S., Hydrogen sulfide slows down progression of experimental Alzheimer's disease by targeting multiple pathophysiological mechanisms. *Neurobiology of Learning and Memory* **2013,** *104*, 82-91.

174. Witt, A.; Macdonald, N.; Kirkpatrick, P., Memantine hydrochloride. *Nature Reviews Drug Discovery* **2004,** *3* (2), 109-110.

175. Sestito, S.; Daniele, S.; Pietrobono, D.; Citi, V.; Bellusci, L.; Chiellini, G.; Calderone, V.; Martini, C.; Rapposelli, S., Memantine prodrug as a new agent for Alzheimer's Disease. *Scientific Reports* **2019,** *9*.

176. Cerda, M. M.; Mancuso, J. L.; Mullen, E. J.; Hendon, C. H.; Pluth, M. D., Use of Dithiasuccinoyl-Caged Amines Enables COS/H2S Release Lacking Electrophilic Byproducts. *Chemistry-a European Journal* **2020,** *26* (24), 5374-5380.

177. Randall, J. B.; Munsell, L. Y.; Morris, J. C.; Swarm, R.; Yarasheski, K. E.; Holtzman, D. M., Human amyloid-beta synthesis and clearance rates as measured in cerebrospinal fluid in vivo. *Nature Medicine* **2006,** *12* (7), 856-861.

178. Bezner, B. J.; Ryan, L. S.; Lippert, A. R., Reaction-Based Luminescent Probes for Reactive Sulfur, Oxygen, and Nitrogen Species: Analytical Techniques and Recent Progress. *Analytical Chemistry* **2020,** *92* (1), 309-326.

179. Lin, V. S.; Chen, W.; Xian, M.; Chang, C. J., Chemical probes for molecular imaging and detection of hydrogen sulfide and reactive sulfur species in biological systems. *Chemical Society Reviews* **2015,** *44* (14), 4596-4618.

180. Jiao, X. Y.; Li, Y.; Niu, J. Y.; Xie, X. L.; Wang, X.; Tang, B., Small-Molecule Fluorescent Probes for Imaging and Detection of Reactive Oxygen, Nitrogen, and Sulfur Species in Biological Systems. *Analytical Chemistry* **2018,** *90* (1), 533-555.

181. Yu, F. B.; Han, X. Y.; Chen, L. X., Fluorescent probes for hydrogen sulfide detection and bioimaging. *Chemical Communications* **2014,** *50* (82), 12234-12249.

182. Henthorn, H. A.; Pluth, M. D., Mechanistic Insights into the H2S-Mediated Reduction of Aryl Azides Commonly Used in H2S Detection. *Journal of the American Chemical Society* **2015,** *137* (48), 15330-15336.

183. Kolb, H. C.; Sharpless, K. B., The growing impact of click chemistry on drug discovery. *Drug Discovery Today* **2003,** *8* (24), 1128-1137.

184. O'Connor, L. J.; Mistry, I. N.; Collins, S. L.; Folkes, L. K.; Brown, G.; Conway, S. J.; Hammond, E. M., CYP450 Enzymes Effect Oxygen-Dependent Reduction of Azide-Based Fluorogenic Dyes. *Acs Central Science* **2017,** *3* (1), 20-30.

185. Lin, V. S.; Lippert, A. R.; Chang, C. J., Cell-trappable fluorescent probes for endogenous hydrogen sulfide signaling and imaging H2O2-dependent H2S production. *Proceedings of the National Academy of Sciences of the United States of America* **2013,** *110* (18), 7131-7135.

186. Cao, D. X.; Liu, Z. Q.; Verwilst, P.; Koo, S.; Jangjili, P.; Kim, J. S.; Lin, W. Y., Coumarin-Based Small-Molecule Fluorescent Chemosensors. *Chemical Reviews* **2019,** *119* (18), 10403-10519.

187. Loudet, A.; Burgess, K., BODIPY dyes and their derivatives: Syntheses and spectroscopic properties. *Chemical Reviews* **2007,** *107* (11), 4891-4932.

188. Lavis, L. D., Teaching Old Dyes New Tricks: Biological Probes Built from Fluoresceins and Rhodamines. In *Annual Review of Biochemistry, Vol 86*, Kornberg, R. D., Ed. 2017; Vol. 86, pp 825-843.

189. Shindy, H. A., Fundamentals in the chemistry of cyanine dyes: A review. *Dyes and Pigments* **2017,** *145*, 505-513.

190. Wang, K.; Peng, H. J.; Ni, N. T.; Dai, C. F.; Wang, B. H., 2,6-Dansyl Azide as a Fluorescent Probe for Hydrogen Sulfide. *Journal of Fluorescence* **2014,** *24* (1), 1-5.

191. Banerjee, S.; Veale, E. B.; Phelan, C. M.; Murphy, S. A.; Tocci, G. M.; Gillespie, L. J.; Frimannsson, D. O.; Kelly, J. M.; Gunnlaugsson, T., Recent advances in the development of 1,8-naphthalimide based DNA targeting binders, anticancer and fluorescent cellular imaging agents. *Chemical Society Reviews* **2013,** *42* (4), 1601-1618.

192. Khan, P.; Idrees, D.; Moxley, M. A.; Corbett, J. A.; Ahmad, F.; von Figura, G.; Sly, W. S.; Waheed, A.; Hassan, M. I., Luminol-Based Chemiluminescent Signals: Clinical and Non-clinical Application and Future Uses. *Applied Biochemistry and Biotechnology* **2014,** *173* (2), 333-355.

193. Fleiss, A.; Sarkisyan, K. S., A brief review of bioluminescent systems (2019). *Current Genetics* **2019,** *65* (4), 877-882.

194. Green, O.; Eilon, T.; Hananya, N.; Gutkin, S.; Bauer, C. R.; Shabat, D., Opening a Gateway for Chemiluminescence Cell Imaging: Distinctive Methodology for Design of Bright Chemiluminescent Dioxetane Probes. *Acs Central Science* **2017,** *3* (4), 349-358.

195. Filipovic, M. R.; Zivanovic, J.; Alvarez, B.; Banerjee, R., Chemical Biology of H2S Signaling through Persulfidation. *Chemical Reviews* **2018,** *118* (3), 377-461.

196. Lavu, M.; Bhushan, S.; Lefer, D. J., Hydrogen sulfide-mediated cardioprotection: mechanisms and therapeutic potential. *Clinical Science* **2011,** *120* (5-6), 219-229.

197. Chen, W. L.; Niu, Y. Y.; Jiang, W. Z.; Tang, H. L.; Zhang, C.; Xia, Q. M.; Tang, X. Q., Neuroprotective effects of hydrogen sulfide and the underlying signaling pathways. *Reviews in the Neurosciences* **2015,** *26* (2), 129-142.

198. Xu, M. T.; Hua, Y. Y.; Qi, Y.; Meng, G. L.; Yang, S. J., Exogenous hydrogen sulphide supplement accelerates skin wound healing via oxidative stress inhibition and vascular endothelial growth factor enhancement. *Experimental Dermatology* **2019,** *28* (7), 776-785.

199. Zhao, H. C.; Lu, S. X.; Chai, J. H.; Zhang, Y. C.; Ma, X. L.; Chen, J. C.; Guan, Q. B.; Wan, M. Y.; Liu, Y. T., Hydrogen sulfide improves diabetic wound healing in ob/ob mice via attenuating inflammation. *Journal of Diabetes and Its Complications* **2017,** *31* (9), 1363-1369.

200. Carballal, S.; Trujillo, M.; Cuevasanta, E.; Bartesaghi, S.; Moller, M. N.; Folkes, L. K.; Garcia-Bereguiain, M. A.; Gutierrez-Merino, C.; Wardman, P.; Denicola, A.; Radi, R.; Alvarez, B., Reactivity of hydrogen sulfide with peroxynitrite and other oxidants of biological interest. *Free Radical Biology and Medicine* **2011,** *50* (1), 196-205.

201. Wallace, J. L.; Wang, R., Hydrogen sulfide-based therapeutics: exploiting a unique but ubiquitous gasotransmitter. *Nature Reviews Drug Discovery* **2015,** *14* (5), 329-345.

202. Wu, L. Y.; Yang, W.; Jia, X. M.; Yang, G. D.; Duridanova, D.; Cao, K.; Wang, R., Pancreatic islet overproduction of H2S and suppressed insulin release in Zucker diabetic rats. *Laboratory Investigation* **2009,** *89* (1), 59-67.

203. Hu, L. F.; Lu, M.; Tiong, C. X.; Dawe, G. S.; Hu, G.; Bian, J. S., Neuroprotective effects of hydrogen sulfide on Parkinson's disease rat models. *Aging Cell* **2010,** *9* (2), 135-146.

204. Sarukhani, M.; Haghdoost-Yazdi, H.; Golezari, A. S.; Babayan-Tazehkand, A.; Dargahi, T.; Rastgoo, N., Evaluation of the antiparkinsonism and neuroprotective effects of hydrogen sulfide in acute 6-hydroxydopamine-induced animal model of Parkinson's disease: behavioral, histological and biochemical studies. *Neurological Research* **2018,** *40* (7), 525-533.

205. Lippert, A. R., Designing reaction-based fluorescent probes for selective hydrogen sulfide detection. *Journal of Inorganic Biochemistry* **2014,** *133*, 136-142.

206. Levinn, C. M.; Cerda, M. M.; Pluth, M. D., Activatable Small-Molecule Hydrogen Sulfide Donors. *Antioxidants & Redox Signaling*.

207. Paley, M. A.; Prescher, J. A., Bioluminescence: a versatile technique for imaging cellular and molecular features. *Medchemcomm* **2014,** *5* (3), 255-267.

208. Rathbun, C. M.; Prescher, J. A., Bioluminescent Probes for Imaging Biology beyond the Culture Dish. *Biochemistry* **2017,** *56* (39), 5178-5184.

209. Yan, Y. C.; Shi, P. F.; Song, W. L.; Bi, S., Chemiluminescence and Bioluminescence Imaging for Biosensing and Therapy: In Vitro and In Vivo Perspectives. *Theranostics* **2019,** *9* (14), 4047-4065.

210. Porterfield, W. B.; Jones, K. A.; McCutcheon, D. C.; Prescher, J. A., A "Caged" Luciferin for Imaging Cell-Cell Contacts. *Journal of the American Chemical Society* **2015,** *137* (27), 8656-8659.

211. Suzuki, K.; Nagai, T., Recent progress in expanding the chemiluminescent toolbox for bioimaging. *Current Opinion in Biotechnology* **2017,** *48*, 135-141.

212. Badr, C. E.; Tannous, B. A., Bioluminescence imaging: progress and applications. *Trends in Biotechnology* **2011,** *29* (12), 624-633.

213. Siraj, N.; El-Zahab, B.; Hamdan, S.; Karam, T. E.; Haber, L. H.; Li, M.; Fakayode, S. O.; Das, S.; Valle, B.; Strongin, R. M.; Patonay, G.; Sintim, H. O.; Baker, G. A.; Powe, A.; Lowry, M.; Karolin, J. O.; Geddes, C. D.; Warner, I. M., Fluorescence, Phosphorescence, and Chemiluminescence. *Analytical Chemistry* **2016,** *88* (1), 170-202.

214. Lee, D.; Khaja, S.; Velasquez-Castano, J. C.; Dasari, M.; Sun, C.; Petros, J.; Taylor, W. R.; Murthy, N., In vivo imaging of hydrogen peroxide with chemiluminescent nanoparticles. *Nature Materials* **2007,** *6* (10), 765-769.

215. Hananya, N.; Green, O.; Blau, R.; Satchi-Fainaro, R.; Shabat, D., A Highly Efficient Chemiluminescence Probe for the Detection of Singlet Oxygen in Living Cells. *Angewandte Chemie-International Edition* **2017,** *56* (39), 11793-11796.

216. Bruemmer, K. J.; Green, O.; Su, T. A.; Shabat, D.; Chang, C. J., Chemiluminescent Probes for Activity-Based Sensing of Formaldehyde Released from Folate Degradation in Living Mice. *Angewandte Chemie-International Edition* **2018,** *57* (25), 7508-7512.

217. An, W. W.; Ryan, L. S.; Reeves, A. G.; Bruemmer, K. J.; Mouhaffel, L.; Gerberich, J. L.; Winters, A.; Mason, R. P.; Lippert, A. R., A Chemiluminescent Probe for HNO Quantification and Real-Time Monitoring in Living Cells. *Angewandte Chemie-International Edition* **2019,** *58* (5), 1361-1365.

218. Bailey, T. S.; Pluth, M. D., Chemiluminescent Detection of Enzymatically Produced Hydrogen Sulfide: Substrate Hydrogen Bonding Influences Selectivity for H2S over Biological Thiols. *Journal of the American Chemical Society* **2013,** *135* (44), 16697-16704.

219. Bailey, T. S.; Pluth, M. D., Chemiluminescent Detection of Enzymatically Produced H2S. In *Hydrogen Sulfide in Redox Biology, Pt A*, Cadenas, E.; Packer, L., Eds. 2015; Vol. 554, pp 81-99.

220. Ke, B. W.; Wu, W. X.; Liu, W.; Liang, H.; Gong, D. Y.; Hu, X. T.; Li, M. Y., Bioluminescence Probe for Detecting Hydrogen Sulfide in Vivo. *Analytical Chemistry* **2016,** *88* (1), 592-595.

221. Tian, X. D.; Li, Z. Y.; Lau, C. W.; Lu, J. Z., Visualization of in Vivo Hydrogen Sulfide Production by a Bioluminescence Probe in Cancer Cells and Nude Mice. *Analytical Chemistry* **2015,** *87* (22), 11325-11331.

222. Schaap, A. P.; Sandison, M. D.; Handley, R. S., CHEMICAL AND ENZYMATIC TRIGGERING OF 1,2-DIOXETANES .3. ALKALINE PHOSPHATASE-CATALYZED CHEMILUMINESCENCE FROM AN ARYL PHOSPHATE-SUBSTITUTED DIOXETANE. *Tetrahedron Letters* **1987,** *28* (11), 1159-1162.

223. Turan, I. S.; Sozmen, F., A chromogenic dioxetane chemosensor for hydrogen sulfide and pH dependent off-on chemiluminescence property. *Sensors and Actuators B-Chemical* **2014,** *201*, 13-18.

224. Gnaim, S.; Green, O.; Shabat, D., The emergence of aqueous chemiluminescence: new promising class of phenoxy 1,2-dioxetane luminophores. *Chemical Communications* **2018,** *54* (17), 2073-2085.

225. Hananya, N.; Shabat, D., Recent Advances and Challenges in Luminescent Imaging: Bright Outlook for Chemiluminescence of Dioxetanes in Water. *Acs Central Science* **2019,** *5* (6), 949-959.

226. Montoya, L. A.; Pearce, T. F.; Hansen, R. J.; Zakharov, L. N.; Pluth, M. D., Development of Selective Colorimetric Probes for Hydrogen Sulfide Based on Nucleophilic Aromatic Substitution. *Journal of Organic Chemistry* **2013,** *78* (13), 6550-6557.

227. Huang, Z. J.; Ding, S. S.; Yu, D. H.; Huang, F. H.; Feng, G. D., Aldehyde group assisted thiolysis of dinitrophenyl ether: a new promising approach for efficient hydrogen sulfide probes. *Chemical Communications* **2014,** *50* (65), 9185-9187.

228. Cao, J.; Lopez, R.; Thacker, J. M.; Moon, J. Y.; Jiang, C.; Morris, S. N. S.; Bauer, J. H.; Tao, P.; Mason, R. P.; Lippert, A. R., Chemiluminescent probes for imaging H2S in living animals. *Chemical Science* **2015,** *6* (3), 1979-1985.

229. Handa, T.; Takeuchi, H.; Takagi, H.; Toriyama, S.; Kawashima, Y.; Komatsu, H.; Nakagaki, M., REACTIVITY OF SINGLET OXYGEN GENERATED BY THE PHOTOSENSITIZATION OF TETRAPHENYLPORPHYRIN IN LIPOSOMES. *Colloid and Polymer Science* **1988,** *266* (8), 745-752.

230. Gurinovich, K. I. S. M. B. P., Lifetime of singlet oxygen in various solvents. *Journal of Applied Spectroscopy* **1981,** *34* (5), 561-564.

231. Roth-Konforti, M. E.; Bauer, C. R.; Shabat, D., Unprecedented Sensitivity in a Probe for Monitoring CathepsinB: Chemiluminescence Microscopy Cell-Imaging of a Natively Expressed Enzyme. *Angewandte Chemie-International Edition* **2017,** *56* (49), 15633-15638.

232. Zhang, W.; Kang, J. Q.; Li, P.; Wang, H.; Tang, B., Dual Signaling Molecule Sensor for Rapid Detection of Hydrogen Sulfide Based on Modified Tetraphenylethylene. *Analytical Chemistry* **2015,** *87* (17), 8964-8969.

233. Cao, X. W.; Lin, W. Y.; Zheng, K. B.; He, L. W., A near-infrared fluorescent turn-on probe for fluorescence imaging of hydrogen sulfide in living cells based on thiolysis of dinitrophenyl ether. *Chemical Communications* **2012,** *48* (85), 10529-10531.

234. Hananya, N.; Boock, A. E.; Bauer, C. R.; Satchi-Fainaro, R.; Shabat, D., Remarkable Enhancement of Chemiluminescent Signal by Dioxetane-Fluorophore Conjugates: Turn-ON Chemiluminescence Probes with Color Modulation for Sensing and Imaging. *Journal of the American Chemical Society* **2016,** *138* (40), 13438-13446.

235. Aucagne, V.; Hanni, K. D.; Leigh, D. A.; Lusby, P. J.; Walker, D. B., Catalytic "click" rotaxanes: A substoichiometric metal-template pathway to mechanically interlocked architectures. *Journal of the American Chemical Society* **2006,** *128* (7), 2186-2187.

236. Denis, M.; Goldup, S. M., The active template approach to interlocked molecules. *Nat. Rev. Chem.* **2017,** *1* (8), 17.

237. Stoddart, J. F., Mechanically Interlocked Molecules (MIMs)-Molecular Shuttles, Switches, and Machines (Nobel Lecture). *Angewandte Chemie-International Edition* **2017,** *56* (37), 11094-11125.

238. Stoddart, J. F., The chemistry of the mechanical bond. *Chemical Society Reviews* **2009,** *38* (6), 1802-1820.

239. Denis, M.; Pancholi, J.; Jobe, K.; Watkinson, M.; Goldup, S. M., Chelating Rotaxane Ligands as Fluorescent Sensors for Metal Ions. *Angewandte Chemie-International Edition* **2018,** *57* (19), 5310-5314.

240. Langton, M. J.; Beer, P. D., Rotaxane and Catenane Host Structures for Sensing Charged Guest Species. *Accounts of Chemical Research* **2014,** *47* (7), 1935-1949.

241. Van Raden, J. M.; White, B. M.; Zakharov, L. N.; Jasti, R., Nanohoop Rotaxanes from Active Metal Template Syntheses and Their Potential in Sensing Applications. *Angewandte Chemie-International Edition* **2019,** *58* (22), 7341-7345.

242. Leonhardt, E. J.; Jasti, R., Emerging applications of carbon nanohoops. *Nat. Rev. Chem.* **2019,** *3* (12), 672-686.

243. Lovell, T. C.; Colwell, C. E.; Zakharov, L. N.; Jasti, R., Symmetry breaking and the turn-on fluorescence of small, highly strained carbon nanohoops. *Chemical Science* **2019,** *10* (13), 3786-3790.

244. White, B. M.; Zhao, Y.; Kawashima, T. E.; Branchaud, B. P.; Pluth, M. D.; Jasti, R., Expanding the Chemical Space of Biocompatible Fluorophores: Nanohoops in Cells. *Acs Central Science* **2018,** *4* (9), 1173-1178.

245. Darzi, E. R.; Jasti, R., The dynamic, size-dependent properties of 5 - 12 cycloparaphenylenes. *Chemical Society Reviews* **2015,** *44* (18), 6401-6410.

246. Golder, M. R.; Jasti, R., Syntheses of the Smallest Carbon Nanohoops and the Emergence of Unique Physical Phenomena. *Accounts of Chemical Research* **2015,** *48* (3), 557-566.

247. Wang, R., Physiological implications of hydrogen sulfide: a whiff exploration that blossomed. *Physiol Rev* **2012,** *92* (2), 791-896.

248. Berna, J.; Goldup, S. M.; Lee, A. L.; Leigh, D. A.; Symes, M. D.; Teobaldi, G.; Zerbetto, F., Cadiot-Chodkiewicz active template synthesis of rotaxanes and switchable molecular shuttles with weak intercomponent interactions. *Angewandte Chemie-International Edition* **2008,** *47* (23), 4392-4396.

249. Movsisyan, L. D.; Franz, M.; Hampel, F.; Thompson, A. L.; Tykwinski, R. R.; Anderson, H. L., Polyyne Rotaxanes: Stabilization by Encapsulation. *Journal of the American Chemical Society* **2016,** *138* (4), 1366-1376.

250. Hartle, M. D.; Meininger, D. J.; Zakharov, L. N.; Tonzetich, Z. J.; Pluth, M. D., NBu4SH provides a convenient source of HS- soluble in organic solution for H2S and anion-binding research. *Dalton Transactions* **2015,** *44* (46), 19782-19785.

251. Scattolin, T.; Senol, E.; Yin, G. Y.; Guo, Q. Q.; Schoenebeck, F., Site-Selective C-S Bond Formation at C-Br over C-OTf and C-Cl Enabled by an Air-Stable, Easily Recoverable, and Recyclable Palladium(I) Catalyst. *Angewandte Chemie-International Edition* **2018,** *57* (38), 12425-12429.

252. The All Results Journals: Chem. AR Journals.

253. Kluger, J., Why Scientists Should Celebrate Failed Experiments. *TIME* 2014.

254. Franco, A.; Malhotra, N.; Simonovits, G., Publication bias in the social sciences: Unlocking the file drawer. *Science* **2014,** *345* (6203), 1502-1505.

255. Board, N. S., Science and Engineering Indicators 2018. Foundation, N. S., Ed. National Science Board: Alexandria, VA, 2018.

256. Federal Tax Revenue by Source, 1934 – 2018. https://taxfoundation.org/federal-tax-revenue-source-1934-2018/ (accessed January 21 2020).

257. Papadakis, M., The economic impacts of public science can be measured. *Scientist* **1997,** *11* (21), 8-8.

258. Salter, A. J.; Martin, B. R., The economic benefits of publicly funded basic research: a critical review. *Research Policy* **2001,** *30* (3), 509-532.

259. Sierra, M. A.; de la Torre, M. C., Dead ends and detours en route to total syntheses of the 1990s. *Angewandte Chemie-International Edition* **2000,** *39* (9), 1538-1559.

260. Martin, K., Publishing Failure in Science. In *Publishing Failure in Science*, goldbio.com, 2018; Vol. 2020.

261. Hilten, L. G. v., Why it's time to publish research “failures”. *Elsevier Connect* 2015.

262. New Negatives in Plant Science. https://www.journals.elsevier.com/new-negatives-in-plant-science.

263. Dr Alexandra Freeman - 'Octopus: a radical new approach to scientific publishing'. https://royalsociety.org/topics-policy/projects/research-culture/research-culture-conference/the-pitch/the-pitch-winner-dr-alexandra-freeman/ (accessed January 21 2020).

264. Freeman, A., Innovator Story: Wrestling the Octopus. *eLife Innovation* 2019.

265. Octopus Octopus - All of Science in One Place. https://octopus-hypothesis.netlify.com/ (accessed January 21 2020).

266. Eshon, J.; Foarta, F.; Landis, C. R.; Schomaker, J. M., alpha-Tetrasubstituted Aldehydes through Electronic and Strain-Controlled Branch-Selective Stereoselective Hydroformylation. *Journal of Organic Chemistry* **2018,** *83* (17), 10207-10220.

267. Park, H.; Verma, P.; Hong, K.; Yu, J. Q., Controlling Pd(IV) reductive elimination pathways enables Pd(II)-catalysed enantioselective C(sp(3))-H fluorination. *Nature Chemistry* **2018,** *10* (7), 755-762.

268. Lee, J.; Ryu, T.; Park, S.; Lee, P. H., Indium Tri(isopropoxide)-Catalyzed Selective Meerwein-Ponndorf-Verley Reduction of Aliphatic and Aromatic Aldehydes. *Journal of Organic Chemistry* **2012,** *77* (10), 4821-4825.

269. Pardeshi, K. A.; Ravikumar, G.; Chakrapani, H., Esterase Sensitive Self-Immolative Sulfur Dioxide Donors. *Organic Letters* **2018,** *20* (1), 4-7.

270. Seki, H.; Xue, S.; Pellet, S.; Silhar, P.; Johnson, E. A.; Janda, K. D., Cellular Protection of SNAP-25 against Botulinum Neurotoxin/A: Inhibition of Thioredoxin Reductase through a Suicide Substrate Mechanism. *Journal of the American Chemical Society* **2016,** *138* (17), 5568-5575.

271. Jessen, H. J.; Schulz, T.; Balzarini, J.; Meier, C., Bioreversible Protection of Nucleoside Diphosphates. *Angewandte Chemie-International Edition* **2008,** *47* (45), 8719-8722.

272. Liu, H. X.; Dang, Y. Q.; Yuan, Y. F.; Xu, Z. F.; Qiu, S. X.; Tan, H. B., Diacyl Disulfide: A Reagent for Chemoselective Acylation of Phenols Enabled by 4-(N,N-Dimethylamino)pyridine Catalysis. *Organic Letters* **2016,** *18* (21), 5584-5587.